University of Bath

PHD

New Generic Synthetic Protocols for Pharmaceutical Intermediates Based on Continuous Flow Multifunctional Platforms

Sobolewska, Anna

Award date:
2015

Awarding institution:
University of Bath

Link to publication

General rights
Copyright and moral rights for the publications made accessible in the public portal are retained by the authors and/or other copyright owners and it is a condition of accessing publications that users recognise and abide by the legal requirements associated with these rights.

- Users may download and print one copy of any publication from the public portal for the purpose of private study or research.
- You may not further distribute the material or use it for any profit-making activity or commercial gain
- You may freely distribute the URL identifying the publication in the public portal ?

Take down policy
If you believe that this document breaches copyright please contact us providing details, and we will remove access to the work immediately and investigate your claim.

Download date: 13. May. 2019

New Generic Synthetic Protocols for Pharmaceutical Intermediates Based on Continuous Flow Multifunctional Platforms

Anna Maria Sobolewska

A thesis submitted for the degree of Doctor of Philosophy

University of Bath
Department of Chemical Engineering

September 2014

COPYRIGHT

Attention is drawn to the fact that copyright of this thesis rests with the author. A copy of this thesis has been supplied on condition that anyone who consults it is understood to recognise that its copyright rests with the author and they must not copy it or use material from it except as permitted by law or with the consent of the author.

This thesis may be made available for consultation within the University Library and may be photocopied or lent to other libraries for the purpose of consultations with effect from ……...

Signed on behalf of the Faculty of Engineering & Design

Abstract

The purpose of this work is to study the synthesis of primary amines under continuous flow conditions using a heterogeneous catalyst. 10 wt% Pd/C catalyst based on mesoporous synthetic carbon was synthesised and used in the form of micro-packed-beds in a structured multichannel compact reactor (developed at the University of Bath) and in a commercially available X-Cube™ flow reactor (developed by ThalesNano). Under continuous flow conditions aliphatic, aromatic and cyclic primary amines were synthesised selectively from aldehydes *via* a tandem reductive amination - hydrogenolysis process with high conversions (>99%) and very good isolated yields (74 - 99%). In this work, two consecutive structured multichannel reactors at different temperatures (T_1 and T_2) were used to ensure hight selectivity (100%) towards the desired products. Optimal conditions at a liquid flow rate of 0.2 mL min^{-1} were obtained with a substrate concentration of 0.2 mol L^{-1}.

Kinetic studies on the reductive amination of hydrocinnamaldehyde and hydrogenolysis of (1-phenylethyl)(3-phenylpropyl)amine were studied with a 10 wt% Pd/C catalyst using a multichannel packed-bed reactor. It was shown that it was possible to neglect mass transport limitations and kinetic models based on the Langmuir-Hinshelwood approach were proposed. The model of competitive dissociative adsorption of hydrogen was found to represent the mechanism of the reaction and fitted the experimental data very well. The reaction rate constant (k_R^*), adsorption equilibrium constants (K_A and K_B) and the apparent activation energy for each reaction were estimated.

The investigation resulted in fundamental information on reactor performance for selected model reactions as well as the development of continuous tandem processes. The results demonstrate that the structured multichannel compact reactor and the commercially available X-Cube™ flow reactor can be used to explore how heterogeneous catalysis may be used to turn a batch reaction into a continuous flow process.

Acknowledgments

I would like to first thank my supervisor, Dr Pawel Plucinski for his continuous support, guidance, suggestions and wide knowledge on chemical engineering which were of immense value in driving this work forward.

I would also like to acknowledge my second supervisor, Professor Jonathan Williams for his constructive discussions of and useful feedback on my work.

I would like to acknowledge the funding support provided by EPSRC and GlaxoSmithKline.

Thanks in particular are due to Dr Robert Watson for hosting my visit to GlaxoSmithKline in Stevenage, for his stimulating ideas and assistance and for making me feel like one of the team. This has been a valuable and unforgettable experience.

I would also like to express my appreciation to the research team; Dr Massimiliano Vezzoli, Dr Sumeet Sharma from the Chemical Engineering Department, and Dr Andrew Watson from the Chemistry Department for their useful discussions, advice and friendship throughout the period I was in Bath.

I am grateful to the technical staff in the Chemical Engineering Department for their kind technical support in helping with the experimental work, especially John Bishop, Fernando Acosta, Merv Newnes and Robert Brain.

Finally, I would like to thank my family and friends for their precious encouragement and support.

Table of Contents

Abstract I

Acknowledgments II

Table of Contents III

List of Figures VIII

List of Schemes XVI

List of Tables XIX

Abbreviations XXII

Nomenclature XXIV

Research Scope 1

Thesis Structure 1

Chapter 1: Literature Review 4

1.1. Introduction 5

1.2. Flow chemistry 7

1.2.1. Microreactors 9

1.2.2. Types of microreactors 10

1.2.3. Properties of microreactors 20

1.2.4. Online analytics in microreactors 23

1.2.5. Application of microreactors 25

1.3. Conclusions 46

1.4. Aim and objectives of the thesis 47

Chapter 2: Reductive Amination of Aldehydes in the Structured Compact Reactor and X-Cube™ Flow Reactor 48

2.1. Introduction 49

2.2. Experimental 58

2.2.1. Pd/C catalyst and reagents 58

2.2.2. Structured compact reactor 59

2.2.3. Continuous catalytic rig and procedure for continuous experiments 60

2.2.4. X-Cube™ flow reactor 62

2.2.5. Analysis techniques 64

2.3. Results and discussion 67

2.3.1. Continuous catalytic rig with multichannel packed-bed reactor 67

2.3.1.1. Imine formation 67

2.3.1.2. Effect of liquid flow rate 70

2.3.1.3. Effect of hydrogen flow rate 73

2.3.1.4. Effect of operating pressure and concentration 74

2.3.1.5. Effect of reaction temperature 76

2.3.1.6. Catalyst stability 79

2.3.1.7. Synthesis of selected secondary amines 82

2.3.1.8. Reactor efficiency with split injection of hydrogen 88

2.3.2. X-Cube™ flow reactor 90

2.3.2.1. Effect of liquid flow rate 90

2.3.2.2. Effect of operating pressure 93

2.3.2.3. Effect of reaction temperature 95

2.3.2.4. Effect of reagent concentration 96

2.3.2.5. Catalyst stability 96

2.3.2.6. Synthesis of selected secondary amines 98

2.4. Conclusions 104

Chapter 3: Deprotection of Secondary Amines in the Structured Compact Reactor and X-Cube™ Flow Reactor 106

3.1. Introduction 107

3.2. Experimental 111

3.2.1. Activated carbon and reagents 111
3.2.2. Preparation of Pd/C catalyst 111
3.2.3. Structured compact reactor 111
3.2.4. Continuous catalytic rig and procedure for continuous experiments 111
3.2.5. Analysis techniques 111
3.3. Results and discussion 113
3.3.1. Characterisation of synthetic carbon and Pd/C catalyst 113
3.3.2. Batch *vs* flow system for 1-phenylethyl group deprotection 115
3.3.3. Continuous catalytic rig with multichannel packed-bed reactor 116
3.3.3.1. Effect of liquid flow rate 116
3.3.3.2. Effect of hydrogen flow rate 119
3.3.3.3. Effect of operating pressure and concentration 121
3.3.3.4. Effect of reaction temperature 124
3.3.3.5. Catalyst stability 125
3.3.3.6. Reactor efficiency with split injection of hydrogen 127
3.3.4. X-Cube™ flow reactor 129
3.3.4.1. Effect of liquid flow rate 129
3.3.4.2. Effect of operating pressure 131
3.3.4.3. Effect of reaction temperature 133
3.3.2.4. Effect of reagent concentration 134
3.3.4.5. Catalyst stability 136
3.4. Conclusions 137
Chapter 4: Tandem - Reductive Amination of Aldehydes and Hydrogenolysis of Secondary Amines 139
4.1. Introduction 140
4.2. Experimental 142
4.2.1. Pd/C catalyst and reagents 142
4.2.2. Structured compact reactor 142
4.2.3. Continuous catalytic rig and procedure for continuous experiments 142
4.2.4. Analysis techniques 145
4.3. Results and discussion 146

4.3.1. Continuous catalytic rig with multichannel packed-bed reactor 146
4.3.1.1. Effect of liquid flow rate 146
4.3.1.2. Effect of hydrogen flow rate 149
4.3.1.3. Effect of reaction temperature 150
4.3.1.4. Reactor efficiency with split injection of hydrogen 151
4.3.1.5. Synthesis of selected primary amines by tandem reductive amination - hydrogenolysis reaction 155
4.3.2. X-Cube™ flow reactor 159
4.3.2.1. Effect of liquid flow rate 159
4.3.2.2. Effect of operating pressure 162
4.3.2.3. Effect of reaction temperature 163
4.3.2.4. Synthesis of selected primary amines by tandem reductive amination - hydrogenolysis reaction 164
4.4. Conclusions 167
Chapter 5: Reaction kinetics for the reductive amination of hydrocinnamaldehyde over a palladium on carbon catalyst 168
5.1. Introduction 169
5.2. Experimental 177
5.2.1. Pd/C catalyst and reagents 177
5.2.2. Analytical technique 177
5.2.3. Structured compact reactor and continuous catalytic rig 177
5.3. Results and discussion 178
5.3.1. Effect of external and internal mass transfer 178
5.3.1.1. Effect of liquid phase flow rate 178
5.3.1.2. Effect of gas phase flow rate 182
5.3.1.3. Effect of internal diffusion 184
5.3.2. Effect of hydrogen partial pressure 186
5.3.3. Effect of reagent concentration 189
5.3.4. Effect of reaction temperature 190
5.3.5. Kinetic model and reaction mechanism 193
5.4. Conclusions 214

Chapter 6: Reaction kinetics for the deprotection of (1-phenylethyl)(3-phenylpropyl) amine over a palladium on carbon catalyst 215

6.1. Introduction 216

6.2. Experimental 220

6.2.1. Pd/C catalyst and reagents 220

6.2.2. Analytical technique 221

6.2.3. Structured compact reactor and continuous catalytic rig 221

6.3. Results and discussion 221

6.3.1. Effect of external and internal mass transfer 221

6.3.1.1. Effect of liquid phase flow rate 221

6.3.1.2. Effect of gas phase flow rate 222

6.3.1.3. Effect of internal diffusion 223

6.3.2. Effect of hydrogen partial pressure 224

6.3.3. Effect of reagent concentration 225

6.3.4. Effect of reaction temperature 226

6.3.5. Kinetic model and reaction mechanism 229

6.4. Conclusions 236

Chapter 7: Final conclusions and recommendations for further work 237

7.1. Conclusions 238

7.2. Recommendations for further work 244

References 247

Appendix I: NMR and MS analysis of secondary amines 271

Appendix II: NMR and MS analysis of primary amines 300

List of Figures

Chapter 1

Figure 1.1. ThalesNano Inc. flow reactor systems: a) H-Cube®, b) X-Cube™, c) H-Cube Pro™ (www.thalesnano.com). 13

Figure 1.2. a) FlowSyn reactor system and b) FlowSyn Polar Bear™ reactor system (www.uniqsis.com). 14

Figure 1.3. The NanoTek microfluidic synthesis system from Advion, USA (www. advison.com). 15

Figure 1.4. The Labtrix®-S1 system from Chemtrix BV, The Netherlands (www.chemtrix.com). 16

Figure 1.5. Vapourtec R-series, a flexible tubular flow reactor system from Vapourtec Ltd.,UK (www.vapourtec.co.uk). 17

Figure 1.6. Glass-based flow reactor platform FlowStart from FutureChemistry BV, The Netherlands (www.futurechemistry.com). 18

Figure 1.7. Glass-based flow reactor platform Africa from Syrris Ltd., UK (www.syrris.com). 18

Figure 1.8. Corning® Advanced - Flow™ Reactors: a) low - flow reactor, b) G1 standard evaluation reactor, c) G3 glass reactor, d) G4 ceramic reactor (www.corning.com) 19

Figure 1.9. Corning® Advanced - Flow™ Reactors: a) reactor modules, b) pilot - scale production (www.corning.com). 20

Figure 1.10. Microreactor used in a synthesis of a vitamin precursor. Adopted fromBrivio *et al.* (2006). 28

Figure 1.11. a) Microreactor used in Reinhoudt's group's work. b) Dedicated chip holder for fitting fused silica fibres into the inlet/outlet chip reservoirs by means of low dead volume Nanoport® connectors. Adopted fromBrivio *et al.* (2006). 30

Figure 1.12. a) The falling film microreactor used in Jähnisch's work. b) Components of the reactor. Adopted from Jähnisch *et al.* (2004). .35

Figure 1.13. a) Construction of the microbubble column used by Jähnisch's group. b) Components of the column. Adopted fromJähnisch *et al.* (2004). .36

Figure 1.14. Raney nickel mediated reduction of nitropyrrolidines. 39
Figure 1.15. Pd/C-mediated reduction and debenzylation of 3-nitropyrrolidines. 40

Chapter 2

Figure 2.1. Structured compact reactor. 59
Figure 2.2. Schematic diagram of the structured compact reactor: (a) general view and (b) cross-section of a channel. Adapted fromFan *et al.* (2009). ...60
Figure 2.3. The continuous catalytic rig with the structured multichannel compact reactor. 61
Figure 2.4. Schematic diagram of the catalytic rig(Plucinski *et al.*, 2005; Bavykin *et al.*, 2005). 62
Figure 2.5. The X-Cube^{TM} flow reactor. 64
Figure 2.6. Calibration curve for the GC analysis of hydrocinnamaldehyde.....65
Figure 2.7. Calibration curve for the GC analysis of α-methylbenzylamine.....65
Figure 2.8. Calibration curve for the GC analysis of (1-phenylethyl)(3-phenylpropyl) amine. 66
Figure 2.9. Imine formation as a function of reagent mixing time. 69
Figure 2.10. Product concentration in the outlet of the reactor as a function of time-on-stream. P_T = 8 bar, F_G = 21.0 mL (STP) min^{-1}, $C_{S,0}$ = 0.4 mol L^{-1},T = 298 K. 70
Figure 2.11. Influence of liquid flow rate on imine conversion during reductive amination of hydrocinnamaldehyde with α-methylbenzylamine reaction. P_T = 8 bar, F_G = 21.0 mL (STP) min^{-1}, $C_{S,0}$ = 0.4 mol L^{-1}, T = 298 K. 71
Figure 2.12. Influence of liquid flow rate on the rate of product formation. P_T = 8 bar, F_G = 21.0 mL (STP) min^{-1}, $C_{S,0}$ = 0.4 mol L^{-1}, T = 298 K, (1 mL min^{-1} = 6.67 m^3 m^{-2} h^{-1}).....72
Figure 2.13. Product concentration as a function of hydrogen flow rate. F_L = 2.0 mL min^{-1}, $C_{S,0}$ = 0.4 mol L^{-1}, T = 298 K. 74
Figure 2.14. Effect of the total pressure on the product concentration. F_G = 21.0 mL (STP) min^{-1}, F_L = 2.0 mL min^{-1}, $C_{S,0}$ = 0.4 mol L^{-1}. 75

Figure 2.15. Effect of the reagent initial concentration on the product concentration P_T = 8 bar, F_G = 21.0 mL (STP) min^{-1}, F_L = 2.0 mL min^{-1}.....75
Figure 2.16. Influence of the reaction temperature on the conversion of imine. P_T = 8 bar, F_G = 21.0 mL (STP) min^{-1}, F_L = 2.0 mL min^{-1}, $C_{S,0}$ = 0.4 mol L^{-1}.....76
Figure 2.17. Influence of the reaction temperature on the conversion of imine to secondary amine. P_T = 8 bar, F_G = 21.0 mL (STP) min^{-1}, F_L = 2.0 mL^{-l} min^{-1}. 79
Figure 2.18. Imine conversion as a function of time-on-stream. P_T = 8 bar, F_G = 21.0 mL (STP) min^{-1}, F_L = 0.5 mL min^{-1}, $C_{S,0}$ = 0.4 mol L^{-1}, T = 298 K. 80
Figure 2.19. The deactivation rate of Pd/C catalyst over 65 hours. 81
Figure 2.20. Channel arrangement for split hydrogen injection experiments. 88
Figure 2.21. Product concentration in the outlet of the reactor as a function of time-on-stream. P_T = 30 bar, $C_{S,0}$ = 0.2 mol L^{-1}, T = 298K. 90
Figure 2.22. Influence of liquid flow rate on the conversion of imine. $C_{S,0}$ = 0.2 mol L^{-1}, T = 298K. 91
Figure 2.23. Influence of liquid flow rate on the overall rate of product formation. $C_{S,0}$ = 0.2 mol L^{-1}, T = 298K. 92
Figure 2.24. Influence of the total pressure on the conversion of imine. $C_{S,0}$ = 0.2 mol L^{-1}, T = 298K. 93
Figure 2.25. Influence of the total pressure on the rate of product formation. $C_{S,0}$ = 0.2 mol L^{-1}, T = 298K. 94
Figure 2.26. Influence of the total pressure on the rate of product formation. $C_{S,0}$ = 0.4 mol L^{-1}, T = 298K. 94
Figure 2.27. Influence of reaction temperature on the imine conversion. P_T = 30 bar, F_L = 0.5 mL min^{-1}, $C_{S,0}$ = 0.4 mol L^{-1}.....95
Figure 2.28. Influence of the initial concentration on the product concentration. P_T = 30 bar, F_L = 0.5 mL min^{-1}, T = 298K. 96
Figure 2.29. The imine conversion as a function of time-on-stream. P_T = 30 bar, F_L = 0.5 mL min^{-1}, $C_{S,0}$ = 0.4 mol L^{-1}, T = 298K. 97
Figure 2.30. The deactivation rate of Pd/C catalyst over 52 hours. 98

Chapter 3

Figure 3.1. Calibration curve of GC analysis for 3-phenylpropan-1-amine. 112
Figure 3.2. Calibration curve of GC analysis for ethylbenzene. 112
Figure 3.3. Nitrogen adsorption/ desorption isotherms for synthetic carbon and the prepared catalyst. 113
Figure 3.4. Nitrogen adsorption/ desorption isotherms of synthetic carbon. 114
Figure 3.5. Product concentration in the outlet of the reactor as a function of time-on-stream. P_T = 8 bar, F_G = 21.0 mL (STP) min^{-1}, $C_{S,0}$ = 0.2 mol L^{-1},T = 393K. 117
Figure 3.6. Influence of the liquid flow rate on the conversion of 2º amine. P_T = 8bar, F_G = 21.0 mL (STP) min^{-1}, $C_{S,0}$ = 0.2 mol L^{-1}, T = 393K. 118
Figure 3.7. Influence of the liquid flow rate on the average rate of product formation. P_T = 8bar, F_G = 21.0 mL (STP) min^{-1}, $C_{S,0}$ = 0.2 mol L^{-1}, T = 393K. 119
Figure 3.8. Influence of the hydrogen flow rate on the product concentration. P_T = 8bar, F_L = 0.5 mL min^{-1}, $C_{S,0}$ = 0.2 mol L^{-1}, T = 393K. 120
Figure 3.9. Influence of the hydrogen flow rate on the overall rate of product formation. P_T = 8bar, F_L = 0.5 mL min^{-1}, $C_{S,0}$ = 0.2 mol L^{-1}, T = 393K. 121
Figure 3.10. Influence of hydrogen pressure on the conversion. F_G = 21.0 mL (STP) min^{-1}, F_L = 0.5 mL min^{-1}, $C_{S,0}$ = 0.2 mol L^{-1}, T = 393K. 122
Figure 3.11. Influence of hydrogen pressure on the rate of product formation. F_G = 21.0 mL (STP) min^{-1}, F_L = 0.5 mL min^{-1}, $C_{S,0}$ = 0.2 mol L^{-1}, T = 393 K. 123
Figure 3.12. Influence of the initial concentration of secondary amine on the product formation. P_T = 8bar, F_G = 21.0 mL (STP) min^{-1}, F_L = 0.5 mL min^{-1}, T = 393K. 124
Figure 3.13. The influence of the reaction temperature on the conversion of secondary amine. P_T = 8bar, F_G = 21.0 mL (STP) min^{-1}, F_L = 0.5 mL min^{-1}, $C_{S,0}$ = 0.2 mol L^{-1} 125

Figure 3.14. The 2º amine conversion as a function of time-on-stream. P_T = 8 bar, F_G = 21.0 mL (STP) min^{-1}, F_L = 0.5 mL min^{-1}, $C_{S,0}$=0.2 mol L^{-1},T = 393K. 126
Figure 3.15. The deactivation rate of Pd/C catalyst over 65 hours during the synthesis of primary amine.....126
Figure 3.16. Channel arrangement for split hydrogen injection experiments.....127
Figure 3.17. The evaluation of steady-state conversion for various reaction conditions. P_T =30 bar, $C_{S,0}$ = 0.1 mol L^{-1}, T = 413K. 129
Figure 3.18. Influence of liquid flow rate on the conversion of the hydrogenolysis of (1-phenylethyl)(3-phenylpropyl)amine. $C_{S,0}$ = 0.1 mol L^{-1}, T = 413K. 130
Figure 3.19. Influence of the liquid flow rate on the rate of hydrogenolysis of (1-phenylethyl)(3-phenylpropyl)amine. $C_{S,0}$ = 0.1 mol L^{-1}, T = 413K. 131
Figure 3.20. Influence of pressure on the conversion of (1-phenylethyl) (3-phenylpropyl)amine. $C_{S,0}$ = 0.1 mol L^{-1},T = 413K. 132
Figure 3.21. Influence of pressure on the rate of product formation of the hydrogenolysis of (1-phenylethyl)(3-phenylpropyl)amine. $C_{S,0}$ = 0.1 mol L^{-1}, T = 413K. 132
Figure 3.22. Influence of the reaction temperature on the product concentration. P_T = 30 bar, F_L = 0.5 mL min^{-1}, $C_{S,0}$ = 0.1 mol L^{-1}.....133
Figure 3.23. Influence of the reaction temperature on the overall rate of product formation. P_T = 30 bar, F_L = 0.5 mL min^{-1}, $C_{S,0}$ = 0.1 mol L^{-1}.....134
Figure 3.24. Effect of the initial concentration of reagent on secondary amine conversion. P_T = 30 bar, F_L = 0.5 mL min^{-1}, T = 413K. 135
Figure 3.25. Effect of the initial concentration of reagent on the rate of product formation. P_T = 30 bar, F_L = 0.5 mL min^{-1}, T = 413K. 135
Figure 3.26. The 2º amine conversion as a function of time-on-stream. P_T = 30 bar, F_L = 0.2 mL min^{-1}, $C_{S,0}$ = 0.1 mol L^{-1}, T = 413K. 136
Figure 3.27. The deactivation rate of Pd/C catalyst during the synthesis of 1º amine.....137

Chapter 4

Figure 4.1.The continuous catalytic rig with the structured multichannel reactors for multi-step synthesis. 143

Figure 4.2. A schematic diagram of the reactors configuration for the consecutive reductive amination of aldehyde (ketone)-hydrogenolysis of secondary amines reaction.....144

Figure 4.3. Influence of the liquid flow rate on the product concentration. P_T = 8 bar, F_G = 21.0 mL (STP) min^{-1}, $C_{S,0}$ = 0.2 mol L^{-1}, T_1 = 298K, T_2= 393K.....148

Figure 4.4. Influence of the liquid flow rate on the average rate of product formation. P_T = 8 bar, F_G = 21.0 mL (STP) min^{-1}, $C_{S,0}$ = 0.2 mol L^{-1}, T_1 = 298K, T_2 = 393K. 148

Figure 4.5. Influence of hydrogen flow rate on the product concentration. P_T = 8 bar, F_L = 0.5 mL min^{-1}, T_1 = 298K, T_2 = 393K.....149

Figure 4.6. Influence of the hydrogen flow rate on product formation. P_T = 8 bar, F_L = 0.5 mL min^{-1}, $C_{S,0}$ = 0.2 mol L^{-1}, T_1 = 298K, T_2 = 393K.....150

Figure 4.7. Reactor channel arrangement for split hydrogen injection experiments. 152

Figure 4.8. Product concentration vs gas flow rate for different hydrogen injection points. P_T = 8 bar, F_L = 0.5 mL min^{-1}, $C_{S,0}$ = 0.4 mol L^{-1}, T_1 = 298K, T_2 = 393K.....153

Figure 4.9. Influence of the hydrogen flow rate on the product concentration for channel arrangement C. P_T = 8 bar, F_L = 0.5 mL min^{-1}, $C_{S,0}$ = 0.4 mol L^{-1}, T_1 = 298K, T_2 = 393K.....154

Figure 4.10. Influence of the liquid flow rate on the product concentration. P_T = 30 bar, $C_{S,0}$ = 0.2 mol L^{-1}, T_1 = 298K and T_2 = 413K.....160

Figure 4.11. Influence of the liquid flow rate on the product concentration. P_T = 30 bar, $C_{S,0}$ = 0.2 mol L^{-1}, T_1 = 298K and T_2 = 403K.....161

Figure 4.12. Influence of the liquid flow rate on the average rate of product formation. P_T = 30 bar, $C_{S,0}$ = 0.2 mol L^{-1}, T_1 = 298K,T_2 = 403K....161

Figure 4.13. Influence of the pressure on the product concentration. F_L = 0.2 mL min^{-1}, $C_{S,0}$ = 0.2 mol L^{-1},T_1 = 298K, T_2 = 403K.....163

Figure 4.14. Influence of the reaction temperature on product concentration. P_T = 30 bar, F_L = 0.2 mL min^{-1}, $C_{S,0}$ = 0.2 mol L^{-1}, T_1 = 298K, T_2 = 403K. 164

Chapter 5

Figure 5.1. Schematic diagram of transport steps in multi-phase catalytic reactions (Hofmann, 1978). 170

Figure 5.2. Influence of the liquid flow rate on the average reaction rate. P_{H_2} = 7.8 bar, F_G = 21.0 mL (STP) min^{-1}, $C_{S,0}$ = 0.4 mol L^{-1}, T = 298K. 179

Figure 5.3. Influence of the gas flow rate on the average reaction rate. P_{H_2} = 7.8 bar, F_L = 1.0 mL min^{-1}, $C_{S,0}$ = 0.4 mol L^{-1}, T = 298 K...182

Figure 5.4. Effect of the hydrogen partial pressure on the average reaction rate. F_G = 21.0 mL (STP) min^{-1}, F_L = 1.0 mL min^{-1}, $C_{S,0}$ = 0.4 mol L^{-1}. ..186

Figure 5.5. Hydrogen solubility in methanol at different temperatures and partial pressures of hydrogen. 189

Figure 5.6. Influence of the initial reagent concentration on the overall rate of reaction. P_{H_2} = 7.8 bar, F_G = 21.0 mL (STP) min^{-1}, F_L = 1.0 mL min^{-1}....190

Figure 5.7. Influence of the reaction temperature on the overall rate of reaction. F_G = 21.0 mL (STP) min^{-1}, F_L = 1.0 mL min^{-1}, $C_{S,0}$ = 0.4 mol L^{-1}. ..190

Figure 5.8. Influence of temperature on the overall reaction rate (in Arrhenius coordinates). F_G = 21.0 mL (STP) min^{-1}, F_L = 1.0 mL min^{-1}, $C_{S,0}$ = 0.4 mol L^{-1}....191

Figure 5.9. Hydrogen solubility in methanol and partial pressure at different temperatures. 192

Figure 5.10. Fits of the competitive and non-competitive dissociative adsorption of hydrogen models. Experimental data obtained at 298K. Lines give the model prediction at higher hydrogen partial pressures. 211

Figure 5.11. Fits of the competitive and non-competitive dissociative adsorption of hydrogen models. Experimental data obtained at 298K. Lines give the model prediction at higher reagent concentrations.....212

Figure 5.12. Fits of the competitive and non-competitive dissociative adsorption of hydrogen models. Experimental data obtained at 298K. 213

Chapter 6

Figure 6.1. Schematic diagram of transport steps in multi-phase catalytic reactions (Hofmann, 1978). 216

Figure 6.2. Influence of the liquid flow rate on the average rate of reaction. P_{H_2} = 2 bar, F_G = 21.0 mL (STP) min^{-1}, $C_{S,0}$ = 0.2 mol L^{-1}, T = 393K. 222

Figure 6.3. Influence of hydrogen flow rate on the average rate of reaction. P_{H_2} = 2 bar, F_L = 0.5 mL min^{-1}, $C_{S,0}$ = 0.2 mol L^{-1}, T = 393K.....223

Figure 6.4. Influence of the hydrogen partial pressure on the overall reaction rate. F_G =21.0 mL (STP) min^{-1}, F_L = 0.5 mL min^{-1}, $C_{S,0}$ = 0.2 mol L^{-1}, T= 393K. 224

Figure 6.5. Hydrogen solubility in methanol at 393K. 225

Figure 6.6. Influence of the initial concentration of (1-phenylethyl) (3-phenylpropyl) amine on the average rate of reaction. P_{H_2} = 2 bar, F_G = 21.0 mL (STP) min^{-1}, F_L = 0.5 mL min^{-1}, T = 393K. 226

Figure 6.7. Influence of the reaction temperature on the overall rate of reaction. F_G = 21.0 mL (STP) min^{-1}, F_L = 0.5 mL min^{-1}, $C_{S,0}$ = 0.2 mol L^{-1}..227

Figure 6.8. Arrhenius plot for apparent activation energy. 227

Figure 6.9. Hydrogen solubility in methanol and partial pressure at different temperatures. 228

Figure 6.10. Fits of the competitive and non-competitive dissociative adsorption of hydrogen models. Experimental data obtained at 393K. Lines give the model prediction at higher hydrogen partial pressure. 234

Figure 6.11. Fits of the competitive and non-competitive dissociative adsorption of hydrogen models. Experimental data obtained at 393K. Lines give the model prediction at higher reagent concentration. 234

Figure 6.12. Fits of the competitive and non-competitive dissociative adsorption of hydrogen models. Experimental data obtained at 393K. 235

List of Schemes

Chapter 1

Scheme 1.1. Synthesis of ethyl cinnamate. 25
Scheme 1.2. Synthesis of monofluorinated toluene in a microreactor. 26
Scheme 1.3. Synthesis of monochlorinated toluene-2,4-diisocyanate. 27
Scheme 1.4. Examples of hydrogenation reactions. 27
Scheme 1.5. Nitration of 1-methyl-3-propyl-1H-pyrazole-5-carboxylic acid. 28
Scheme 1.6. Synthesis of pyrenebutyric acid ethyl ester. 30
Scheme 1.7. Synthesis of 1-hexane. 31
Scheme 1.8. Suzuki reaction carried out in a borosilicate microreactor. 31
Scheme 1.9. Synthesis of 4-methoxybiphenyl (The Kumana-Corriu reaction). 32
Scheme 1.10. Diazo coupling reaction carried out in a pressure-driven glass microreactor. 32
Scheme 1.11. The benzylation reaction of ethyl 2-oxocyclopentanecarboxylate..33
Scheme 1.12. Mukaiama aldol reaction of benzaldehyde in a "fluorous nano flow" system. 33
Scheme 1.13. Synthesis of an isoxazole and a substituted pyrazole. 34
Scheme 1.14. 1,2-azoles formation. 34
Scheme 1.15. Synthesis of monofluorinated toluene. 35
Scheme 1.16. Synthesis of a pharmaceutically interesting intermediate *via* continuous flow azidation. 37
Scheme 1.17. Selected NK 1-antagonists. 38
Scheme 1.18. Flow synthesis of Tramadol. 39
Scheme 1.19. Model reaction used to demonstrate the Diels-Alder cycloaddition at high temperatures and pressure. 40
Scheme 1.20. Schematic illustrating the oxidation of testosterone. 41
Scheme 1.21. Synthesis of indigo. 42
Scheme 1.22. Synthesis of *N,N'*-dicyclohexylethylenediimine. 42
Scheme 1.23. Synthesis of 4-chloro-*N*-methylbenzamide. 43
Scheme 1.24. Cu-catalysed cycloaddition of benzyl azide and phenylacetylene. .43

Scheme 1.25. Macrocyclization reaction under continuous flow conditions using a copper tube reactor.....44
Scheme 1.26. The Knoevenagel condensation reaction under continuous flow conditions using 30-cm tubing packed with AO-TBD. 44
Scheme 1.27. Synthesis of Vitamin D analogues in microstructured reactors. 45

Chapter 2

Scheme 2.1. Synthesis of secondary and tertiary amines by alkylation.....50
Scheme 2.2. Reduction of *N*-containing functional groups to amines. 50
Scheme 2.3. Reduction of nitrogen containing carbonyl derivatives to amines. ...51
Scheme 2.4. Reductive amination of cyclohexanone.....51
Scheme 2.5. Stoichiometric reduction of imines. 52
Scheme 2.6. Transition-metal reduction of imines. 52
Scheme 2.7. Diversity from secondary amines prepared by reductive amination(Nicolaou *et al.*, 2002).....53
Scheme 2.8. General reductive amination pathway. 53
Scheme 2.9. A self-modulated system with four-stage cyclic pathway proposed by Xing *et al.*(2008).....55
Scheme 2.10. Equilibrium in the synthesis of imines from an aldehyde and an amine(Patil and Adimurthy, 2013). 68
Scheme 2.11. Overall steps in reductive amination of hydrocinnamaldehyde. 68
Scheme 2.12. Imine formation for the model reductive amination reaction of hydrocinnamaldehyde with α-methylbenzylamine. 68
Scheme 2.13. Proposed pathway for the tertiary amine formation. 78

Chapter 3

Scheme 3.1. Deprotection of DHPM benzyl ester. 108
Scheme 3.2. Synthesis of Polyhydroxylated Oxamacrolide. 108
Scheme 3.3. Debenzylation and dehalogenation of 5-(1-benzyl-4-phenylpiperidin-4-yl)-2-chloropyridine.....109
Scheme 3.4. Hydrogenation of (*S*)-2-(1*H*-tetrazol-5-yl)-pyrrolidine-1-carboxylic acid benzyl ester. 109
Scheme 3.5. Deprotection of (1-phenylethyl)(3-phenylpropyl)amine. 110

Chapter 4

Scheme 4.1. General scheme of the synthesis of 1^{o} amines *via* coupling of reductive amination of aldehyde and hydrogenolysis of 2^{o} amine....141

Scheme 4.2. Tandem reductive amination of hydrocinnamaldehyde – hydrogenolysis of (1-phenylethyl)(3-phenylpropyl) amine to 3-phenylpropan-1-amine. 141

Scheme 4.3. Tandem reductive amination of hydrocinnamaldehyde - hydrogenolysis of (1-phenylethyl)(3-phenylpropyl) amine to 3-phenylpropan-1-amine with an (unwanted) deamination reaction to ethylbenzene.....147

Chapter 5

Scheme 5.1. Imine formation from hydrocinnamaldehyde and α-methylbenzylamine. 171

Scheme 5.2. Hydrogenation of an imine.....172

Chapter 6

Scheme 6.1. Deprotection of (1-phenylethyl)(3-phenylpropyl)amine.....226

List of Tables

Chapter 2

Table 2.1. Influence of temperature on the selectivity of the reductive amination of hydrocinnamaldehyde at higher temperatures. 77

Table 2.2. Formation of selected secondary amines[a] by reductive amination of aldehydes in the packed-bed multichannel reactor over a Pd/C catalyst.....84

Table 2.3. Formation of selected secondary amines by reductive amination of ketones in the packed-bed multichannel reactor over a Pd/C catalyst.....87

Table 2.4. The influence of the hydrogen split injection on reactor efficiency. P_T = 8 bar, F_G = 21.0 mL(STP)min^{-1}, F_L = 2.0 mL min^{-1}, $C_{0,S}$ = 0.4 mol L^{-1}, T=298K. 89

Table 2.5. Formation of selected secondary amines[a] by reductive amination of aldehyde in the X-Cube™ flow reactor over a Pd/C catalyst. 100

Table 2.6. Formation of selected secondary amines by reductive amination of ketones in the X-Cube™ flow reactor over a Pd/C catalyst. 103

Table 2.7. Comparison of the optimal reaction conditions for both reactors at 298 K. 105

Table 2.8. Comparison of the optimal reaction conditions for both reactors at higher temperatures. 105

Chapter 3

Table 3.1.Porous structure characterisation data (by nitrogen adsorption at 77K) for synthetic carbons and the synthesised Pd/C catalyst. 115

Table 3.2. Deprotection of 1-phenylethyl group over Pd/C for different reactors. 116

Table 3.3. The influence of the hydrogen split injection on reactor efficiency. P_T = 8 bar, F_G = 21.0 mL(STP) min^{-1}, F_L = 0.5 mL min^{-1}, $^{a}C_{0,S}$ = 0.2 mol L^{-1}, $^{b}C_{0,S}$ = 0.4 mol L^{-1}, T = 393K. 128

Table 3.4. Comparison of the reaction conditions for both reactors. 138

Chapter 4

Table 4.1. Influence of the second reactor temperature on the tandem reductive amination-hydrogenolysis process. 151

Table 4.2. Primary amines synthesised by tandem reductive amination of aldehydes-hydrogenolysis of secondary amines in the packed-bed multichannel reactor over Pd/C catalyst.....156

Table 4.3. Primary amines synthesised by tandem reductive amination of ketones - hydrogenolysis of secondary amines in the packed-bed multichannel reactor over Pd/C catalyst.....158

Table 4.4. Primary amines[a] synthesised *via* tandem: reductive amination of aldehydes - hydrogenolysis of secondary amines in the X-Cube™ flow reactor over a Pd/C catalyst. 165

Table 4.5. Comparison of the reaction conditions for the tandem process. 167

Chapter 5

Table 5.1. Various models for Reductive Amination of hydrocinnamaldehyde with α-methylbenzylamine over 10% Pd/C catalyst.....209

Table 5.2. Kinetic and adsorption parameters for reductive amination at 298K. 210

Table 5.3. Kinetic and adsorption parameters for reductive amination at 323K. 210

Table 5.4. Kinetic and adsorption parameters for reductive amination at 298K. 213

Table 5.5. Kinetic and adsorption parameters for reductive amination at 323K. 213

Table 5.6. Kinetic and adsorption parameters for reductive amination at 298 and 323K. 214

Chapter 6

Table 6.1. Various models for the hydrogenolysis of secondary (1-phenylethyl)(3-phenylpropyl)amine over 10% Pd/C catalyst at 393K. 232
Table 6.2. Kinetic and adsorption parameters for hydrogenolysis of (1-phenylethyl)(3-phenylpropyl)amine at 393K. 233
Table 6.3. Kinetic and adsorption parameters for reductive amination at 393K. 235
Table 6.4. Kinetic and adsorption parameters for hydrogenolysis reaction at 393K. 236

Chapter 7

Table 7.1. Optimal reaction conditions for the tandem reductive amination-hydrogenolysis reaction for both reactors. 239
Table 7.2. Optimal reaction conditions for reaductive amination of aldehydes reaction for both reactors at 298 K. 240
Table 7.3. Optimal reaction conditions for reaductive amination of aldehydes reaction for both reactors at higher temperature. 241
Table 7.4. Optimal reaction conditions for the hydrogenolysis reaction for both reactors. 242
Table 7.5. Kinetic and adsorption parameters for reductive amination at 298 and 323K. 243
Table 7.6. Kinetic and adsorption parameters for hydrogenolysis reaction at 393K. 244

Abbreviations

AC	Activated Carbon
AHPCS	Allylhydridopolycarosilane
API	Active Pharmaceutical Intermediate
ATR	Attenuated Total Reflectance
BJH	Barrett-Joyner-Halenda
Bn	Benzyl
Bz	Benzoyl
BPR	Back Pressure Regulator
CatCart	Catalyst Cartridge
Cbz	Benzyloxycarbonyl
CFD	Computatotional Fluid Dynamics
DAST	Diethylaminosulfur trifluoride
DCE	1,2-dichloroethane
DCM	Dichloromethane
DIPEA	N,N-diisopropylethylamine
DMSO	Dimethyl sulfoxide
DPT	Differential Pressure Transducer
DRA	Direct Reductive Amination
EtOH	Ethanol
FEP	Fluorinated Ethylene Propylene
GS	Gas Chromatography
IR	Infrared

Me	Methyl
MeOH	Methanol
NMR	Nuclear Magnetic Resonance
PBR	Packed-bed Reactor
PCTFE	Polychlorotrifluoroethylene
PCV	Pressure Control Valve
PDMS	Polydimethylsiloxane
PEEK	Polyether Ether Ketone
PET	Positron Emission Tomography
Ph	Phenyl
PMMA	Polymethylmethacrylate
PPDA	*p*-phenylenediamine
PPS	Polyphenylsulfide
PTFE	Polytetrafluoroethylene
PVC	Polyvinyl Chloride
PVSZ	Polyvinylsilizane
RIE	Reactive Ion Etching
SPECT	Single-Photon Emission Computed Tomography
TBAB	Tetrabutylammonium bromide
TFFA	Trifluoroacetic Anhydride
THF	Tetrahydrofuran
TOF	Turn Over Frequency
UV	Ultraviolet

Nomenclature

A	Channel cross-section area (m^2)
A, B, C	*Antoine* coefficients (-)
a_s	External specific area of pellet ($m^2\ kg_{cat}^{-1}$)
$a_{G/L}$	gas-liquid interfacial area / volume of bed ($m^2\ m^{-3}$)
C_{AS}	Reactant concentration at the particle surface (mol m^{-3})
C_{2^o}	Concentration of the product (2º amine) in the outlet of the reactor (mol L^{-1})
$C_{2^o \text{amine},b}$	(1-phenylethyl)(3-phenylpropyl)amine concentration in the bulk liquid (mol m^{-3})
$C_{2^o \text{amine},s}$	(1-phenylethyl)(3-phenylpropyl)amine concentration at the solid-liquid interface (mol m^{-3})
$C_{H_2,b}$	Hydrogen concentration in the bulk liquid (mol m^{-3})
$C_{H_2,i}$	Hydrogen interfacial concentration (mol m^{-3})
$C_{H_2,s}$	Hydrogen concentration at the solid-liquid interface (mol m^{-3})
$C_{\text{imine},b}$	*(E)*-(1-phenylethyl)(3-phenylpropylidene)amine concentration in the bulk liquid (mol m^{-3})
$C_{\text{imine},s}$	*(E)*-(1-phenylethyl)(3-phenylpropylidene)amine concentration at the solid-liquid interface (mol m^{-3})
C_p	Product concentration (mol L^{-1})
D_{AB}	Binary diffusion coefficient of A in B ($cm^2\ s^{-1}$)
D_e	Effective diffusivity ($cm^2\ min^{-1}$)
d_p	Diameter of pellet (m)
E_a	Apparent activation energy (kJ mol^{-1})

e_g	bed porosity (-)
F_G	Volumetric gas flow rate (mL min^{-1})
F_L	Volumetric liquid flow rate (mL min^{-1})
F_G	Volumetric gas flow rate (mL min^{-1})
H	Henry's constant of hydrogen in the reaction mixture (bar)
k	Specific reaction constant / m^3 of liquid (mol^{-1} $kg_{cat}^{-1}s^{-1}$)
k_c	Mass transfer coefficient (m s^{-1})
k_{G/H_2}	Gas phase mass transfer coefficient (m s^{-1})
$k_{L,G}$	Gas-liquid mass transfer coefficient (m s^{-1})
$k_{L/S}$	Liquid-solid mass transfer coefficient (m s^{-1})
m_{cat}	Mass of catalyst in an individual channel (kg)
m_{Pd}	Mass of metallic palladium on the catalyst (g)
M_B	Molecular weight of solvent B (g mol^{-1})
$M_{w,Pd}$	Atomic weight of palladium (kg mol^{-1} or g mol^{-1})
p_{MeOH}^{sat}	Vapour pressure (bar)
P_{H_2}	Partial pressure of hydrogen (bar)
P_T	Total pressure (bar)
Re_L	Reynolds number of the liquid phase (-)
Re_G	Reynolds number of the gas phase (-)
(R_A)	Rate of product formation (mol kg_{cat}^{-1} s^{-1})
$(-r_A)$	Overall reaction rate (mol kg_{cat}^{-1} s^{-1})
$(-r_{AS})$	Surface reaction rate (mol m^{-3} s^{-1})
$-r_A^{'}(obs)$	Observed reaction rate per volume of the catalyst (mol kg_{cat}^{-1} s^{-1})
R	Catalyst particle radius (cm)

Sh	Sherwood number (-)
T	Temperature (K)
U	Free-stream velocity (m s^{-1})
x_{H_2}	mole fraction of the hydrogen in the liquid phase (-)

Greek symbols

η	Effectiveness factor (-)
ρ_L	Fluid density (kg m^{-3})
U	Free-stream velocity (m s^{-1})
μ_L	Liquid viscosity (Pa · s)
ρ_G	Gas density (kg m^{-3})
μ_G	Gas viscosity (Pa · s)
ρ_c	Density of catalyst pellet (kg m^{-3})
$\tilde{\tau}$	Tortuosity (-)
ϕ_p	Pellet porosity (-)
σ_c	Constriction factor (-)
χ	Association factor of solvent (-)
μ	Viscosity of solvent (cP)
υ_A	Molar volume of A (cm^3 mol^{-1})

Research Scope

The main objective of this thesis is to evaluate the synthesis of primary amines under continuous flow conditions using the structured multichannel compact reactor developed at University of Bath and the commercially available X-Cube^{TM} flow reactor (ThalesNano, Hungary) for the manufacture of speciality chemicals which lead to the production of APIs in the presence of a suitable catalyst. The structured multichannel reactor is part of a continuous catalytic rig which was constructed at an early stage of the project. Amines are very important industrial organic compounds which are widely used as fine chemicals and pharmaceutical intermediates. Secondary amines were synthesised *via* reductive amination of aldehydes and then they were hydrogenolysed to primary amines. These were used as model reactions to assess the continuous-flow process in both reactors. Detailed kinetics and process optimisation studies of each reaction, as well as the tandem process, were investigated. The performance of the structured multichannel compact reactor developed at the University of Bath was compared with the commercially available X-Cube^{TM} flow reactor available from ThalesNano. The effects of operating parameters on the reactors' performance were investigated. The structured multichannel compact reactor was also used for studying reaction kinetics.

Thesis Structure

The thesis is divided into seven Chapters.

Chapter 1 reviews the state of the art in microtechnology and flow chemistry and focuses on commercially available microreactors. This chapter also includes the motivation for moving from batch to continuous flow processing in the fine chemicals and pharmaceutical industries.

Chapter 2 describes the application of the compact packed-bed reactor and the commercially available X-Cube^{TM} flow reactor for a continuous reductive amination of aldehydes. The catalytic liquid-phase hydrogenation of

hydrocinnamaldehyde to (1-phenylethyl)(3-phenylpropyl)amine was chosen as the model reaction. The performance of the structured multichannel compact reactor and the X-Cube™ flow reactor for the continuous hydrogenation of an intermediate imine is investigated and a comparison is made between the experimental results from both reactors. The optimisation of flow conditions is systematically investigated by varying concentration, gas and liquid flow rates, pressure and temperatures. A variety of secondary amines, which are either commercially unavailable or very expensive compounds to purchase, were synthesised for use in further studies, with excellent conversion and isolated yield.

In Chapter 3 the hydrogenolysis of secondary amine synthesised via reductive amination of hydrocinnamaldehyde with α-methylbenzylamine (see Chapter 2) is investigated. The hydrogenolysis of (1-phenylethyl)(3-phenylpropyl)amine to 3-phenylpropan-1-amine over Pd/C catalyst is studied as a model reaction. Performance of the structured compact reactor in terms of calculated product yield, selectivity and average rate of product formation for continuous deprotection is evaluated and compared with the data obtained using the X-Cube™ flow reactor, commercially available from ThalesNano. The effect of reaction parameters, *i.e.* gas/liquid flow rates, concentration, staged injection of hydrogen; pressure and temperature are studied in detail.

In Chapter 4 the tandem reductive amination of aldehydes-deprotection of secondary amines is presented and the performance of the structured compact reactor and the X-Cube™ flow reactor is investigated and compared. A variety of primary amines were synthesised with very good conversion, selectivity and isolated yield.

Chapter 5 presents studies on the chemical kinetics of reductive amination of aldehydes for the model reaction, *i.e.* reductive amination of hydrocinnamaldehyde with α-methylbenzylamine in the structured multichannel compact reactor. In a set of experiments, appropriate experimental conditions are established to achieve a better understanding of the effect of the key variables. The work aims at identifying the main factors that influence the reaction, *i.e.* liquid and gas flow rates, hydrogen partial pressures, temperatures and reactant concentrations.

A possible reaction mechanism is proposed and the rate equations that describe the reactions involved in the process are developed and used to obtain the necessary kinetic parameters. The equations are then used to fit experimental data obtained using Matlab software. The experimental conditions tested were chosen so that the effect of all the main influencing parameters could be investigated and the validity of the assumptions made tested.

Chapter 6 reports the chemical kinetics studies for the deprotection of secondary amines for the model reaction, *i.e.* deprotection of (1-phenylethyl)(3-phenylpropyl) amine in the structured multichannel compact reactor. The chapter describes experiments that were performed with a palladium catalyst supported on activated carbon, leading to a better understanding of the effect of the key variables on the process. The work aims at identifying the main factors that influence the reaction *i.e.* liquid and gas flow rates, hydrogen partial pressures, temperatures and reactant concentrations. A possible reaction mechanism is proposed and the rate equations that describe the reactions involved in the process are developed and used to obtain the necessary kinetic parameters. The equations are used to fit experimental data obtained using Matlab software. The experimental conditions tested were chosen so that the effect of all the main influencing parameters could be investigated and the validity of the assumptions made tested.

Note that, for technical reasons, in Chapters 2, 3 and 4 all pressure data is presented as the total pressure (P_T) whereas in Chapters 5 and 6 (kinetic studies) the calculated partial pressure of hydrogen (P_{H_2}) is used.

Chapter 7 presents the final conclusions of the work and provides suggestions/ recommendations for further work.

Chapter 1

Literature Review

1.1. Introduction

The development of flow chemistry for the manufacturing of speciality chemicals and pharmaceuticals has been advanced by the development of microtechnology, *i.e.* microdevices. The applications of microtechnology have developed very rapidly in many areas, and in recent years the use of microstructured devices for chemical processes has shown very impressive results. A patent containing all the essential features for how a microstructured system for chemistry should be built was lodged in 1986 from the former East Germany. Although this patent showed the path to the production of microstructured reactors, its principles could not be implemented due to the prevailing economic circumstances in East Germany at that time. The first micro-heat exchanger was subsequently built in Germany in 1989 (at the Forschungszentrum Karlsruhe) (Schubert *et al.* 1989) and similar work was started in 1993 at the Pacific Northwest National Laboratory (PNNL, USA), focusing on the energy sector (Jähnisch *et al.* 2004; Gavriilidis *et al.* 2002; Ehrfeld *et al.* 2000; Hessel *et al.* 2004; Jensen 2001; Fichtner *et al.;* Mello and Wootton 2002).

Initially microtechnology was adopted mainly by process engineers rather than by chemists, probably because it took several years for its potential to be demonstrated. Many of the well-known chemical syntheses, *i.e.* Wittig, Knoevenagel, Ugi, Michael-addition, Suzuki-coupling (Fletcher *et al.* 2002), Aldol (Wiles *et al.* 2001), Hantzsch (Garcia-Egido *et al.* 2002) Diels–Alder (Fernandez-Suarez *et al.* 2002), Azo-coupling (Wootton *et al.* 2002) and Enamin reactions (Sands *et al.* 2001) have since been performed with the use of microreactors. In most cases, the results obtained using microstructured reactors were better than for their macrostructured counterparts. The following examples of chemical reactions, such as fluorination (Chambers and Spink 1999; Chambers *et al.* 2001; Jähnisch *et al.* 2000), chlorination, nitration (Burns and Ramshaw 1999), hydrogenation (Wie and Honicke 1996; Wießmeier and Hönicke 1996), and oxidation (Veser 2001; Kestenbaum *et al.* 2002; Kestenbaum *et al.* 2000) have all been described in literature. Many well-known types of chemical reactions, such as additions (Kestenbaum *et al.* 2000; Kestenbaum *et al.* 2002; Wiles *et al.* 2002),

eliminations (Rouge *et al.* 2001), nucleophilic substitutions on aliphatics, electrophilic substitutions on aromatics (Jähnisch *et al.* 2000), cycloadditions (Fernandez-Suarez *et al.* 2002) are included in a broad spectrum of chemical transformations.

It should be pointed out that the increase in automation and a wide variety of new synthetic methods are revolutionizing the synthesis of complex molecules related to the fine and pharmaceutical industries. In a classical synthesis methodology, the synthesis of a pharmaceutically active compound often requires at least ten intermediate steps. This type of synthesis, therefore, requires patience and a profound knowledge of reaction mechanisms. It also produces lots of by-products as waste (although some of these may be useful), which reduces the efficiency of the process and the final amount of the desired product. Each stage is also extremely time-consuming, involving preparation, work-up and purifications. This type of synthesis clearly shows, therefore, the limitations of current chemical transformations and a major challenge for synthetic chemists is to develop faster and more efficient clean synthesis procedures, especially related to the fine and pharmaceutical industries (Kündig 2007; Anastas and Kirchhoff 2002).

Microtechnology allows chemical reactions to be carried out in much less time (milliseconds in some cases) due to effective mixing, which also helps to improve the yield of the desired products. Another advantage of microtechnology is the better control over reaction parameters. Due to these advantages, the potential applications of microreactors have been widely recognised in the chemical and pharmaceutical industry in recent years. Nowadays, some commercial suppliers are offering microstructured devices for entire chemical process plants (Wootton *et al.* 2002; Bökenkamp *et al.* 1998) and many research institutes and universities are working with industry to explore the potential of microtechnology for the development of clean and sustainable chemical processes.

Gas-liquid reactions involving solid catalysts play a crucial role in many industries. In the pharmaceutical industry, for example, hydrogenation reactions are carried out on a large scale, mostly in batch reactors. Indeed, nearly 20% of all reaction steps in a typical fine chemical synthesis are catalytic hydrogenation. In this case, the use of microreactor geometry in the pharmaceutical industry would greatly benefit the miniaturization of the chemical process. The main purpose of such miniaturization is to achieve clean and efficient on-site, on-demand, and on-time distributed production of chemicals (McGovern *et al.* 2008; Ehrfeld *et al.* 2000; Jensen 2001; Jensen 1998; Al-Dahhan *et al.* 1997; Gavriilidis *et al.* 2002; Wörz *et al.* 2001b; Mills and Chaudhari 1997).

1.2. Flow chemistry

Continuous flow chemistry is a rapidly growing research area which offers the opportunity to change the way synthetic chemistry is performed both in research and in industry. In synthetic chemistry, for example, it is very important to discover, develop and perform organic transformations quickly. In research laboratories, microwave chemistry, as well as combinatorial applications, are widely used, but when it comes to the scaling-up of the process, round-bottom flasks are used instead. Flow chemistry is an attractive method to drive down the time required to put compounds into production because the reaction methodology can be rapidly obtained, thereby giving high-quality chemical information about the compound of interest. Flow chemistry offers a number of other advantages, such as reducing exposure to hazardous chemicals, increasing the atom efficiency as well as allowing in-line control over the process by integration of the analytical tools with the microreactor system. Reactions can be performed safely above the boiling point of the organic solvents with very precise control of chemical reactivity and reaction conditions. Microreaction technology, therefore, allows the chemist to perform organic transformation with higher selectivity, yield and purity in comparison to traditional batch systems, as has been observed by many researchers (Wiles and Watts 2011, 2012; McQuade and Seeberger 2013).

While continuous flow chemistry is now successfully serving the bulk and petrochemical industry, over the last two decades, there has also been increased interest in using continuous systems to perform reactions related to the synthesis of fine chemicals (Jas and Kirschning 2003; Kobayashi *et al.* 2006). Reactions which have traditionally been performed in a batch mode have been demonstrated in the flow-mode, *i.e.* hydrogenation reactions, C-C couplings, inorganic syntheses and synthesis of pharmaceutical intermediates (Takasuga *et al.* 2006; Liu *et al.* 2004; Baumann *et al.* 2008; LaPorte and Wang 2007; Kirschning *et al.* 2006).

Previously published examples on the use of continuous processes in the pharmaceutical sector include simple devices that exploit sequences of static mixers, residence time flow tubes and simple inefficient heat exchangers. It is likely that the more interesting applications have not been disclosed (Takasuga *et al.* 2006; LaPorte and Wang 2007). Continuous flow systems have several advantages in comparison with batch processes based on the characteristic features of micro spaces (Mason *et al.* 2007; Marre *et al.* 2010; Hessel 2009; Anastas and Kirchhoff 2002; Kaupp 2006; Schwalbe *et al.* 2004; Löwe *et al.* 2006; Renken *et al.* 2007; Yoshida *et al.* 2013).

These days, apart from the fact that the reaction conditions must be controlled precisely and must be performed in a safe manner, pharmaceutical industries keep changing the restrictions on the amount of waste that can be generated during the production process in order to decrease the volume of waste generated and move towards production on-demand (Tucker 2006; Jiménez-González *et al.* 2011; Leahy *et al.* 2013; Bryan *et al.* 2013). For example, for each kilogram of the product prepared, pharmaceutical companies generate *ca.* 25 kg of wastewater. Companies must improve their processes in order to generate less waste and reduce the negative impact on the environment (Lerou *et al.* 2010).

In the literature, the advantages of continuous flow processes in chemicals and pharmaceuticals manufactures over the traditional batch systems have been very well documented in terms of cost, quality and safety. Continuous flow reactors offer a number of benefits including lower plant and production costs as well as improved quality and safety of the process and faster and cheaper scale-up (Roberge *et al.* 2005;

Malhotra 2005; Stitt 2002; Calabrese and Pissavini 2011; Wiles and Watts 2014; Roberge *et al.* 2008; Plumb 2005; Schaber *et al.* 2011; Elvira *et al.* 2013; Poechlauer *et al.* 2013). Specifically, Kolehmainen *et al.* (2009) compared the synthesis of peracetic acid using a traditional batch reactor and microreactors and concluded that the continuous flow processes reduce operating costs, increase the safety of the synthesis and also gives the opportunity to generate potentially hazardous and explosive chemicals at the site of use, which will contribute to lower operating costs and fewer potential transportation risks. Another example of on-site synthesis was demonstrated by Jensen and Schmidt (2001), who reported the synthesis of phosgene using a silicon microreactor.

1.2.1. Microreactors

Microreactors are described as a miniaturized reaction system. They are made using, at least partially, microtechnology and precision engineering. The dimensions of the reaction channels inside the microreactor are in the sub-milimeter and sub-micrometer range. Very often, the terms nanoreactors or milli-/minireactors are used for these devices because of their dimensional range (Ehrfeld *et al.* 2000). Many advantages of microreactors have become apparent in the last decade. Since they are smaller, microreactors need less space, materials and energy and often have shorter response times. Accordingly, it is possible to return more results in a shorter time. It is also possible to integrate them into parallel systems, which allows an increased rate of production at relatively low costs. They have already found the way into organic synthesis, because they offer various advantages over traditional chemistry, which is performed in flask or vessels (Singh *et al.* 2005; Yoshida *et al.* 2008; Yoshida 2008; Wirth 2008; Brandt and Wirth 2009).

1.2.2. Types of microreactors

In recent years, a variety of microdevices has been developed for gas - liquid, liquid - liquid or gas - liquid - solid systems, with most of these now widely available. The use of microreactors is affected by many factors, for example: the construction material and the means by which the reactants and solvents are delivered to the system (Ehrfeld *et al.* 2000; Wirth 2008, 2013). Microreactors can be fabricated from a wide range of materials *i.e.* glass (Hibara *et al.* 2001), quartz (Beato *et al.* 2008), diamond (Adamschik *et al.* 2001), polymethylmethacrylate (PMMA) (Becker and Gärtner 2001), polydimethylsiloxane (PDMS) (McCreedy 2001; Schudel *et al.* 2009), polyimide (Min *et al.* 2010), allylhydridopolycarbosilane (AHPCS) or polyvinylsilazane (PVSZ) (Yoon *et al.* 2008), ceramic (Ueno *et al.* 2003a), silicon (Leonel *et al.* 2007), stainless steel (Santamaría *et al.* 2007), nickel (Jensen *et al.* 2005), and Hastelloy (Okafor *et al.* 2010). Microreactors must be chemically inert to the reactants/products and solvents (Manz *et al.* 1991; Hartman and Jensen 2009). It is also important to consider the operating conditions that will be used when choosing the appropriate reactor material (Tiggelaar *et al.* 2007; Trachsel *et al.* 2008).

Glass is a very popular material from the synthetic chemist's point of view, both for its transparency, which allows visual control of a reaction, and for the fact that it is inert to the majority of organic solvents and reagents (Watts and Haswell 2005; McCreedy 2000, 2001; Watts *et al.* 2001; Fletcher *et al.* 1999). Pyrex®, Borofloat®, and Foturan® can be used as a glass substrate to fabricate microreactors using photolithography and wet etching (Rodriguez *et al.* 2003) or powder blasting (Oosterbroek *et al.* 2006). Glass microreactors have been widely used by researchers but they do have some limitations: the use of hydrofluoric acid can lead to channel etching, changing the reactor's dimensions, so this cannot be used as a reagent or a by-product (Fletcher *et al.* 2002) Africa is one of the devices that can be equipped with glass reactors, and is commercially available from Syris Company.

Silicon is another material which is of great interest in the construction of microreactors: it is chemically inert and its oxidation behaviour is also similar to glass. Silicon-based microreactors can be fabricated using either wet or dry techniques, depending on the requirements (Jensen 2006). Reactive ion etching (RIE) is an example of a dry technique which is used for more complex features, eg. high aspect ratio channels or mixing elements. During the development of silicon microreactors all features can be fusion bonded to a second silicon layer, or anodically bonded to a glass plate. A thermal oxide layer is also grown on the microchannels to increase the chemical stability of the device (Murphy *et al.* 2007). This type of microdevice can be used for exothermic reactions as well as reactions that require very high or low temperatures due to the excellent thermal conductivity of silicon (Jensen 2001; Lu *et al.* 2001; Geyer *et al.* 2006).

Microreactors can also be made based on polymers such as polymethylmethacrylate (PMMA) (Becker and Gärtner 2001), polydimethylsiloxane (PDMS) (McCreedy 2001; Schudel *et al.* 2009), polyimide (Min *et al.* 2010) or polyvinylsilazane (PVSZ) (Yoon *et al.* 2008). Polymer-based microreactors can be fabricated using a number of techniques *i.e.* hot embossing (Alonso-Amigo 2000), injection moulding (Lee *et al.* 2005; Attia *et al.* 2009), casting (Zhou and Chan-Park 2005) as well as gas-entrained polymer extrusion (Hallmark *et al.* 2005; Hornung *et al.* 2007) depending on the selected material. PDMS microreactors have limited mechanical stability, low thermal conductivity and no resistance against many organic solvents but they are widely used for aqueous chemistries performed at atmospheric pressure (Lee *et al.* 2003; Duan *et al.* 2006; Geyer *et al.* 2006). Polytetrafluoroethylene (PTFE) and PVSZ microreactors have much better heat and chemical resistance in comparison to PDMS (Wiles and Watts 2011).

The most popular material for the construction of microreactor is stainless steel, although the dimensions are generally larger than those made of glass or silicon (Wirth 2008; Ehrfeld *et al.* 2000). One example of this is the microreactor designed by Ehrfeld Mikrotechnik which is a part of commercially available system, which includes the Cytos Lab system, with an internal volume of 1.0 and 1.1 mL. The Institut für Mikrotechnik Mainz (IMM) offers a wide range of micromixers,

heat exchangers, as well as reactors for multi-phase reactions. Stainless steel is the material selected for process chemistry (Geyer *et al.* 2006; Hartman and Jensen 2009).

Microreactors can be also fabricated from ceramics using a 3D mould or a low-pressure injection moulding process. These devices can be used for high temperature processes (Knitter *et al.* 2001; Müller *et al.* 2005; Jain *et al.* 2009).

Once a suitable material has been identified and the reactor has been fabricated, the next step is to choose the appropriate connection for delivering the reagents into the reaction channel. Gas and/or liquid feed lines can be connected to the reactor using a variety of techniques such as commercially available Swagelok® connectors (Unnikrishnan *et al.* 2009), soldering (Murphy *et al.* 2007), adhesive ports (Fredrickson and Fan 2004; Shintani *et al.* 2004) and gluing using epoxy resins (Ashish and Mayuresh 2003).

Today, a variety of microreactors as well as flow reactor platforms are commercially available. The flow reactor platforms can be used for fast reaction optimisation in research laboratories in a relatively short time. They also allow small-scale production of material. A few examples of the commercially available flow platforms are presented below since they are of great interest to researchers who are more concerned with the chemistry than the design and fabrication of a device (Wiles and Watts 2011).

ThalesNano Nanotechnology Inc. has a variety of flow reactors (Figure 1.1) including, the X-Cube™ for heterogeneous catalysis (dual cartridge system, 473K and 150 bar), the H-Cube® continuous flow hydrogenator (373K, 100 bar), the H-Cube Pro™ (423K, 100 bar), the H-Cube Mini™ (373K, 100 bar) and the H-Cube Midi™, designed for process scale flow hydrogenation (423K, 100 bar). In addition, the Phoenix Flow Reactor™ multifunctional platform is compatible with H-Cube Pro™, H-Cube Midi™ and X-Cube™ for heterogeneous or homogeneous catalysis (723K, 100 bar) and the Ice Cube™ Flow Reactor (203 - 353K, 6 bar) can be used for exothermic reactions.

a)

b)

c)

Figure 1.1. ThalesNano Inc. flow reactor systems: a) H-Cube®, b) X-Cube™, c) H-Cube Pro™ (www.thalesnano.com).

Uniqsis UK offers the FlowSyn system, which is an integrated continuous flow reactor operating in the temperature range from 233K up to 533K. Reactions can be optimized using a glass mesoreactor. This reactor allows the production of chemicals using a series of tubular reactors which can be fabricated from a variety of compatible materials such as PEEK and PTFE, PTFE, PTFE and stainless steel or PTFE and Hastelloy®. Figure 1.2 presents examples of the FlowSyn systems.

a) **b)**

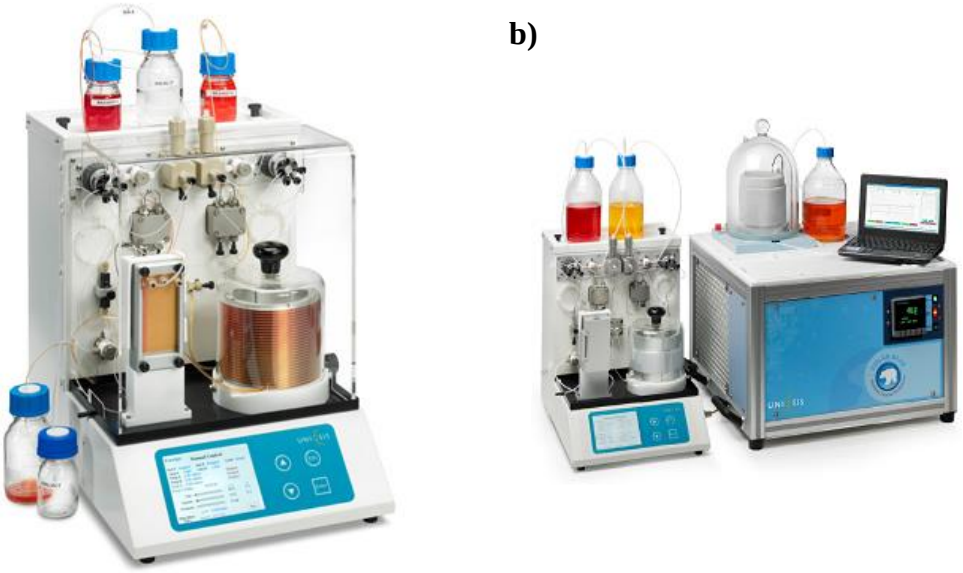

Figure 1.2. a) FlowSyn reactor system and b) FlowSyn Polar Bear™ reactor system (www.uniqsis.com).

Accedo Corporation (USA) has developed the Conjure™ system with online LC - MS reaction monitoring (www.accendocorporation.com). The reactor can be operated in the temperature range from 253K up to 573K and pressures of 150 bar. The system is based on a segmented flow and the on-line analysis, with a maximum injection frequency of 5 minutes, allows precise reaction monitoring and rapid identification of the materials/ products. Accedo Corporation has also developed the Propel™ flow reactor which can be used for reaction screening, optimisation and scale-up. This system allows the programming of up to nine experiments and is capable of performing syntheses over 100 grams.

The NanoTek® microfluidic synthesis system (Figure 1.3), developed by Advion Biosciences Inc. (USA), is a suitable tool for the synthesis of positron emission tomography (PET) and single-photon emission computed tomography (SPECT) compounds. The initial reaction conditions can be optimised within 1 - 2 minutes using μg of reagents.

Figure 1.3. The NanoTek microfluidic synthesis system from Advion, USA (www. advison.com).

Chemtrix BV (The Netherlands) has developed systems for continuous processing from laboratory to industrial production scale. The Labtrix®-S1 system (Figure 1.4) can be operated in a temperature range from 253K up to 468K and can be pressurized up to 25 bar. This system is a fully automated platform for laboratory-based optimisation of reactions. The company offers a variety of materials from which the parts of the system can be made, for example PEEK, which has excellent chemical resistance to most organic solvents, PPS and perfluoroelastomer which have excellent chemical resistance to hydrochloric acid, trifluoroacetic acid, nitrobenzene, sulphuric acid, acetic acid and butyl lithium, as well as ETFE and perfluoroelastomer which have excellent resistance when corrosive and hazardous reagents like nitric acid, sulphuric acid and sodium hypochlorite are used. The Labtrix®-S1 system can produce mg of product. The company also offers KiloFlow® and Plantrix® systems which allow kg-scale and tonne-scale production.

Figure 1.4. The Labtrix®-S1 system from Chemtrix BV, The Netherlands (www.chemtrix.com).

Vapourtec Ltd., UK, offers the R - Series modular system (Figure 1.5). The system is very flexible and can be operated in the temperature range from 203K to 523K and up to 50 bar of pressure, depending on the reactor used. The company offers a standard PFA coiled tube reactor, stainless steel or Hastelloy® coils and Omnifit glass columns. The system can be connected to the Flow Commander™ software, fractional collector, autosampler or additional pump channels. The company also offers the E - Series system which can be equipped with a range of reactors available for the R - Series as well as a photochemical reactor suitable for both the E - Series and R - Series.

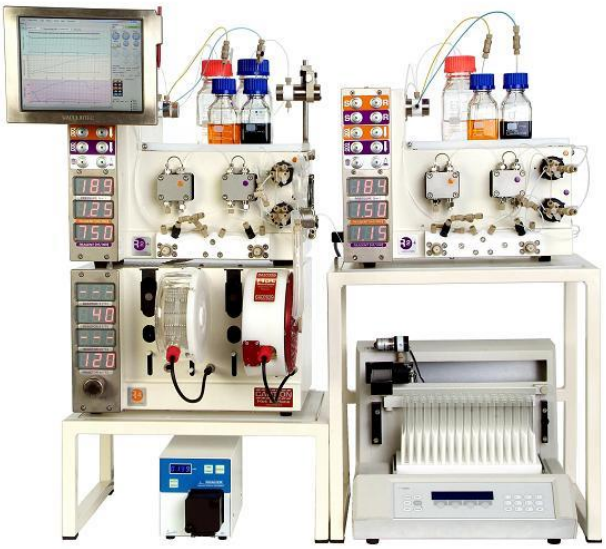

Figure 1.5. Vapourtec R-series, a flexible tubular flow reactor system from Vapourtec Ltd.,UK (www.vapourtec.co.uk).

FutureChemistry (Nijmegen, The Netherlands) offers the FlowStart system (Figure 1.6), which has an operating temperature range of 273 – 363K. This system contains glass microreactors which can produce mg - g quantities of material per day. The company offers a variety of complete systems such as FlowStartEvo and FlowExpertBasic, as well as a variety of modules which can be combined with each system, for example a gas module or photochemistry set. A range of microreactors compatible with FlowExpert, FlowStart and FlowStartEvo systems are also available.

Figure 1.6. Glass-based flow reactor platform FlowStart from FutureChemistry BV, The Netherlands (www.futurechemistry.com).

Syrris Ltd. (Royston, UK) offers the Asia and Africa (Figure 1.7) microreactor flow systems. The company offers a variety of materials from which the parts of the system can be made, such as glass and PTFE/ fluoropolymer, PCTFE as well as stainless steel and Hastelloy. The systems can be used across a wide range of temperatures, from 258K to 523K, allowing fast optimisation of the reaction conditions and compound synthesis from micrograms to kilograms.

Figure 1.7. Glass-based flow reactor platform Africa from Syrris Ltd., UK (www.syrris.com).

In addition to these commercially available microreactors and microreactor-based systems, some companies are also able to design and fabricate customized devices, for example Corning S.A.S located in France. Corning Advanced - Flow™ reactors (Figure 1.8) can be easily transferred from the laboratory scale to process development and industrial - scale production (Figure 1.9). The company also offers technology for photochemical systems through the G1 photo reactor.

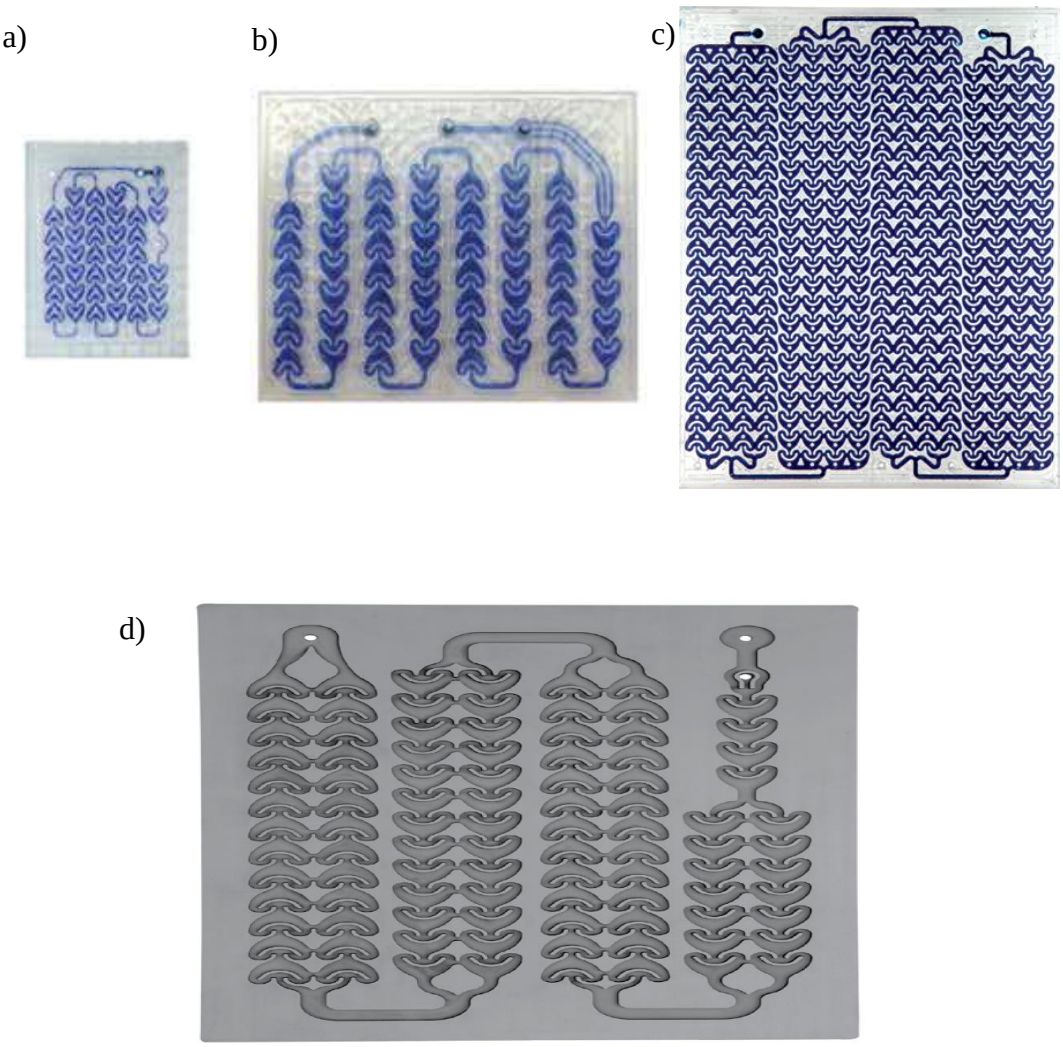

Figure 1.8. Corning® Advanced - Flow™ Reactors: a) low - flow reactor, b) G1 standard evaluation reactor, c) G3 glass reactor, d) G4 ceramic reactor (www.corning.com)

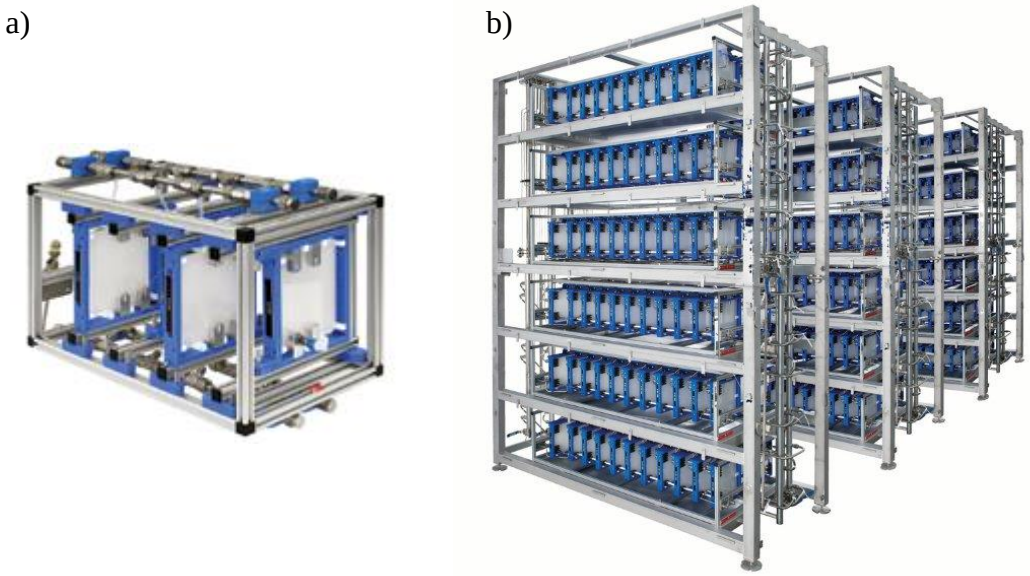

Figure 1.9. Corning® Advanced - Flow™ Reactors: a) reactor modules, b) pilot - scale production (www.corning.com).

1.2.3. Properties of microreactors

The main feature of microreactors is their high surface-to-volume ratio, which can result in rapid mixing of reagents, uniform reaction conditions due to precise temperature control, as well as rate enhancements because of short diffusion distances. Generally, but not exclusively, they have a three-dimensional structure. The inner dimensions are between 10 and 100 micrometres while the specific surface area is between 10 000 and 50 000 m^2m^3. Further, due to the size of the microchannels, the convective heat transfer coefficient is typically in the range of 6×10^4 $Wm^{-2}K^{-1}$ for effective heat transfer to be achieved. In comparison, for the batch reactor, the convective heat transfer coefficient is usually *ca.* 740 $Wm^{-2}K^{-1}$ (Wiles and Watts 2011). Similarly, reactions which require cryogenic conditions can be performed without any risk. In constrast, with batch processes, whereas when performing exothermic reactions on a laboratory scale it is easy to control the reaction temperature (*e.g.* by immersing a round-bottom flask into an ice bath), at larger scales it is a real challenge for an engineer to control the reactor

temperature precisely (Wiles and Watts 2011). It is well known that under laminar flow conditions the heat-transfer coefficient is inversely proportional to the channel diameter. The high heat-exchanging efficiency allows fast cooling and heating within the microreactor, which means that reactions can be carried out under isothermal conditions. This ability to perform reactions under isothermal conditions, with well-defined residence times, leads to a higher selectivity, yield and product quality in most cases. Microstructured reactors can also be used for fast and/or strongly exothermic/endothermic reactions (Jähnisch *et al.* 2004; McGovern *et al.* 2008). Both heat transfer and mass transfer are improved in microreactors. The influence of mass transfer on the speed of the reaction can be reduced due to the small dimensions of the reaction channel. Mixing time in micromixers is shorter than in conventional systems because of their smaller sizes and the diffusion time is also very short (Hessel and Löwe 2003; Jähnisch *et al.* 2004). The mixing time can range from seconds to a few milliseconds for liquids (Hessel *et al.* 2003). During the mixing process any turbulence cannot be observed and the process is limited to diffusion and secondary flows (Franzen 2000). Another important feature of microreactors is the hydrodynamic flow in the microchannels. In most cases, the flow is laminar, directed and highly symmetric. The Reynolds numbers lie between 1 and 1000 and depend on velocity as well as on the channel dimensions. Parameters such as temperature, pressure, and residence time and flow rate are very well controlled during the reaction which takes place at low volumes. Strongly exothermic or explosive reactions as well as reactions with toxic substances (as only very small amount of reagents are handled) or under higher operating pressure can be performed in microreactors due to their higher safety (Jähnisch *et al.* 2004; McGovern *et al.* 2008).

Microreactors also allow chemists to use organic solvents above their boiling point by pressurizing the system (Hessel *et al.* 2008; Hessel 2009; Razzaq *et al.* 2009a; Illg *et al.* 2010). Compared to batch reactions, which are usually carried out under atmospheric pressure, microreactors therefore open a thermal window for each reaction solvent (Lin *et al.* 2009). In the literature, lots of reports indicate that pressures below 30 bar have been employed by means of backpressure regulation or via the fabrication of narrow, restrictor channels within devices. However, systems pressurised in the range of 140-600 bar have also been reported, resulting in dramatic

rate enhancements compared to reactions performed using standard temperatures and pressures (Benito-Lopez *et al.* 2005; Razzaq *et al.* 2009b; Verboom 2009). Microreactors, therefore, provide more opportunities for synthetic chemists since specialized equipment is no longer required to perform reactions under extreme conditions (Darvas *et al.* 2009). Reactors can be fabricated in such a way that they contain heating elements, like heating blocks or Peltier elements (Kusakabe *et al.* 2001; Fortt *et al.* 2003), also microwaves have been widely used in connection with microreactors for thermal activation (Glasnov and Kappe 2007; Moseley *et al.* 2007).

The main advantages of microreactors which have significant implications for future innovation are therefore (Fan *et al.* 2008; Kirschning *et al.* 2006; Wiles and Watts 2011; Ehrfeld *et al.* 2000):

- small dimensions of reaction elements:
    - better mixing and good control over concentrations and temperatures within a small reaction volume;
    - potential to use nonthermal activation of molecules, *i.e.* microwaves, light, electric and magnetic fields, etc;
    - the possibility to use high pressures.

- high surface-to-volume ratio of reactor space:
    - fast cooling/heating;
    - extended surface as catalyst support;
    - electrical or optical signal carrier.

- modular design and novel manufacturing methods:
    - fabrication by inexpensive rapid prototyping or rolling/stamping;
    - possibility of combining different materials in 3D structured reactors;
    - simultaneous fabrication of functional elements of reactors.

Flow processes also have some limitations for the pharmaceutical or chemical sector. These include (Fan *et al.* 2008; Kirschning *et al.* 2006):

- the need for reactor materials to be inert for a large variety of organic solvents;
- the need to determine an efficientway of regenerating reaction columns;
- the need to determine purification steps for intermediates and/or final products;
- different kinetics of reactions;
- different solvents for multistep syntheses under the flow conditions.

Microstructured reactors can be advantageously used as process engineering tools for acquiring information about organic reactions, which could be transferred to the production scale. Results can be obtained in a short time and with greater safety. Information can also be used for optimizing process plants, which already exist, as well as giving opportunities for new production concepts. Many examples from chemical production have been documented (Wörz *et al.* 2001a; Löwe and Ehrfeld 1999; Jähnisch *et al.* 2004).

1.2.4. Online analytics in microreactors

The integration of microreactor technology with online analytical techniques is a significant development for the increase of sample throughput. Constant process evaluation is very important, especially in an industry where consistent product quality is very important. Online analytical techniques can give more detailed data on the physical - chemical processes as well as reducing the time and costs of the optimisation process. A variety of such techniques have been coupled with microreactors, including Raman and UV/Vis/IR spectroscopy, high-speed microscopy, NMR or HPLC systems.

Mechtilde *et al.* (2006), Nitta *et al.* (2012) and Gavriilidis *et al.* (2011) have each demonstrated the use of Raman Spectroscopy as an example of *in situ* monitoring of reaction process within microchannels. The FTIR Spectroscopy has been used for *in situ* reaction monitoring in terms of reactant consumption and formation of products, allowing rapid optimization of the continuous flow processes.

Tagawa *et al.* (2011) used the FTIR Spectroscopy for gas phase reactions performed in the microreactor in which the catalyst was deposited within the channels to evaluate the catalyst activity and monitor the progress of the reaction. Jensen *et al.* (2004) reported kinetic studies on the hydrogenolysis of methyl formate using a silicon micromixer. The conventional bench-top FTIR spectrometer was used in this investigation and the micromixer was placed within its sample holder. Another example of FTIR online analysis under continuous flow conditions was reported by Jähnisch *et al.* (2006; 2009). The authors used a novel fibre-optical diamond ATR sensor for gas-liquid reaction monitoring in Vitamin D analogue synthesis, as well as during the pharmaceutical intermediates synthesis during the ozonolysis - reduction sequence. The advantage of the FTIR spectroscopy technique for *in situ* monitoring of the reaction progress has also been reported by Ley *et al.* (2009; 2010).

Nuclear magnetic resonance (NMR) has also been used for the *in situ* monitoring of chemical reactions within microreactors. Bart *et al.* (2009) reported the use of a high - resolution NMR flow probe for the *in situ* monitoring of kinetic studies performed in microreactor of the acetylation of benzyl alcohol in the presence of DIPEA.

The use of chromatographic techniques as *in-situ* monitoring of the reaction under continuous flow conditions has also been demonstrated. Welch and Gong (2009) presented the use of the Express RT online HPLC system at ambient pressure for the thermal isomerization of the Diels-Alder adduct of cyclopentadiene and maleic anhydride. The HPLC technique, in combination with Raman and IR spectroscopy, as an online analytical technique has also been presented by Ferstl *et al.* (2004). The authors used the combination of these techniques for product quality monitoring and for process development, as well as long-term process monitoring during the synthesis of 2-(4-chloro-3-nitrobenzoyl)benzoic acid *via* the nitration reaction.

From the examples described above it can be seen that analytical techniques such as Raman and UV/Vis/IR spectroscopy, high-speed microscopy, NMR or HPLC can be used as an online analytical tools for reaction monitoring under continuous flow conditions

1.2.5. Application of microreactors

Many reactions have been successfully carried out using systems containing microreactors, for example, Grignard reactions, glycosylations, olefinations (Skelton *et al.* 2001b; Skelton *et al.* 2001a), Swern oxidations (Kawaguchi *et al.* 2005), nitrations (Doku *et al.* 2001), natural product syntheses and multi-step reactions (Acke *et al.* 2006; Kirschning *et al.* 2012; Ley *et al.* 2013), and many others.

Chemical transformations performed in microreactors should be relatively fast and should not cause precipitation of any reactants/products while the reaction is in progress, in order to avoid the possibility of blocking the system and thus restricting the continuous flow. However, some of them require the use of solid catalysts. The active catalyst (metal or metal complex), supported either on polymeric materials or on porous inorganic materials, is placed in the channels of the microreactor (Geyer *et al.* 2006).

Metal-catalyzed cross coupling reactions are one of the key transformations, which lead to the carbon-carbon bond formation. A Heck reaction leading to the formation of ethyl cinnamate was successfully carried out under the flow conditions in a stainless steel microreactor (Scheme 1.1). Product was obtained in 95% yield in 30 minutes of residence time at 403K while in the batch process 100% conversion was obtained at 413K using a pre-conditioned catalyst. A carbon supported (10% Pd/C) catalyst was loaded in a cartridge and the starting solution of the substrates was passed through it (Geyer *et al.* 2006; Jensen 2001; Greenway *et al.* 2000).

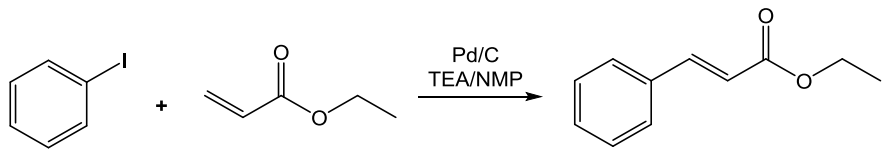

Scheme 1.1. Synthesis of ethyl cinnamate.

Reactions that make use of corrosive and toxic gases are usually difficult or impossible to perform in a batch mode due to the hazardous and highly reactive nature of the gases, which include fluorination, chlorination, oxygenation and nitration reactions (Chambers *et al.* 2001; Chambers and Spink 1999; De Mas *et al.* 2003; Jähnisch *et al.* 2000; Chambers *et al.* 2005). In microreactors, however, since they allow a controlled gas flow rate and regulation of the contact time between the liquid and gas, these transformations can be performed. Liquid-gas reactors are often integrated with phase separators in order to separate the liquid from the gas phase at the end of the reaction (Geyer *et al.* 2006).

Geyer *et al.* (2006) used a silicon microreactor coated with nickel to perform the direct fluorination of toluene (Scheme 1.2). Monofluorinated products were achieved with very good selectivity, ortho-, meta- and para- isomers were obtained in a 3:1:2 ratio. 96% conversion has been obtained using five equivalents of elemental fluorine in methanol. It is well known that these reactions are highly exothermic and difficult to control in conventional devices due to the use of elemental fluorine.

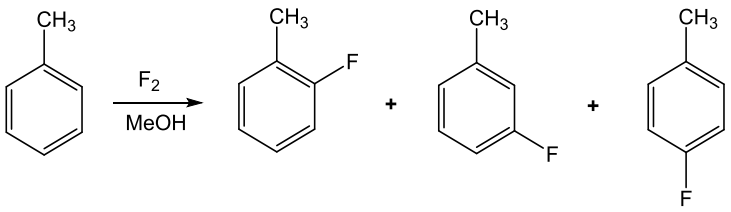

Scheme 1.2. Synthesis of monofluorinated toluene in a microreactor.

The side-chain chlorination of toluene-2,4-diisocyanate (Scheme 1.3) has also been performed in a nickel microreactor equipped with a quartz window. This helped in the formation of chlorine radicals from gaseous chlorine by irradiation of the reaction mixture, because light penetrated through the channels of the microreactor. As has been discussed, one of the advantages of microdevices is their high surface to volume ratio, which results here in a low concentration of free radicals and high selectivity of the reaction. 55% conversion and 80% selectivity was obtained for 1-chloromethyl-2,4-diisocyanatobenzene while in the batch mode 65% conversion and 45% selectivity was achieved (Geyer *et al.* 2006).

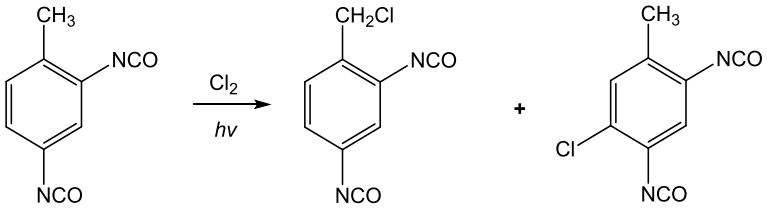

Scheme 1.3. Synthesis of monochlorinated toluene-2,4-diisocyanate.

Kobayashi *et al.* (2004) has investigated a palladium-coated microreactor to perform debenzylation of benzyl ether and reduction of alkenes and alkynes in gas-liquid-solid reactions (Scheme 1.4). The small dimensions of microreactors allow great interaction between all the phases and consequently lead to higher efficiency and yields compared to the traditional process.

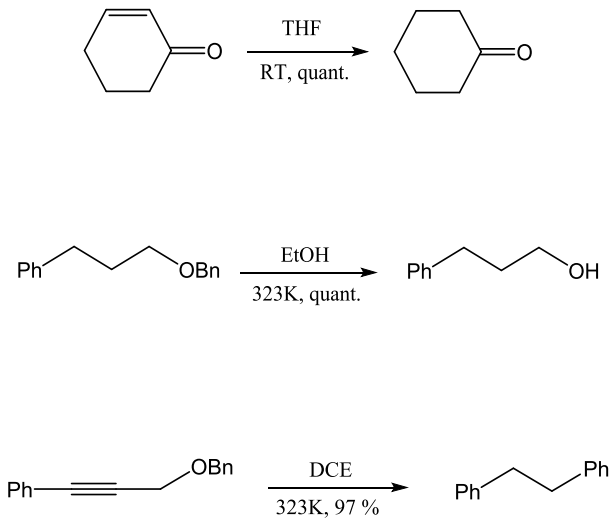

Scheme 1.4. Examples of hydrogenation reactions.

One of the most desirable reactions from the industrial point of view is the electrophilic nitration of aromatic compounds. These reactions are difficult to perform on a large scale due to safety concerns. The nitration of 1-methyl-3-propyl-1H-pyrazole-5-carboxylic acid is particularly problematic in a batch mode because of the temperature control and long reaction time (Scheme 1.5). A large amount of carbon dioxide is also generated by undesired decarboxylation. This reaction has, however, been performed under flow conditions using the stainless steel microreactor of the Cytos lab system, which led to the highly controlled formation of nitropyrazole. The

decarboxylation reaction was minimized due to accurate temperature control. The desired product was obtained in a 73% yield with a residence time of 35 minutes. This synthesis is a key intermediate for the synthesis of the drug Sildenafil® (Panke *et al.* 2003)

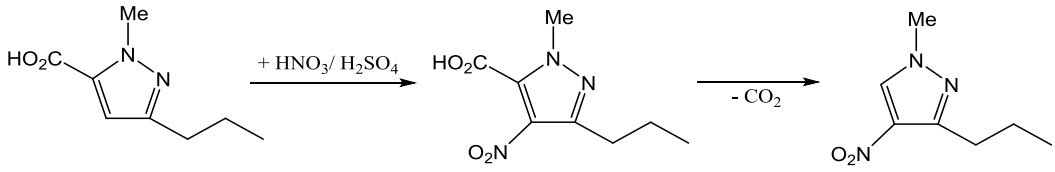

Scheme 1.5. Nitration of 1-methyl-3-propyl-1H-pyrazole-5-carboxylic acid.

A very fast, highly exothermic and homogeneously catalyzed reaction which gives a vitin precursor as a product has been demonstrated by Ehrfeld *et al.* (2000) and Wörz *et al.* (2001a). 80-85% yield of product was obtained in a continuous mixer/heat exchanger reactor, whereas, a 70% yield was achieved in a semi-batch process. When the reaction was performed under isothermal conditions in a microreactor with thirty-two channels (900 × 62μm^2) (Figure 1.10), about 85% yield was obtained at a residence time of 4 s at 323K. Higher yields (90-95%) could be obtained at a residence time of 30 s at 293K (Brivio *et al.* 2006).

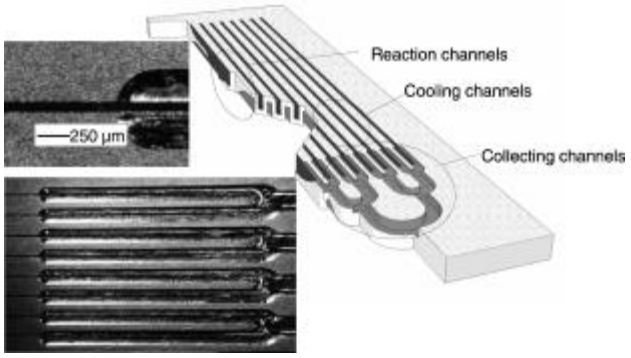

Figure 1.10. Microreactor used in a synthesis of a vitamin precursor. Adopted from Brivio *et al.* (2006).

Kawaguchi *et al.* (2005) carried out the Swern oxidation in continuous flow microreactors at much higher temperatures (between 253K and 293K) than those required in batch reactors (223K or lower).

The nitration of benzene in a glass microreactor has been reported by Doku *et al.* (2001). Nitrobenzene, 1,3-dinitrobenzene and 1,3,5-trinitrobenzene were obtained in 65, 8 and 5% yields, respectively.

The nitration of benzene and toluene in stainless steel and polytetrafluoroethylene (PTFE) microreactors has been presented by Fletcher *et al.* (2002). The authors found a linear dependency of the conversion with the temperature; the conversion could be increased by reducing the microchannel diameter or by increasing the flow rates. They showed the possibility of optimizing reactions by studying the effect of independent parameters on reaction rates.

Hessel *et al.* (2000) presented the synthesis of hydrogen cyanide via the Andrussow route. They showed that a micro heat-exchanger prevents the hydrogenolysis of the reaction to produce ammonia. The high degree of temperature control prevents side-reactions occurring in microreactors and decomposition of the target product is reduced, thus increasing the overall product yield, selectivity and purity, compared to the macroscale process.

Side reactions are minimized in microreactors due to the high mixing efficiency, which prevents the formation of concentration gradients. Jensen *et al.* (2001) reported that mass transfer coefficients for the catalytic hydrogenation of cyclohexene to cyclohexane in a silicon-glass microreactor is about two orders of magnitude larger than those reported in the literature for standard laboratory scale reactors. Jensen *et al.* (2000) performed the reaction of acid chlorides and hydrogen peroxide to organic peroxides. This reaction could be performed due to the high temperature control, which eliminated the risk of explosion during the process. The accurate control of the temperature was possible due to the heat transfer from the reaction.

Reinhoudt *et al.* (2003) demonstrated the acid catalyzed esterification of 9-pyrenebutyric acid with ethanol as a solvent to pyrenebutyric acid ethyl ester (Scheme 1.6).

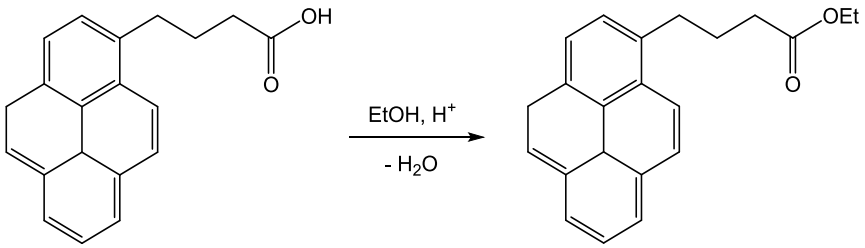

Scheme 1.6. Synthesis of pyrenebutyric acid ethyl ester.

Product was obtained with a higher yield when a pressure-driven continuous flow glass microreactor was used (Figure 1.11), leading to the conclusion that the reaction rate is significantly higher in comparison with conventional procedures.

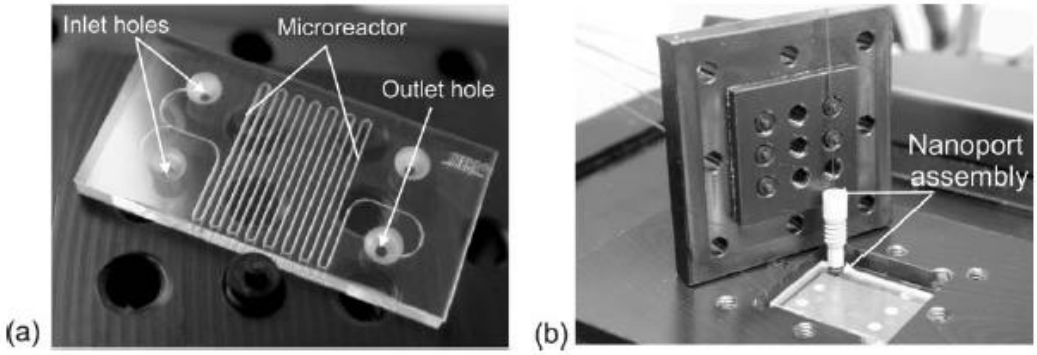

Figure 1.11. a) Microreactor used in Reinhoudt's group's work. b) Dedicated chip holder for fitting fused silica fibres into the inlet/outlet chip reservoirs by means of low dead volume Nanoport® connectors. Adopted from Brivio *et al.* (2006).

Wilson and McCreedy (2000), meanwhile, presented the heterogeneously catalyzed dehydration of alcohols (Scheme 1.7) in a glass/PDMS hybrid microreactor in which the catalyst (sulfated zirconia) was dusted over the PDMS surface before the top and bottom ones were joined together by photolithography and chemical etching of glass. The reaction was performed at 428 - 433K, in which the liquid transport took place through an injection pump. The conversion of 1-hexanol to 1-hexane was about 95% instead of 30% in the conventional process.

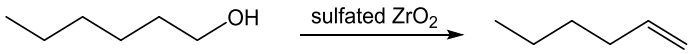

Scheme 1.7. Synthesis of 1-hexane.

The Suzuki reaction in a borosilicate microreactor with a channel width of 300 μm and depth of 115 μm has been performed as an example of a catalytic liquid-phase reaction by Greenway *et al.* (2000). The catalyst (1.8% Pd/SiO_2) was scattered as a suspension and by heating up to 373K for 1 h. Aryl cyanide was periodically injected into the continuous flow of the phenylboronic acid by electro-osmotic flow to give 4-cyanobiphenyl in 10% higher yields (67%) than the batch process (Scheme 1.8).

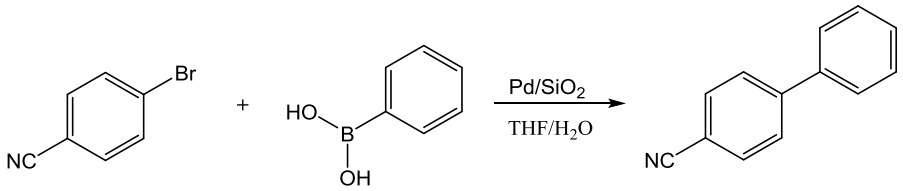

Scheme 1.8. Suzuki reaction carried out in a borosilicate microreactor.

Haswell's group performed the Kumada-Corriu reaction in microstructured reactor. Small pellets of catalyst were placed into 1-2 mm diameter polypropylene capillaries. 4-Methoxybiphenyl was obtained by reacting *p*-bromoanisol with phenylmagnesium bromide (Scheme 1.9) in the presence of the Merrfield-resin-immobilized nickel complex catalyst. The results showed that the product can be obtained in a few minutes under flow conditions while 24 h is required to obtain the same yield in the traditional process. This phenomenon was explained by the fact that the reactants can reach deeper into the pores of the resin under the high pressure conditions and thus a larger

number of active sites become accessible for the reaction compared to the traditional process (Haswell *et al.* 2001).

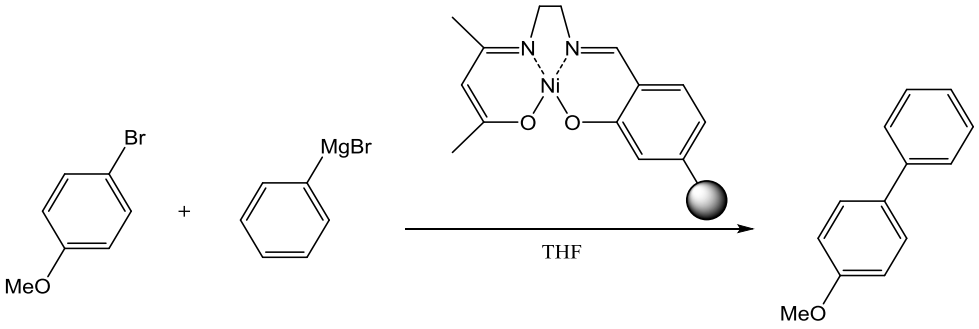

Scheme 1.9. Synthesis of 4-methoxybiphenyl (The Kumana-Corriu reaction).

A phase transfer diazo coupling reaction in a pressure-driven glass microreactor was presented by Kitamori's group (Scheme 1.10). This liquid-liquid multi-phase reaction allowed almost a 100% yield of the desired product to be obtained, due to the short diffusion process and large active surface area at the interface. Two solutions: 5-methylresorcinol in ethyl acetate and 4-nitrobenzene diazonium tetrafluoroborate in water were introduced under continuous flow conditions (Hisamoto *et al.* 2001)

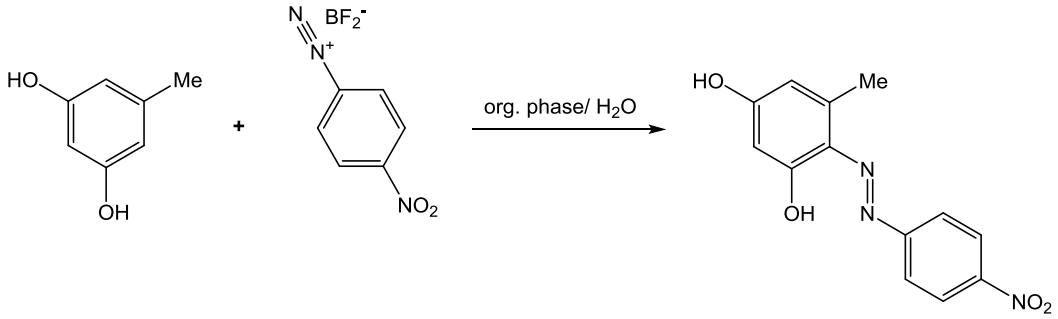

Scheme 1.10. Diazo coupling reaction carried out in a pressure-driven glass microreactor.

Ueno *et al.* (2003b), meanwhile, carried out a phase-transfer benzylation reaction of ethyl 2-oxocyclopentanecarboxylate with benzyl bromide and tetrabutylammonium bromide in a pressure-driven glass microreactor (Scheme 1.11). The benzylated

product was obtained at a higher conversion rate compared to experiments performed on the macroscale with different stirring speeds in the batch process.

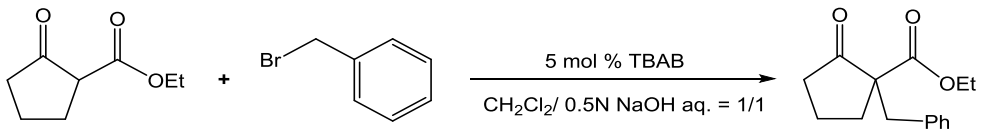

Scheme 1.11. The benzylation reaction of ethyl 2-oxocyclopentanecarboxylate

In a microreactor controlled by a nano-feeder the Mukaiyama aldol reaction of benzaldehyde with trimethylsilyl enol ether has been carried out by Mikami *et al.* (2003) (Scheme 1.12). Both reagents in toluene were injected in one inlet, while the catalyst solution was injected through a second one. Only 0.1% (by mol) of the scandium complex was used under the flow conditions. The reaction was completed within seconds, giving the product in 97% yield while in the batch mode only 11% of product was obtained using 1-10% (by mol) of catalyst, a vigorous stirring at 328K for 2 h.

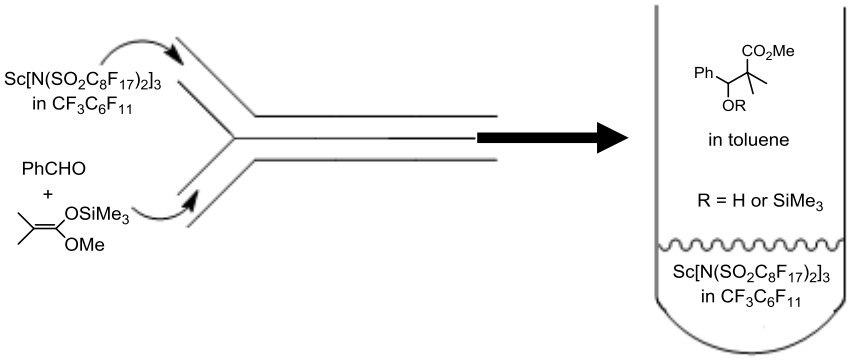

Scheme 1.12. Mukaiama aldol reaction of benzaldehyde in a "fluorous nano flow" system.

Watts *et al.* (2004) reported the synthesis of isoxazole and substituted pyrazole (Scheme 1.13) starting from 1-phenylbutene-1,3-dione using electro-osmotic flow to move reagents within the microchannels. They also published the preparation of an array of pyrazoles using the same microreactors (Scheme 1.14) (Watts and Haswell 2005).

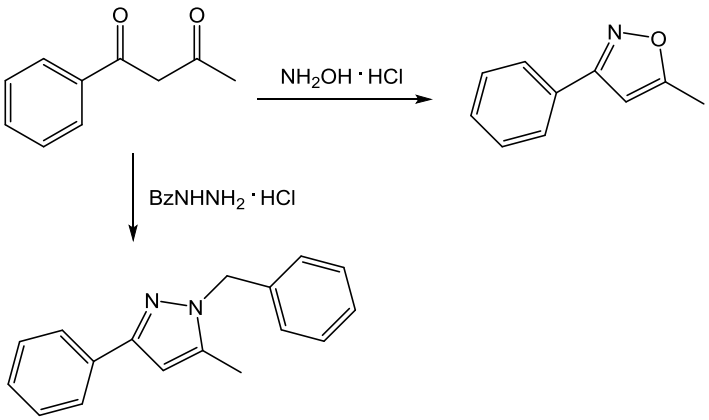

Scheme 1.13. Synthesis of an isoxazole and a substituted pyrazole.

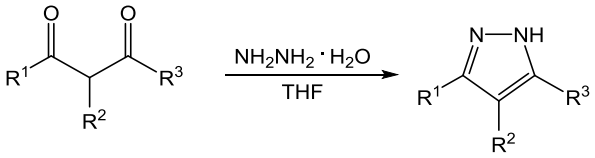

R^1 = Me, Ph, $(CH_2)_4$-
R^2 = H, Me
R^3 = Me, Ph

Scheme 1.14. 1,2-azoles formation.

The authors estimated that 339 g of product could be produced per day by 1000 microreactors working in parallel. Based on this assessment, and the library of 1,4-azoles, it was found that an EOF-based microreactor could be used in the large-scale production of chemical and pharmaceutical products. Garcia-Egido *et al.* (2003) has created the same type of libraries using a pressure-driven microreactor.

The falling-film microreactor (Figure 1.12) and the microbubble column (Figure 1.13) have also been investigated in fluorination reactions (Scheme 1.15) with molecular fluorine by Jähnisch *et al.* (2000; 2004).

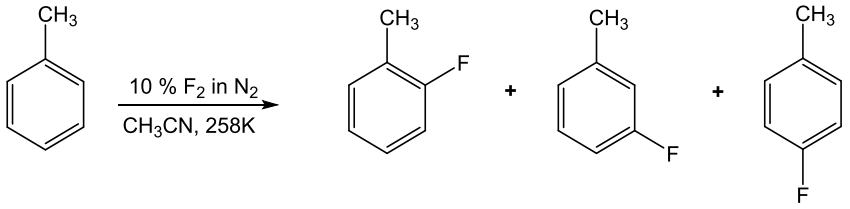

Scheme 1.15. Synthesis of monofluorinated toluene.

A stainless steel falling film microreactor (Figure 1.12) with a quartz window to perform photochemical gas-liquid reactions has been reported by Jähnisch *et al.* (2004). The heat and mass transfer was found to be increased by the development of a thin liquid film (up to 15 μm thick corresponded to the specific phase interface of up to 20 000 $m^2 m^{-3}$) in the microreactor's channels. The design principles of the falling-film microreactor are presented in Figure 1.12a.

The reactor is built from four components:

- bottom housing section with heat exchanger;
- reaction plate;
- contact-zone mask;
- top housing section with a quartz window.

a) **b)**

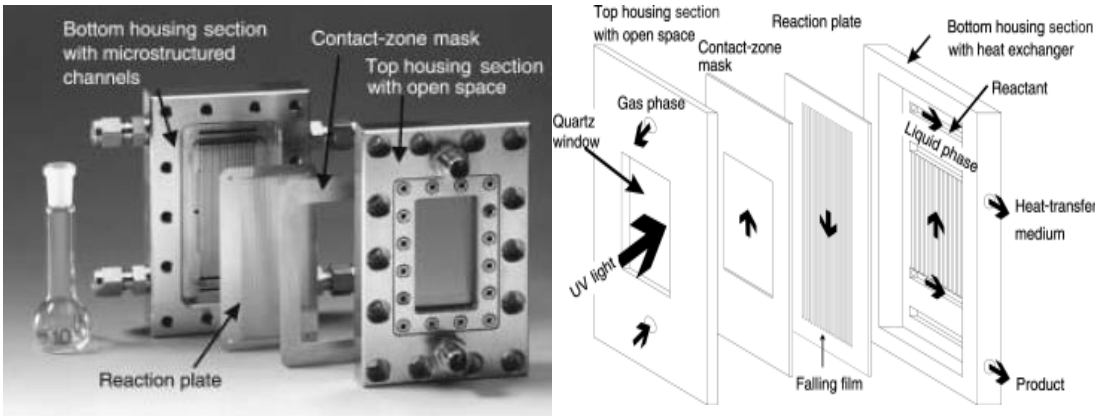

Figure 1.12. a) The falling film microreactor used in Jähnisch's work.
b) Components of the reactor. Adopted from Jähnisch *et al.* (2004).

The monofluorinated toluene was obtained with higher selectivity in the falling-film microreactor compared to the microbubble column (Figure 1.13). De Mas *et al.* (2001; 2008)showed that fluorination with F_2 can be performed at room temperature in a two-channel reactor made of silica.

In the microbubble column, the reaction plate has microchannels with a width ranging from 100 to 1200 µm and a depth from 100 to 600 µm. The top housing section is in rectangular-shaped open space through which the gaseous reagents can flow while the liquid flows downwards due to gravity above the reaction channel (Adam and Prein 1996).

a) **b)**

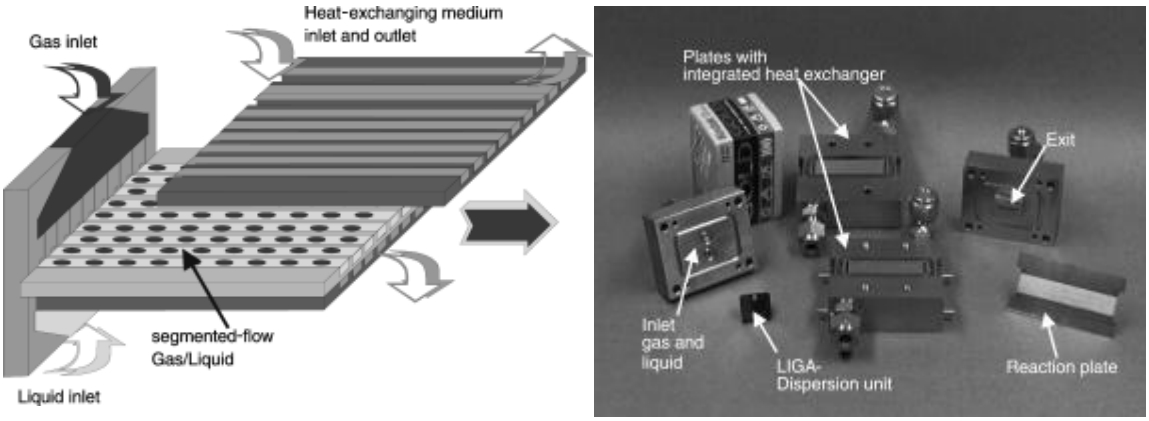

Figure 1.13. a) Construction of the microbubble column used by Jähnisch's group.
b) Components of the column. Adopted from Jähnisch *et al.* (2004).

A static microdisperser unit made of a nickel/copper alloy is the central part of the microbubble column (Figure 1.13). The gas and liquid inlet is no wider than 5 and 20 µm, respectively. Flow distribution is achieved through the construction of a pressure barrier in the feed part of the microdisperser for both phases. The thermal effects are controlled through the use of a heat-transfer fluid that flows in counterflow to the reagents. The microbubble column reactor is designed for gas-liquid reactions with a short contact time (Jähnisch *et al.* 2004). Both of the reactors presented in Figure 1.12 and Figure 1.13 are suitable for gas-liquid reactions and have been developed by

Institut für Mikrotechnik Mainz (IMM) and their collaborators (Jähnisch *et al.* 2000; 2004).

Shen *et al.* (2009) reported the exothermic nitration of 2-ethylhexanol to 2-ethylhexylnitrate in a microreactor. The reaction is considered as highly exothermic with the possibility of explosion or associated side reactions. They investigated the effect of mixed acid composition and operating conditions on the conversion of iso-octanol and the average reaction rate. The reaction was performed safely at 298 – 313K, whereas in conventional reactors the temperature is kept at 288K or below for the safety reasons. The authors obtained 2-ethylhexylnitrite at a 98.2% conversion at 308K and 7.2 s of residence time. Using flow chemistry to perform nitration reactions increases the safety aspect of the process due to the exothermic and corrosive nature of nitration reactions (Burns and Ramshaw 2002; Ferstl *et al.* 2004).

Another example of selective nitration using neat HNO_3 was reported by Braune *et al.* (2009). Commercially available glass microreactors supplied by Corning Incorporated were used and the authors reported that the target product could be obtained at a rate of 100 kg h^{-1} by operating eight reactors in parallel.

The synthesis of 1-(azidomethyl)-3,5-bis-(trifluoromethyl)benzene (Scheme 1.16) using a continuous flow reactor was presented by Kopach *et al.* (2009). A stainless steel tube reactor operated at 363K afforded the desired product in 97% conversion at a residence time of 20 min and the authors were able to produce 25 g of 1-(azidomethyl)-3,5-bis-(trifluoromethyl)benzene by operating the reactor continuously for almost 3 hours.

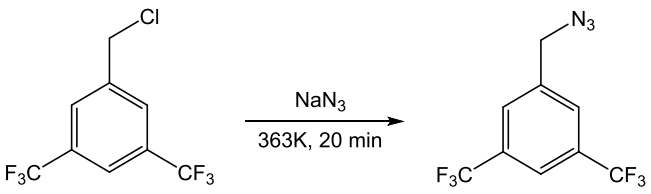

Scheme 1.16. Synthesis of a pharmaceutically interesting intermediate via continuous flow azidation.

A regioselective condensation of 1-(azidomethyl)-3,5-bis-(trifluoromethyl)benzene with a β - ketoester is a key step in the preparation of compounds (2) and (3) (Scheme 1.17) which are NK-1- antagonists and have been approved for emesis treatment (Kopach *et al.* 2009).

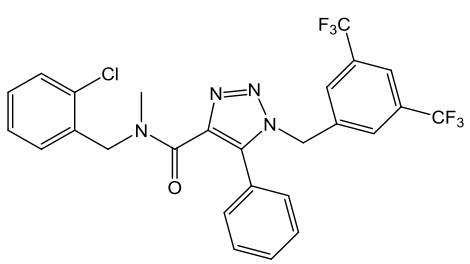

(2)

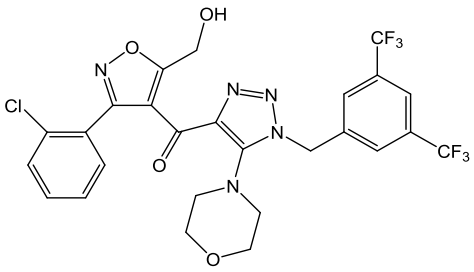

(3)

Scheme 1.17. Selected NK 1-antagonists.

Using diethylaminosulfur trifluoride (DAST) Seeberger *et al.* (2008) reported the deoxyfluorination reaction of alcohols, lactols, aldehydes and carboxylic acids using a continuous flow microstructured reactor at 343K, 16 min of reaction time and *in situ* quenching of excess DAST and HF. Fluorinated products were obtained with a 40 - 100% isolated yield.

Rencurosi *et al.* (2010) described the synthesis of substituted alcohols using a tubular reactor, commercially available from Vapourtec. A variety of carbonyl containing compounds reacted with Grignard reagents and was successfully converted to secondary and tertiary alcohols. Using a PTFE tube reactor this methodology was extended to the synthesis of the analgesic Tramadol (Scheme 1.18) which was isolated in 96% yield as a hydrochloride salt in an 8 : 2 ratio of the two diastereoisomers.

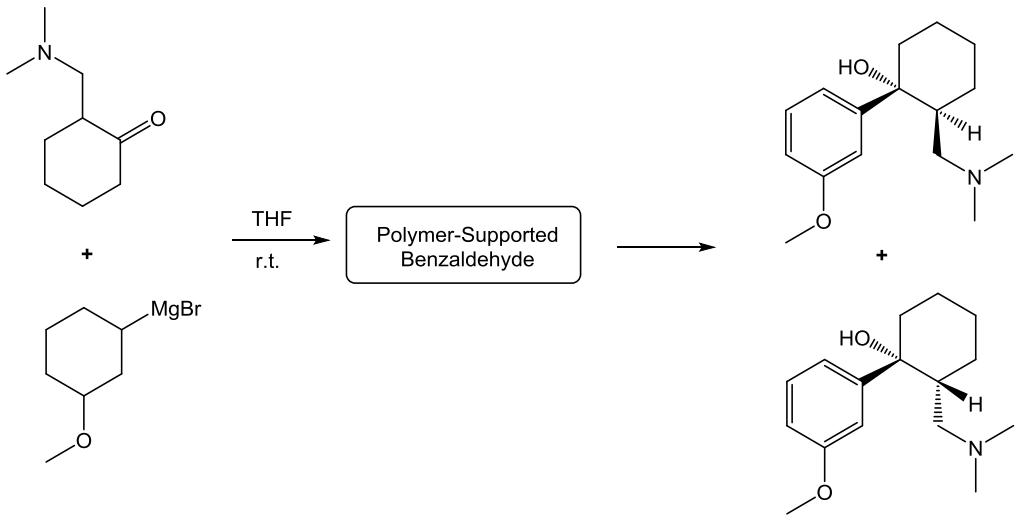

Scheme 1.18. Flow synthesis of Tramadol.

Baumann *et al.* (2010) reported a preparation of 3-nitropyrrolidine derivatives using a dipolar cycloaddition reaction involving azomethine ylides and nitro alkenes under continuous flow conditions using commercially available R2+/R4 system from Vapourtec at the temperature range 333 - 393K and 30 - 90 min of reaction time. They extended their work to the chemoselective hydrogenation of 3-nitropyrrolidines using the H-Cube® flow reactor to perform the reduction of the nitro group over the benzyl group to the corresponding amine (Figure 1.14) in the presence of acetic acid at 333K, using a cartridge filled with the Raney nickel catalyst. Amines were synthesised in high yield ranging from 93% to 97%. Furthermore, when 10% Pd/C was used instead of Raney nickel catalyst a reduction of the nitro group, as well as debenzylation, was observed and products were obtained in 90 - 97% yield (Figure 1.15).

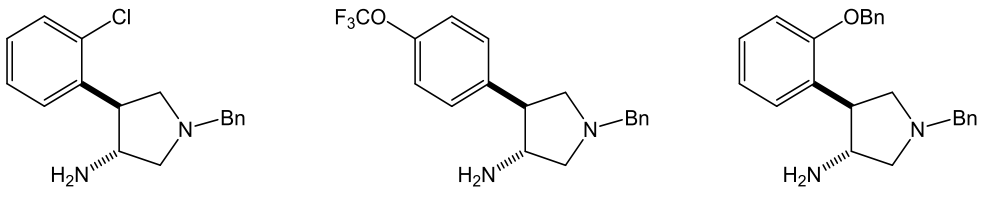

Figure 1.14. Raney nickel mediated reduction of nitropyrrolidines.

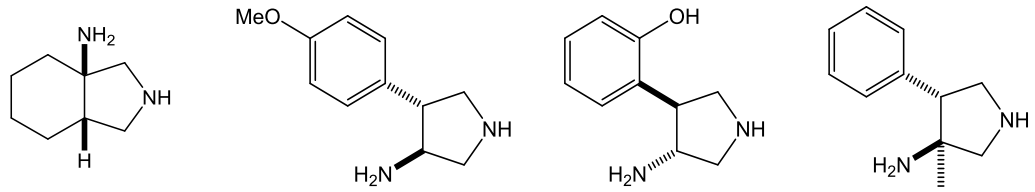

Figure 1.15. Pd/C-mediated reduction and debenzylation of 3-nitropyrrolidines.

Kappe *et al.* (2009) used the X-Cube^{TM} flow reactor to demonstrate the cycloaddition of 2,3-dimethylbutadiene and acrylonitrile to the cyclohexene adduct (Scheme 1.19). The cycloaddition process under batch microwave conditions takes 20 min at 513K but can be reduced to 10 min at 523K using toluene as the solvent (Kremsner and Kappe 2006). Performing the reaction under continuous flow

conditions at 523K, 60 bar set pressure and at 0.8 mL min^{-1} of liquid flow rate, the authors achieved the cycloadduct in a near quantitative isolated yield. Changing the solvent from toluene to MeCN, THF or 1,2-dimethoxyethane gave identical results.

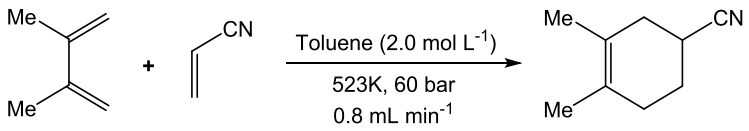

Scheme 1.19. Model reaction used to demonstrate the Diels-Alder cycloaddition at high temperatures and pressure.

The cycloaddition of isoamylene and α-methylstyrene using a microreactor to synthesised indane compounds was performed by Okafor *et al.* (2010). The authors carried out the acid catalysed cycloaddition using a tube reactor containing silica beads. The packed-bed reactor allowed efficient mixing of the biphasic reactant streams and at 308K using a sulphuric acid catalyst concentration of 98 wt %, converted 96% of reactants in 30 min of reaction time.

Kawaguchi *et al.* (2005) reported the Swern oxidation at temperatures between 253K and 293K using a microreactor. This temperature range is much higher than that required for conventional batch reactors (*i.e.* 223K or below). Primary, secondary,

cyclic and benzylic alcohols gave the corresponding carbonyl compounds in good yields and selectivity at 253K which can be attributed to the precise temperature control and fast and efficient mixing. In comparison, a conventional batch macroscale reactor with a 30 mL volume resulted in very low carbonyl compound formation at the same reaction temperature.

The Moffat-Swern was also investigated by Linden *et al.* (2008) using a microreactor system from the Ehrfeld Mikrotechnik BTS company. They reported that when the microreactor was operated for over 1.5 h it had a production rate of 60 g h^{-1} and a throughput of 23.6 g L^{-1} h^{-1} of 4-androstene-3,17-dione (Scheme 1.20).

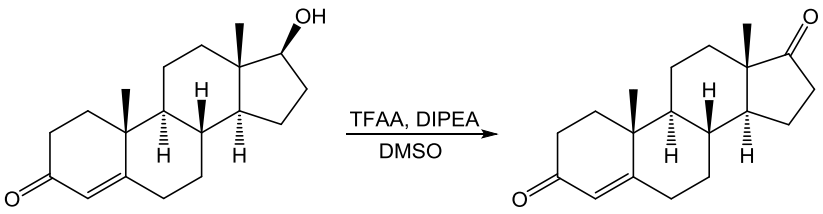

Scheme 1.20. Schematic illustrating the oxidation of testosterone.

Sedelmeier *et al.* (2010) reported the synthesis of carboxylic acids from alcohols and aldehydes, carbonyls and carboxylic acids from nitroalkanes using permanganate as the oxidant under continuous flow conditions using the Uniqsis FlowSyn. In this work, the T-piece mixer was immersed within an ultrasound bath to prevent the T-piece connector from blocking due to the fouling of manganese dioxide. The oxidation of nitroalkanes, alcohols and aldehydes to corresponding carboxylic acids was performed at room temperature with the reaction times ranging from 10 to 30 min under continuous flow conditions, giving the products in high yield (71 - 98%). Nef oxidation of nitroalkanes was also investigated. The use of a single equivalent of potassium permanganate converts nitroalkanes into aldehydes (or ketones) at room temperature, 5 - 8 min reaction times and a yield in the range of 58 to 95%.

Poe *et al.* (2006) used mineral oil as a carrier phase during the synthesis of indigo (Scheme 1.21). This base-catalysed aldol condensation resulted in the precipitation of a solid, as well as fouling of the product on the poly(vinyl chloride) tubing when the reactions was carried out in the absence of the carrier phase.

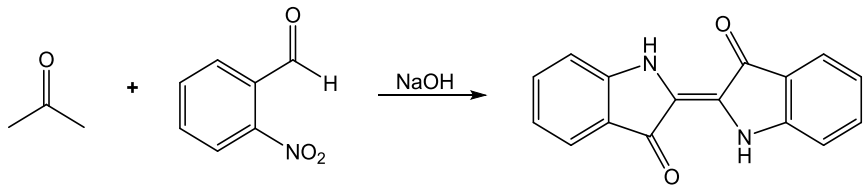

Scheme 1.21. Synthesis of indigo.

The authors extended their approach of monodispersed droplet flow to the synthesis of *N,N'*-dicyclohexylethylenediimine from glyoxal and cyclohexylamine (Scheme 1.22). In this case, however, hexane was used as the carrier phase due to the fact that the product was soluble in mineral oil and difficult to recover.

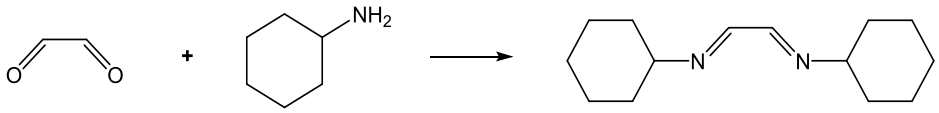

Scheme 1.22. Synthesis of *N,N'*-dicyclohexylethylenediimine.

Using toluene as a carrier phase they reported the synthesis of 4-chloro-*N*-methylbenzamide (Scheme 1.23), in a highly exothermic reaction using a microreactor and compared this with a batch process. The isolated yields of the product were 87.6% and 76.9% for continuous flow and the batch process, respectively, with high product purity. The space-time yields (STY) were reported as 9.150 mol m^{-3} min^{-1} using the continuous microfluidic device and 0.7140 mol m^{-3} min^{-1} for the batch synthesis.

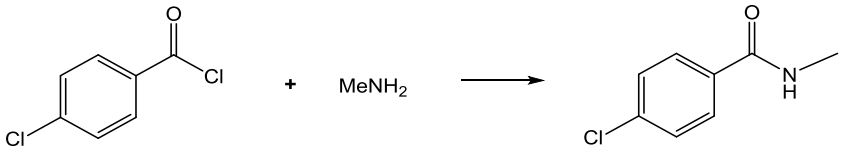

Scheme 1.23. Synthesis of 4-chloro-*N*-methylbenzamide.

Using the X-Cube^{TM} flow reactor provided by ThalesNano, Fuchs *et al.* (2010) reported the azide-alkyne cycloaddition reaction catalysed by Cu-C. The model reaction is presented in Scheme 1.24 and by varying the reaction parameters, the authors were able to show that the product can be synthesised in 99% isolated yield at 443K and 12 s residence time under continuous flow conditions. When increasing the system productivity by an increase of the reagent throughput, however, Cu leaching from the charcoal support increased, indicating that the support acts as a reservoir for the Cu, operating a release-recapture mechanism (Lipshutz *et al.* 2007). As the quantity of the Cu in the target products was far above the quantity allowed in pharmaceuticals, authors used Quadrapure^{TM} TU (thiourea) resin for metal scavenging via thiol complexation (Hinchcliffe *et al.* 2007). This allowed them to decrease the Cu contamination from 600 mg kg^{-1} to < 1 mg kg^{-1}.

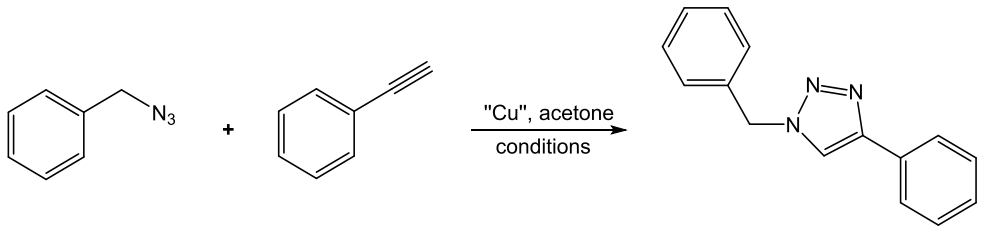

Scheme 1.24. Cu-catalysed cycloaddition of benzyl azide and phenylacetylene.

Bogdan and James (2010) reported a series of cycloadditions using an Accendo Conjure flow reactor with copper tubing (3m length, 0.75 mm inner diameter). The optimisation process of the macrocyclization was performed using the azidoalkyne as a model reaction (Scheme 1.25). A series of macrocycles was synthesised using EtOH as a solvent at 423K and 5 min residence time and 0.1 mol L^{-1} of azide concentration. Products were isolated in yields ranging from 28%

to 80%. A very low level of Cu (< 5 ppm) was measured in the reaction mixture, indicating that the catalytic copper could be in a deadsorbed form, before being readsorbed to the surface of the reactor tube.

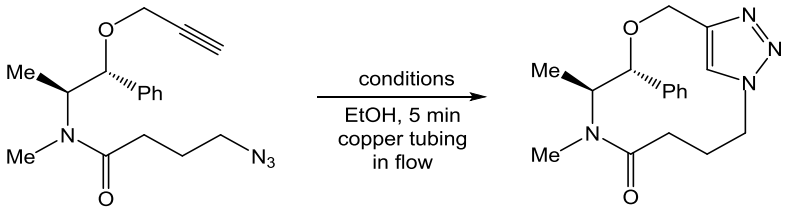

Scheme 1.25. Macrocyclization reaction under continuous flow conditions using a copper tube reactor.

The Knoevenagel condensation reaction is commonly used for the production of the fine chemical for coumarin derivatives (Ramani *et al.* 1999; Scott and Raston 2000) and for pharmaceutical production, e.g. nifendipine and nitrendipine derivatives for hypertension drugs (Saunders 2000). This C - C bond forming reaction using heterogeneous catalysis is widely studied under continuous flow conditions.

Bogdan *et al.* (2007) reported the Knoevenagel condensation of benzaldehyde and ethyl cyanoacetate (Scheme1.26) using a packed-bed reactor with pressure-driven flow. They compared their results with batch experiments and found 90% conversion at 50 µL min^{-1} (3 mL total volume in 1 hour) under continuous flow conditions whereas, using a batch system (reaction volume of 3 mL), the conversion was only 69% after 1 hour.

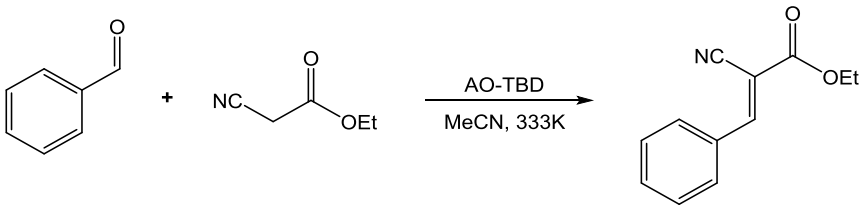

Scheme 1.26. The Knoevenagel condensation reaction under continuous flow conditions using 30-cm tubing packed with AO-TBD.

The Knoevenagel condensation under continuous flow conditions has also been successfully applied using a packed-bed reactor and electro-osmotic flow (Wiles *et al.* 2007), zeolite catalysts (Lau *et al.* 2008), monoliths (El Kadib *et al.* 2009) as well as wall-coated reactors (Costantini *et al.* 2009), in each case giving the desired compounds in high purity and yield.

The synthesis of Vitamin D precursor (Scheme 1.27) using ozonolysis-reduction sequence under continuous flow conditions has also been reported by Hübner *et al.* (2009).

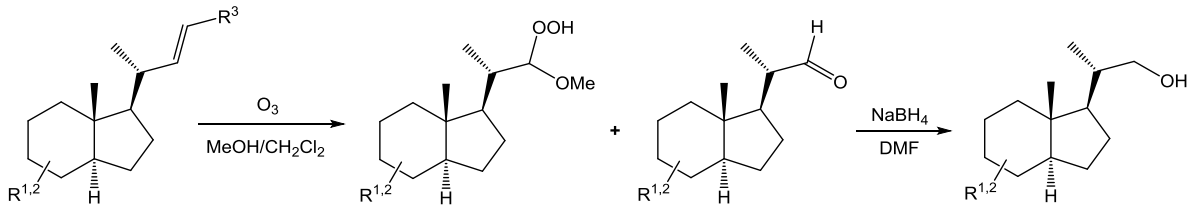

Scheme 1.27. Synthesis of Vitamin D analogues in microstructured reactors.

Apart from the examples presented above, it can be seen that flow chemistry has been widely used for a variety of liquid and multi-phase reaction systems. It can also be successfully used for multi-step syntheses and in the area of photochemistry (Hook *et al.* 2005; Coyle and Oelgemöller 2008; Wiles and Watts 2012). The formation of tricyclic aziridines from pyrrole derivatives has been presented by Maskill *et al.* (2013). The authors used single fluorinated ethylene propylene (FEP) flow reactor and demonstrated that multigram quantities of products can be synthesised under continuous flow conditions. The use of photochemistry under continuous flow conditions has also been reported by Lévesque and Seeberger (2012) for the synthesis of the anti-malaria drug artemisinin. The authors reported that aphotoinducted singlet-oxygen ($^1O_2$), which is a highly reactive molecule, can be generated under continuous flow conditions. Since microreactors offer a great control over reaction parameters, it is possible to eliminate the low rate of gaseous oxygen mass transfer into the solution which is typical of traditional batch systems, meaning that 200 g of artemisinin per day could be produced.

Overall, flow chemistry represents a significant breakthrough towards improved efficiency through automation and process optimization. The number of examples presented above shows that microreactors are promising tools in synthetic chemistry and can be used at different application scales. Continuous flow processing and microreactors together offer a number of advantages in comparison with conventional chemical processes.

1.3. Conclusions

Microreactors allow many chemical reactions to be performed with a higher level of productivity, more cleanly and more safely. In comparison with conventional chemical processes, microreactors offer much better control of the reaction parameters, including heat and mass transfer, simple scale-up and increased atom efficiency. Continuous flow chemistry allows the chemist to generate data on the reaction kinetics and pathways, as well as to optimise the reaction conditions in a relatively short time compared to traditional batch processes. It has also been demonstrated that microreactors can be combined with online analytical techniques like Raman and UV/Vis/IR spectroscopy, high-speed microscopy, NMR or chromatographic techniques. It has been shown that there are a variety of microreactors and microreactor-based systems commercially available for researchers and that these include gas-liquid, liquid-liquid or gas-liquid-solid reaction systems, with most of these now widely available. Some companies are also able to design and fabricate customized devices as well as pilot and production plants apart from the R&D platforms. For example Chemtrix offers the KiloFlow® system which allows researchers to perform rapid, predictable scale-up from mg (Labtrix®) to kg (KiloFlow®) without re-optimization or change in mixing efficiency. The company also offers the Plantrix® Industrial Flow Reactor which allows the user to produce at the tonne-scale, for the execution of highly profitable processes. All of these make the continuous flow process easily accessible for researchers and ensure that this technology will have a substantial impact on the future of chemistry and the chemical industries.

1.4. Aim and objectives of the thesis

Microreactors have proved to be a very powerful tool in the area of flow chemistry, especially in the synthesis of speciality chemicals, chemical intermediates and pharmaceutical intermediates. The concept of flow chemistry has not previously been investigated for the synthesis of primary amines and a tandem: reductive amination-hydrogenolysis process. Amines are very important industrial organic compounds which are widely used as fine chemicals and pharmaceutical intermediates. The main goal of this work is to evaluate the synthesis of primary amines under continuous flow conditions using the structured multichannel compact reactor developed at the University of Bath and the commercially available X-Cube^{TM} flow reactor (ThalesNano, Hungary) for the manufacture of speciality chemicals which lead to the production of APIs in the presence of Pd/C catalyst.

To the best of the author's knowledge the synthesis of primary amines *via* tandem reductive amination of aldehydes - hydrogenolysis of secondary amines process has not previously been investigated in the context of continuous flow processing.

The following research activities are necessary to achieve the aim and objectives of this project:

- evaluation of optimum conditions for reductive amination under continuous flow conditions;
- evaluation of optimum conditions for hydrogenolysis reaction under continuous flow conditions;
- evaluation of optimum conditions for tandem process under continuous flow conditions;
- evaluation of a kinetic model and mechanism for each reaction.

Chapter 2

Reductive Amination of Aldehydes in the Structured Compact Reactor and X-Cube™ Flow Reactor

2.1. Introduction

Amines are considered as very useful intermediates in the pharmaceutical and fine chemicals industry among many other functional groups in organic chemistry (Trost and Fleming 1991; Brown 1994). In the area of drug discovery, especially, secondary amines have gained special attention since they are extremely important pharmacophores in numerous biologically active compounds (Insaf and Witiak 1999). It is well known that secondary amines can be used as important scaffoldings for further reactions in combinatorial library generation (Balkenhohl *et al.* 1996) as well as in solid phase synthesis (Albericio 2000). In the literature many traditional methods have been reported for the synthesis of secondary amines but this can often be problematic due to poor yields and/ or low chemical selectivity, as well sometimes entailing harsh reaction conditions (Patai 1968; Salvatore *et al.* 2001).

One of the most common and straightforward methods for secondary amine formation is direct *N*-alkylation, commonly known as the "Hofmann alkylation", where the primary amine is treated with alkyl halides or their equivalents, such as dialkyl sulphates or sulphonates (Katritzky *et al.* 1995). Secondary and tertiary amines can be synthesised using this method depending on the conditions used (Scheme 2.1). It is well known, however, that the selectivity of this synthetic method is very limited due to the over-alkylation which very often occurs (Trost and Fleming 1991). Traditionally, secondary amines could be obtained by the treatment of an alkyl halide with a large excess of a primary amine, but this is a very expensive and wasteful process which requires the excess of starting primary amine to be removed at the end of the process, usually by applying distillation techniques (Solomons 2000; Abdel-Magid and Mehrman 2006).

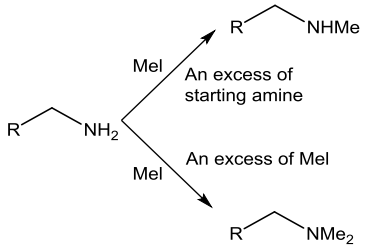

Scheme 2.1. Synthesis of secondary and tertiary amines by alkylation.

One of the most convenient methods for secondary amine synthesis is the reduction of compounds containing higher oxidation state nitrogen atoms to amines using a variety of reducing agents (Scheme 2.2 and Scheme 2.3). Nitro compounds, amides and nitriles (Scheme 2.2) can all be reduced through to the amine. Imines, enamines and iminium ions formed by reaction of amines with carbonyl compounds, can all be reduced to amines (Scheme 2.3) (Roe and Montgomery 1953; Rylander 1967; Brown and Heim 1973; Kuehne and Shannon 1977; Larock 1999).

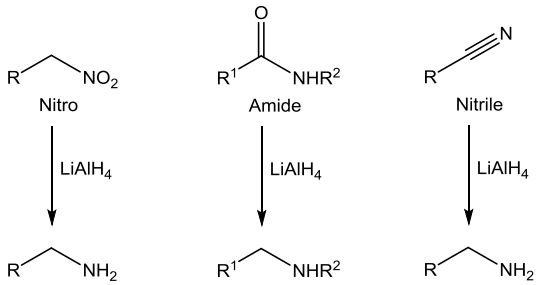

Scheme 2.2. Reduction of *N*-containing functional groups to amines.

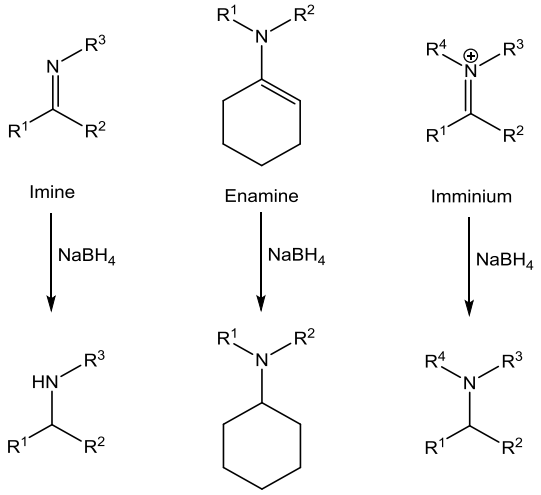

Scheme 2.3. Reduction of nitrogen containing carbonyl derivatives to amines.

The reductive amination reaction (Scheme 2.4) is a key transformation used in industry for amine formation due to its reliability and ease of use. The ability to reduce an imine to the amine has been the centre of much research. The reaction can be done using stoichiometric amounts of reducing agent; however, the use of reducing agents is not atom efficient because it also requires stoichiometric amounts of reagents (Scheme 2.5). The reduction can also be done using catalytic amounts of Pd/C and H_2 gas. Since the 1940s, more and more catalysts have been developed to hydrogenate imines. For catalytic hydrogenation many transition metals have been used, including Ni, Pd, Pt, and Cu (Scheme 2.6). The use of heterogeneous catalysis allows easy purification and removal of the catalyst from the product at the end of the reaction (Basu *et al.* 2003).

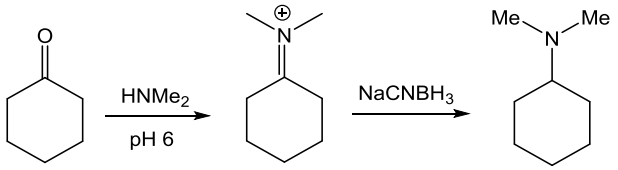

Scheme 2.4. Reductive amination of cyclohexanone.

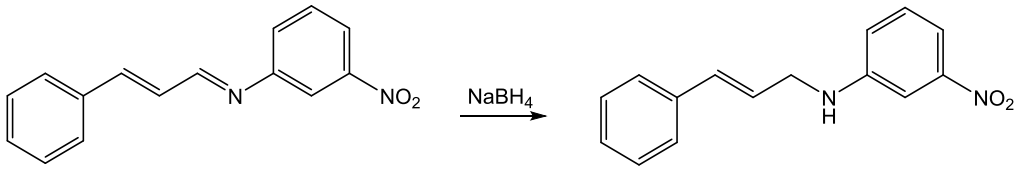

Scheme 2.5. Stoichiometric reduction of imines.

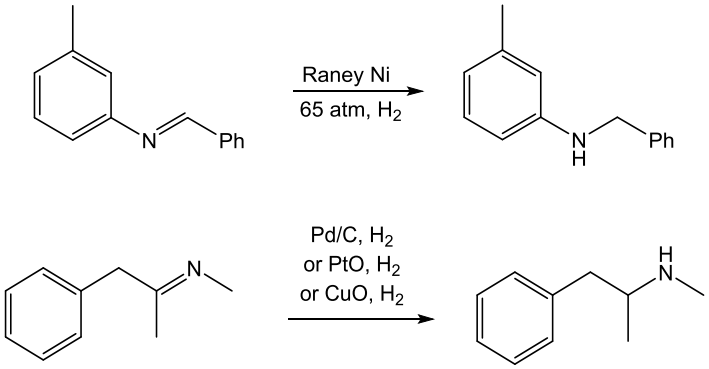

Scheme 2.6. Transition-metal reduction of imines.

Hydrogenation reactions play important roles in the chemical and pharmaceutical industries. In a batch reactor, the heterogeneous catalyst is suspended in a solution of substrate molecules while hydrogen gas is bubbled through. This approach has been used in many organic syntheses because of its simplicity. However, slow mass transfer between phases can be a disadvantage of this three phase reaction system. Furthermore, hydrogenation reactions are carried out at elevated pressures in an autoclave so as to increase the reaction rate. For reasons of safety and economy such high pressure batch reactors should be avoided in industry (Yoswathananont *et al.* 2005).

In combinatorial chemistry the reductive amination reaction is one of the most widely applied techniques and is an excellent method for generating diversity (Scheme 2.7).

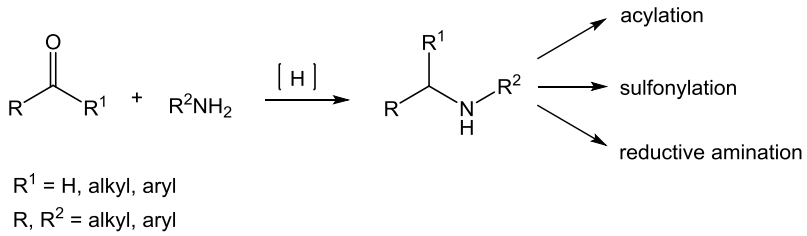

Scheme 2.7. Diversity from secondary amines prepared by reductive amination (Nicolaou *et al.* 2002).

Reductive amination is very well established reaction in organic chemistry (Kim *et al.* 1985; Bomann *et al.* 1995; Abdel-Magid *et al.* 1996). The main advantage of this reaction is the fact that amines, aldehydes and ketones are usually inexpensive and commercially available, and a variety of protocols for a wide range of reaction conditions and reagents, for both imine formation and reduction, are described in the literature (Wakchaure *et al.* 2007; Patil and Adimurthy 2013). The reductive amination of the carbonyl compounds is the most useful and important tool in the synthesis of amines. The reaction involves the initial formation of an intermediate carbinolamine, which dehydrates to form an imine (Scheme 2.8), the imine is then protonated to form an iminium ion. Reduction of the iminium ion produces the alkylated amine product. Literature is also available for direct reduction of the carbinolamine to the alkylated amine. Here, the reducing agent must reduce imines or iminium ions selectively over aldehydes or ketones, which means that the choice of reducing agent is critical for the success of the reaction (Abdel-Magid *et al.* 1996; Abdel-Magid and Mehrman 2006).

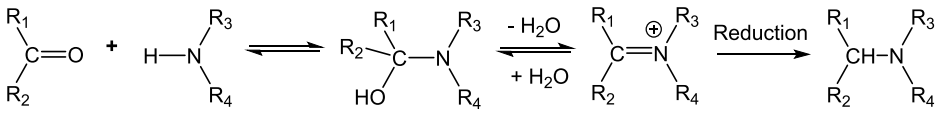

Scheme 2.8. General reductive amination pathway.

The reductive amination reaction is described as either a direct (without formation of the intermediate imine or iminium salt) or indirect (involving formation of the intermediate imine) reaction (Abdel-Magid *et al.* 1996). Many examples of reductive amination reagents, including sodium cyanoborohydride ($NaBH_3CN$) (Borch *et al.* 1971), borane-pyridine (Bomann *et al.* 1995; Burkhardt and Coleridge 2008), $Ti(OiPr)_4/NaBH_3CN$ (Bhattacharyya 1994), borohydride exchange resin (Yoon *et al.* 1993), Zn/AcOH (Mićović *et al.* 1991), $NaBH_4/Mg(ClO_4)_2$ (Brussee *et al.* 1990) have been reported for batch processing. Other reducing methods include catalytic hydrogenation (Freifelder 1978), sodium borohydride, iron pentacarbonyl and alcoholic KOH (Watanabe *et al.* 1974), BH_3-pyridine (Pelter *et al.* 1984; Bomann *et al.* 1995), and formic acid (March 1997). The over-alkylation can be circumvented by using less than one equivalent of the carbonyl compound (Szardenings *et al.* 1996). Most of these methods for the reduction of imines involve employing borohydride reagents, although a few general methods using main group Lewis acid catalysts have been also reported (Piers *et al.* 2000).

Abdel-Magid *et al.* (1996) published a procedure for direct reductive amination of aldehydes and ketones with a variety of aliphatic and aromatic amines using sodium triacetoxyborohydride [$NaBH(OAc)_3$] as a reducing agent. This borohydride reagent is mild and exhibits remarkable selectivity as a reducing agent.

Palladium on carbon (Pd/C) is the most widely used catalyst for the reductive amination reaction. Activated carbon has many advantages as a supporting material: it is stable in strongly acidic or alkaline conditions, cheap, and has a high surface area, due to its high porosity. Moreover, in the case of a noble metal catalyst, the precious metal can easily be recovered by burning off the carbon. Carbon comes from natural products such as peat or wood, however, so each batch of activated carbon may have different properties which may alter the effectiveness of the catalyst (Heinen *et al.* 2000).

The Pd/C catalysed reductive amination of aldehydes in methanol (MeOH) using formic acid (HCOOH), with ammonium formate (HCO_2NH_4) (Byun *et al.* 2007) as the *in situ* hydrogen donor and molecular hydrogen at 1 atm, has been reported in chloroform as a solvent at room temperature.

Xing *et al.* (2008) proposed a four-stage cyclic pathway for self-modulated highly chemoselective direct reductive amination (DRA) using a Pd/C catalyst (Scheme 2.9). The reaction scheme was as follows: HCl was released *in-situ* from the Pd/C catalyzed hydrodechlorination of $CHCl_3$ and partially poisoned the catalyst. The second stage involved the efficient condensation of an aldehyde and an amine, catalyzed by the HCl formed in step 1. During the third stage, the hydrogenation of benzylideneamine catalyzed by the "mild Pd/C catalyst" took place, which had a high selectivity to reduce the imine over the carbonyl compound. In the last stage, the benzylamine hydrochloride was formed when benzylamine captured an HCl molecule and the "mild Pd/C catalyst" was reactivated to be an "active Pd/C catalyst" again.

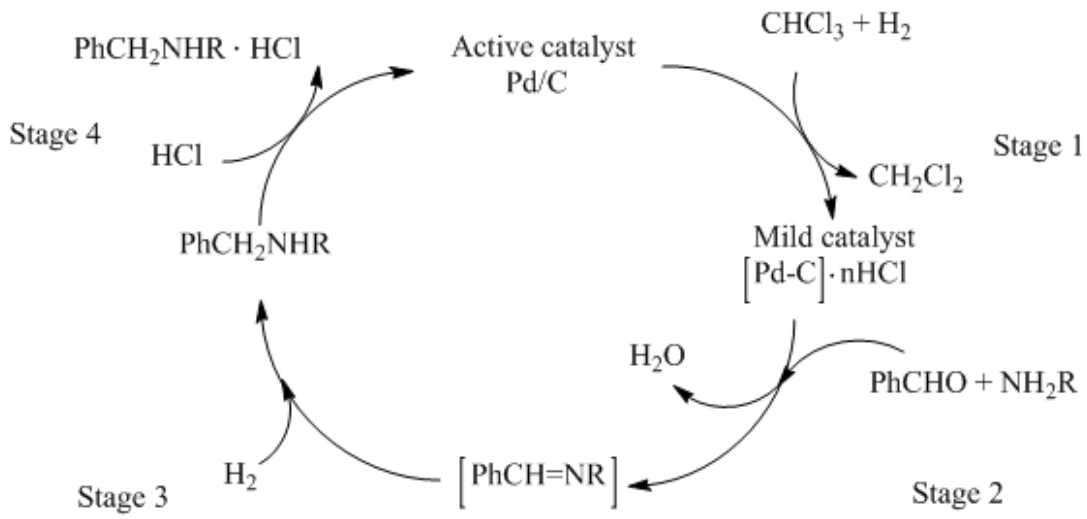

Scheme 2.9. A self-modulated system with four-stage cyclic pathway proposed by Xing *et al.* (2008).

Reductive amination is used in the synthesis of many drugs, but side reactions may occur, decreasing the selectivity towards the desired product. The process can be related to reversibility, compound/functional group incompatibility or over-reduction. Secondary amines are very often contaminated with the primary amine from the over-reduced product and debenzylation during the reduction of aryl imines (Saaby *et al.* 2005).

One of the most important issues in reductive amination reactions is controlling the selectivity, since the specification for the purity of amines is often very strict. The reaction intermediate (imine) is very reactive so many parallel and consecutive reactions can take place, decreasing the selectivity of the reductive amination of aldehydes or ketones. The desired product is then contaminated with a mixture of primary and tertiary amines, which are usually difficult to separate due to their very similar boiling points. The choice of the catalyst is crucial to achieve good selectivity in the reductive amination reaction (Gomez *et al.* 2002).

Dialkylation of amines is one of the side reactions which may occur in the reductive amination of aldehydes with primary amines. It is recommended to use 5 % or more molar excess of primary amine if dialkylation occurs (Abdel-Magid and Mehrman 2006).

In solvents such as MeOH, THF and DCE, the imine from aldehydes and primary amines is formed relatively quickly. Methanol is the preferred solvent for faster imine formation, which can then be reduced directly to the amine in a relatively short time, helping to avoid the formation of dialkylamines (Abdel-Magid and Mehrman 2006).

Another side-reaction which may occur in the reductive amination process is the formation of an alcohol from the unreacted carbonyl group. The hydrogenation of the carbonyl group adds to the loss of material and may disturb the reaction itself. Reaction conditions and the catalyst must be chosen carefully so the rate at which the carbonyl compound is being reduced to the alcohol remains relatively slow (Gomez *et al.* 2002).

In the reductive amination of benzaldehyde with dimethylamine and methyl isopropyl ketone with ethylamine, Pd/C produced less alcohol by-product than Pt/C *i.e.* it was a more selective catalyst. Birtill *et al.* (1998) has proposed a mechanism through carbinolamine intermediates in which the hydrogenolysis of the C-N bond of the carbinolamine provides for the formation of alcohol, which occurs more readily over Pt than over Pd. Even through Pt/C was much more active than Pd/C, the selectivity towards the desired secondary amine is higher for the latter than the former (Gomez *et al.* 2002).

The reductive amination reaction requires a selective reducing agent. The imine intermediate can be reduced using formic acid, certain metal hydrides or sodium cyanoborohydride etc., as stated before. Nevertheless, molecular hydrogen in the presence of a supported catalyst as the reducing agent is more environmentally friendly, and seems to be the ideal reducing agent for the reductive amination since water is the only by-product (Gomez *et al.* 2002).

In recent years, microreactors have begun to incorporate new practical preparative methods for organic transformations. Flow chemistry replaces traditional glassware with channels and cartridges that can be pre-packed with catalysts or immobilised reagents. Microreactors permit controlled mixing and precise temperature control while the reaction takes place (Baxendale *et al.* 2006a).

There are only a few reports on reductive amination of aldehydes or ketones by flow hydrogenation. Saaby *et al.* (2005) reported the reduction of imines to amines using an H-Cube® continuous-flow hydrogenation reactor, Cooper *et al.* (2011) presented reductive amination with secondary amines, Falus *et al.* (2011) reported reductive amination of ketones using an X-Cube™ flow reactor and $HCOONH_4$ as the *in situ* hydrogen donor, while Liu *et al.* (2012) presented a synthesis of a benzylpiperazine from piperazine and benzaldehyde *via* reductive amination using an H-Cube Midi™ reactor.

As a part of this project, a procedure for the continuous flow reductive amination of aldehydes or ketones with primary amine into secondary amine with high purity of the product is required for the next step of the overall process.

This chapter describes the reductive amination of aldehydes with the extension to ketones in the structured compact reactor developed at the University of Bath and the commercially available X-Cube^{TM} flow reactor manufactured by ThalesNano. The reaction was investigated in detail from the point of view of the optimisation of liquid and gas flow rates, pressures, temperatures and reagent concentrations. The secondary amines synthesised via reductive amination of aldehydes (ketones) are a starting point for further studies into the hydrogenolysis of secondary amines in Chapter 3 and Chapter 6.

2.2. Experimental

2.2.1. Pd/C catalyst and reagents

The Pd/C catalyst (Pd 10% by weight) was prepared by impregnation of the mesoporous microspherical synthetic activated carbon (AC) support, with an average particle size of 155 μm supplied by Mast Carbon Ltd., Guildford, UK. In a typical Pd/C catalyst synthesis procedure, 1.0 g $PdCl_2$ was dissolved in 2 mL of concentrated hydrochloric acid and 10.0 mL distilled water. This mixture was kept at 353K under stirring for 30 min. Then sodium acetate (17.5 g in 50 mL water) and AC (~5.2 g) were added and kept at 353K for 3 hours. Aqueous sodium borohydride solution (3 × 10 mL) was added dropwise to the slurry and stirred for 1.5 h at 353K. Then, the slurry was left for 18 hours at room temperature under gentle stirring. Following impregnation, the suspension was filtered and washed with distilled water, to pH 7. The catalyst was then dried under vacuum at 308K for 22 hours and stored in a sealed container before use. The loading capacity of the compact reactor is *ca.* 0.45 g of catalyst per 3 × 3 × 100 mm channel.

All chemicals used in this study were purchased from Acros Organics, Sigma-Aldrich, Fluka or Lancaster and were used without further purification.

2.2.2. Structured compact reactor

The structured compact packed-bed reactor shown in Figure 2.1 is an essential part of the continuous catalytic rig which was built during the first year of the project.

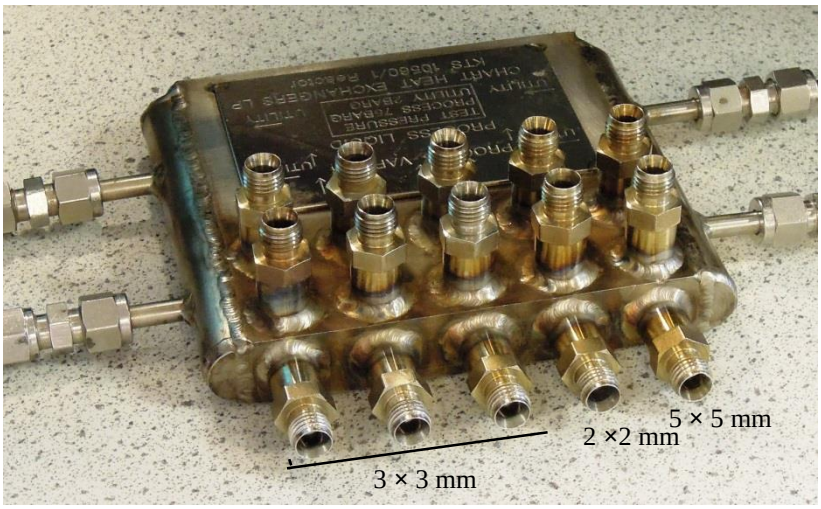

Figure 2.1. Structured compact reactor.

The structured multichannel reactor has five channels. The reaction channels are arranged in parallel between two heat exchangers and have a length of 100 mm and a square cross-section with three different sizes: 2mm × 2mm, 3mm × 3mm (3 channels) and 5mm × 5mm. Liquid and gas feed lines can be connected to the channels with Swagelok® fittings. The micro-heat exchangers are located above and below all the reaction channels to ensure an even temperature field for each channel. The structured compact reactor also has static mixers located above the reaction channels: these are used for premixing and preheating liquid and gas reactants before introducing them into the reaction channels. The reactor was constructed using thin stainless steel shims, with an operating pressure up to 75 bar. A schematic diagram of the structured multichannel reactor is shown in Figure 2.2. Further information about the reactor, *i.e.* design concepts and hydrodynamic properties, is available elsewhere (Plucinski *et al.* 2005; Bavykin *et al.* 2005).

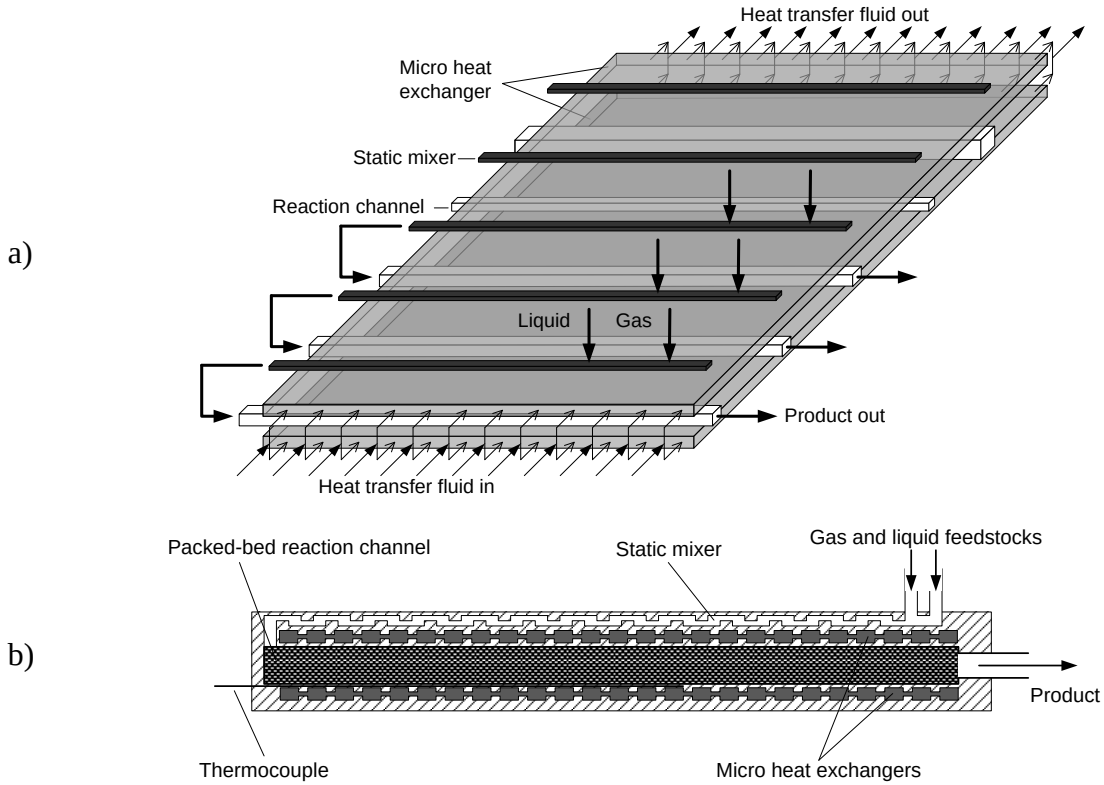

Figure 2.2. Schematic diagram of the structured compact reactor: (a) general view and (b) cross-section of a channel. Adapted from Fan *et al.* (2009).

2.2.3. Continuous catalytic rig and procedure for continuous experiments

The continuous catalytic rig is shown in Figure 2.3 and the schematic diagram in Figure 2.4. The main element of the system is the packed-bed (PB) structured multichannel compact reactor. Liquid reagents were introduced into the feed vessel using a syringe after mixing. A HPLC pump (Kontron, No 422M) was used to pump the feed through the reaction channels. The product was collected in another vessel *via* a low dead-volume six-way valve with a 250 µl sample loop. A re-circulating bath was used to control the temperature in the system. The mineral oil was recycled through the micro-heat exchangers. A back pressure regulator (BPR) (Brooks, No F00574/001) was used to control the operating pressure and a differential pressure transducer (DPT) (Bronkhorst®, No M9201747B) was used to monitor the pressure drop across the reactor. The hydrogen gas was supplied to the reaction channels

using a mass flow controller (MFC) (Brooks, No F00562/001). Thermocouples were connected at each of the two ends of the structured microreactor to control the temperature inside the microreactor.

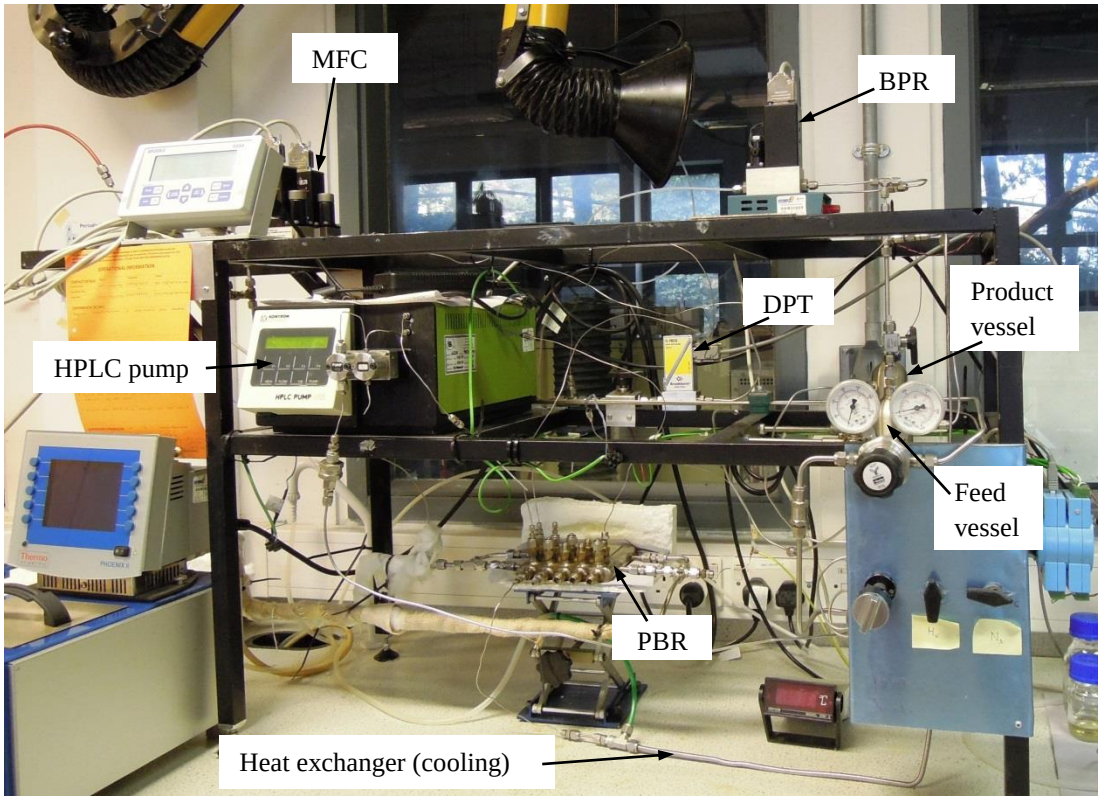

Figure 2.3. The continuous catalytic rig with the structured multichannel compact reactor.

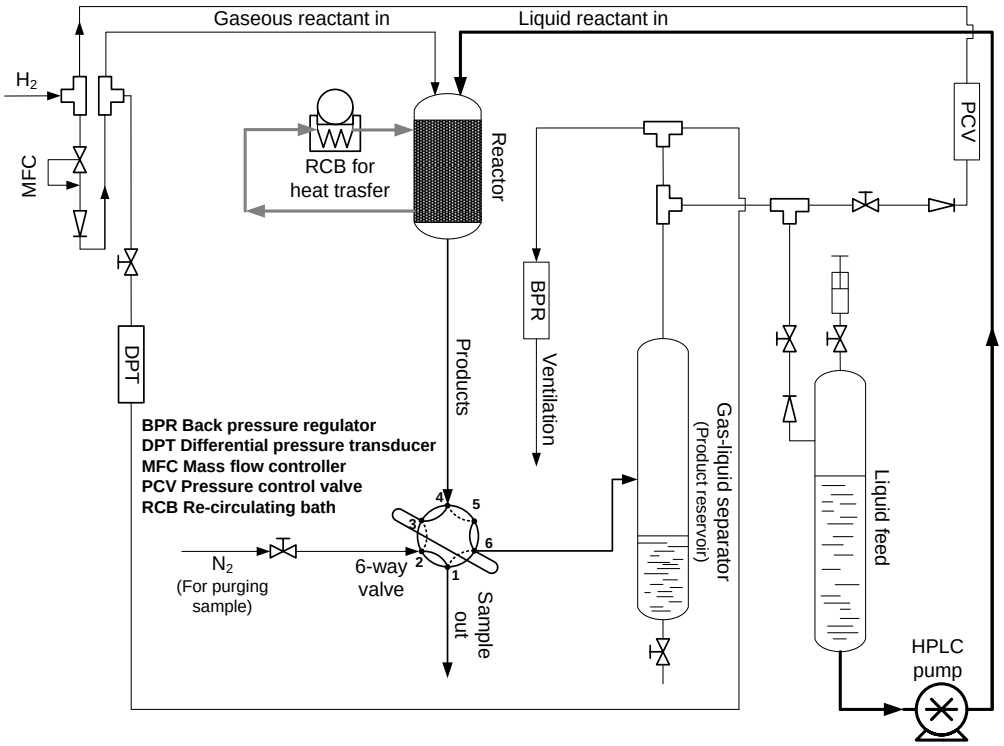

Figure 2.4. Schematic diagram of the catalytic rig (Plucinski *et al.* 2005; Bavykin *et al.* 2005).

2.2.4. X-Cube™ flow reactor

The X-Cube™ (Figure 2.5) is a high-pressure continuous flow reactor manufactured by ThalesNano. According to the manufacturer, reactions can be performed under inert conditions, temperatures up to 473K (intervals of 278K), pressures up to 150 bar (at intervals of 5 bar) and flow rates up to 3 mL min^{-1} (at intervals of 0.1 mL min^{-1}). The system can work with or without the introduction of gases from an external source. An HPLC pump passes the reagents/solvents through the system and prepacked catalyst/reagent cartridges (CatCarts), where the actual reaction takes place and the product can be collected into the vial. The CatCart technology allows the use of air-sensitive catalyst/reagents without the need for an inert atmosphere.

According to the manufacturer, the X-Cube™ flow reactor has a number of advantages:

1. Substrates can be rapidly heated up due to the small-volume reaction line;
2. Exothermic or unstable reactions can be performed in a safer way;
3. The reaction can take place in minutes instead of hours due to the rapid heat and mass transfer from the small volume reaction line to the high surface area catalysts;
4. Catalysts/reagents are confined to cartridges for easier handling and work-up procedure;
5. Due to the versatility of the reactor it is possible to perform multistep reactions:
    a. dual cartridge system;
    b. several mixer units;
    c. dual pump system;
    d. flexible configuration;
6. Gas can be introduced into the system from an external cylinder *via* the gas inlet on the back of the instrument, allowing tri-phasic reactions to be performed;
7. Reaction parameters can be adjusted using a touch-screen interface.

Figure 2.5. The X-Cube^{TM} flow reactor.

2.2.5. Analysis techniques

Gas chromatography (GC, Varian CP-3800) was used to analyse reaction substrates/ intermediates/ products using a polar capillary column (CP Sil - 8CB). All samples collected during the experiments were analysed without further purification.

Pure compounds were used to determine the retention times of each component. Standard samples of analytes with known concentrations were prepared for calibration. The calibration curves were obtained by plotting the ratio of the analyte signal (peak area) as a function of the analyte concentration of the pure compound. For the model reaction, *i.e.* reductive amination of hydrocinnamaldehyde with α-methylbenzylamine, calibration curves are presented in Figure 2.6 for

hydrocinnamaldehyde, Figure 2.7 for α-methylbenzylamine and Figure 2.8 for (1-phenylethyl)(3-phenylpropyl)amine.

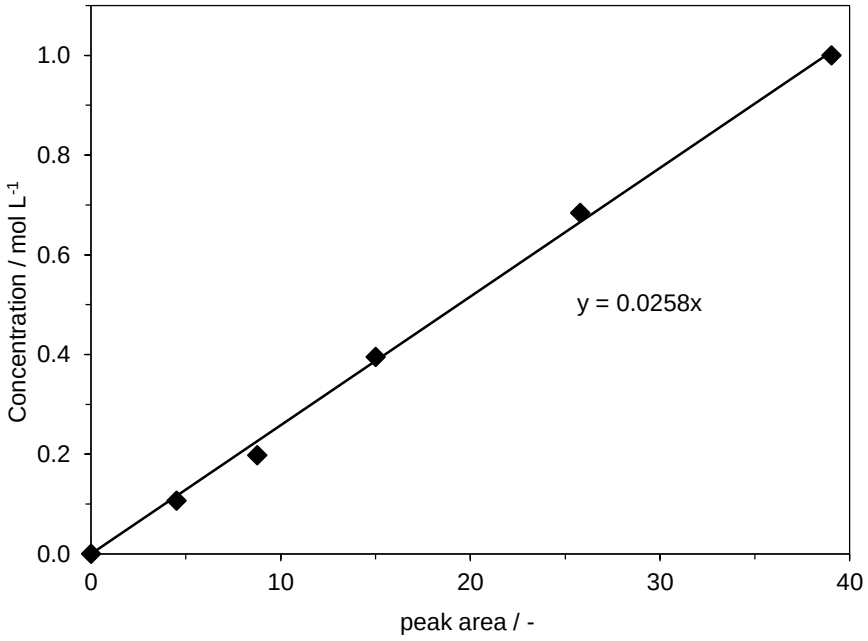

Figure 2.6. Calibration curve for the GC analysis of hydrocinnamaldehyde.

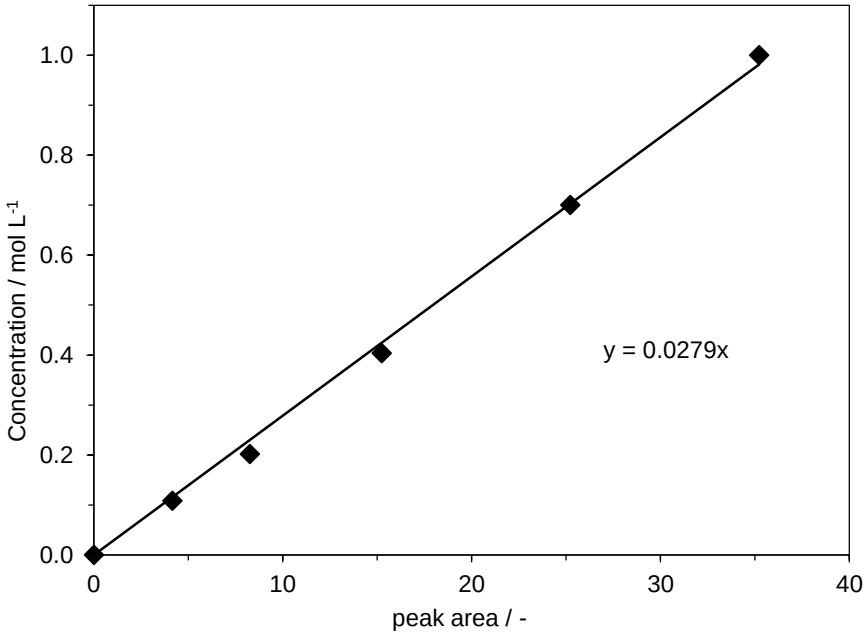

Figure 2.7. Calibration curve for the GC analysis of α-methylbenzylamine.

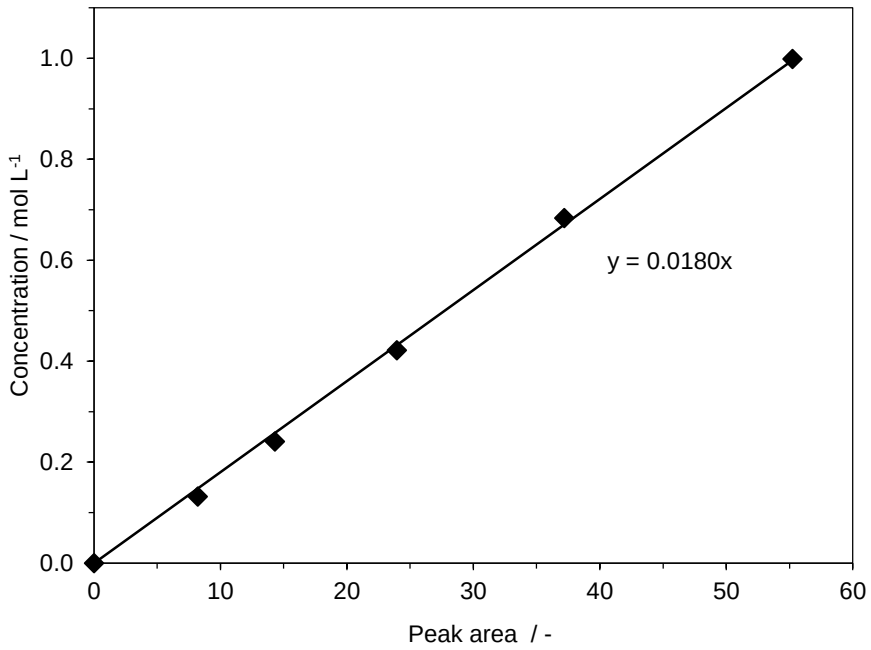

Figure 2.8. Calibration curve for the GC analysis of (1-phenylethyl)(3-phenylpropyl) amine.

^{1}H NMR/ and ^{13}C NMR analysis spectra were run in deuterated (≥99.5%) chloroform ($CDCl_3$) purchased from Fluorochem on a Bruker Avance 400 (400MHz) at GlaxoSmithKline for the determination of the chemical structures of the synthesised products. Results are presented in the Appendix I.

Mass spectrometry analysis was performed using a microTOF electrospray time-of-flight (ESI-TOF) mass spectrometer (Bruker Daltonik, GmbH, Bremen, Germany) coupled to an Agilent 1200 LC system (Agilent Technologies, Waldbronn, Germany). Results are presented in the Appendix I.

Products were purified by column chromatography (SiO_2, 20% NH_3 in MeOH/ DCM) using a Biotage SP HPFC Flash Purification System at GlaxoSmithKline (Stevenage, UK).

A Micrometric ASAP 2020 analyser was used to perform the gas adsorption analysis using N_2 as a probing gas for obtaining the nitrogen adsorption isotherms of the carbon support and the catalyst (see Chapter 3, section 3.3.1). The following parameters were obtained from the analysis:

- the specific surface area (S_{BET});
- average pore diameter (d_{ave});
- pore volume (V_p).

2.3. Results and discussion

2.3.1. Continuous catalytic rig with multichannel packed-bed reactor

The optimisation of flow conditions for the reductive amination of aldehydes was systematically investigated by varying liquid and gas flow rates, pressure, temperature and reagent concentration. Results obtained for the reductive amination of aldehydes in a continuous catalytic rig (Figure 2.3, see Chapter 2, section 2.2.3) with the structured compact reactor developed at the University of Bath are presented in the next section of this chapter.

2.3.1.1. Imine formation

Before discussion of the obtained results, it is worthwhile to discuss the reaction pathway for the synthesis of secondary amine from the reductive amination of aldehydes.

Imines are formed by the condensation of amines and aldehydes or ketones with loss of water (Scheme 2.10). The classic methods for water removal are azeotrope formation or trapping with molecular sieves. In combinatorial chemistry, therefore, a number of different approaches have been developed for imine formation to support these techniques (Wakchaure *et al.* 2007; Patil and Adimurthy 2013).

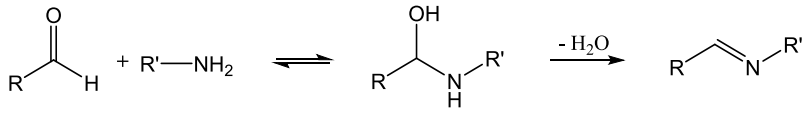

Scheme 2.10. Equilibrium in the synthesis of imines from an aldehyde and an amine (Patil and Adimurthy 2013).

In this study no additives were used to remove the water formed during the imine formation.

The reductive amination of hydrocinnamaldehyde with α-methylbenzylamine over Pd/C catalyst was chosen as a model reaction (Scheme 2.11).

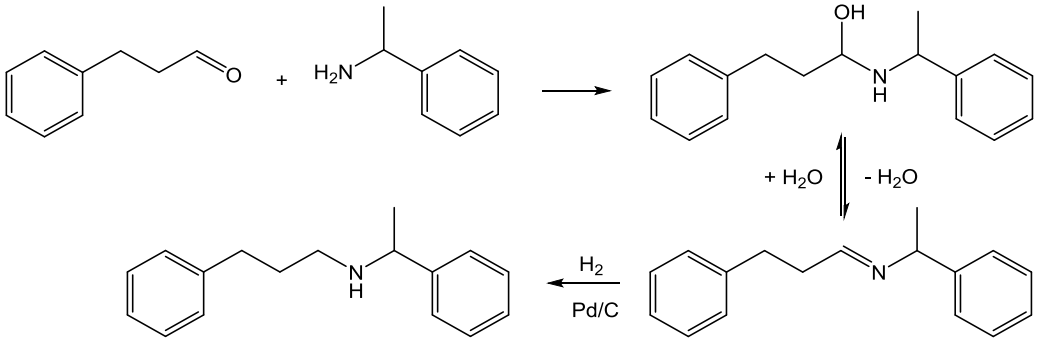

Scheme 2.11. Overall steps in reductive amination of hydrocinnamaldehyde.

The first step of this reaction is the formation of an imine (Scheme 2.12).

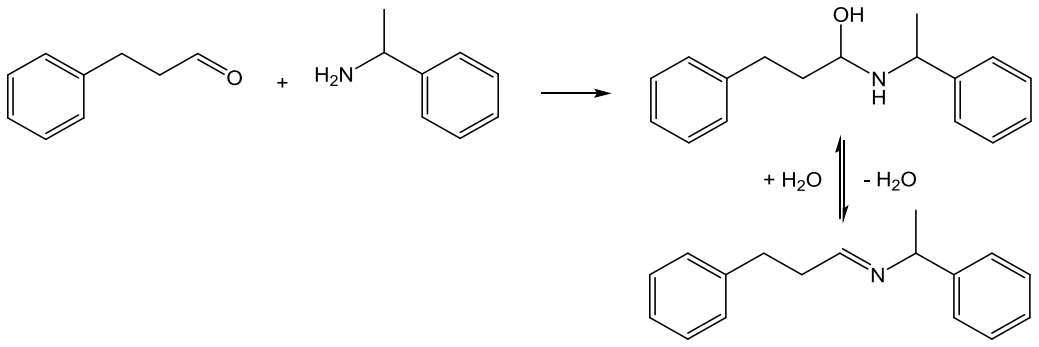

Scheme 2.12. Imine formation for the model reductive amination reaction of hydrocinnamaldehyde with α-methylbenzylamine.

This step is very fast and is a non-catalytic reaction. The imine is formed to 97 and 99% after 5 and 15 minutes of reagent mixing, respectively (Figure 2.9).

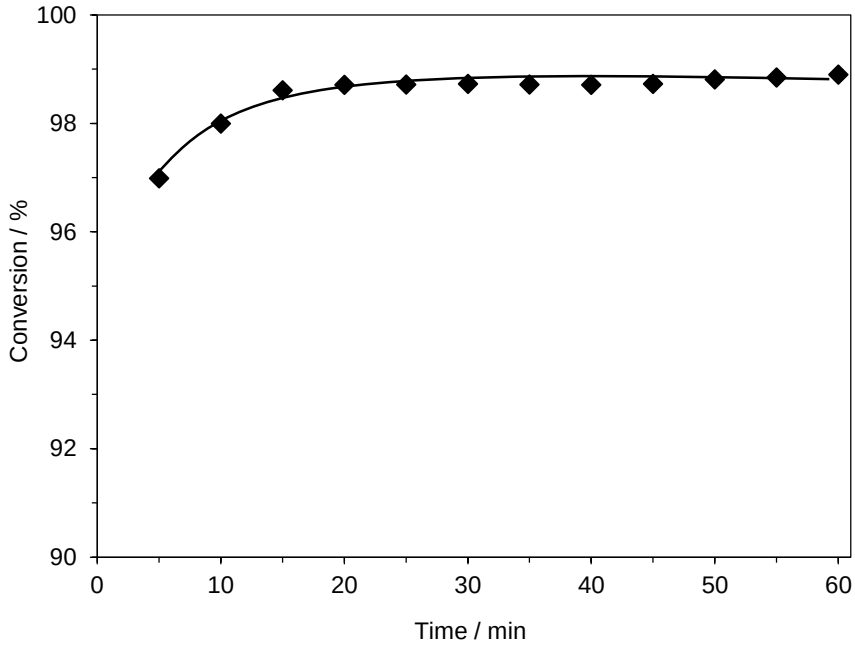

Figure 2.9. Imine formation as a function of reagent mixing time.

It is worth noting that the residence time in the static mixer part of the reactor was long enough to complete the imine formation.

The conversion was monitored using GC analysis. After mixing the reagents for 10 minutes, the solution was introduced to the feed vessel in order to perform the reductive amination reaction.

All further calculations (conversion, selectivity, yield and rate of product formation) are based on the imine not on the carbonyl compound (aldehyde), since the imine formation step is a very fast, homogeneous, noncatalytic reaction in the liquid phase.

2.3.1.2. Effect of liquid flow rate

Figure 2.10 shows the product concentration as a function of time-on-stream at two liquid flow rates, 1.0 and 2.0 mL min^{-1}. The product concentration initially decreased with time followed by a plateau after *ca.* 12 minutes time-on-stream, indicating that a steady state was achieved in the reactor 12 minutes after introducing the reagents. At a higher liquid flow rate the product concentration was lower due to the decrease of the residence time in the reaction channel.

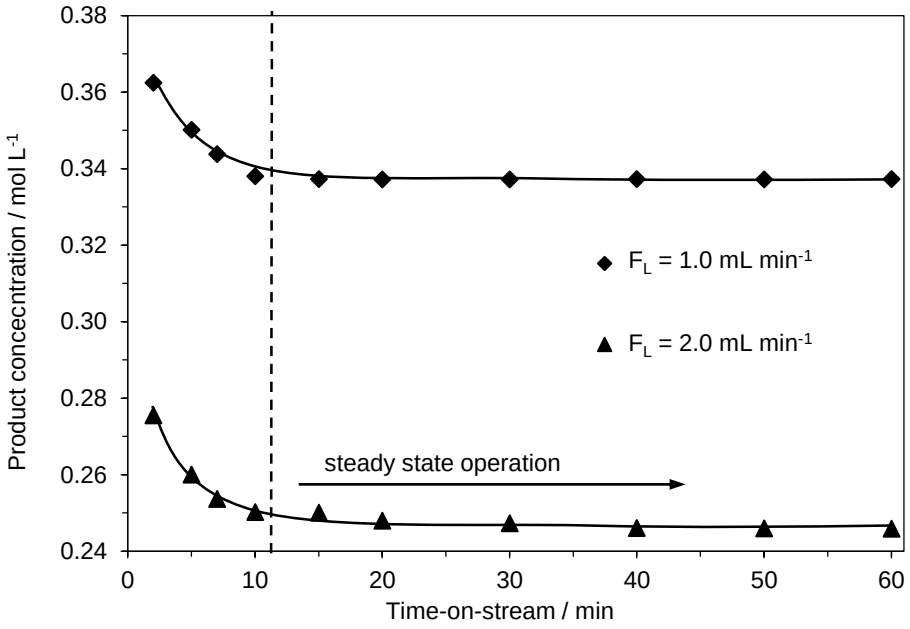

Figure 2.10. Product concentration in the outlet of the reactor as a function of time-on-stream. P_T = 8 bar, F_G = 21.0 mL (STP) min^{-1}, $C_{S,0}$ = 0.4 mol L^{-1},T = 298 K.

For the substrate concentration used in this study, *i.e.* $C_{S,0}$ = 0.4 mol L^{-1}, a 100% conversion of the imine was achieved in a single pass through a fully loaded 3 mm × 3 mm × 100 mm channel with 10% Pd/C under mild operation conditions, *i.e.* 8 bar of total pressure, temperature of 298K, 21.0 mL (STP) min^{-1} of hydrogen flow rate and 0.5 mL min^{-1} of liquid flow rate. A lower conversion of imine was measured for higher liquid flow rates due to the reduction of the liquid phase residence time in the reaction channel (Figure 2.11).

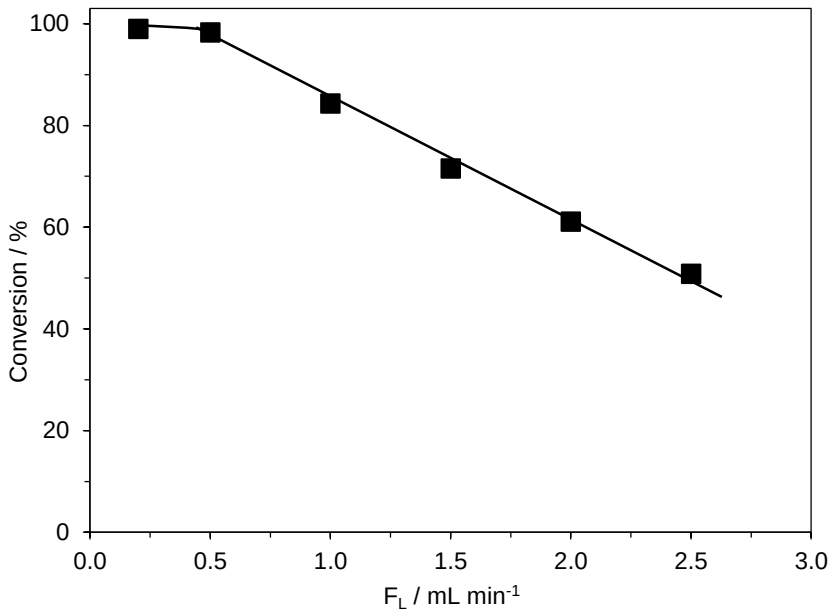

Figure 2.11. Influence of liquid flow rate on imine conversion during reductive amination of hydrocinnamaldehyde with α-methylbenzylamine reaction.
P_T = 8 bar, F_G = 21.0 mL (STP) min^{-1}, $C_{S,0}$ = 0.4 mol L^{-1}, T = 298 K.

Figure 2.12 shows the influence of liquid flow rate on the overall rate of the product formation (Equation 2.1). The rate of product formation depends strongly on the liquid flow rate up to 1.5 mL min^{-1}. With further increases of the liquid flow rate, however, only a very slight increase in the overall rate of product formation was noticed. The increase in the overall rate of product formation with liquid flow rate highlights the influence of mass transfer for the liquid flow rate up to 1.5 mL min^{-1}. A further increase in liquid flow rate indicates that the reaction is almost independent of the external mass transfer. Higher liquid flow rates promote the transition of the rate-limiting step from mass transfer to the kinetic regime.

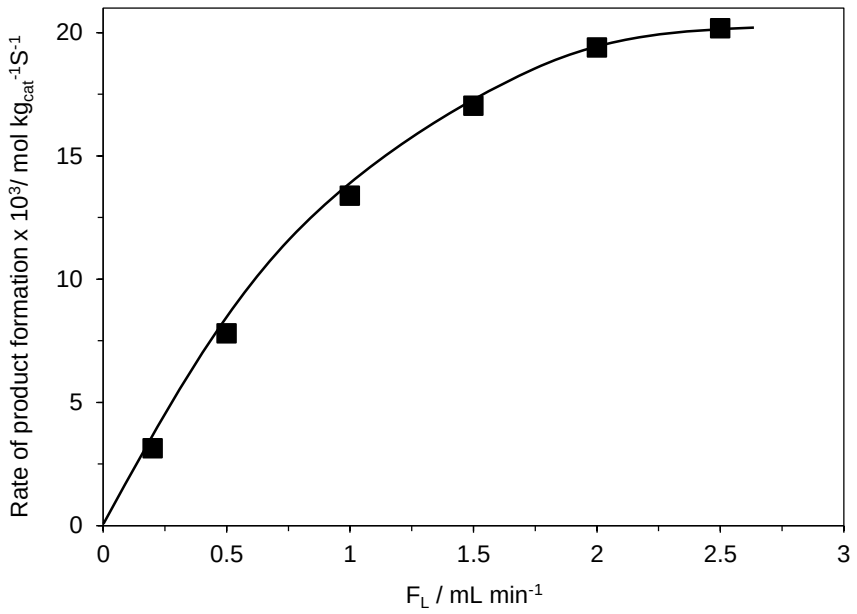

Figure 2.12. Influence of liquid flow rate on the rate of product formation. P_T = 8 bar, F_G = 21.0 mL (STP) min^{-1}, $C_{S,0}$ = 0.4 mol L^{-1}, T = 298 K, (1 mL min^{-1} = 6.67 m^3 m^{-2} h^{-1})

The rate of product formation (R_A) was calculated based on the following equation:

$$(R_A) = \frac{F_L C_p}{m_{cat}} \qquad (2.1)$$

where:

(R_A) rate of product formation (mol kg_{cat}^{-1} s^{-1});
F_L volumetric flow rate of liquid phase (L s^{-1});
C_p exit concentration of product (mol L^{-1});
m_{cat} mass of catalyst in an individual channel (kg).

It is worth noting that the rate of product formation is not a rate of reaction; it is an integral value of the rate of reaction (integral reactor) for the entire length of the reactor.

The rate of product formation is related to the Turn Over Frequency (TOF) (Bavykin *et al.* 2005):

$$TOF = M_{w,Pd}(R_A) \qquad (2.2)$$

where:

TOF Turn Over Frequency (s^{-1});

$M_{w,Pd}$ atomic weight of palladium (kg mol^{-1});

(R_A) rate of the product formation (mol $kg_{cat}^{-1} s^{-1}$).

2.3.1.3. Effect of hydrogen flow rate

Figure 2.13 shows the product concentration as a function of hydrogen flow rate at 298K, and at 1 and 6 bar of total pressure, respectively. At low gas flow rates (F_G < 8 mL (STP) min^{-1}), the concentration of (1-phenylethyl)(3-phenylpropyl)amine depends on the hydrogen flow rate and is therefore limited by hydrogen supply. The product concentration was found to be almost independent for a higher range of gas flow rates (F_G > 8 mL (STP) min^{-1}). The hydrogen supply line presented in Figure 2.13 represents the theoretical stoichiometric volumetric flow rate of hydrogen for a given product concentration.

The independence of the product concentration from the gas flow rate excludes the possibility of any influence of external mass transfer on the reaction and indicates that the reaction could be limited by internal diffusion or by the chemical reaction itself.

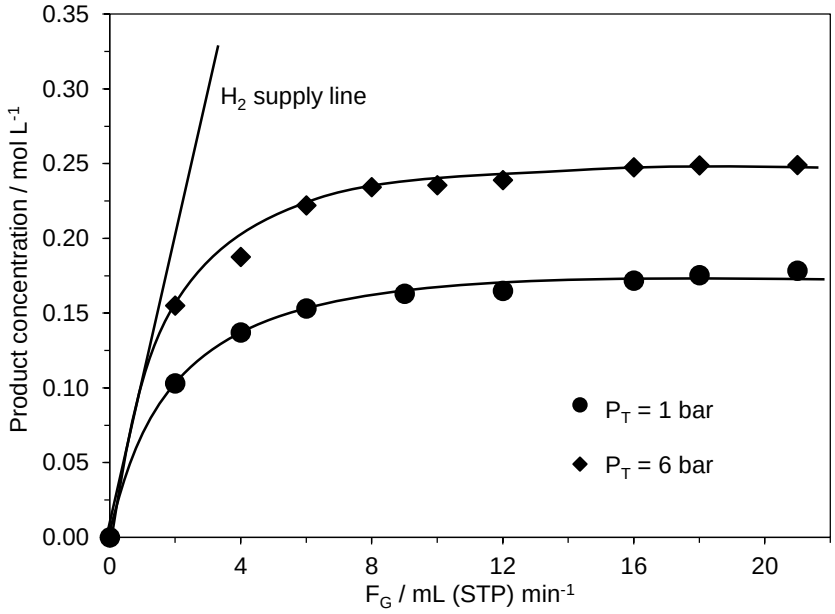

Figure 2.13. Product concentration as a function of hydrogen flow rate. F_L = 2.0 mL min^{-1}, $C_{S,0}$ = 0.4 mol L^{-1}, T = 298 K.

2.3.1.4. Effect of operating pressure and concentration

The influence of the total pressure was studied at a constant liquid flow rate of 2.0 mL min^{-1} to avoid mass transfer limitations on the product concentration (Figure 2.14). The reaction was investigated at two temperatures: 298K and 323K.

The product concentration increased from 0.18 mol L^{-1} to 0.25 mol L^{-1} with an increase in the pressure from 1 to 6 bar at the temperature of 298K. Further increases in pressure increased the product concentration at the exit from the reactor to 0.27 mol L^{-1} at 10 bar.

At 323K, the product concentration increased slightly as pressure increased, *i.e.* 0.36 mol L^{-1} at 1 bar and 0.38 mol L^{-1} at 6 bar. Further increases in pressure increased the product concentration to 0.39 mol L^{-1} at 8 and 10 bar.

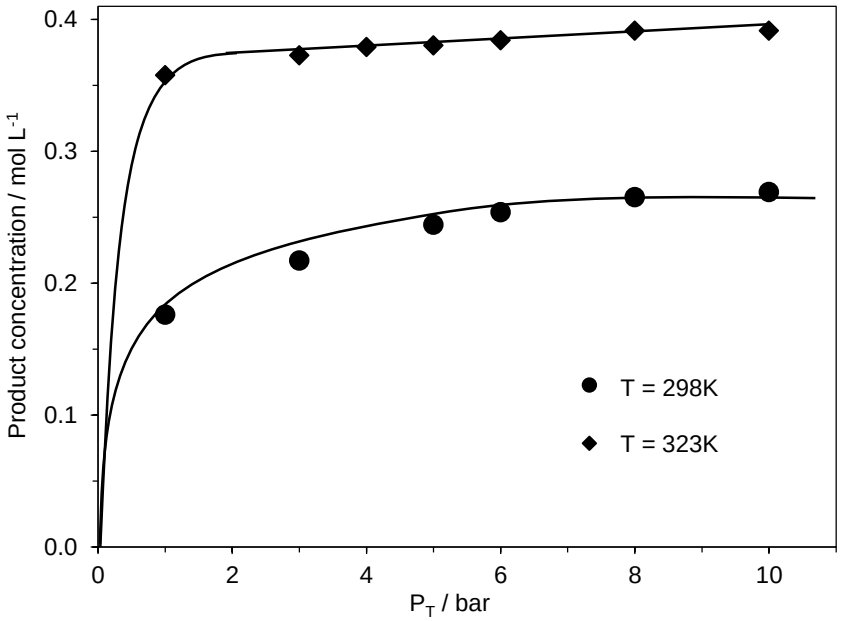

Figure 2.14. Effect of the total pressure on the product concentration.
F_G = 21.0 mL (STP) min^{-1}, F_L = 2.0 mL min^{-1}, $C_{S,0}$ = 0.4 mol L^{-1}.

The influence of the initial reagent concentration on the product concentration is presented in Figure 2.15. The experiments performed in this section were all run on the same catalyst bed, which could suggest that the catalyst was not deactivated during the reaction. Furthermore, the assumption was made that no leaching of palladium took place (see Chapter 2, section 2.3.1.6 - catalyst stability).

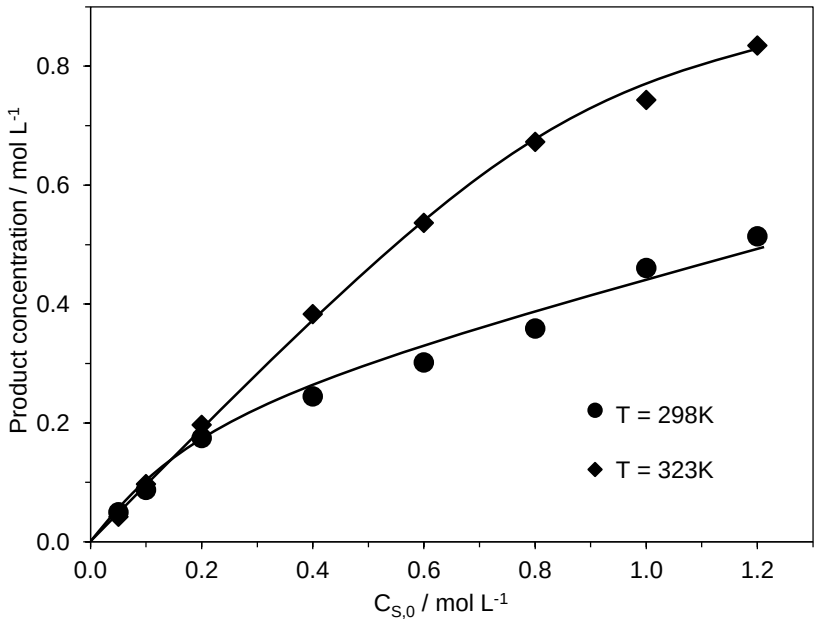

Figure 2.15. Effect of the reagent initial concentration on the product concentration
P_T = 8 bar, F_G = 21.0 mL (STP) min^{-1}, F_L = 2.0 mL min^{-1}.

The selectivity remained 100% for all the experiments, apart from the one performed at 323K and 0.05 mol L^{-1} of initial concentration reagents. Under these reaction conditions, the selectivity for the secondary amine decreased to 84%. This is due to the hydrogenolysis of (1-phenylethyl)(3-phenylpropyl)amine and, as a result, 16% of 3-phenylpropan-1-amine was formed. No tertiary amine was found to be formed under these reaction conditions.

2.3.1.5. Effect of reaction temperature

Figure 2.16 shows the influence of temperature on the imine conversion and the yield of (1-phenylethyl)(3-phenylpropyl)amine. As the temperature was increased from 298K to 333K the total conversion increased from 61% to 97%. Further increases in the reaction temperature, however, *i.e.* T ≥ 363K, decreased the selectivity of the reaction (Table 2.1), indicating that the optimal temperature was 333 K.

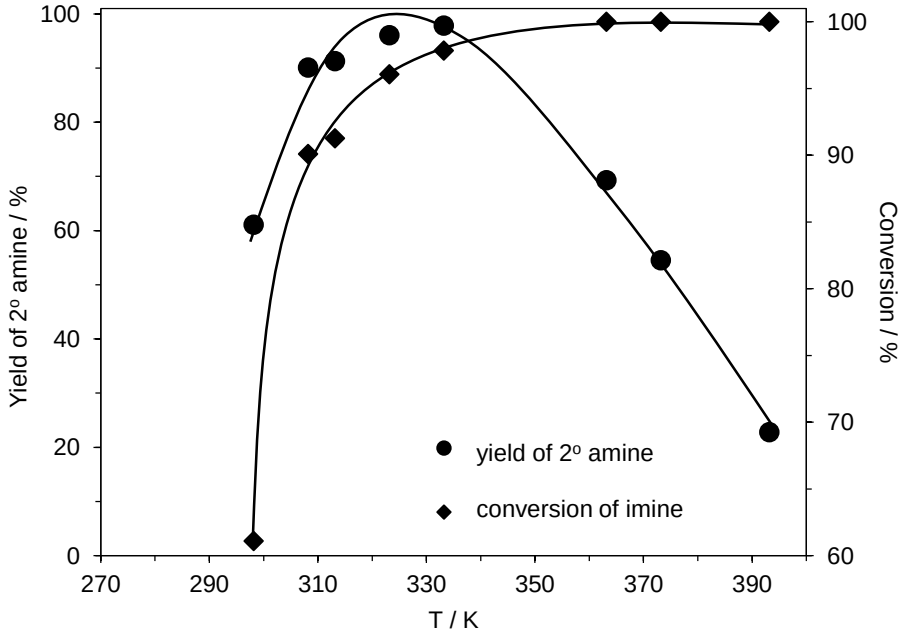

Figure 2.16. Influence of the reaction temperature on the conversion of imine. P_T = 8 bar, F_G = 21.0 mL (STP) min^{-1}, F_L = 2.0 mL min^{-1}, $C_{S,0}$ = 0.4 mol L^{-1}.

Table 2.1. Influence of temperature on the selectivity of the reductive amination of hydrocinnamaldehyde at higher temperatures.

Temperature	**Selectivity[a]**		
K	**3º amine**	**2º amine**	**1º amine**
363	19	69	12
373	20	55	25
393	29	23	48

[a] Selectivity was determined by GC analysis

It is possible that at higher temperatures ($T \geq 363K$) the imine was being hydrolysed back to the aldehyde and amine, since the imine formation step is an equilibrium reaction.

The most likely tertiary amine formation pathway is the reduction of hydrocinnamaldehyde which reacts with the α-methylbenzylamine. It is then cleaved to form 3-phenyl-1-propylamine, which subsequently reacts with the hydrocinnamaldehyde and is reduced forming the secondary amine. The secondary amine then reacts with another equivalent of hydrocinnamaldehyde and is reduced again to give the tri(phenylpropyl)amine as the tertiary amine (Scheme 2.13).

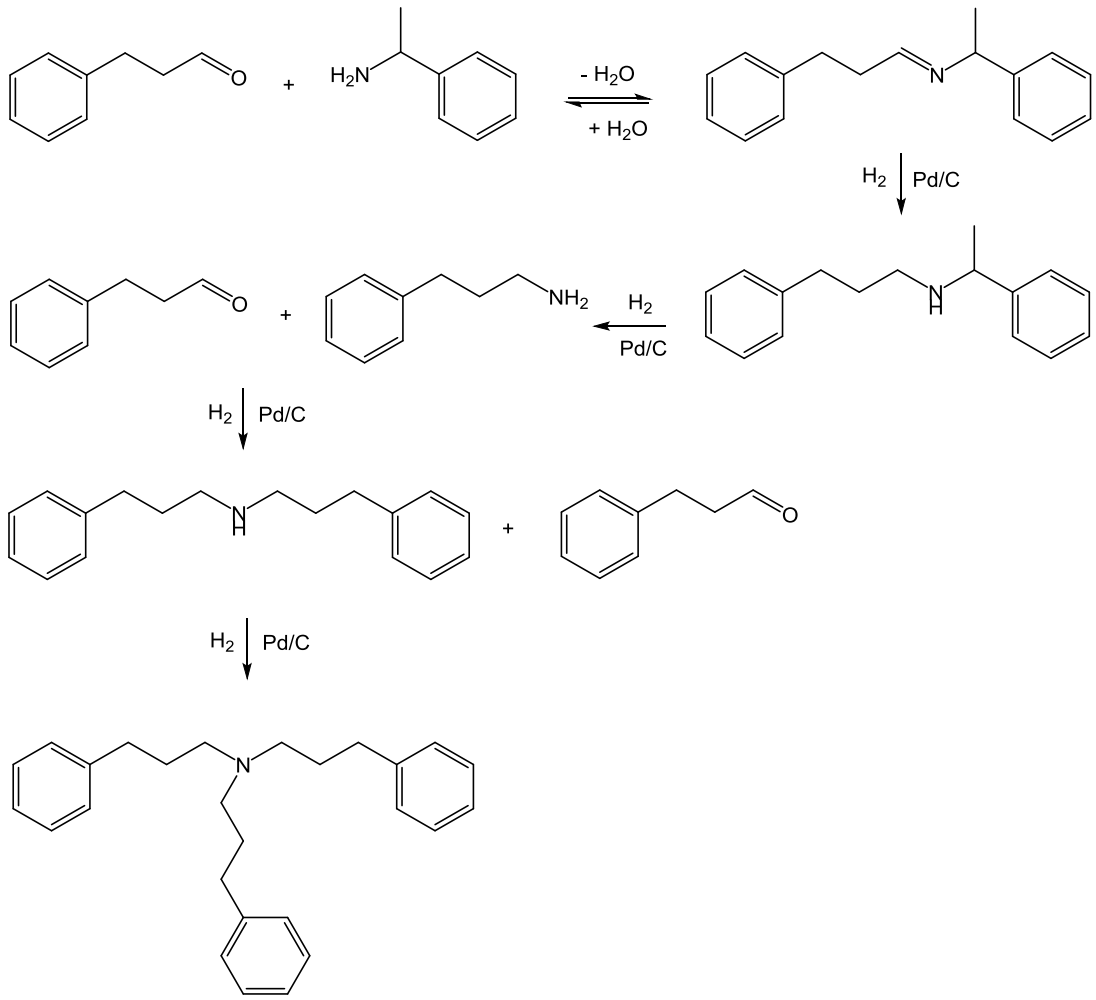

Scheme 2.13. Proposed pathway for the tertiary amine formation.

The dimerization of α-methylbenzylamine, which reacts with hydrocinnamaldehyde, is also possible, but the 3-phenyl-1-propylamine formed *via* hydrogenolysis of 2º amine is less hindered than the α-methylbenzylamine and so is more likely to form the tri(phenylpropyl)amine.

The positive effect of the temperature on the imine conversion is in the range of 298K - 333K. The temperature dependence of the imine conversion is shown in Figure 2.17. As the temperature was increased from 298K to 333K the total conversion of the imine was observed to increase significantly, *e.g.* at 0.4 mol L^{-1}, the total conversion increased from 61% to 97%. In the temperature range from 323K to 333K,

however, the total conversion remained the same, *ca.* 98%. At higher initial reagent concentrations (0.8 mol L^{-1}) conversion was higher with increasing temperature.

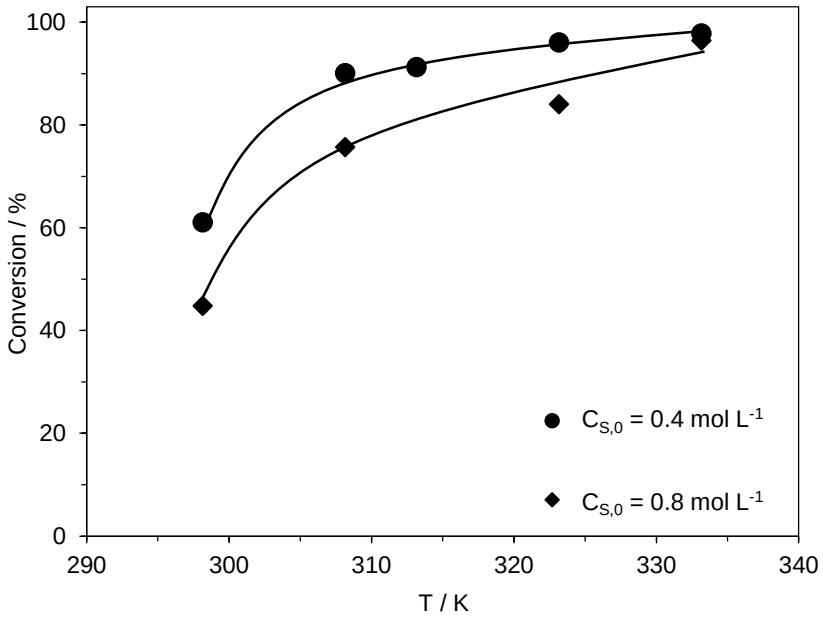

Figure 2.17. Influence of the reaction temperature on the conversion of imine to secondary amine. P_T = 8 bar, F_G = 21.0 mL (STP) min^{-1}, F_L = 2.0 mL^{-l} min^{-1}.

2.3.1.6. Catalyst stability

The time-on-stream experiments were carried out in the 3 × 3 × 100 mm reactor channel, which was fully loaded with the catalyst to evaluate the activity of 10% Pd/C. The conversion of imine and selectivity to secondary amine remained almost constant in each run (Figure 2.18). Each experiment was carried out for 13 hours. After each experiment, the system was washed with solvent (MeOH) to prevent any blockage in the line from residue caused by the reactants.

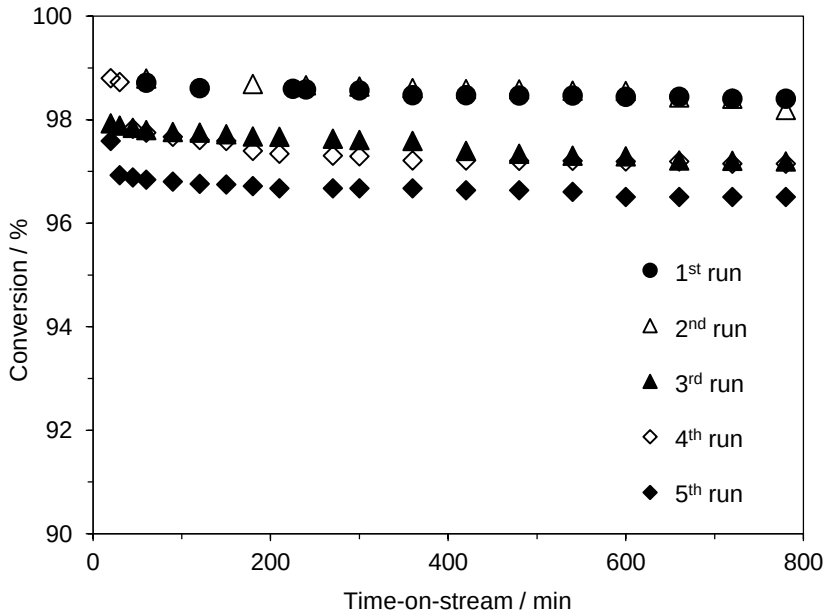

Figure 2.18. Imine conversion as a function of time-on-stream. P_T = 8 bar, F_G = 21.0 mL (STP) min^{-1}, F_L = 0.5 mL min^{-1}, $C_{S,0}$ = 0.4 mol L^{-1},T = 298 K.

For the first two runs, over 13 hours of continuous flow, the average conversion of imine into 2º amine remained constant: *ca.* 99%. The third and fourth run, meanwhile, showed a slight decrease in conversion. Further decreases in the conversion were observed in the fifth run, with an average conversion of *ca.* 97%. The overall decrease in conversion between the first and fifth run was very small, however (*ca.* 2%), which suggests that the Pd/C catalyst synthesised for this work had a high activity and good stability.

In order to evaluate the catalyst deactivation, Figure 2.19 shows the relationship between logarithmic Turn Over Frequency (TOF) and catalyst life time. The TOF was calculated using the following equation:

$$TOF = \frac{C_{2^o} F_L M_{w,Pd}}{m_{Pd}} \qquad (2.3)$$

where:

TOF Turn Over Frequency (h^{-1});

C_{2^o} product (2º amine) concentration in the outlet of the reactor (mol L^{-1});

F_L volumetric liquid flow rate of the reactant (L h^{-1});

$M_{w,Pd}$ atomic weight of palladium (g mol^{-1});

m_{Pd} mass of metallic palladium on the catalyst (g).

The rate of catalyst deactivation was calculated using the following equation (Bavykin *et al.* 2005):

$$TOF = TOF_{(0)} \times e^{-k_d t} \qquad (2.4)$$

where:

TOF Turn Over Frequency (h^{-1});

$TOF_{(0)}$ Turn Over Frequency at time zero;

k_d catalyst deactivation rate constant (h^{-1});

t catalyst life time (h).

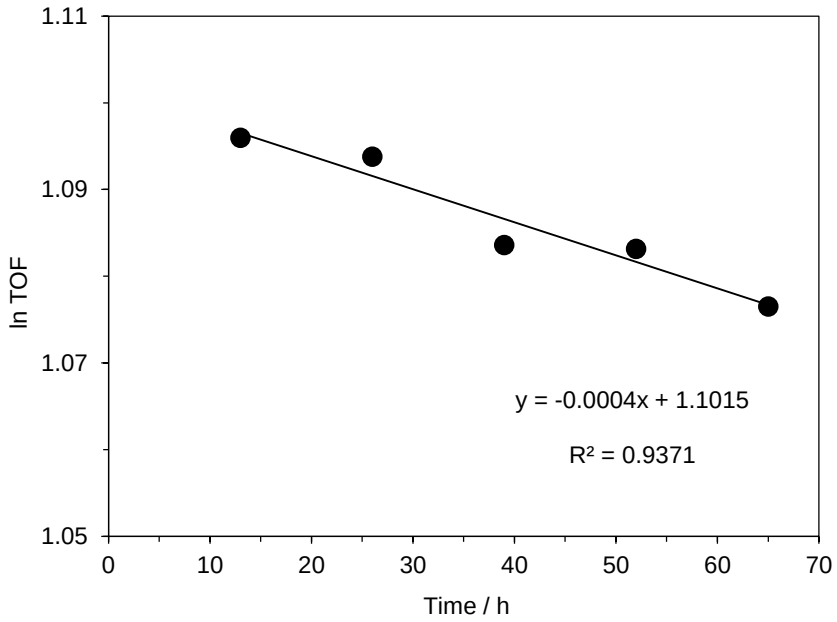

Figure 2.19. The deactivation rate of Pd/C catalyst over 65 hours.

The data presented in Figure 2.19 indicates that the catalyst deactivation rate constant is very small and was estimated to be *ca.* $4.0 \cdot 10^{-4}$ h^{-1}.

2.3.1.7. Synthesis of selected secondary amines

According to Wakchaure *at al.* (2007) the reactivity of carbonyl compounds follows the order aldehyde > cyclic ketones > acyclic ketones. Reductive amination reactions can require harsh conditions due to the steric hindrance. The reaction may require very long reaction time or more than one cycle of the process for adequate results.

Another important factor in reductive amination is the electronic factor. The more reactive nature of the carbonyl compound or amine can lead the reaction to over-alkylation or a mixture of products. Furthermore, solvent choice is also important since the reductive amination may be sensitive to it (Wakchaure *et al.* 2007).

Reductive amination of various aldehydes was carried out continuously in the compact multichannel reactor. The results of these syntheses are summarised in Table 2.2. The reductive amination of aldehydes was very efficient in most of these cases. Aromatic, cyclic, aliphatic and methoxy-substituted aldehydes afforded the products with 100 % conversion and very good isolated yield (89 - 99%).

In the case of cinnamaldehyde (Entry 11, Table 2.2) no (*E*)-2-phenyl-*N*-(1-phenylethyl)ethenamine was formed due to the C - C double bond hydrogenation. For Entry 1 and 11 (Table 2.2), the same product was obtained with very good isolated yields. No product formation was observed for 3-(methylthio)propanal (Entry 12, Table 2.2) due to catalyst poisoning by sulphur.

The reductive amination reaction was extended to ketones using the standard conditions for reductive amination of aldehydes, *i.e.* P_T = 8 bar, F_L = 0.5 mL min^{-1}, F_G = 21.0 mL (STP) min^{-1}, T = 298K, $C_{S,0}$ = 0.4 mol L^{-1}.

In the case of ketones as a starting material, the intermediate imine was formed during the mixing of α-methylbenzylamine with a ketone only in the case of cyclohexanone (Entry 1, Table 2.3). In all other cases (Entry 2 and 3, Table 2.3) the intermediate formation was a catalytic reaction.

Results obtained for the reductive amination of ketones were not as good as the one obtained for reductive amination of aldehydes due to the fact that ketones are not as reactive as aldehydes.

The reductive amination of ketones gave the product at lower conversions compared to that for aldehydes (Table 2.3).

Cyclohexanone (Entry 1, Table 2.3) gave the product in 88% of isolated yield under reaction conditions: P_T = 8 bar, F_L = 0.2 mL min^{-1}, F_G = 21.0 mL (STP) min^{-1}, $C_{S,0}$ = 0.2 mol L^{-1}, T = 298K, confirming that the cyclic ketones are more reactive than acyclic ketones. In order to increase the conversion, an increase in the reaction temperature was necessary in the case of the 4-phenyl-2-butanone (Entry 2, Table 2.3 and 3'-methoxyacetophenone (Entry 3, Table 2.3). Increasing the reaction temperature to 323K led to product formations of 66% and 37% isolated yield for Entries 2 and 3 (Table 2.3), respectively.

Further studies on the reductive amination of ketones are required in order to increase the conversion. At this point, longer residence time might be suggested as a means of achieving this, rather than a temperature increase, since further increases in the reaction temperature may result in the deprotection of the methoxy group in the case of 3'-methoxyacetophenone (Entry 3, Table 2.3), and a mixture of products in the case of 4-phenyl-2-butanone (Entry 2, Table 2.3).

Table 2.2. Formation of selected secondary amines[a] by reductive amination of aldehydes in the packed-bed multichannel reactor over a Pd/C catalyst.

Entry	Substrate	Product	Conversion[b]	Yield[c]
1	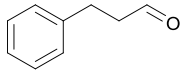	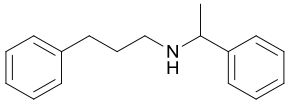	100	98
2	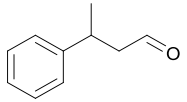	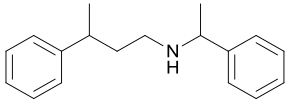	99	96
3	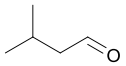	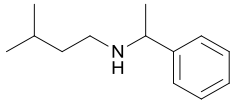	100	93
4	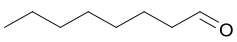	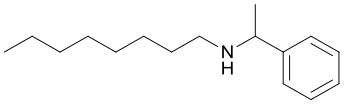	99	92
5	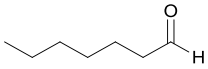	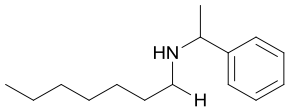	96	92

6	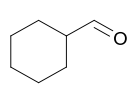	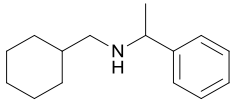	100	98
7	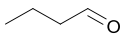	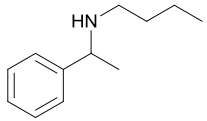	100	97
8		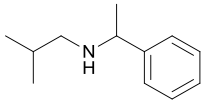	99	92
9	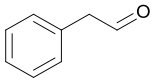	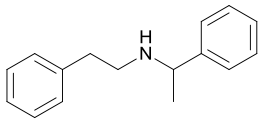	100	98
10	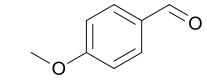	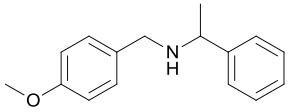	100	89
11	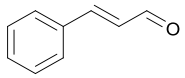	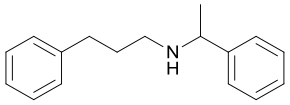	100	99

12	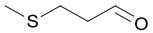	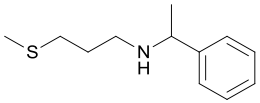	-	-
13	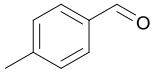	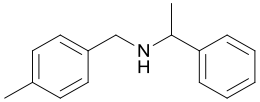	97	95

[a] Reaction conditions: P_T = 8 bar, F_G = 21.0 mL (STP) min^{-1}, F_L = 0.5 mL min^{-1}, $C_{S,0}$ = 0.4 mol L^{-1}, T = 298K, methanol as a solvent.

[b] Conversion was determined by GC analysis

[c] Isolated yield after column chromatography

Table 2.3. Formation of selected secondary amines by reductive amination of ketones in the packed-bed multichannel reactor over a Pd/C catalyst.

Entry	Substrate	Product	Conversion[c]	Yield[d]
1[a]	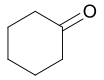	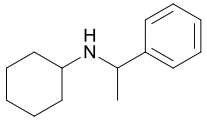	94	88
2[b]	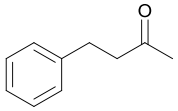	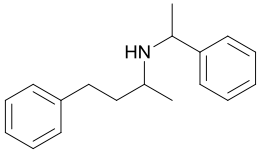	72	66
3[b]	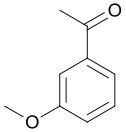	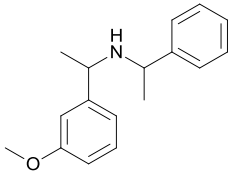	44	37

[a] Reaction conditions: P_T = 8 bar, F_G = 21.0 mL (STP) min^{-1}, F_L = 0.2.mL min^{-1}, $C_{S,0}$ = 0.2 mol L^{-1}, T = 298K, methanol as a solvent.

[b] Reaction conditions: P_T = 8 bar, F_G = 21.0 mL (STP) min^{-1}, F_L = 0.2 mL min^{-1}, $C_{S,0}$ = 0.2 mol L^{-1}, T = 323K, methanol as a solvent.

[c] Conversion was determined by GC analysis

[d] Isolated yield after column chromatography

2.3.1.8. Reactor efficiency with split injection of hydrogen

The possibility that different hydrogen injection strategies might increase reactor efficiency was also investigated for the reductive amination of aldehydes. The reaction channel arrangements with the different gas injection options are illustrated in Figure 2.20. For all configurations, the amount of hydrogen supplied remained in the same relationship to the amount of catalyst. Compared to arrangement A, double the amount of hydrogen was used to maintain a consistent amount of gas along the reaction bed in arrangements B and C.

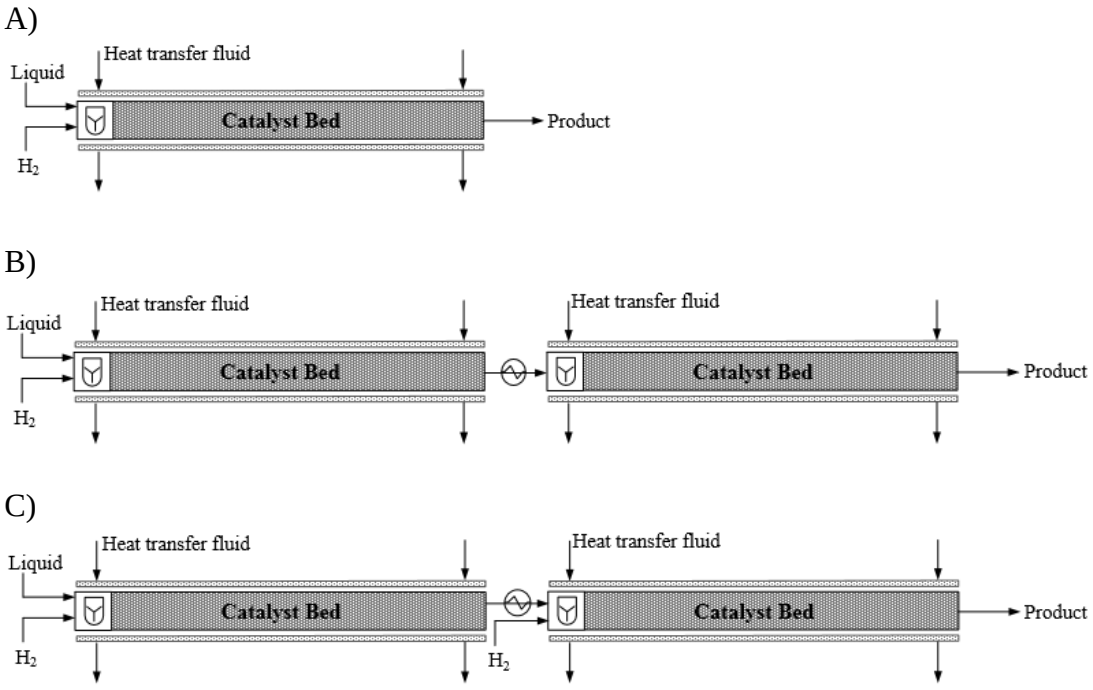

Figure 2.20. Channel arrangement for split hydrogen injection experiments.

An increase in the imine conversion of *ca.* 5% was measured with arrangement A by increasing the hydrogen flow rate from 21.0 to 42.0 mL (STP) min^{-1}. For arrangement C, an identical total amount of hydrogen as in the case of B was split and injected at the entrance of the two consecutive channels. The hydrodynamic regime in the two channels was, therefore, believed to be identical to that in case A.

The product yield increased up to 95% using channel arrangement C. It should be noted here that the difference between the results obtained with channel arrangements B and C is less than 1% (Table 2.4). The increase in conversion between cases A and B/C is due to the doubling of the total residence time. In all three cases, selectivity to (1-phenylethyl)(3-phenylpropyl)amine remained the same at 100% (which was confirmed by GC analysis).

Table 2.4. The influence of the hydrogen split injection on reactor efficiency. P_T = 8 bar, F_G = 21.0 mL(STP)min^{-1}, F_L = 2.0 mL min^{-1}, $C_{0,S}$ = 0.4 mol L^{-1}, T=298K.

Channel arrangement	**Conversion (%)**
A	61
B	94
C	95

Performing another set of experiments for all configurations at 323K provoked no change in selectivity. Furthermore, in all arrangements, the conversion remained at between 95 - 97% with no side reactions such as over-alkylation, for instance, which could take place in cases B and C due to the presence of twice the number of active centres on the catalyst in these cases.

This simple model of the split gas distribution along the length of the reaction channel resulted in a higher yield of the desired product for experiments performed at 298K. The concept of dosing the required amount of gaseous reactant at different positions along the catalyst bed can be a flexible method for performing more complex reactions under continuous flow conditions using microreactors. This aspect will also be investigated in Chapters 3 and 4, where the hydrogenolysis of secondary amines, and a tandem process of reductive amination of aldehydes (ketones) - deprotection of secondary amines is presented.

2.3.2. X-Cube™ flow reactor

In this part of the project, a commercially available X-Cube™ flow reactor was employed for the reductive amination of aldehydes. The reaction was studied in detail by varying different parameters, *i.e.* liquid flow rate, pressure, temperature and the initial reagent concentration. Results are presented in the next subsections.

2.3.2.1. Effect of liquid flow rate

Figure 2.21 shows the product concentration in the outlet solution as a function of time-on-stream at two liquid flow rates, 1.5 and 2.5 mL min^{-1}. The product concentration initially decreased with time followed by a plateau after *ca.* 20 minutes time-on-stream, which indicated the time at which a steady state was achieved in the reactor. At higher liquid flow rates the product concentration was lower due to the decrease of the residence time in the reaction channel

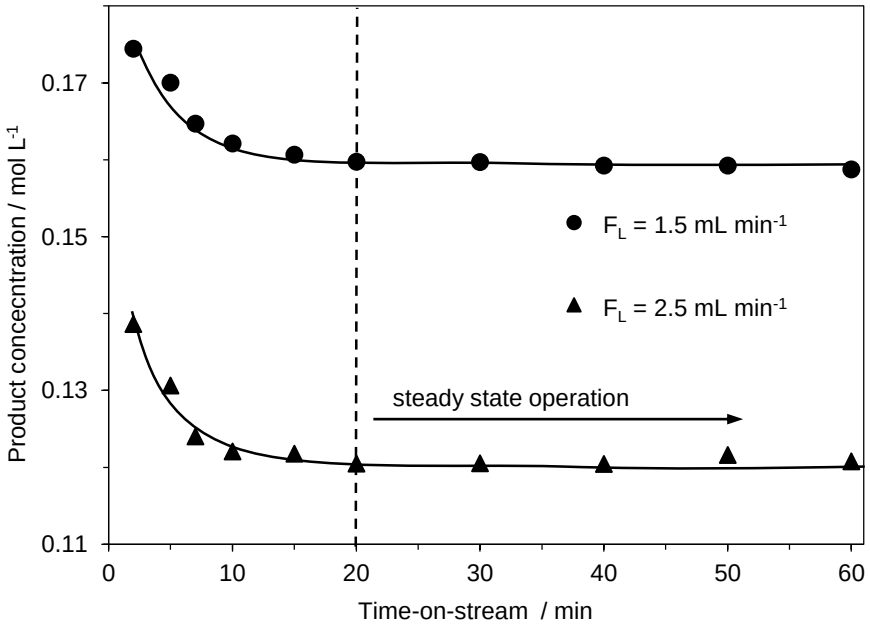

Figure 2.21. Product concentration in the outlet of the reactor as a function of time-on-stream. P_T = 30 bar, $C_{S,0}$ = 0.2 mol L^{-1}, T = 298K.

Figure 2.22 shows the influence of liquid flow rate at 5 and 30 bar on the conversion of imine into secondary amine. The conversion of imine was observed to decrease as the liquid flow rate increased from 0.5 to 3.0 mL min^{-1} at 5 and 30 bar of total pressure, respectively. A linear decrease in the conversion of imine was noticed at all liquid flow rates investigated in this work. The decrease in the conversion of imine at higher liquid flow rates is due to the lower residence time of the liquid phase in the reactor. The excess concentration of liquid reactant compared to the concentration of dissolved hydrogen might be another reason for the lower conversion of the imine at higher liquid flow rates. Increasing hydrogen pressure results in an enhanced solubility of hydrogen in the liquid phase and therefore higher saturation is expected at higher hydrogen pressures.

According to the manufacturer, the gas flow rate in this particular reactor cannot be controlled. The gas is mixed with the reagents in the mixing unit and then directed through a bubble detector. The amount of gas bubbles in the liquid is measured by an optical detector. The rate of bubbles in the liquid phase is regulated by a valve so as to keep a near constant value of 5% of gas in the liquid at any time, independent of the applied pressure.

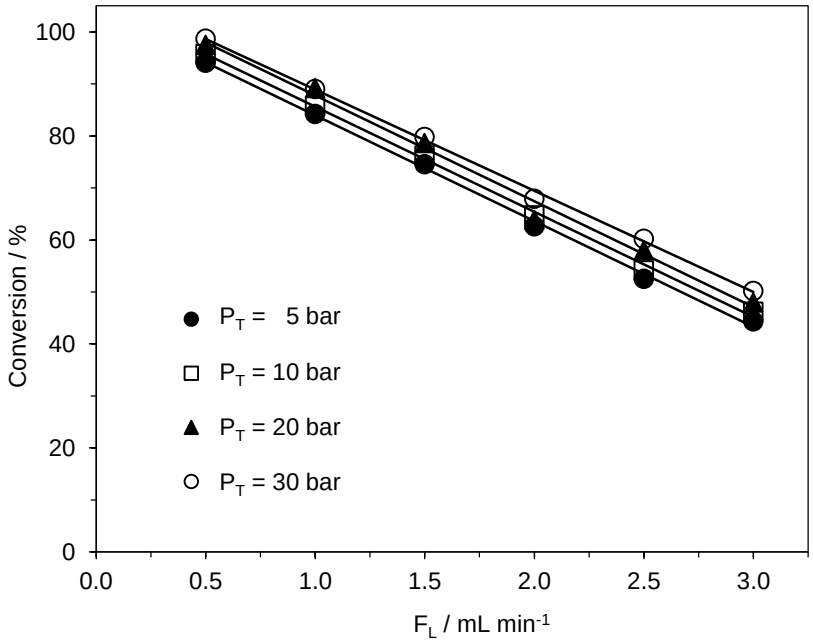

Figure 2.22. Influence of liquid flow rate on the conversion of imine.
$C_{S,0}$ = 0.2 mol L^{-1}, T = 298K.

The overall rate of product formation increased strongly as the liquid flow rate increased up to 2.0 mL min^{-1} (Figure 2.23). When the liquid flow rate was increased further to 3.0 mL min^{-1}, a slight increase in the overall rate of product formation was observed. The increase in the overall rate of product formation with liquid flow rate indicates the influence of mass transport ($0.5 \leq F_L < 2.0$ mL min^{-1}). For higher flow rates, $F_L \geq 2.0$ mL min^{-1}, the reaction is almost independent of mass transfer limitations and is very likely to be in the kinetic regime.

Increasing the liquid flow rate up to 2.5 mL min^{-1} resulted in a higher rate of product formation. Comparing the data obtained at 2.5 mL min^{-1} liquid flow rate and at 5 and 30 bar of total pressure, shows that the rate of product formation increased by only 15% while the pressure increased six times, whereas at a liquid flow rate of 0.5 mL min^{-1} the rate of product formation increased only 5% while the pressure increased six times.

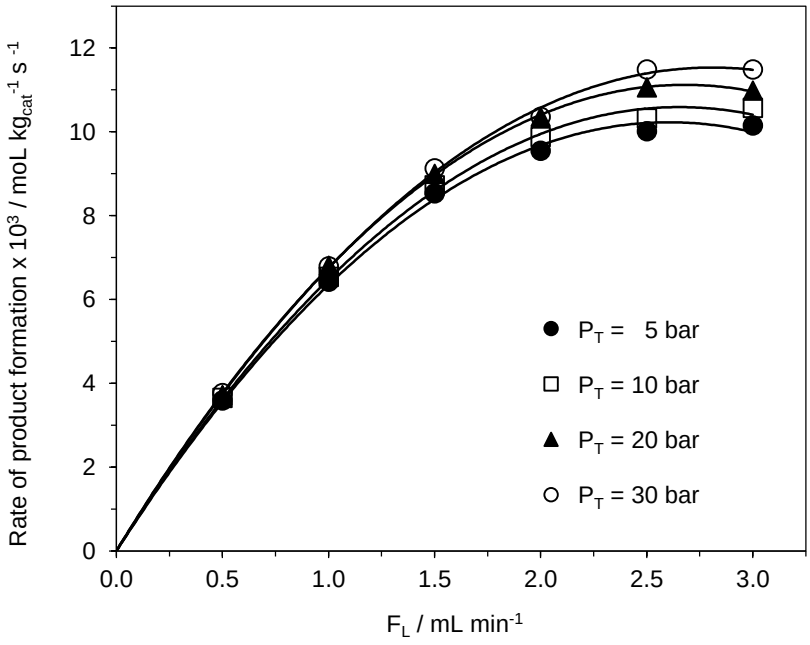

Figure 2.23. Influence of liquid flow rate on the overall rate of product formation. $C_{S,0}$ = 0.2 mol L^{-1}, T = 298K.

2.3.2.2. Effect of operating pressure

No significant effect of hydrogen pressure on the conversion of imine was noted (Figure 2.24). The conversion increased from 94 to 99% at 5 and 30 bar, respectively and at a 0.5 mL min^{-1} liquid flow rate. At a 1.5 mL min^{-1} liquid flow rate, meanwhile, the conversion increased by only 6% and by 13% at 2.5 mL min^{-1} while the pressure increased six times. The overall rate of product formation was also found to be almost independent of the total pressure (Figure 2.25), indicating that the active sites of the catalyst were fully occupied with hydrogen and that the saturation region of Langmuir-Hinshelwood rate expression could be observed.

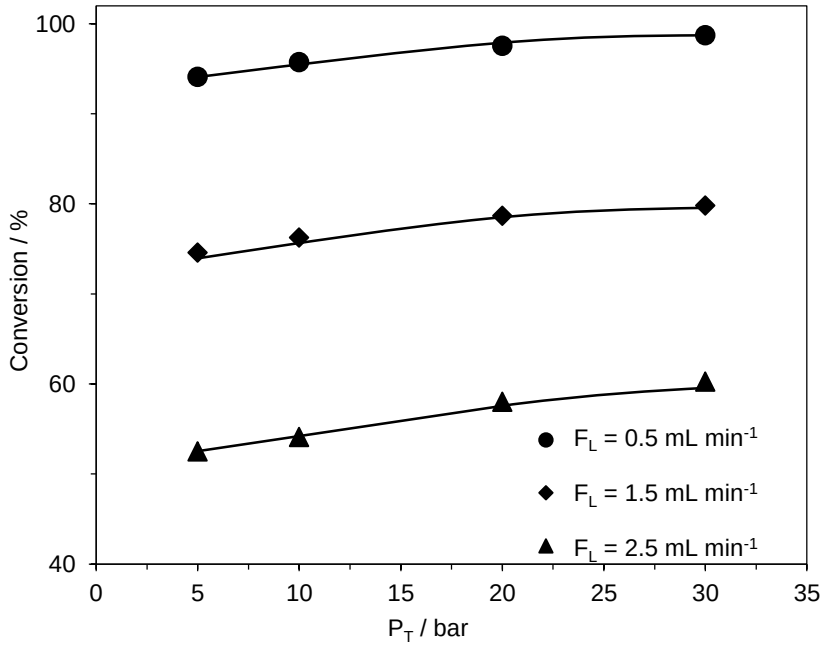

Figure 2.24. Influence of the total pressure on the conversion of imine.
$C_{S,0}$ = 0.2 mol L^{-1}, T = 298K.

The influence of the total pressure on the overall rate of product formation was also studied at an initial reagent concentration of 0.4 mol L^{-1} (Figure 2.26). The overall rate of product formation increased by only *ca.* 13% while the total pressure in the reactor increased from 5 to 20 bar at 3.0 mL min^{-1} and by *ca.* 9% at a liquid flow rate of 1.0 mL min^{-1}.

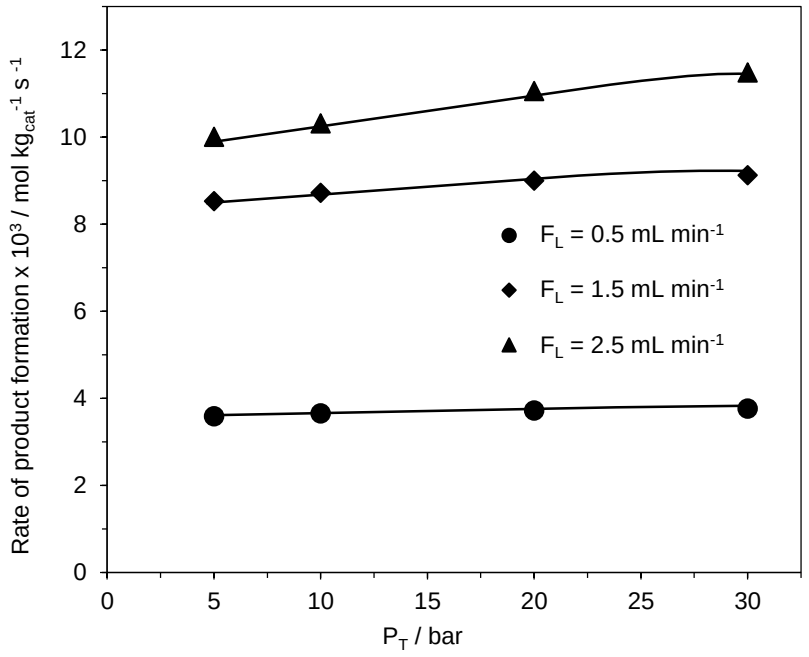

Figure 2.25. Influence of the total pressure on the rate of product formation. $C_{S,0}$ = 0.2 mol L^{-1}, T = 298K.

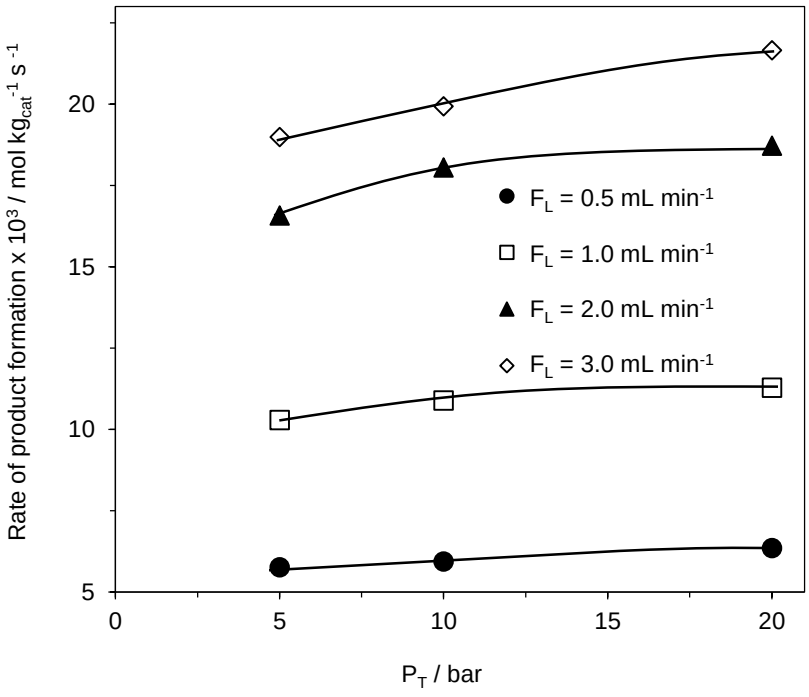

Figure 2.26. Influence of the total pressure on the rate of product formation. $C_{S,0}$ = 0.4 mol L^{-1}, T = 298K.

2.3.2.3. Effect of reaction temperature

The effect of reaction temperature on the imine conversion was studied at 0.4 mol L^{-1} initial reagent concentration and is presented in Figure 2.27.

The conversion increased from 64% to 88% at 298K and 308K. Further increases in temperature increased the conversion up to 99% at 343K, indicating the high efficiency of the catalytic system and reactor for the given conditions.

Performing the experiments at 0.2 mol L^{-1} initial reagent concentration and in the temperature range of 298 - 343K showed no change to the selectivity. At all temperatures 99% conversion was obtained and secondary amine was the only product, indicating that at this temperature range reductive amination can be carried out selectively with no concerns about additional product formation.

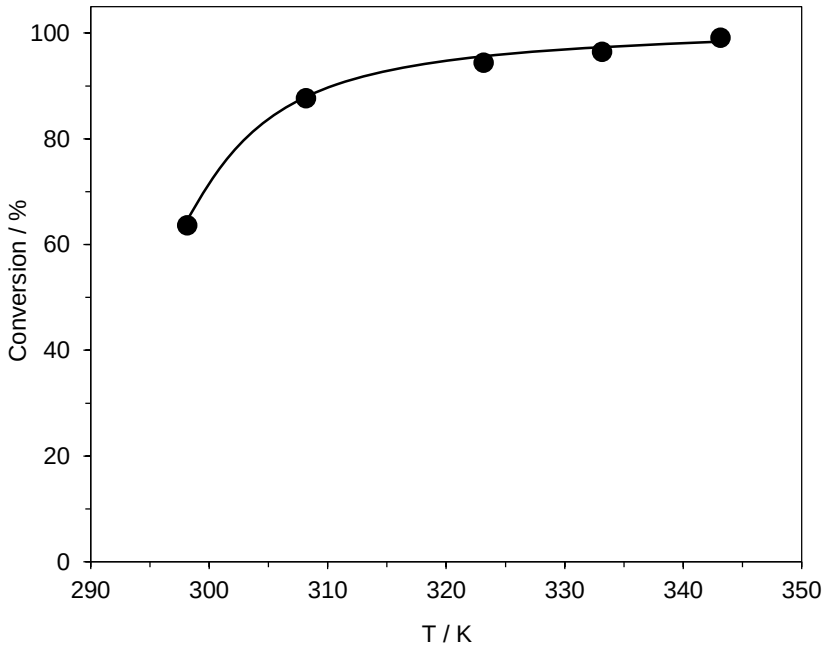

Figure 2.27. Influence of reaction temperature on the imine conversion.
P_T = 30 bar, F_L = 0.5 mL min^{-1}, $C_{S,0}$ = 0.4 mol L^{-1}.

2.3.2.4. Effect of reagent concentration

The influence of the initial reagent concentration on the product concentration is presented in Figure 2.28. An increase in the substrate concentration increased the product concentration due to the higher number of collisions between molecules. The selectivity remained 100% for all the experiments and no tertiary amine was found to be formed under these reaction conditions. The experiments were performed on the same CatCart which might suggest that the catalyst was not deactivated during the reaction and it was also assumed that no leaching of palladium took place.

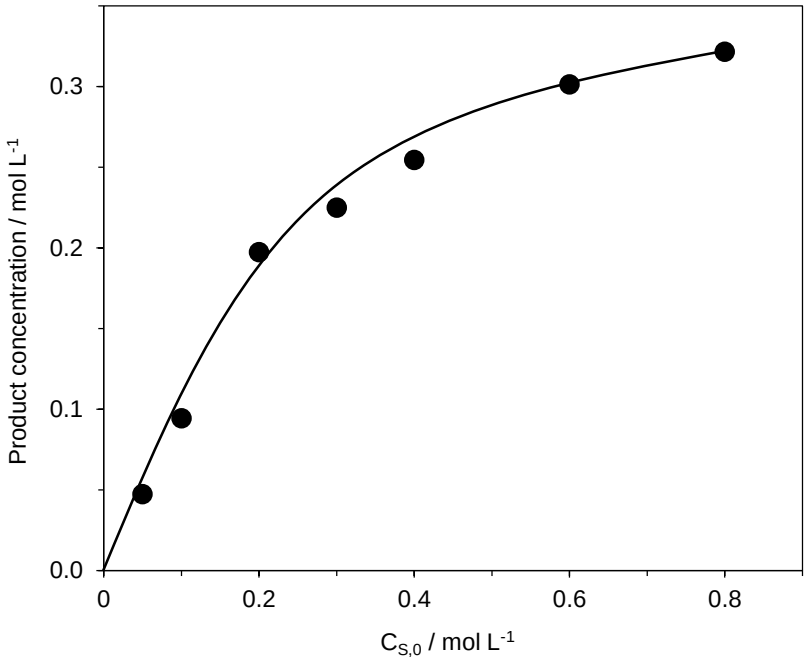

Figure 2.28. Influence of the initial concentration on the product concentration. P_T = 30 bar, F_L = 0.5 mL min^{-1}, T = 298K.

2.3.2.5. Catalyst stability

Time-on-stream experiments were carried out to evaluate the activity of 10% Pd/C catalyst in the X-Cube™ reactor. The conversion of imine and selectivity to secondary amine remained constant in each run (Figure 2.29). Each experiment was carried out for 13 hours with a liquid flow rate of 0.5 mL min^{-1}. After each experiment,

the system was washed with solvent (MeOH) to prevent any blockage in the line from residue caused by the reactants/ products.

For the first three runs, over 13 hours of continuous flow the average conversion of imine into 2^{o} amine remained constant, *ca.* 98%, the fourth run showed a slight decrease in conversion to 97%, but the fact that the decrease between the first and the fourth run was so small indicates that the Pd/C catalyst synthesised for this work had a high activity and good stability over 52 hours of experiments.

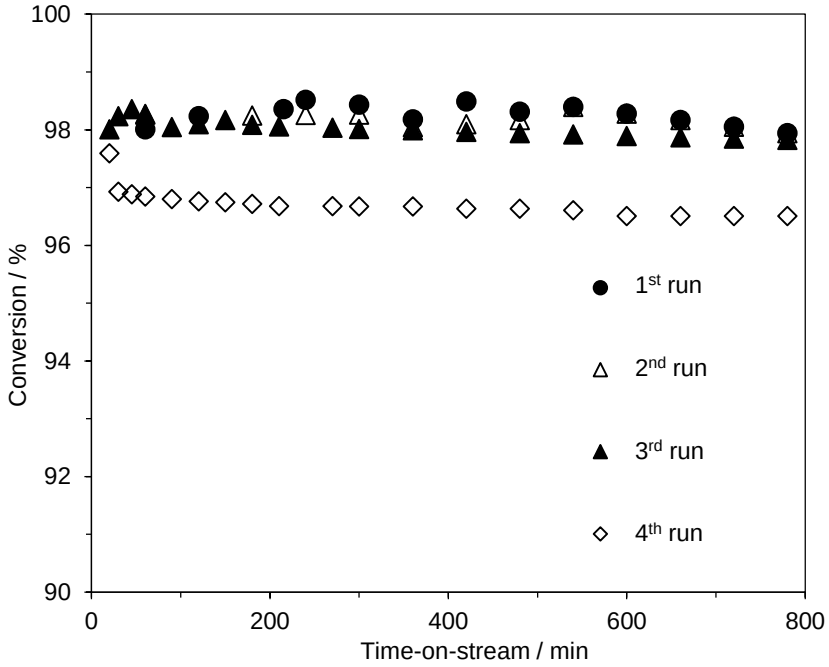

Figure 2.29. The imine conversion as a function of time-on-stream.
P_T = 30 bar, F_L = 0.5 mL min^{-1}, $C_{S,0}$ = 0.4 mol L^{-1}, T = 298K.

In order to evaluate the catalyst deactivation, Figure 2.30 shows the relationship between logarithmic Turn Over Frequency (TOF) and catalyst life-time. The TOF was calculated based on Equation 2.2 while the rate of catalyst deactivation was calculated using Equation 2.3.

The data presented in Figure 2.34 indicates that the rate of catalyst deactivation was very small, estimated to be *ca.* 4.0 · 10^{-4} h^{-1}.

It is worth noting that the values of the catalyst deactivation constant calculated for the X-Cube^{TM} flow reactor and the PBR (see Chapter 2, section 2.3.1.6) are the same, indicating that this value is characteristic to the reaction (*i.e.* chemical system), not the reactor.

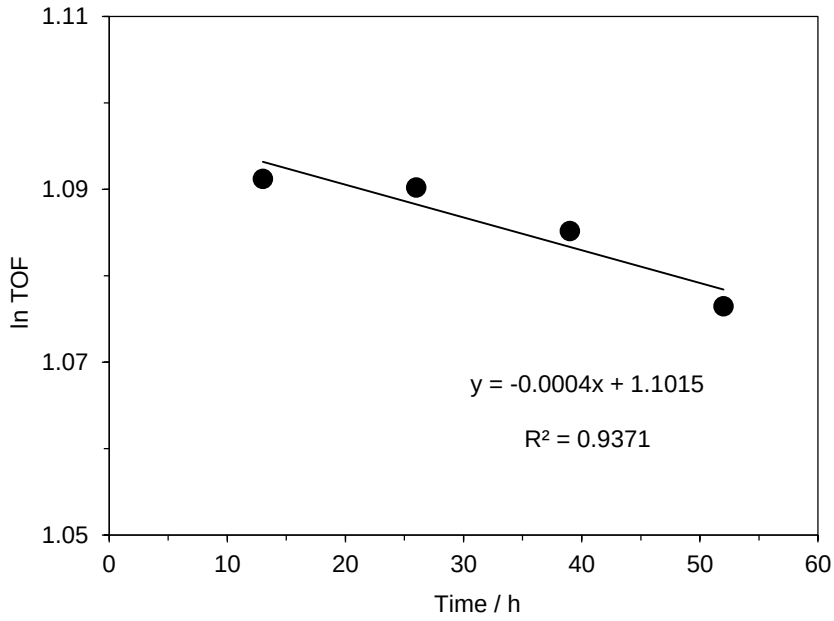

Figure 2.30. The deactivation rate of Pd/C catalyst over 52 hours.

2.3.2.6. Synthesis of selected secondary amines

A series of aldehydes were screened to determine the reaction's tolerance to the prevailing conditions, *i.e.* $C_{S,0}$ = 0.2 mol L^{-1}, T = 298K, P_T = 30 bar, F_L= 0.5 mL min^{-1}, for consecutive substrates.

The data presented in Table 2.5 shows that the secondary amines can be synthesised with very good isolated yield.

In the case of cinnamaldehyde (Entry 11, Table 2.5) no (*E*)-2-phenyl-*N*-(1-phenylethyl)ethenamine was formed due to C - C double bond hydrogenation. For Entries 1 and 11 (Table 2.4), the same product was obtained with very good isolated yield. No product formation was observed for 3-(methylthio)propanal (Entry 12, Table 2.4) due to poisoning of the catalyst by sulphur. The same situation

was observed when the multichannel packed-bed reactor was used (see section 2.3.1.7.).

The results presented in Table 2.6 show that the reductive amination of ketones at 0.2 mol L^{-1} initial reagent concentrations gave much lower conversions in comparison to aldehydes.

The intermediate was formed during the mixing of α-methylbenzylamine with a ketone only in the case of cyclohexanone (Entry 1, Table 2.6). In all other cases (Entries 2 and 3, Table 2.6) the intermediate formation was a catalytic reaction.

Cyclohexanone (Entry 1, Table 2.6) gave the product in 65% of isolated yield under reaction conditions: P_T = 30 bar, F_L = 0.2 mL min^{-1}, $C_{S,0}$ = 0.2 mol L^{-1}, T = 298K. In the case of the 4-phenyl-2-butanone (Entry 2, Table 2.6) and 3'-methoxyacetophenone (Entry 3, Table 2.6) the reductive amination was unsuccessful under these reaction conditions: no secondary amine was formed, even when the liquid flow rate was decreased to 0.2 mL min^{-1}. Increasing the reaction temperature up to 373K, however, led to a product formation of 48% and 35% isolated yield for Entries 2 and 3 (Table 2.6), respectively.

The results obtained under certain reaction conditions were not as good as the ones obtained for reductive amination of aldehydes due to the fact that ketones are not as reactive as aldehydes. This requires further study.

Table 2.5. Formation of selected secondary amines[a] by reductive amination of aldehyde in the X-Cube™ flow reactor over a Pd/C catalyst.

Entry	Substrate	Product	Conversion[b]	Yield[c]
1	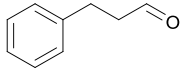	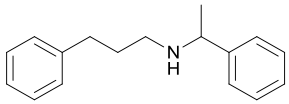	100	97
2	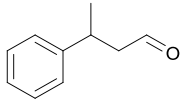	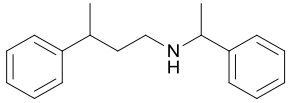	99	95
3	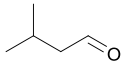	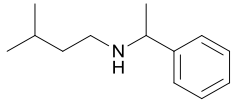	99	92
4	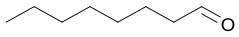	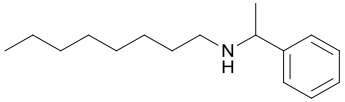	99	91
5	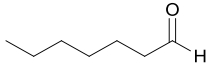	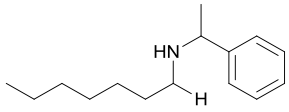	89	85

6	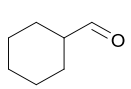	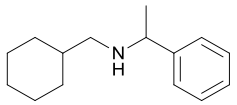	99	94
7	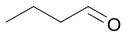	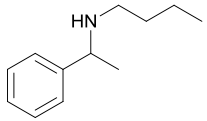	97	94
8		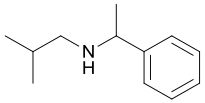	99	95
9	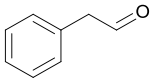	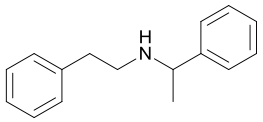	99	96
10	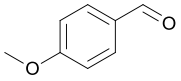	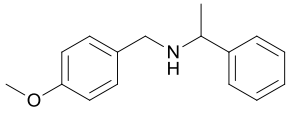	97	88
11	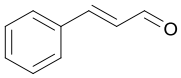	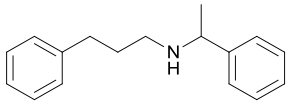	100	97

12	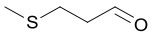	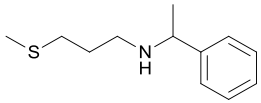	-	-
13	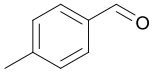	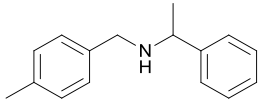	100	90

[a] Reaction conditions: P_T = 30 bar, F_L = 0.5 mL min^{-1}, $C_{S,0}$ = 0.2 mol L^{-1}, T = 298K, methanol as a solvent.

[b] Conversion was determined by GC analysis

[c] Isolated yield after column chromatography

Table 2.6. Formation of selected secondary amines by reductive amination of ketones in the X-Cube™ flow reactor over a Pd/C catalyst.

Entry	Substrate	Product	Conversion[c]	Yield[d]
1[a]	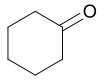	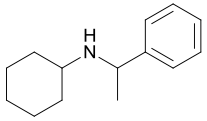	72	65
2[b]	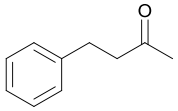	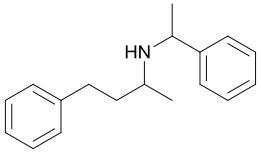	56	48
3[b]	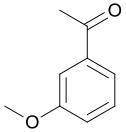	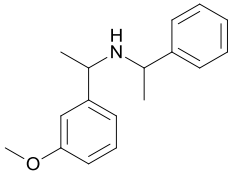	43	35

[a] Reaction conditions: P_T = 30 bar, F_L = 0.2 mL min^{-1}, $C_{S,0}$ = 0.2 mol L^{-1}, T = 298K, methanol as a solvent.

[b] Reaction conditions: P_T = 30 bar, F_L = 0.2 mL min^{-1}, $C_{S,0}$ = 0.2 mol L^{-1}, T = 373K, methanol as a solvent.

[c] Conversion was determined by GC analysis

[d] Isolated yield after column chromatography

2.4. Conclusions

In conclusion, the reductive amination of aldehydes with α-methylbenzylamine was successfully investigated using a continuous catalytic rig with a multichannel packed-bed reactor, and a commercially available X-Cube™ flow reactor. The reaction was extended to ketones, however further studies are required in order to increase the conversion in the case of ketones.

The most significant result was the ability to synthesise for further studies a variety of secondary amines (protected primary amines) which are either commercially unavailable or very expensive to purchase.

It was shown that a variety of protected primary amines can be synthesised with high yield in a continuous process. The reaction time is also much shorter than when using a batch process.

Comparison of the results obtained from both reactors showed that the packed-bed multichannel reactor was more efficient than the X-Cube™ (Table 2.7). For example, 0.012 mol h^{-1} of product can be obtained in a single pass through the reaction channel with an undiluted catalyst bed using the continuous catalytic rig, while the X-Cube™ flow reactor can only produce 0.006 mol h^{-1}.

In order to increase the productivity it would be necessary to increase the reaction temperature (Table 2.8) or catalyst amount, *i.e.* by using more than one reaction channel. However, we did not want to double the catalyst amount, work on the tandem reductive amination-deprotection was halted.

The effectiveness of the packed-bed multichannel reactor for performing continuous catalytic reductive amination of aldehydes was much better than that of the X-Cube™ flow reactor. The results also showed that the staged injection of hydrogen was beneficial for the model reaction (*i.e.* reductive amination of hydrocinnamaldehyde), which was attributed to a better hydrodynamic regime.

At this stage it was important to prove that the reductive amination of aldehydes can be done using these systems, since this reaction is an important part of the main goal of this project - multi-step synthesis of pharmaceutical intermediates.

Table 2.7. Comparison of the optimal reaction conditions for both reactors at 298 K.

	PBR	**X-Cube™**
P_T (bar)	8	30
T (K)	298	298
F_L (mL min^{-1})	0.5	0.5
F_G (mL min^{-1})	21.0	-
$C_{S,0}$ (mol L^{-1})	0.4	0.2
m_{cat} (g)	0.45	0.45
Productivity (mol h^{-1})	0.012	0.006

Table 2.8. Comparison of the optimal reaction conditions for both reactors at higher temperatures.

	PBR	**X-Cube™**
P_T (bar)	8	30
T (K)	323	343
F_L (mL min^{-1})	2.0	0.5
F_G (mL min^{-1})	21.0	-
$C_{S,0}$ (mol L^{-1})	0.4	0.4
m_{cat} (g)	0.45	0.45
Productivity (mol h^{-1})	0.048	0.012

Chapter 3

Deprotection of Secondary Amines in the Structured Compact Reactor and X-Cube™ Flow Reactor

3.1. Introduction

Primary amines are important in human life and for the chemical industry. It is well known that they are particularly useful as pharmaceutically active substances and fine chemicals. In this regard, fundamental transformation in modern organic synthesis is *N*-debenzylation of benzylamines. One of the preferred methods for *N*-debenzylation of benzylamines is Pd/C catalytic hydrogenolysis, which is characterized by high conversion and selectivity. In multi-step organic syntheses a manipulation of functional groups is essential to avoid side reactions during a chemical transformation. Benzyl groups are often the protective group of choice for amines and can be removed from the N atom by various reactions at the end of transformation (Cheng *et al.* 2009; Gross *et al.* 2002).

Hydrogenolysis reactions, as well as catalytic heterogeneous hydrogenation processes of organic compounds, are of great interest in research laboratories as well as in the chemical and pharmaceutical industries (Irfan *et al.* 2011).

Traditional batch deprotection protocols usually require long reaction times or, when performed on a large scale, high pressures of hydrogen gas in autoclave reactors, which pose a potential hazard during the processing (Irfan *et al.* 2011).

Over the past few years, the application of continuous flow processes for deprotection reactions has increased significantly. The syntheses performed under continuous flow conditions using microreactors are more efficient and allow better heat management and mixing control than standard batch processes (Wirth 2008; Luis and García-Verdugo 2010; Ehrfeld *et al.* 2000). An additional advantage of the three phase reaction system is attributed to the gas-liquid-solid interactions within microchannels for better molecular diffusion (Kobayashi *et al.* 2006). Furthermore, the small hold-up reduces the potential risk of explosion, which is important when flammable hydrogen gas is used. Catalyst separation and recovery from the reaction products is also eliminated in this method. Taken together, these advantages are in good agreement with the principles of "Green Chemistry'' (Irfan *et al.* 2011).

From the synthetic point of view, protecting groups are very important in the synthesis of many compounds. The removal of the different protecting groups, for example, benzyl, carbobenzyloxy and 1-phenylethyl, at the end of the synthesis may cause some difficulties, however. Catalytic hydrogenation is one of the most common ways of removing protecting groups (Irfan *et al.* 2011).

Desai *et al.* (2006) reported *O*-benzyl deprotection of DHPM benzyl esters using the H-Cube flow reactor. The desired product was synthesised in 95% isolated yield using 0.025 mol L^{-1} of feed solution (Scheme 3.1).

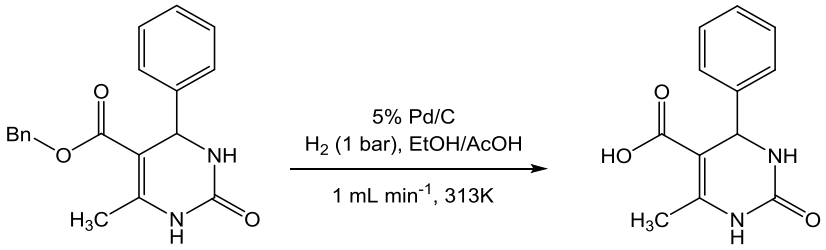

Scheme 3.1. Deprotection of DHPM benzyl ester.

Another example of flow debenzylation was presented by Matos and Murphy (2007). The synthesis of various oxamacrolides included the ring-closing metathesis macrocyclization which was followed by a flow debenzylation and a double bond reduction. The H-Cube flow reactor gave the desired products in 47 - 71% isolated yield (Scheme 3.2).

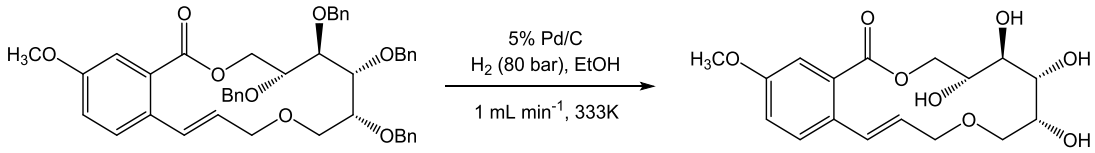

Scheme 3.2. Synthesis of Polyhydroxylated Oxamacrolide.

The cyclohexanamine derivatives as antagonists to the neuropeptide Y (Y1) receptor were synthesised by Cho *et al.* (2009). The benzyl ether continuous flow deprotection and dehalogenation gave 3-(4-phenylpiperidin-4-yl)-pyridine (Scheme 3.3).

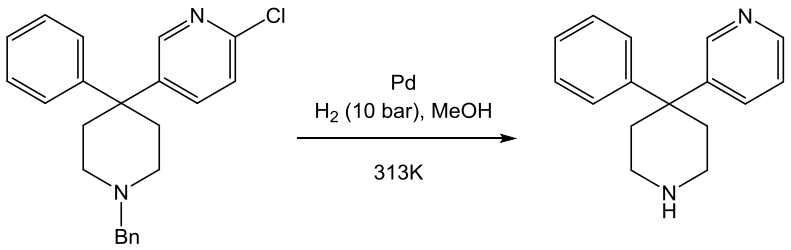

Scheme 3.3. Debenzylation and dehalogenation of 5-(1-benzyl-4-phenylpiperidin-4-yl)-2-chloropyridine

Ley *et al.* (2006) described the *O*- and *N*-deprotection approach using the H-Cube flow reactor. The benzyl carbamate protecting group was successfully removed from the (S)-2-(1*H*-tetrazol-5-yl)-pyrrolidine-1-carboxylic acid benzyl ester (Scheme 3.4). 3g of (*S*)-5-pyrrolidin-2-yl-1*H*-tetrazole was synthesised in 3.5 hours under continuous flow conditions instead of three days under the standard conditions.

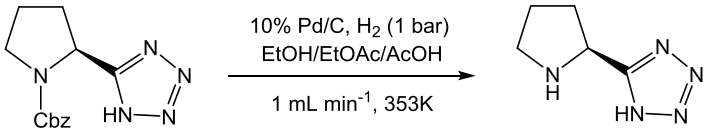

Scheme 3.4. Hydrogenation of (*S*)-2-(1*H*-tetrazol-5-yl)-pyrrolidine-1-carboxylic acid benzyl ester.

As an extension of the above work, Ley *et.al* (2006b) investigated the deprotection of Cbz group to the synthesis of small di- and tripeptides. The same group further showed the optimisation of an effective *O*- and *N*-deprotection reaction for a range of substrates, for example amino acids, simple amines and dipeptides by varying different reaction parameters (Ley *et al.* 2007).

The functional group deprotection protocols using the H-Cube flow reactor have been presented in numerous synthetic studies: deprotection of Cbz and benzyl ether protecting groups (Clapham *et al.* 2007), hydrogenolytic deprotection of the Cbz group (Huang *et al.* 2009), Boc-deprotection (Simerska *et al.* 2009) and Cbz-deprotection (Petersen *et al.* 2009), which are each mostly performed in the context of drug application discovery.

In this chapter, the hydrogenolysis of secondary amine synthesised *via* reductive amination of hydrocinnamaladehyde with α-methylbenzylamine (see Chapter 2) is investigated in the multichannel packed-bed reactor and the X-Cube^{TM} flow reactor. Deprotection of (1-phenylethyl)(3-phenylpropyl)amine to 3-phenylpropan-1-amine (Scheme 3.5) was chosen as a model reaction. Performance of the structured compact reactor in terms of calculated product yield, selectivity and average rate of product formation for continuous deprotection was evaluated and compared with the data obtained using the X-Cube^{TM} flow reactor. The effect of reaction parameters, *i.e.* gas and liquid flow rates, concentration, staged injection of hydrogen; pressure and temperature were studied in detail.

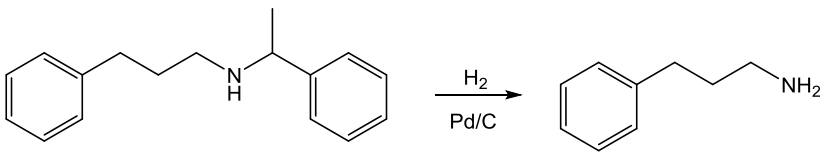

Scheme 3.5. Deprotection of (1-phenylethyl)(3-phenylpropyl)amine.

3.2. Experimental

3.2.1. Activated carbon and reagents

The carbon support used in this study was mesoporous phenolic resin derived synthetic carbon, which was kindly provided by MAST Carbon (UK). The synthetic carbons possess a tailored pore structure (a bimodal micro and meso-pore structure) and were produced in the form of beads.

The (1-phenylethyl)(3-phenylpropyl)amine used was synthesised *via* the reductive amination of aldehydes reaction. The hydrocinnamaldehyde, α-methylbenzylamine and methanol were purchased from Sigma-Aldrich and used without further purification.

3.2.2. Preparation of Pd/C catalyst

The synthesis of the catalyst has been described in Chapter 2, section 2.2.1.

3.2.3. Structured compact reactor

Details of the structured multichannel reactor and of the continuous catalytic system used are given in Chapter 2, section 2.2.2.

3.2.4. Continuous catalytic rig and procedure for continuous experiments

The procedure for the continuous experiments is presented in Chapter 2, section 2.2.3.

3.2.5. Analysis techniques

Gas chromatography (GC, Varian CP - 3800) was used to analyse reaction substrates/ intermediates/ products using a polar capillary column (CP Sil - 8CB). All samples collected during the experiments were analysed without further purification.

Standard samples of 3-phenylpropan-1-amine and ethylbenzene (by-product), with known concentrations, were prepared for calibration. The calibration curves were obtained by plotting the ratio of the analyte signal as a function of the analyte concentration. The calibration curve for (1-phenylethyl)(3-phenylpropyl)amine is presented in Chapter 2 (see section 2.2.5), Figure 3.1 shows the curve for 3-phenylpropan-1-amine and Figure 3.2 for ethylbenzene.

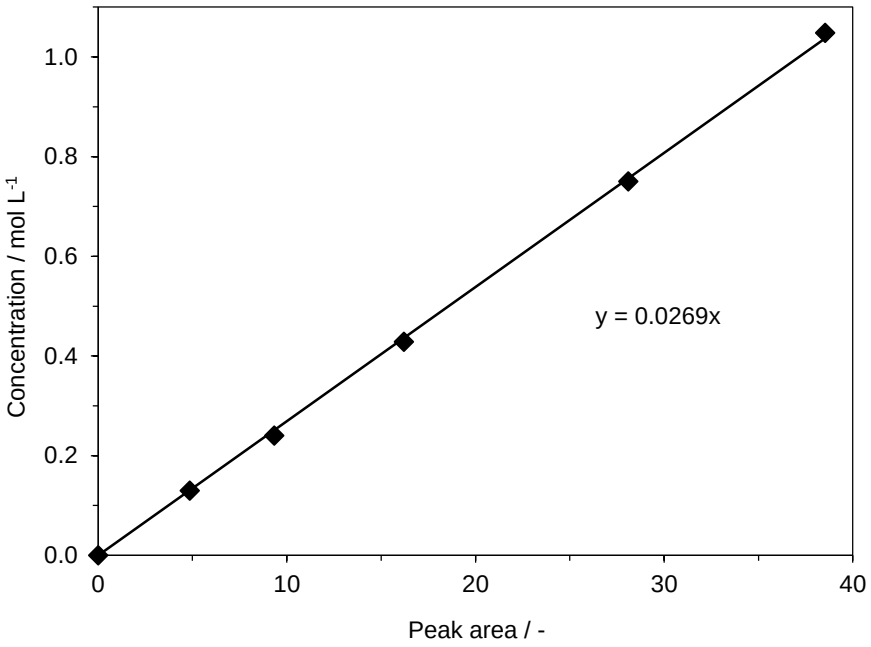

Figure 3.1. Calibration curve of GC analysis for 3-phenylpropan-1-amine.

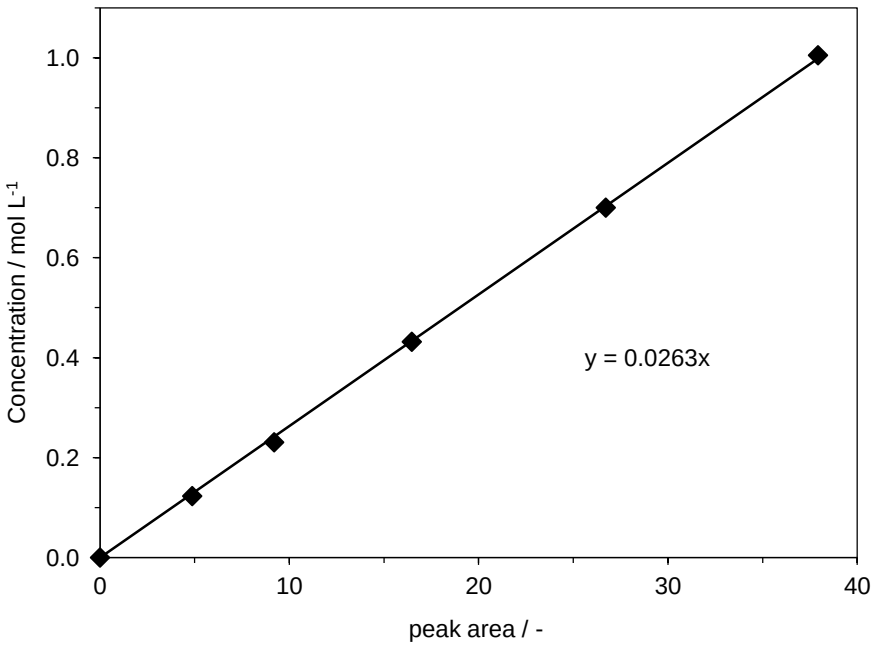

Figure 3.2. Calibration curve of GC analysis for ethylbenzene.

3.3. Results and discussion

3.3.1. Characterisation of synthetic carbon and Pd/C catalyst

A Micrometric ASAP 2020 analyser was used to perform the gas adsorption analysis using N_2 as a probing gas for obtaining the nitrogen adsorption isotherms of the carbon support and the catalyst (Figure 3.3).

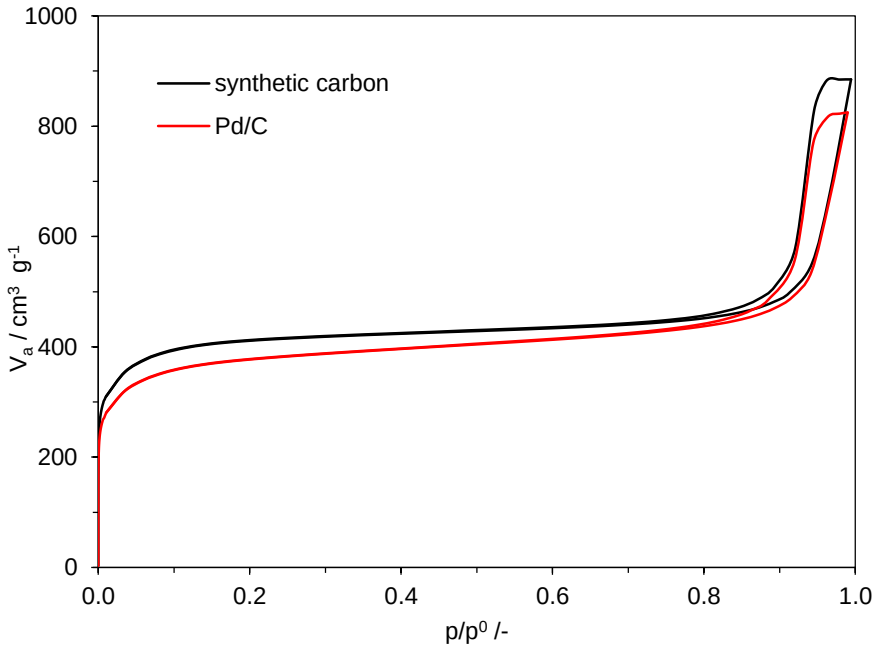

Figure 3.3. Nitrogen adsorption/ desorption isotherms for synthetic carbon and the prepared catalyst.

The specific surface area (S_{BET}) was calculated using a relative pressure range of 0.05 - 0.30. The original Barrett-Joyner-Halenda (BJH) method was used to calculate the median pore diameter from the adsorption branch of the isotherm. This method presumes that all pores are open-ended cylindrical pores and applies only to the mesopore and small macropore size range (Figure 3.4).

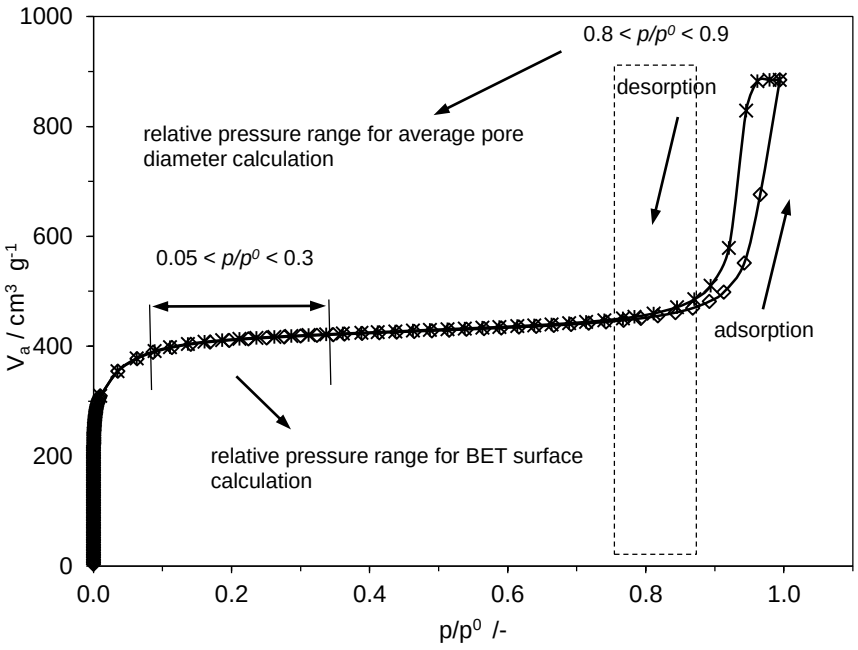

Figure 3.4. Nitrogen adsorption/ desorption isotherms of synthetic carbon.

The porous structure characteristics of both the carbon and the prepared Pd/C catalyst are reported in Table 3.1. The synthesised catalyst used a new synthetic carbon support (mesoporous) specifically designed for deposition of metal nanoparticles with a controlled particle size distribution. The average pore diameter ($d_{av.}$) was 22.8 nm for the carbon support and 16.5 nm for the Pd/C catalyst. The prepared Pd/C catalyst had a specific surface area of 983 m^2 g^{-1}, which is lower than that of the carbon support (1306 m^2 g^{-1}); that is, the support lost 25% of its area after impregnation of the palladium. It might be that this surface area loss was due to palladium nanoparticles blocking some pores.

Table 3.1.Porous structure characterisation data (by nitrogen adsorption at 77K) for synthetic carbons and the synthesised Pd/C catalyst.

	S_{BET} [a] / $m^2\ g^{-1}$	V_{micro} [b] / $cm^3\ g^{-1}$	V_{meso} [c] / $cm^3\ g^{-1}$	d_{ave} [c] / nm
Carbon support	1306	0.494	1.369	22.8
10% Pd/C	983	0.416	1.276	16.5

[a] Total surface area, calculated using a relative pressure range of 0.05 – 0.3 (to ensure that positive BET constants were obtained by using BET equation).
[b] Calculated using t-plot method. t-plot estimates of micropore volume and external surface area correspond here to the slit-shaped pore model.
[c] Determined from adsorption isotherms using the BJH method. The (4V/A) term was used in the estimation of average pore diameters, which corresponds to the assumed cylindrical model pore size.

3.3.2. Batch *vs* flow system for 1-phenylethyl group deprotection

To highlight the effectiveness of the flow process compared to the batch system for the deprotection of (1-phenylethyl)(3-phenylpropyl)amine to 3-phenylpropan-1-amine, some initial experiments were performed in a stainless steel batch reactor.

In the literature no data was found for 1-phenylethyl group deprotection under continuous flow conditions.

Lamb *et al.* (2009) has investigated the reaction in a batch system using borrowing hydrogen methodology. The authors performed the formation of *N*-protected primary amines from alcohols and *in situ* deprotection to give the primary amine. In this case, the hydrogenolysis reaction was carried out for 14 h.

Another example has been reported by Nugent *et al.* (2011). Here, secondary amines were synthesised *via* reductive amination of ketones which, after purification, underwent the hydrogenolysis reaction. Primary amines were synthesised in good isolated yield with a reaction time of 24 hours.

The data presented in Table 3.2 summarises the results obtained and clearly shows the advantage of flow processes over the traditional batch ones.

Table 3.2. Deprotection of 1-phenylethyl group over Pd/C for different reactors.

Reactor	Temperature / K	Pressure/ bar	Conversion / %	Reaction time / h
PBR[a]	393	8	100	0.03
X-Cube[b]	403	30	100	0.03
Batch reactor[c]	393	10	99	4
Batch reactor[d]	338	1	83[e]	14

[a] continuous three phase catalysis, 10 wt % Pd/C, 0.2 mol L^{-1} initial concentration (this work)
[b] continuous three phase catalysis, 10 wt % Pd/C, 0.1 mol L^{-1} initial concentration (this work)
[c] batch three phase catalysis, 10 wt % Pd/C, 0.2 mol L^{-1} initial concentration (this work)
[d] batch three phase catalysis, 10 wt % Pd/C (commercial catalyst), 0.2 mol L^{-1} initial concentration, (Lamb *et al.* 2009).
[e] isolated yield

3.3.3. Continuous catalytic rig with multichannel packed-bed reactor

In this section, the deprotection of (1-phenylethyl)(3-phenylpropyl)amine is investigated using a continuous catalytic rig with a multichannel packed-bed reactor developed at the University of Bath. The optimisation of the reaction was studied in detail by varying different process parameters, *i.e.* liquid and gas flow rates, pressure, temperature and initial concentration of reagents.

3.3.3.1. Effect of liquid flow rate

Figure 3.5 shows the product concentration as a function of time-on-stream at two liquid flow rates: 0.5 and 1.0 mL min^{-1}. The product concentration initially decreased with time, followed by a plateau after *ca.* 15 minutes time-on-stream, indicating that a steady state was achieved in the reactor 15 minutes after introducing the reagents.

A lower conversion of secondary amine was measured for higher liquid flow rates, due to the reduction of the liquid phase residence time in the reaction channel.

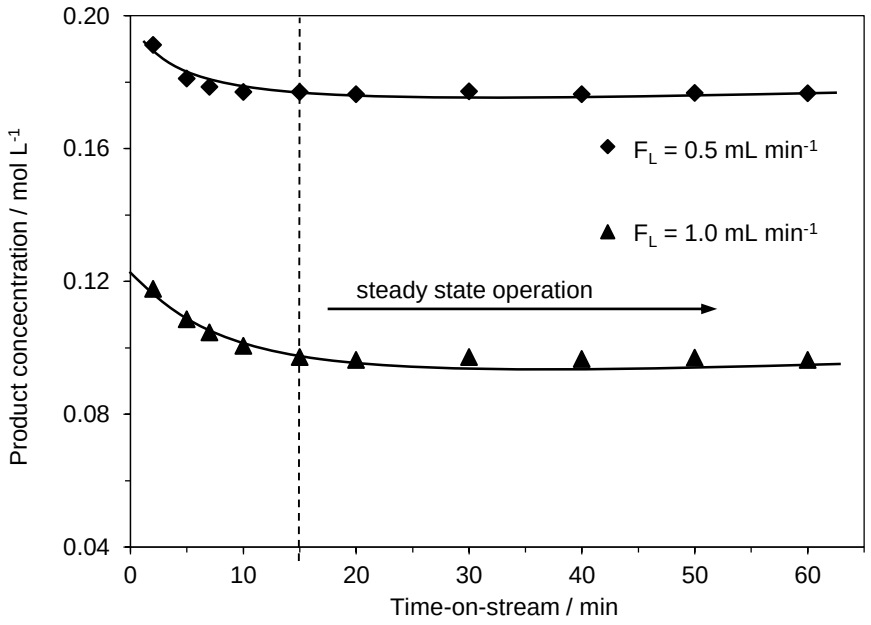

Figure 3.5. Product concentration in the outlet of the reactor as a function of time-on-stream. P_T = 8 bar, F_G = 21.0 mL (STP) min^{-1}, $C_{S,0}$ = 0.2 mol L^{-1},T = 393K.

The effect of the liquid flow rate on the conversion of secondary amine into primary amine is presented in Figure 3.6. In these studies, the 3 × 3 × 100 mm channel was used with about 0.45g of catalyst. Increasing the liquid flow rate resulted in a decrease in conversion, which is consistent with a reduction in residence time of the liquid phase in the reactor. Maximum conversion of secondary amine was achieved at a flow rate of 0.2 mL min^{-1} with a substrate concentration of 0.2 mol L^{-1}. The selectivity to primary amine remained the same (100%) for all the liquid flow rates studied in this work. No side products were detected.

Based on the obtained results of conversion (Figure 3.6) the rate of product formation was calculated according to Equation 2.1 (Chapter 2, section 2.3.1.2).

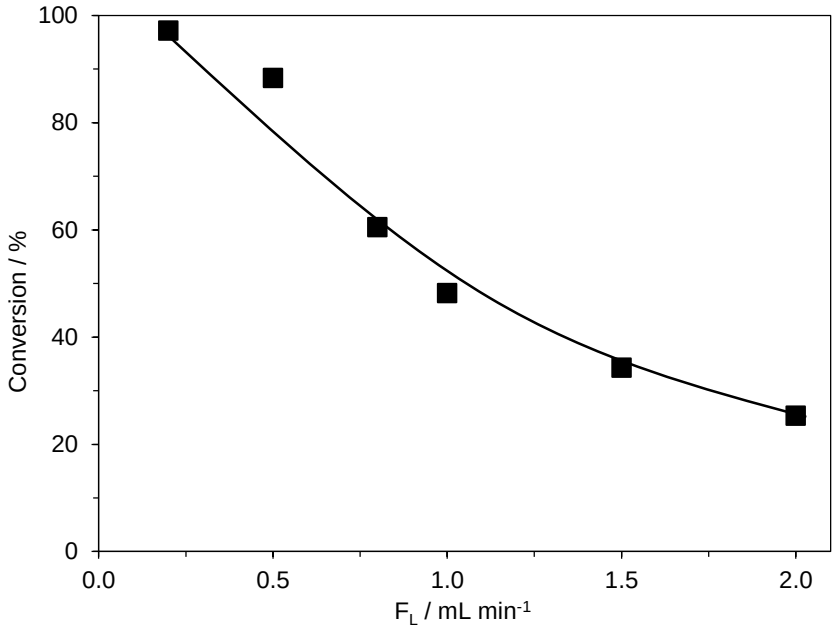

Figure 3.6. Influence of the liquid flow rate on the conversion of 2° amine. P_T = 8 bar, F_G = 21.0 mL (STP) min^{-1}, $C_{S,0}$ = 0.2 mol L^{-1}, T = 393K.

Figure 3.7 shows the influence of the liquid flow rate on the overall rate of the product formation. As can be seen, the rate of product formation depends strongly on the liquid flow rate up to 0.5 mL min^{-1}, but when the flow rate is increased further only a very slight increase in the overall rate of product formation was noticed. The increase in overall rate of product formation with liquid flow rate indicates the influence of mass transfer for the liquid flow rate up to 0.5 mL min^{-1}; thereafter, however, the reaction is almost independent of the external mass transfer. Higher liquid flow rates, therefore, promote the transition of the rate-limiting step from mass transfer to the kinetic regime.

Based on the data presented in Figure 3.7 it is possible to distinguish between the mass transfer and the kinetic regimes. The overall catalytic process is independent of the liquid flow rate, which means it becomes independent of the mass transfer limitations at $F_L \geq$ 0.5 mL min^{-1}.

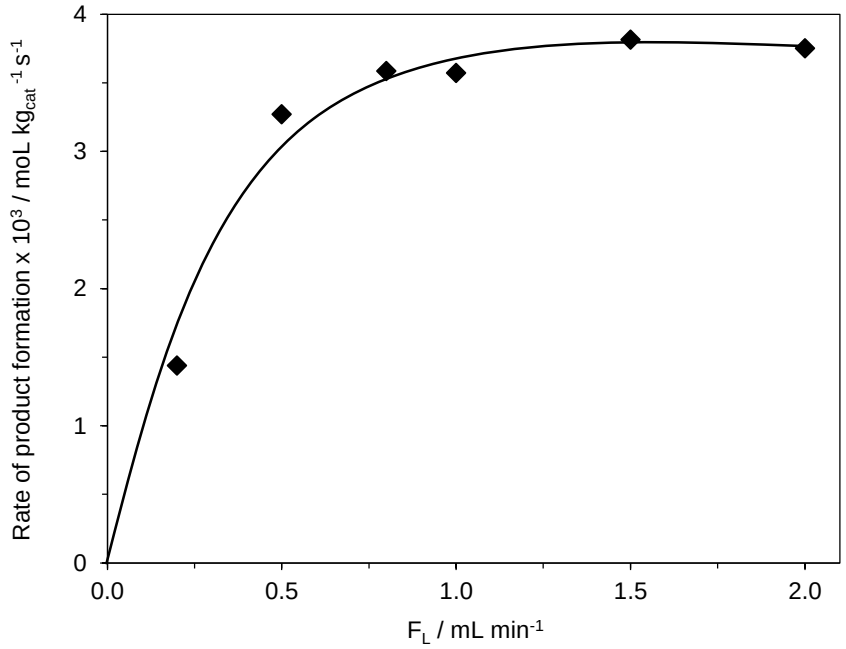

Figure 3.7. Influence of the liquid flow rate on the average rate of product formation. P_T = 8bar, F_G = 21.0 mL (STP) min^{-1}, $C_{S,0}$ = 0.2 mol L^{-1}, T = 393K.

3.3.3.2. Effect of hydrogen flow rate

Figure 3.8 shows the influence of the hydrogen flow rate on the product concentration at 393K. The product concentration increased significantly when the hydrogen flow rate was increased up to 15 ml (STP) min^{-1} at 393K, but further increases in the hydrogen flow rate had no significant effect on product formation.

The most probable reason for the increase in the product concentration at increased hydrogen flow rates is the presence of higher concentrations of hydrogen in the reactor. At low gas flow rates (F_G < 15 mL (STP) min^{-1}) the product concentration depends on the hydrogen flow rate and this was limited by its supply. The hydrogen supply line presented on the Figure 3.8 represents the theoretical stoichiometric volumetric flow rate of hydrogen for a given product concentration. Additionally, the change in the flow rate of the gas phase affects the volumetric fraction of the liquid phase (saturation, β_L) in the reactor, thereby changing the superficial velocity of the liquid phase. The increase in the gas flow rate, therefore, decreases the liquid phase

saturation, β_L, (Equation 3.1) and increases the linear velocity of the liquid phase (Duduković *et al.* 2002; Larachi *et al.* 1991a; Larachi *et al.* 1991b).

$$\beta_L = \frac{F_L}{F_L + F_G} \tag{3.1}$$

where:

β_L liquid saturation (-);

F_L volumetric flow rate of the liquid phase (mL min^{-1});

F_G volumetric flow rate of the gas phase (mL min^{-1}).

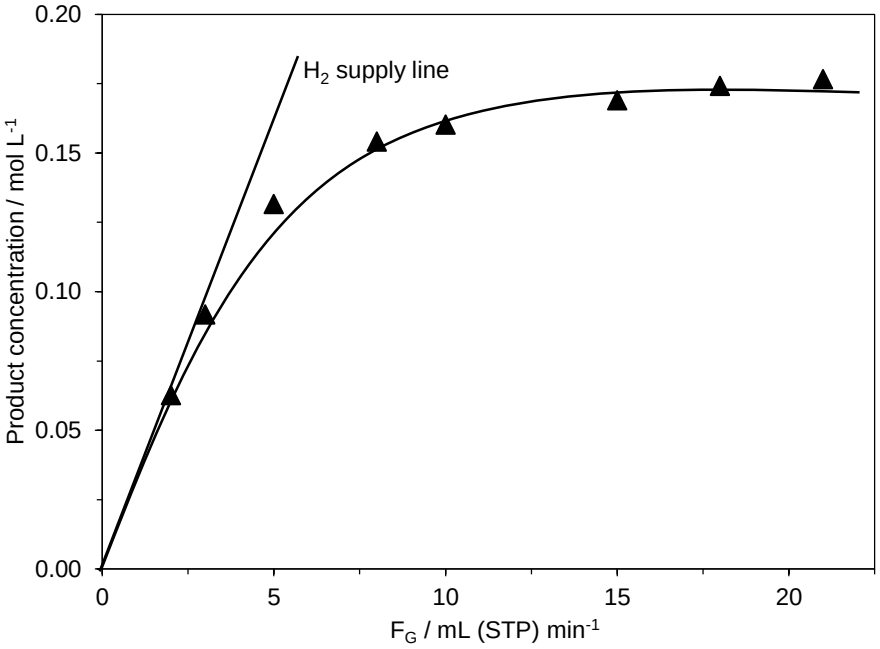

Figure 3.8. Influence of the hydrogen flow rate on the product concentration.
P_T = 8bar, F_L = 0.5 mL min^{-1}, $C_{S,0}$ = 0.2 mol L^{-1}, T = 393K.

The influence of the hydrogen flow rate on the overall rate of product formation was calculated according to Equation 2.1, Chapter 2, section 2.3.1.2 and is presented in Figure 3.9. The rate of product formation increased from 1.16 up to $3.13 \cdot 10^{-3}$ mol kg_{cat}^{-1} s^{-1} at 2.0 and 15.0 mL (STP) min^{-1} of hydrogen flow rate, respectively. For flow rates higher than 15.0 mL (STP) min^{-1} however, the rate of product formation was found to be almost independent of the hydrogen flow rate: only increasing by *ca.* 4%. Therefore, the possibility of mass transfer limitations can be

neglected after 15.0 mL (STP) min^{-1} of hydrogen flow rate at 393K and at 8 bar of total pressure.

Further experiments were carried out at 393K and with a hydrogen flow rate of 21.0 mL (STP) min^{-1} to neglect the effect of the mass transfer resistance.

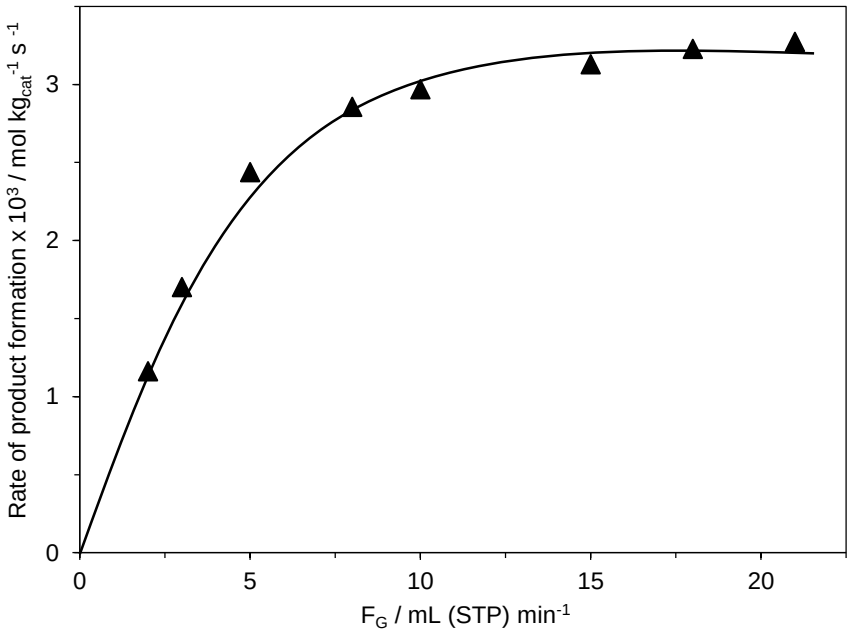

Figure 3.9. Influence of the hydrogen flow rate on the overall rate of product formation. P_T = 8bar, F_L = 0.5 mL min^{-1}, $C_{S,0}$ = 0.2 mol L^{-1}, T = 393K.

3.3.3.3. Effect of operating pressure and concentration

The influence of the total pressure on the secondary amine conversion was studied at a constant liquid flow rate of 0.5 mL min^{-1} and a hydrogen flow rate of 21.0 mL (STP) min^{-1} to avoid the mass transfer limitations on product formation (Figure 3.10). Here, the conversion increased from 84 to 89% at 7 and 8 bar of the system pressure and remained constant as the pressure increased further.

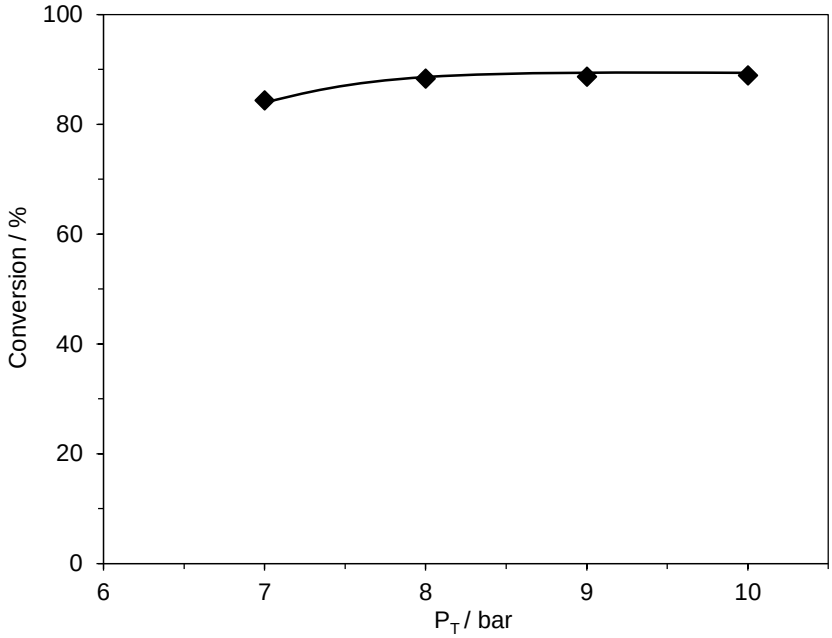

Figure 3.10. Influence of hydrogen pressure on the conversion.
F_G = 21.0 mL (STP) min^{-1}, F_L = 0.5 mL min^{-1}, $C_{S,0}$ = 0.2 mol L^{-1}, T = 393K.

Figure 3.11 presents the influence of total system pressure on the rate of product formation. The rate of product formation increased by *ca.*5% as the total pressure increased from 7 to 8 bar. No significant effect of total pressure on the rate of product formation was noticed with further increases in the system pressure.

Increasing the total pressure of hydrogen in the system increases the solubility of hydrogen in the liquid phase and thus larger saturation is expected at higher pressures. The effect of the system pressure on the rate of product formation confirmed that the reaction is not limited by the diffusional resistances.

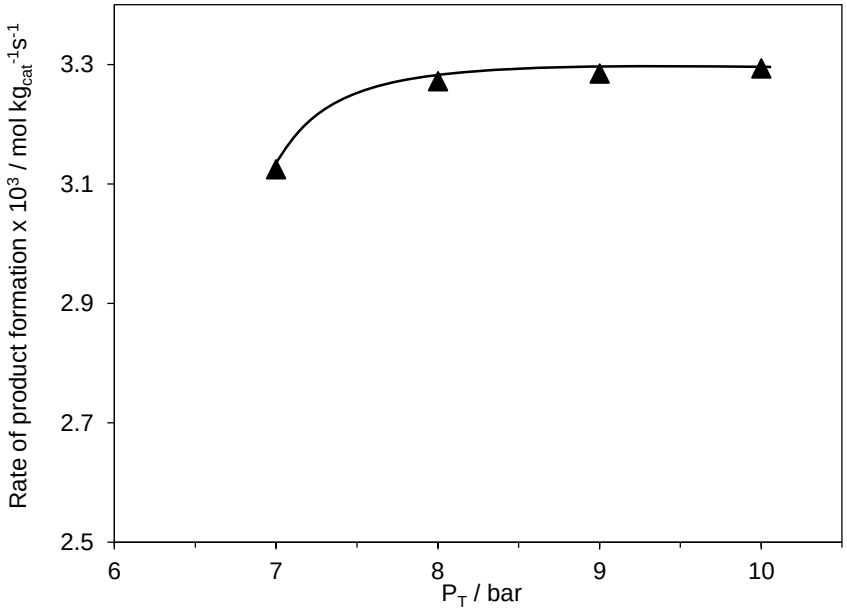

Figure 3.11. Influence of hydrogen pressure on the rate of product formation. F_G = 21.0 mL (STP) min^{-1}, F_L = 0.5 mL min^{-1}, $C_{S,0}$ = 0.2 mol L^{-1}, T = 393 K.

The influence of the initial reagent concentration on the product formation is presented in Figure 3.12. An increase of the substrate concentration increased the product concentration due to saturation of the catalyst surface with reactant. The product formation was observed to increase as the initial concentration of secondary amine was increased up to 0.3 mol L^{-1} of the initial reagent concentration. Further increases in the reagent concentration had no significant effect on the product formation. This asymptotic approach at higher concentrations may imply a Langmuir-Hinshelwood type of kinetic effect exists for the secondary amine deprotection (see Chapter 6).

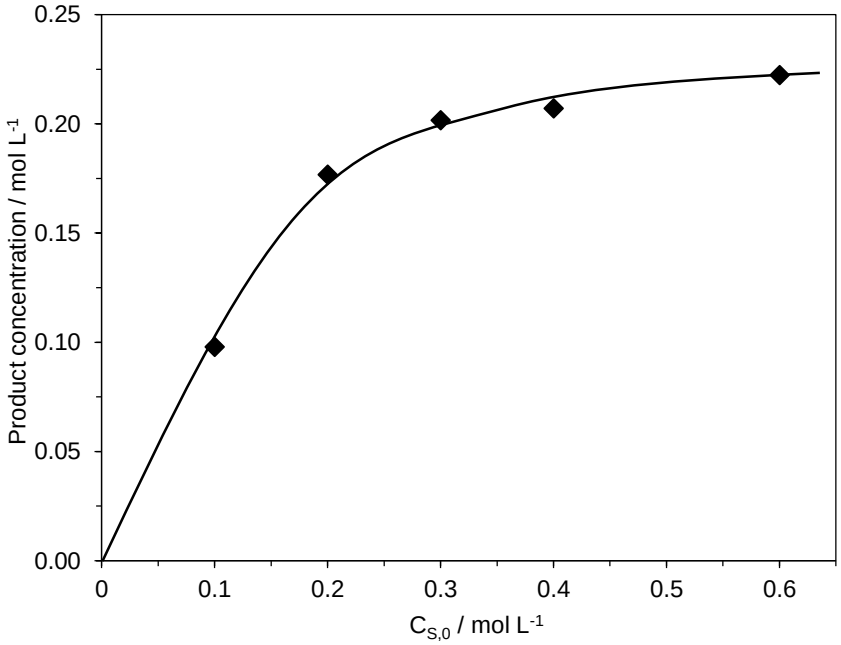

Figure 3.12. Influence of the initial concentration of secondary amine on the product formation. P_T = 8bar, F_G = 21.0 mL (STP) min^{-1},F_L = 0.5 mL min^{-1}, T = 393K.

3.3.3.4. Effect of reaction temperature

The effect of the reaction temperature on the conversion of secondary amine is presented in Figure 3.13 and was studied in the temperature range of 353 to 393K. Isothermal conditions were kept at all conversion levels, which were proven by temperature measurements in close proximity to the reaction channel (distance from thermocouple to reaction fluid *ca.* 100 µm). The hydrogenolysis of (1-phenylethyl)(3-phenylpropyl)amine is an mildly exothermic reaction with standard reaction enthalpy of - 86 kJ mol^{-1} (the thermodynamic properties of compounds involved in the reaction were obtained from ChemBioDraw Ultra 12.0). However, the very effective heat transfer characteristics of the compact reactor ensured an isothermal mode of operation (Kolios *et al.* 2000; Losey *et al.* 2001; Rouge *et al.* 2001; Kandlikar 2002; Watel 2003; Plucinski *et al.* 2005).

The conversion increased from 67 to 88% when the temperature increased from 353 to 393K. The increase in the reaction temperature had no influence on the reaction selectivity, which remained constant for the whole range of temperatures investigated, *i.e.* 100%.

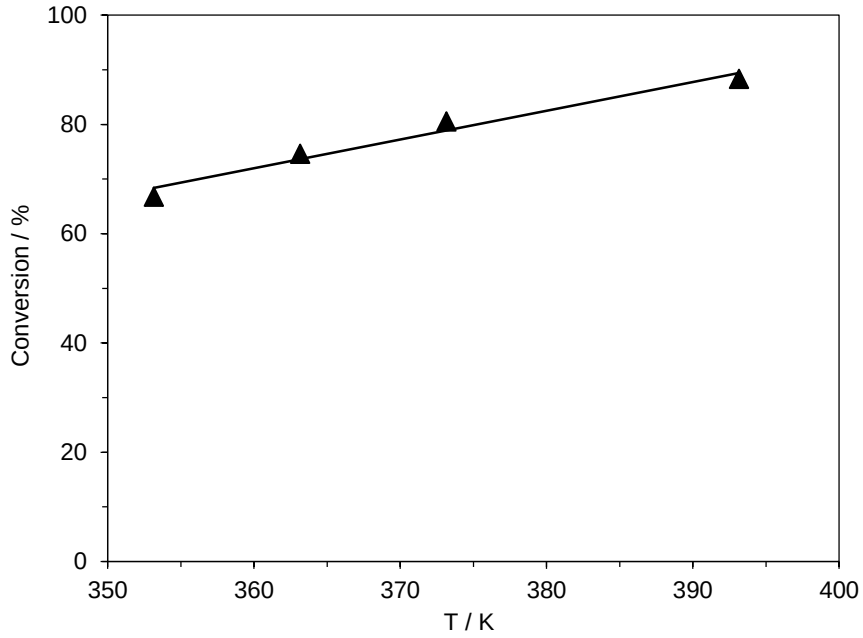

Figure 3.13. The influence of the reaction temperature on the conversion of secondary amine. P_T = 8bar, F_G = 21.0 mL (STP) min^{-1}, F_L = 0.5 mL min^{-1}, $C_{S,0}$ = 0.2 mol L^{-1}

3.3.3.5. Catalyst stability

The time-on-stream experiments were carried out in the 3 × 3 × 100 mm reactor channel which was fully loaded with the catalyst to evaluate the activity of 10% Pd/C. The conversion of 2^o amine to 1^o amine remained constant for the first three runs, *ca.* 88%; runs 4 and 5, meanwhile, showed a decrease in conversion of *ca.* 4% (Figure 3.14). Each experiment was carried out for 13 hours with breaks after 5 hours of continuous running in order to supply more feed solution. The feed tank volume was *ca.* 250 - 300 mL. After each experiment, the system was washed with the solvent (MeOH) to prevent any blockage in the line from the residue of the reactants and products.

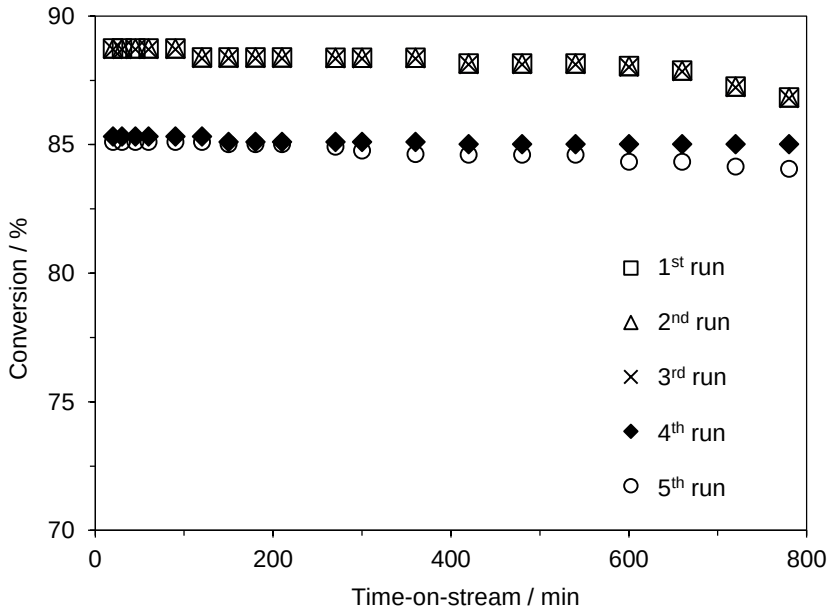

Figure 3.14. The 2^{o} amine conversion as a function of time-on-stream. P_T = 8 bar, F_G = 21.0 mL (STP) min^{-1}, F_L = 0.5 mL min^{-1}, $C_{S,0}$=0.2 mol L^{-1},T = 393K.

Figure 3.15 shows a relation between logarithmic Turn Over Frequency (TOF) and catalyst life time. The TOF was calculated using Equation 2.1 (see Chapter 2) and the rate of catalyst deactivation was calculated using Equation 2.2 (see Chapter 2). The data presented in Figure 3.15 indicates that the rate of catalyst deactivation is very small and was estimated to be 2 ·10^{-4} h^{-1}.

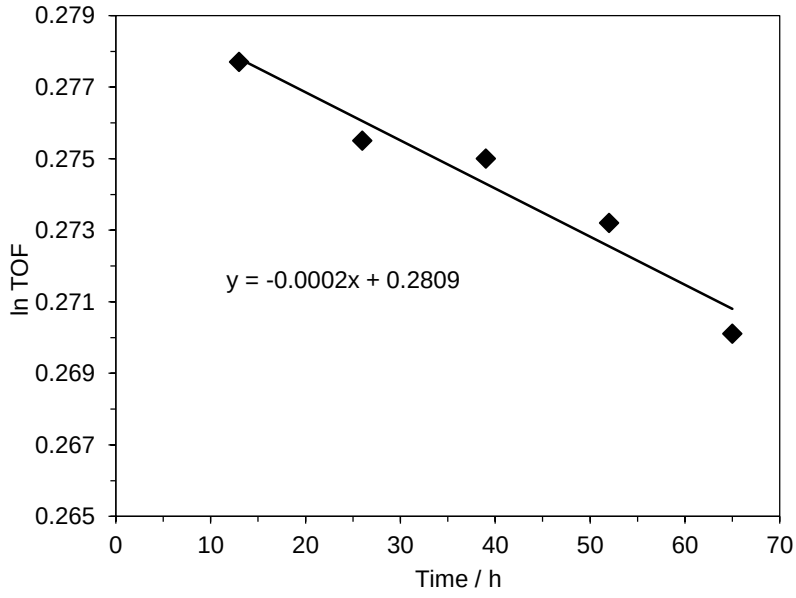

Figure 3.15. The deactivation rate of Pd/C catalyst over 65 hours during the synthesis of primary amine.

3.3.3.6. Reactor efficiency with split injection of hydrogen

In the multichannel compact reactor the gas and liquid phases can be introduced to the reactor in various ways. In this section the possibility of using different injection points for the gas phase was investigated. The reactor has three channels of the same dimensions (3 × 3 × 100 mm) and therefore two of them were interconnected. The reaction channel arrangements with different gas injection options are illustrated in Figure 3.16. For all configurations, the amount of hydrogen supplied relative to the catalyst amount used remained the same. Compared with the arrangement A, a double amount of hydrogen was used due to the increase of the catalyst amount in the arrangements B and C. It was considered very likely that the conversion would change since the mass of the catalyst in the reactor had changed (Table 3.3).

A)

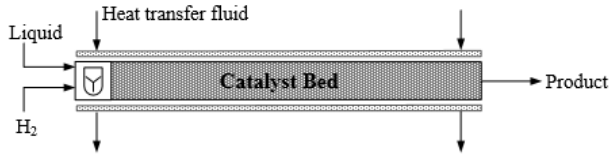

B)

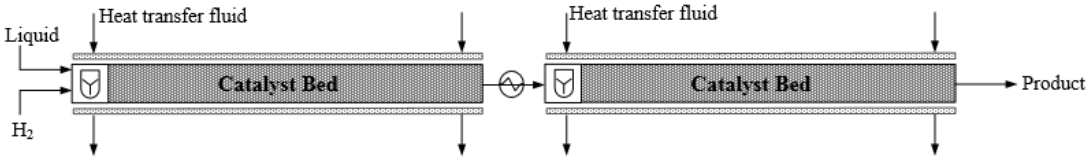

C)

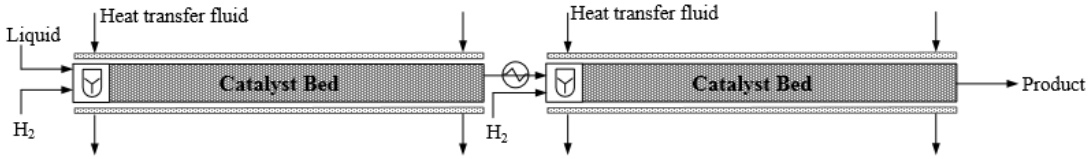

Figure 3.16. Channel arrangement for split hydrogen injection experiments.

The conversion of secondary amine increased from 88% to 93%, for the arrangements A and B, respectively. The hydrogen flow rate used in arrangement A was 21.0 mL (STP) min^{-1} and for arrangement B was 42.0 mL (STP) min^{-1}, due to the double amount of catalyst at 0.2 mol L^{-1} of reagent initial concentration, 8 bar of total pressure, 0.5 mL min^{-1} liquid flow rate and a reaction temperature of 393K. An identical total amount of hydrogen as in case B was split and injected at the entrance of the two channels for arrangement C. The product yield increased up to 98% using channel arrangement C.

Another set of experiments for all channel arrangements was performed at a higher initial reagent concentration, *i.e.* at 0.4 mol L^{-1}. The conversion of secondary amine increased by *ca.* 5% for arrangement B in comparison with arrangement A, *i.e.* from 52% to 57%. For arrangement C, an identical total amount of hydrogen as in case B was split and injected at the entrance of the two consecutive channels. The conversion increased up to 84% using channel arrangement C. In all three cases selectivity to primary amine remained the same, *i.e.* 100%.

The increase in the conversion between case A and B/C is due to the doubling of the mass of the catalyst. Furthermore, the split gas distribution along the length of the reaction channel resulted in a higher yield of the desired product. However, the concept of dosing the required amount of gaseous reactant at different positions along the catalyst bed might represent a flexible method of performing more complex reactions under continuous flow conditions using the packed-bed multichannel reactor developed at the University of Bath.

Table 3.3. The influence of the hydrogen split injection on reactor efficiency.
P_T = 8 bar, F_G = 21.0 mL(STP) min^{-1}, F_L = 0.5 mL min^{-1}, $^{a}C_{0,S}$ = 0.2 mol L^{-1}, $^{b}C_{0,S}$ = 0.4 mol L^{-1}, T = 393K.

Channel arrangement	**[a]Conversion (%)**	**[b]Conversion (%)**
A	88	52
B	93	57
C	98	84

3.3.4. X-Cube™ flow reactor

In this section the deprotection of (1-phenylethyl)(3-phenylpropyl)amine was investigated using the commercially available X-Cube™ flow reactor manufactured by ThalesNano. The optimisation of the reaction was studied in detail by varying process parameters such as, liquid flow rate, pressure, temperature and initial concentration of the reagents, using onechannel fully loaded with catalyst.

3.3.4.1. Effect of liquid flow rate

Figure 3.17 shows the product concentration in the outlet solution as a function of time-on-stream at two two liquid flow rates used: 1.0 and 1.5 mL min^{-1}. The product concentration initially decreased with time followed by a plateau after *ca.* 20 minutes time-on-stream indicating that a steady state was achieved in the reactor. At higher liquid flow rates the product concentration was lower due to the decreased residence time in the reaction channel.

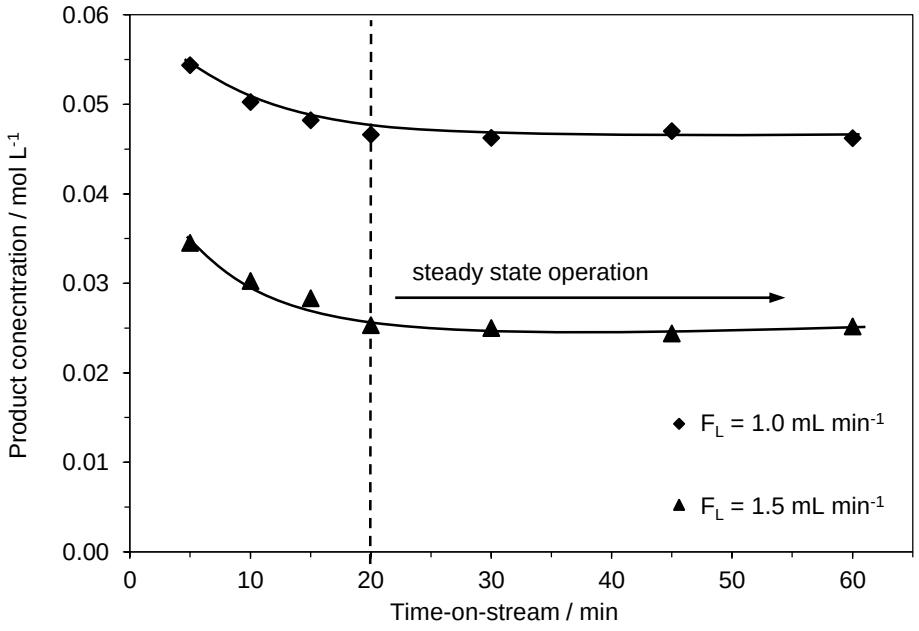

Figure 3.17. The evaluation of steady-state conversion for various reaction conditions. P_T =30 bar, $C_{S,0}$ = 0.1 mol L^{-1}, T = 413K.

Figure 3.18 shows the influence of liquid flow rate at various total pressures on the conversion of secondary amine into primary amine. At a liquid flow rate of 0.2 mL min^{-1} the conversion of (1-phenylethyl)(3-phenylpropyl)amine remained constant at *ca.* 98 - 99% for all the pressures investigated. For higher liquid flow rates, $F_L \geq 2.0$ mL min^{-1}, the conversion continued to be independent of the supplied pressure (Figure 3.18), although it was slightly higher for a reactor pressure of 30 bar.

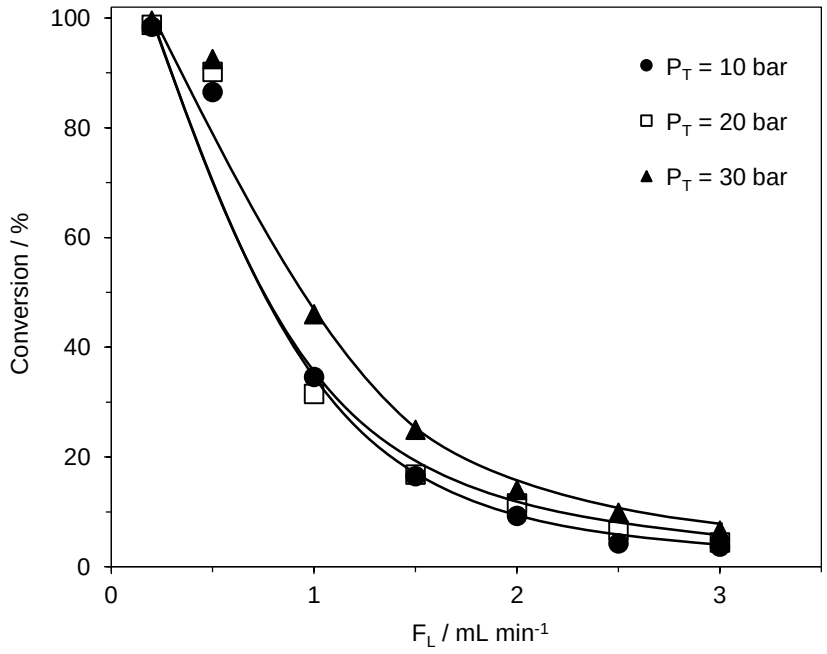

Figure 3.18. Influence of liquid flow rate on the conversion of the hydrogenolysis of (1-phenylethyl)(3-phenylpropyl)amine. $C_{S,0}$ = 0.1 mol L^{-1}, T = 413K.

An increase in the liquid flow rate decreased the rate of product formation (Figure 3.19). The results presented in Figure 3.19 shows that for liquid flow rates of 0.2 and 0.5 mL min^{-1} the rate of product formation is independent of the pressure. Experiments were performed at 10, 20 and 30 bar of total pressure.

It is worth mentioning here that the reductive amination and hydrogenolysis reactions behave differently when performed using the X-Cube™ flow reactor since the gas flow rate in the X-Cube™ flow reactor is unknown (Figure 3.19 and Figure 2.23, Chapter 2). It is also worth noting that in the PBR the rate of product formation and rate of reaction both increased as the liquid flow rate increased, and the different

behaviour exhibited in the X-Cube™ flow reactor may be a consequence of the unknown hydrodynamic reaction conditions in the reactor.

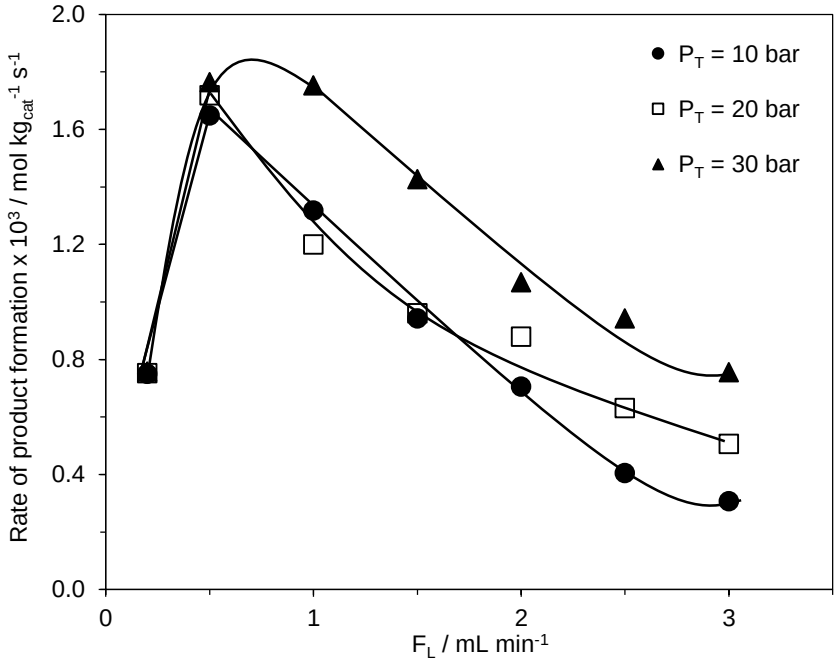

Figure 3.19. Influence of the liquid flow rate on the rate of hydrogenolysis of (1-phenylethyl)(3-phenylpropyl)amine. $C_{S,0}$ = 0.1 mol L^{-1},T = 413K.

3.3.4.2. Effect of operating pressure

The data presented in Figure 3.20 shows the influence of the total reactor pressure on the conversion of secondary amine. The value of conversion increased by only *ca.* 7% at 0.5 mL min^{-1} of liquid flow rate, while the pressure was increased from 10 to 30 bar, indicating that the conversion is almost independent of the applied system pressure.

The influence of the system pressure on the rate of product formation is presented in Figure 3.21. The overall rate of product formation was found to be almost independent of the applied pressure at 0.5 mL min^{-1} of liquid flow rate, while increasing the liquid flow rate up to 2.0 mL min^{-1} increased the rate of product formation from 0.7 to $1.07 \cdot 10^{-3}$ mol kg_{cat}^{-1} s^{-1}.

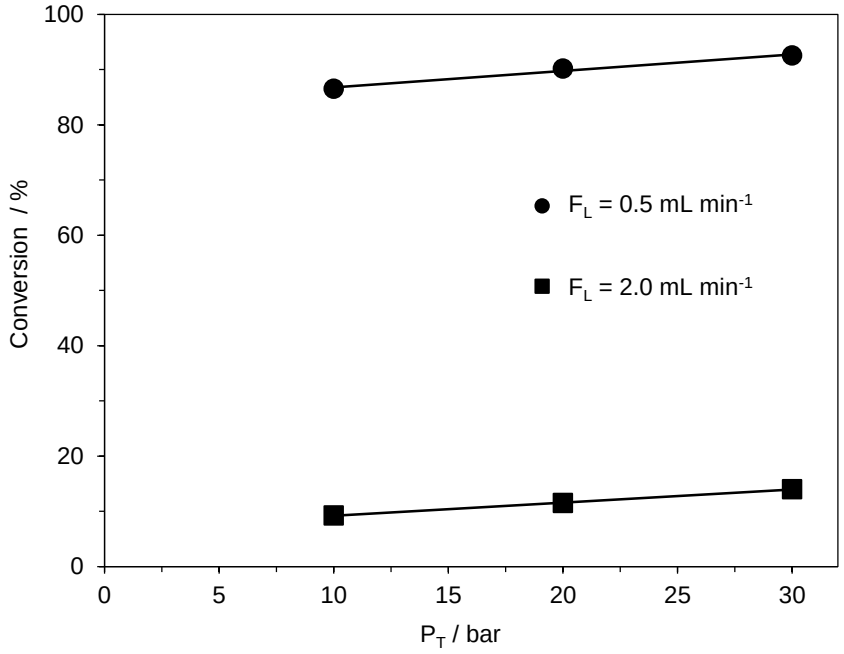

Figure 3.20. Influence of pressure on the conversion of (1-phenylethyl) (3-phenylpropyl)amine. $C_{S,0}$ = 0.1 mol L^{-1},T = 413K.

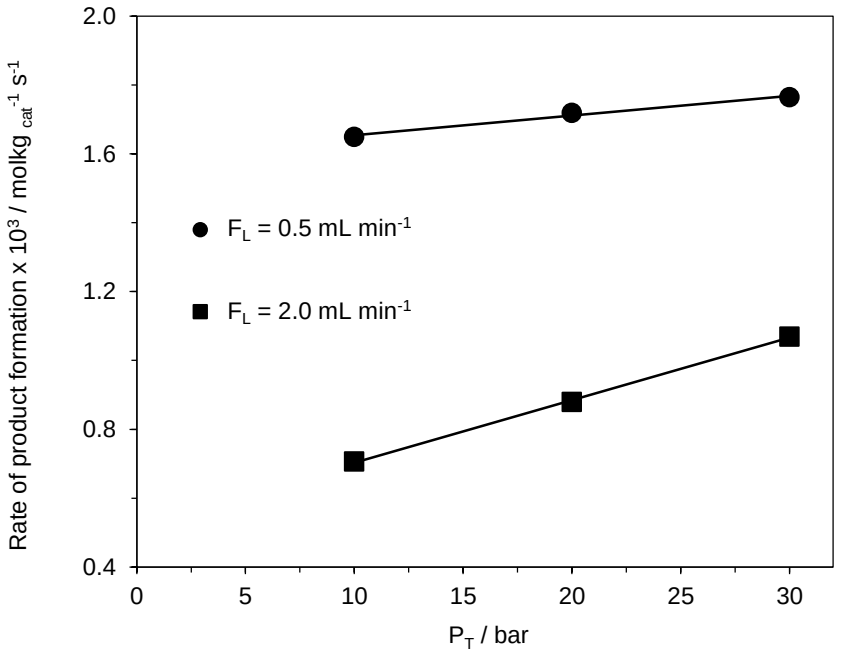

Figure 3.21. Influence of pressure on the rate of product formation of the hydrogenolysis of (1-phenylethyl)(3-phenylpropyl)amine. $C_{S,0}$ = 0.1 mol L^{-1}, T = 413K.

3.3.4.3. Effect of reaction temperature

The data presented in Figure 3.22 shows the influence of the reaction temperature on the product concentration. Experiments were performed in the temperature range of 353 – 433K. As the temperature was increased from 353K to 413K, the product concentration increased from 0.02 to 0.09 mol L^{-1}. Further increases in the reaction temperature, *i.e.* T ≥ 433K, decreased the product concentration. At 433K, 100% conversion was achieved; however a 40% loss of primary amine was noticed due to the deamination of the desired product. Altogether, therefore, under these reaction conditions, 413K was the optimal temperature for the reaction. A higher concentration of by-product (ethylbenzene) was measured by GC.

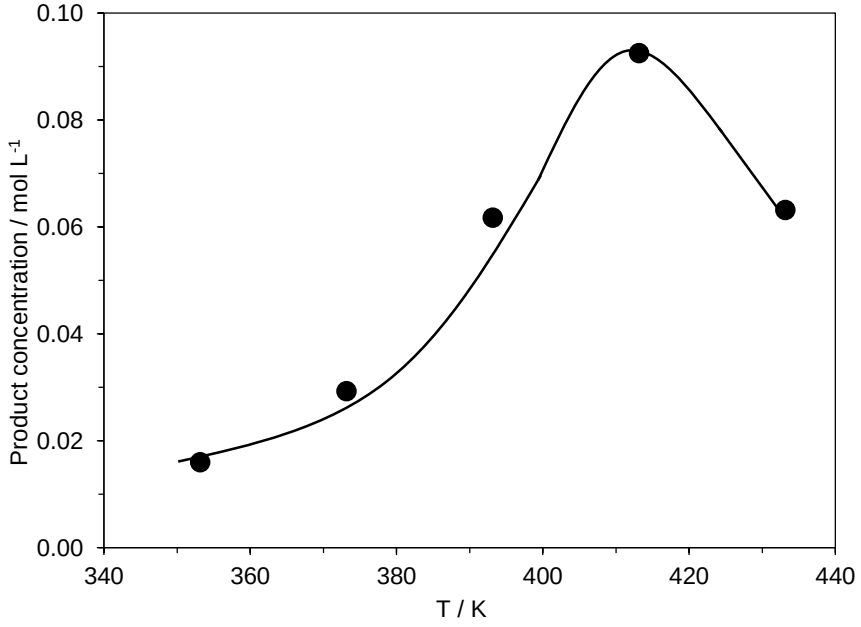

Figure 3.22. Influence of the reaction temperature on the product concentration. P_T = 30 bar, F_L = 0.5 mL min^{-1}, $C_{S,0}$ = 0.1 mol L^{-1}.

The effect of reaction temperature on the rate of product formation is presented in Figure 2.23. The positive effect of temperature on the secondary amine conversion is in the range of 353 - 413K, with the rate of product formation increasing from 0.35 to 1.76· 10^{-3} mol kg_{cat}^{-1} s^{-1} as the temperature increased from 353 to 413K.

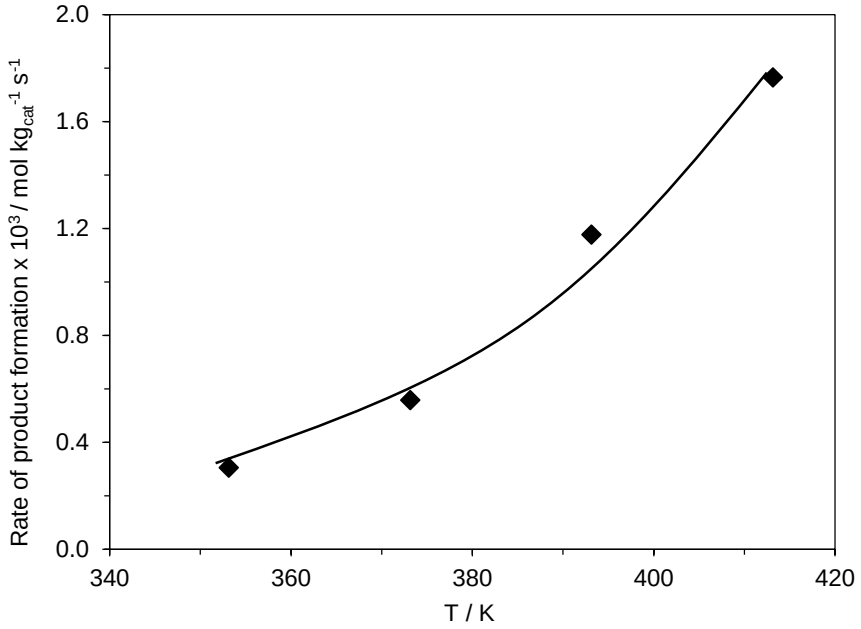

Figure 3.23. Influence of the reaction temperature on the overall rate of product formation. P_T = 30 bar, F_L = 0.5 mL min^{-1}, $C_{S,0}$ = 0.1 mol L^{-1}.

3.3.2.4. Effect of reagent concentration

The influence of the reagent concentration on secondary amine conversion is presented in Figure 3.24. Experiments were performed at 413K and in the range 0.05 to 0.6 mol L^{-1} substrate concentration. An increase in the substrate concentration decreased the conversion from 100% to 25% for the reagent concentrations of 0.05 and 0.6 mol L^{-1}.

Figure 3.25 presents the influence of the substrate concentration on the overall rate of product formation. As the initial reagent concentration was increased from 0.05 to 0.2 mol L^{-1}, the rate of product formation increased *ca.* 58%. Further increases in reagent concentration, however, only increased the rate of product formation by *ca.* 15%. A saturation-like isotherm was observed, suggesting a heterogeneous catalytic mechanism for the hydrogenolysis reaction.

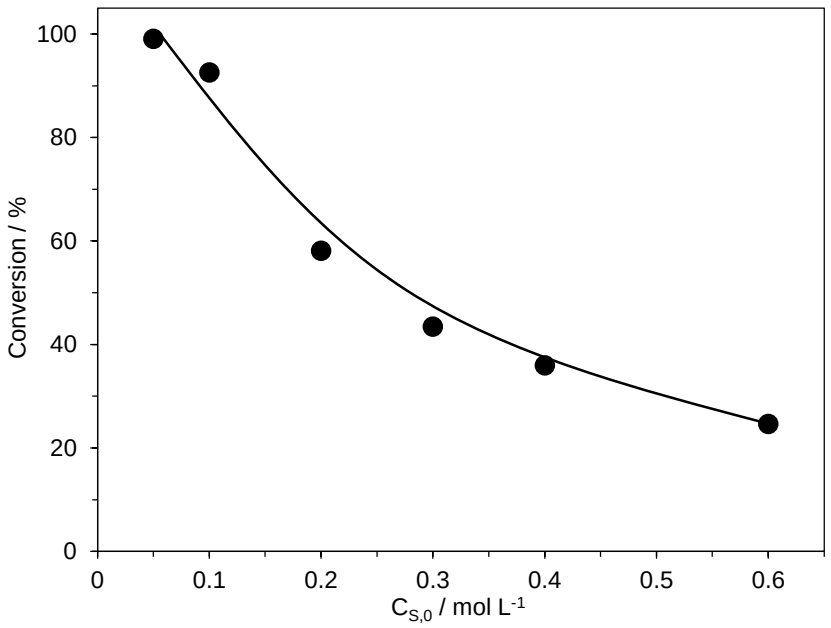

Figure 3.24. Effect of the initial concentration of reagent on secondary amine conversion. P_T = 30 bar, F_L = 0.5 mL min^{-1}, T = 413K.

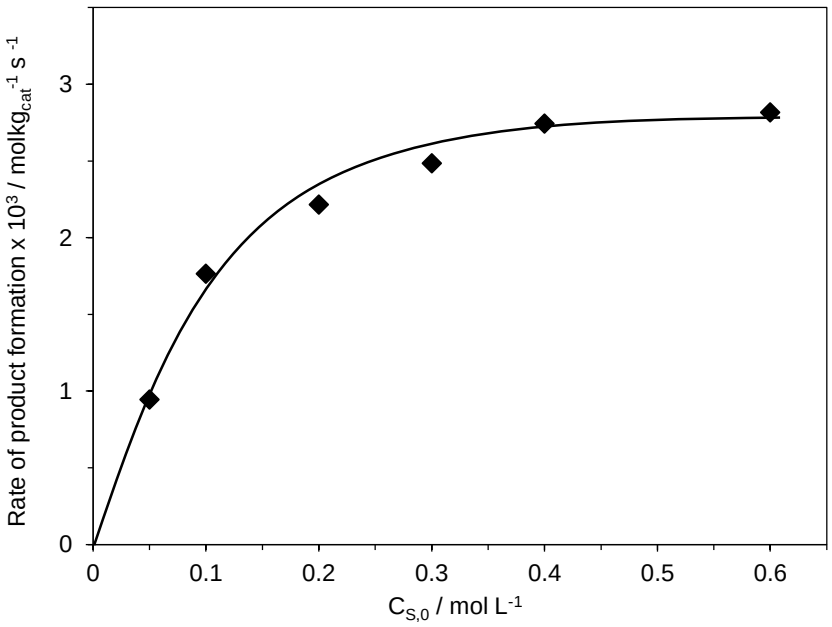

Figure 3.25. Effect of the initial concentration of reagent on the rate of product formation. P_T = 30 bar, F_L = 0.5 mL min^{-1}, T = 413K.

3.3.4.5. Catalyst stability

The time-on-stream experiments were carried out to evaluate the activity of 10% Pd/C in the X-Cube^{TM} reactor for the hydrogenolysis of (1-phenylethyl) (3-phenylpropyl)amine (Figure 3.26). Each experiment was carried out for 13 hours with a liquid flow rate of 0.2 mL min^{-1}. After each experiment, the system was washed with a solvent (MeOH) to prevent any blockage in the line from the residue of the reactants.

For the first run, over 13 hours of continuous flow, the average conversion of the 2^{o} amine to the desired primary amine was 99%. The second and third runs showed a slight decrease in the conversion to 98%. Since the decrease in the conversion between the first and the third run was only 1% it is evident that the Pd/C catalyst synthesised for this work had a high activity and good stability over the 65 hours of the experiment.

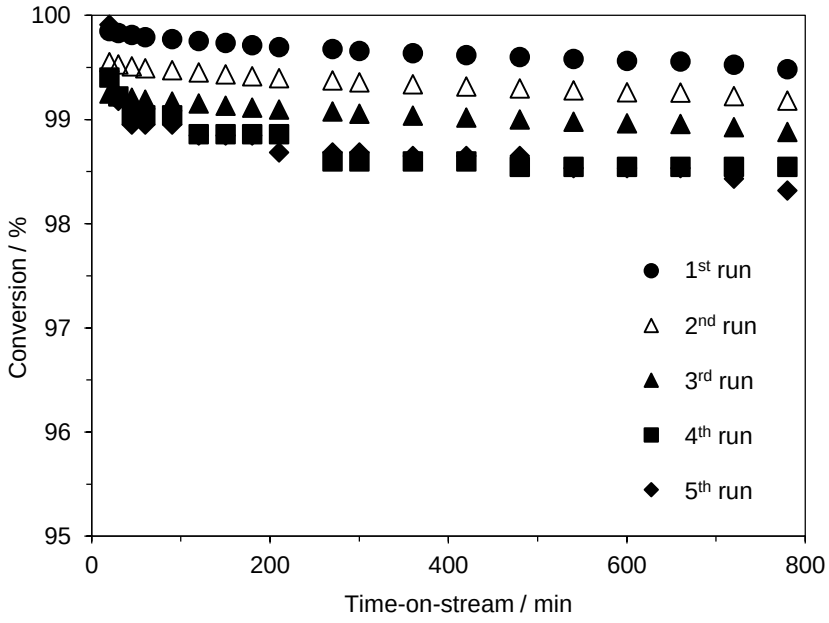

Figure 3.26. The 2^{o} amine conversion as a function of time-on-stream. P_T = 30 bar, F_L = 0.2 mL min^{-1}, $C_{S,0}$ = 0.1 mol L^{-1}, T = 413K.

In order to evaluate the catalyst deactivation Figure 3.27shows the relationship between logarithmic Turn Over Frequency (TOF) and catalyst life-time. The TOF was calculated based on Equation 2.3 (see Chapter 2, section 2.3.1.6), while the rate of catalyst deactivation was calculated using Equation 2.4 (see Chapter 2, section 2.3.1.6). The data presented in Figure 3.27 indicates that the rate of catalyst deactivation was very small; just *ca.* $2.0 \cdot 10^{-4}$ h^{-1}.

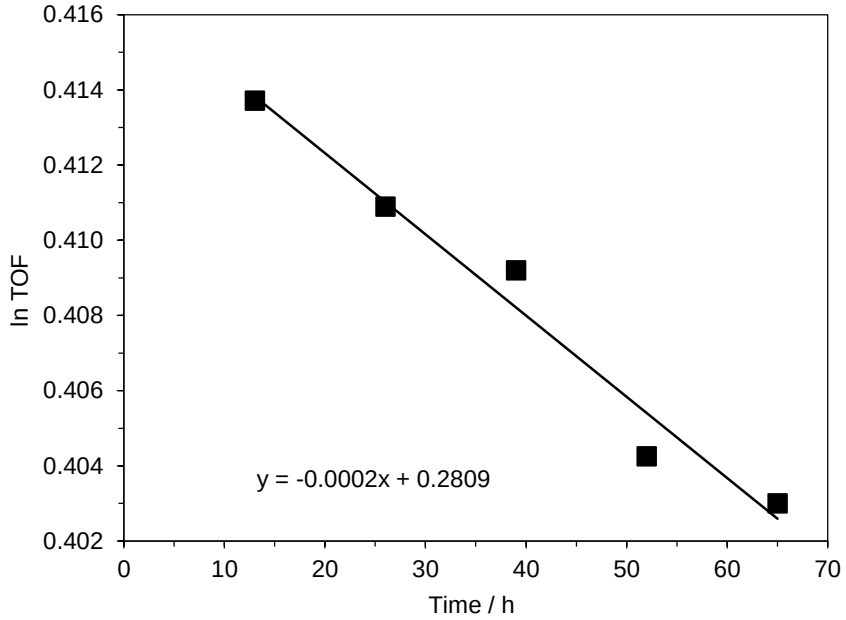

Figure 3.27. The deactivation rate of Pd/C catalyst during the synthesis of 1° amine.

It is worth noting that the values of the catalyst deactivation constant calculated for the X-Cube™ flow reactor and the PBR (see Chapter 3, section 3.3.3.6) are the same, indicating that this value is characteristic to the reaction, not the reactor.

3.4. Conclusions

The deprotection of secondary amine, (1-phenylethyl)(3-phenylpropyl)amine was successfully investigated using a continuous catalytic rig with multichannel packed-bed reactor, and a commercially available X-Cube™ flow reactor.

To the best of the author's knowledge this approach has not previously been investigated in the context of continuous flow processing.

A comparison of the results obtained from both reactors showed that the continuous catalytic rig with a multichannel packed-bed reactor was more efficient than the X-Cube™ (Table 3.4). For example, 0.0024 mol h^{-1} of product can be obtained in a single pass through the reaction channel (3 × 3 × 100 mm) with an undiluted catalyst bed, while the X-Cube™ flow reactor can only produce 0.0012 mol h^{-1} in a single pass through the reaction channel (70 × 4 mm). In comparison with the multichannel packed-bed reactor used in the continuous catalytic rig, a higher pressure and temperature must be used in order to achieve 100% of conversion when using the X-Cube™ flow reactor. As was mentioned before, however, temperature is a very important parameter for the deprotection reaction: too low temperature leads to no product formation while one that is too high may lead to the decomposition of the desired primary amine. Furthermore, too long contact time with the catalyst active sites may also contribute to this problem.

Table 3.4. Comparison of the reaction conditions for both reactors.

	PBR	**X-Cube™**
P_T (bar)	8	30
T (K)	393	413
F_L (mL min^{-1})	0.2	0.2
F_G (mL min^{-1})	21.0	-
$C_{S,0}$ (mol L^{-1})	0.2	0.1
m_{cat} (g)	0.45	0.45
Productivity (mol h^{-1})	0.0024	0.0012

The effectiveness of the packed-bed multichannel reactor for performing the model deprotection reaction was much better, with a more intensified process being achieved compared to that obtained when, the X-Cube™ flow reactor was used. The results also showed that the staged injection of hydrogen was beneficial for this model reaction.

Chapter 4

Tandem - Reductive Amination of Aldehydes and Hydrogenolysis of Secondary Amines

4.1. Introduction

Amines are used in a variety of chemical industry sectors in the production of pharmaceuticals, agrochemicals, fine chemicals, polymers and pigments (Lawrence 2004). Primary amines are the most useful, however their high reactivity makes their selective synthesis very challenging (Ayedi *et al.* 2013; Gunanathan and Milstein 2008).

This group of compounds can be prepared using various methods although reductive amination is the most widely used. This process is based on the conversion of aldehydes into amines followed by a reduction step (Gross *et al.* 2002; Kadyrov and Riermeier 2003; Dangerfield *et al.* 2010; Gunanathan and Milstein 2008; Ayedi *et al.* 2013).

In this chapter, the results of a one-pot continuous flow reductive amination-hydrogenolysis reaction are presented. The aldehyde was reductively aminated under very similar reaction conditions to those found in Chapter 2, except now, without work-up; the second reactor with a channel containing 10% Pd/C was connected, allowing *in situ* deprotection of the secondary amine into a primary amine. Determination of the success of the overall reaction is based on the isolated yields of the primary amines (see section 4.3.1.5 and 4.3.2.4).

The primary amine synthesised by the hydrogenolysis reaction can undergo an unwanted deamination reaction under certain reaction conditions, as seen in Chapter 3.

Nugent *et al.* (2011) has performed a sequential reductive amination-hydrogenolysis reaction in a batch system, finding the following rate depressing factors for the hydrogenolysis step in the one-pot (batch) procedure:

1. non-alcoholic reaction solvents;
2. in some cases slightly lower reaction temperatures;
3. the heterogeneous reaction mixture from the reductive amination stage may reduce the availability of the catalyst active sites for hydrogenolysis reaction.

The coupling of the reductive amination of aldehyde and hydrogenolysis of secondary amine is presented on Scheme 4.1.

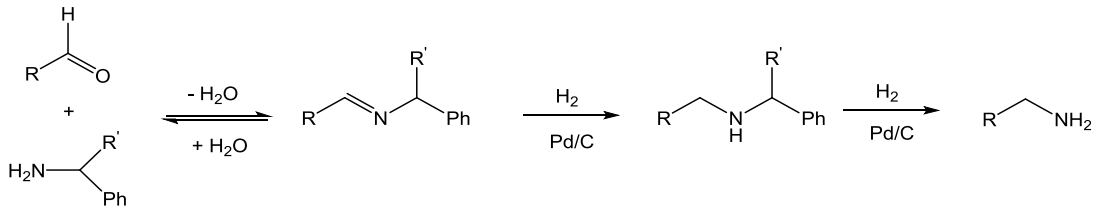

Scheme 4.1. General scheme of the synthesis of 1º amines via coupling of reductive amination of aldehyde and hydrogenolysis of 2º amine.

In this study, the synthesis of 3-phenylpropan-1-amine has been chosen as a model reaction. This tandem process involves two steps, reductive amination of hydrocinnamaldehyde and hydrogenolysis of (1-phenylethyl)(3-phenylpropyl)amine to 3-phenylpropan-1-amine (Scheme 4.2). Each of these steps has been studied in detail previously (see Chapters 2 and 3).

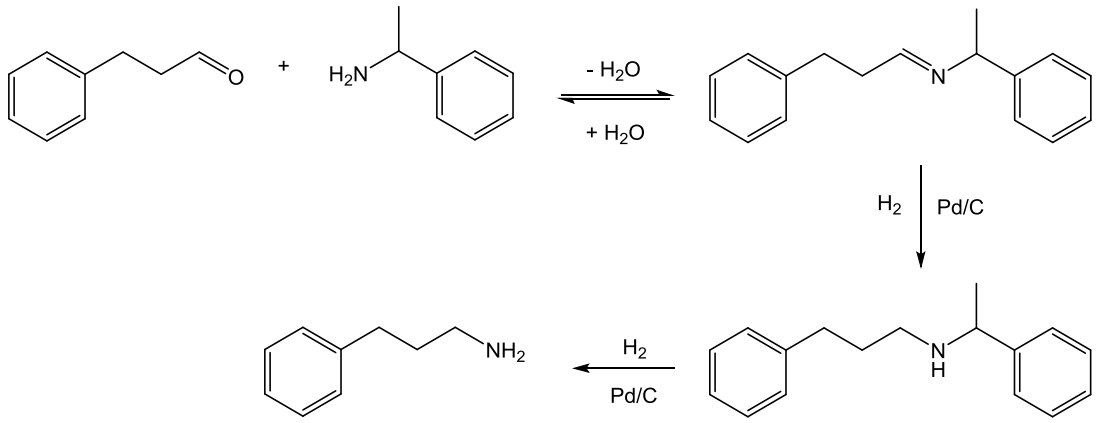

Scheme 4.2. Tandem reductive amination of hydrocinnamaldehyde – hydrogenolysis of (1-phenylethyl)(3-phenylpropyl) amine to 3-phenylpropan-1-amine.

4.2. Experimental

4.2.1. Pd/C catalyst and reagents

The synthesis of the catalyst has been described in Chapter 2, section 2.2.1, using mesoporous microspherical synthetic carbon as a support (kindly supplied by Mast Carbon Ltd).

All chemicals used in this study were purchased from Acros Organics, Sigma-Aldrich, Fluka or Lancaster and were used without further purification.

4.2.2. Structured compact reactor

Details of the structured multichannel reactor are given in Chapter 2, section 2.2.2.

4.2.3. Continuous catalytic rig and procedure for continuous experiments

The tandem reductive amination of aldehydes (ketones) - hydrogenolysis of secondary amines reaction was performed using a continuous catalytic rigas shown in Figure 4.1.

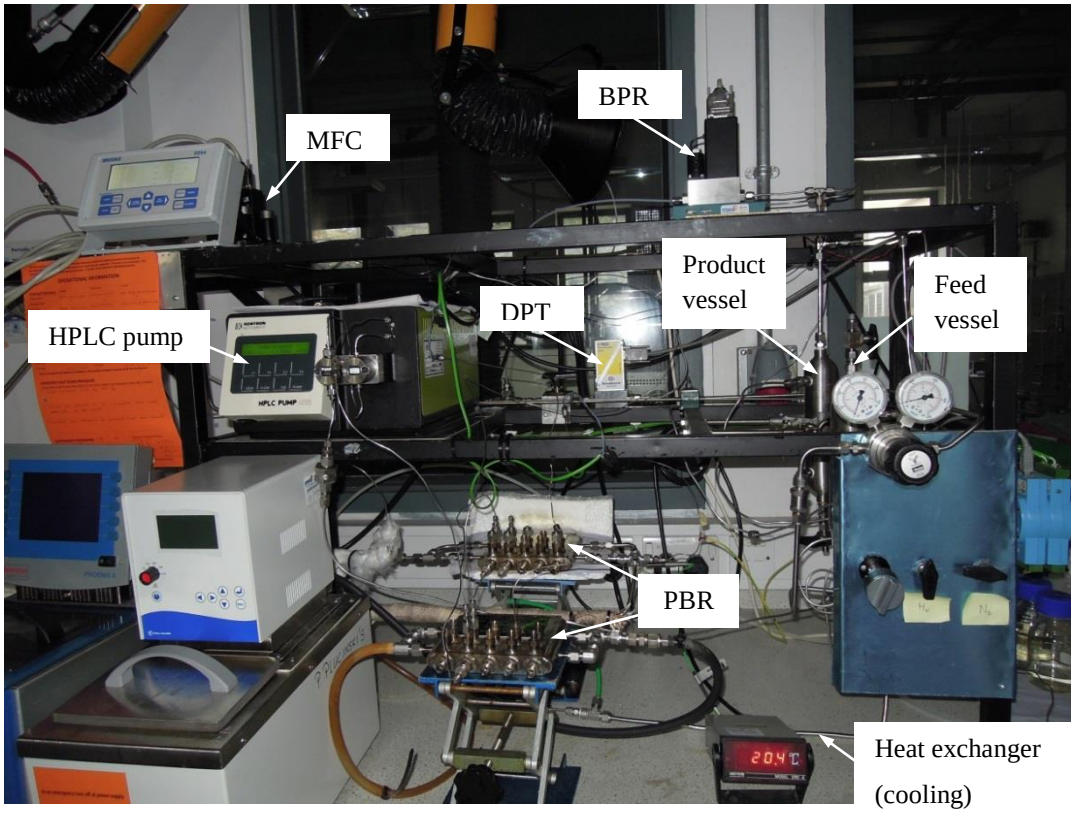

Figure 4.1.The continuous catalytic rig with the structured multichannel reactors for multi-step synthesis.

The experimental rig is similar to the one used in previous studies (see Chapter 2, section 2.2.3.). In this work, two consecutive structured multichannel reactors were used. Based on the previous studies on reductive amination of aldehydes (ketones) (Chapter 2) and hydrogenolysis of secondary amines (Chapter 3) it has been found that in order to achieve high conversion and selectivity the reductive amination reaction must be performed at a temperature lower than 363K, while the deprotection reaction has to be carried out at higher temperature (T > 363K). For this reason two multichannel packed-bed reactors were connected in series as part of the continuous catalytic rig for the tandem process.

The reaction channels used in this study had a square cross-section of 3 × 3 mm and were 100 mm length. Figure 4.2 presents a schematic diagram of the reactor's channel configuration for the multi-step synthesis.

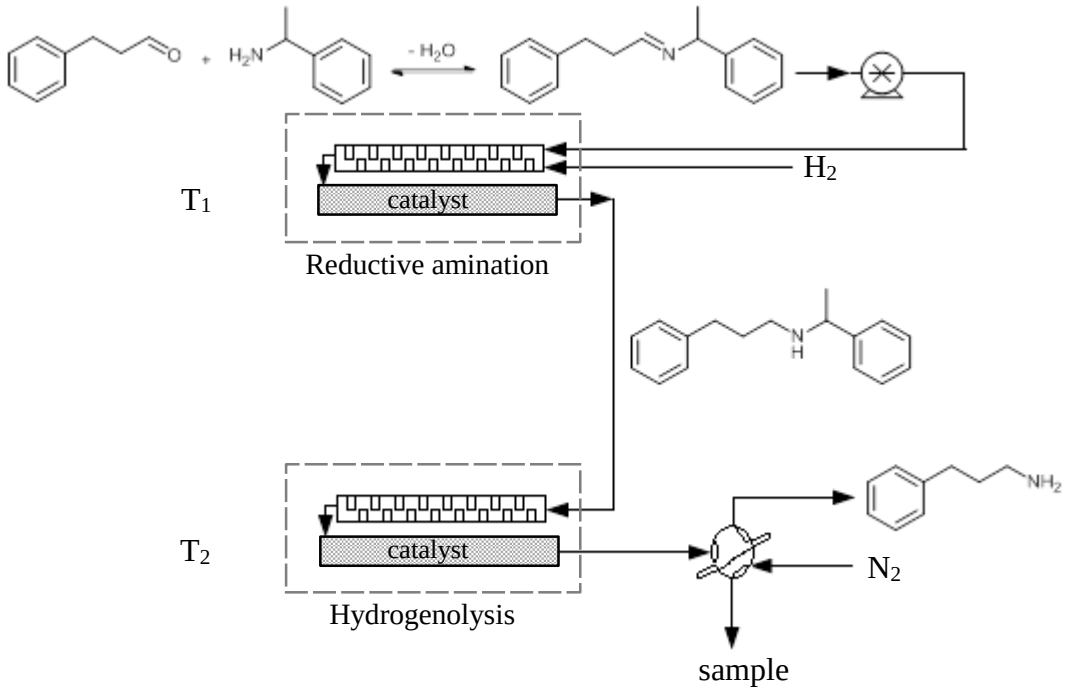

Figure 4.2. A schematic diagram of the reactors configuration for the consecutive reductive amination of aldehyde (ketone)-hydrogenolysis of secondary amines reaction.

The liquid reagents (aldehyde/ ketone and primary amine) were premixed in MeOH and introduced to the feed vessel. The reaction channels were equipped with standard Swagelok® fittings for connecting the liquid and gas lines. The system was pressurised with hydrogen gas and the operating pressure was set by a back pressure regulator (BPR) (Brooks, No F00574/001), the pressure drop across the reactor was monitored by a differential pressure transducer (DPT) (Bronkhorst®, No M9201747B). The hydrogen gas was supplied to the reaction channels at the desired flow rate using mass flow controllers (MFC) (Brooks, No F00562/001). The temperature of the reactors was controlled by re-circulating baths using heat transfer fluid (water - in the first reactor and mineral oil - in the second reactor) flowing through the micro-heat exchangers in both reactors. An HPLC pump (Kontron, No 422M) was used to flow the liquid reactants at the desired flow rate from the feed vessel through the reaction channels packed with the catalyst. The product was collected in the second vessel via a low dead-volume six-way valve (Valco Instruments) equipped with a 250 μL sample loop.

4.2.4. Analysis techniques

Gas chromatography (GC, Varian CP - 3800) was used to analyse reaction substrates/ intermediates/ products using a polar capillary column (CP Sil - 8CB). All samples collected during the experiments were analysed without further purification.

The calibration curves for the model reaction, *i.e.* reductive amination of hydrocinnamaldehyde with α-methylbenzylamine and hydrogenolysis of (1-phenylethyl)(3-phenylpropyl)amine to 3-phenylpropan-1-amine and ethylbenzene (by-product) were presented previously in Chapter 2, section 2.2.5 and Chapter 3, section 3.2.5.

Products were isolated as amine hydrochloride salts. After removing the solvent under vacuum, the clear solution was acidified using 1M HCl in diethyl ether. Samples were concentrated under vacuum to a solid and then recrystallized by dissolving in EtOH and adding EtOAc.

For the determination of the chemical structures of the synthesised products ^{1}H NMR analysis spectra were run in DMSO - d_6 (≥99.9%), purchased from Fluorochem on a Bruker Avance 250 (250 MHz).

Mass spectrometry analysis was performed using a micrOTOF electrospray time-of-flight (ESI - TOF) mass spectrometer (Bruker Daltonik, GmbH, Bremen, Germany) coupled to an Agilent 1200 LC system (Agilent Technologies, Waldbronn, Germany).

The results of the ^{1}H NMR and mass spectrometry analysis are presented in Appendix II.

4.3. Results and discussion

4.3.1. Continuous catalytic rig with multichannel packed-bed reactor

The optimisation of flow conditions for the reductive amination of aldehydes was systematically investigated by varying liquid and gas flow rates, pressure, temperature and reagent concentration. The results obtained for the reductive amination of aldehydes in a continuous catalytic rig (Figure 4.1, Chapter 4, section 4.2.3) with the structured compact reactor developed at the University of Bath are presented in the next section of this chapter.

4.3.1.1. Effect of liquid flow rate

The effect of the liquid flow rate on the average rate of product formation for the tandem - reductive amination of aldehydes and *in-situ* hydrogenolysis of secondary amines was studied in two reactors at various temperatures, T_1 and T_2, for reductive amination and hydrogenolysis, respectively.

The initial reaction conditions were chosen based on the results of the earlier experiments in Chapters 2 and 3:

- pressure - 8 bar;
- hydrogen flow rate - 21.0 mL (STP) min^{-1};
- concentration - 0.2 mol L^{-1};
- temperature of first and second reactor - 298K and 393K.

Each of the reactors had a channel with the dimensions of 3 × 3 × 100 mm loaded with the 10% Pd/C catalyst.

The influence of the liquid flow rate on the product concentration is shown in Figure 4.3. For the substrate concentration used in this study, *i.e.* $C_{S,0}$ = 0.2 mol L^{-1}, a 100% conversion of the imine was achieved in a single pass through a fully loaded reactor channel with 10% Pd/C in the first reactor at 298K and at 0.1 and

0.2 mL min^{-1} liquid flow rate. It was found, however, that when the liquid flow rate was 0.1 mL min^{-1} the concentration of the by-product (ethylbenzene) was higher than the concentration of primary amine, *i.e.* 0.23 mol L^{-1} (ethylbenzene) and 0.17 mol L^{-1} (primary amine). This indicates a 15% loss of the 1° amine. Too high concentration of the by-product is a consequence of this unwanted deamination reaction of the primary amine (Scheme 4.3), which has probably occured due to the liquid phase residing for too long a time in the second reactor.

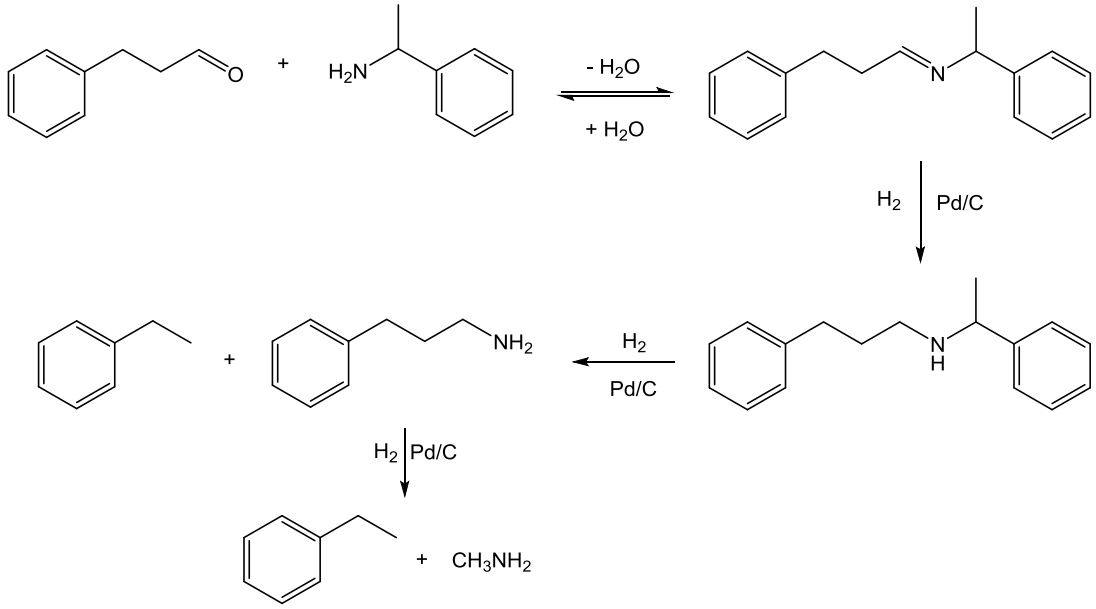

Scheme 4.3. Tandem reductive amination of hydrocinnamaldehyde - hydrogenolysis of (1-phenylethyl)(3-phenylpropyl) amine to 3-phenylpropan-1-amine with an (unwanted) deamination reaction to ethylbenzene.

A lower product concentration was measured for higher liquid flow rates. This was due to the reduction of the liquid phase residence time in the reaction channel. Primary amine was obtained with 100% selectivity and conversion at 0.2 mL min^{-1} of the liquid flow rate.

Figure 4.4 presents the influence of the liquid flow rate on the average rate of primary amine formation. As was shown in Chapter 2, for the given process conditions, the conversion of imine in the first reactor was 100%, therefore, in order to calculate the overall rate of primary amine formation, the mass of catalyst in the second reactor was used. The average rate of product formation depends strongly on the liquid flow rate up to 0.5 mL min^{-1}. When the liquid flow rate was increased further than this only a very slight increase in the overall rate of product formation was noticed. The increase

in overall reaction rate with liquid flow rate indicates the influence of mass transfer for liquid flow rates up to 0.5 mL min^{-1}. A further increase in the liquid flow rate indicates that the reaction is almost independent of the mass transfer limitation, as was seen for the individual reactions (Chapter 2 and 3).

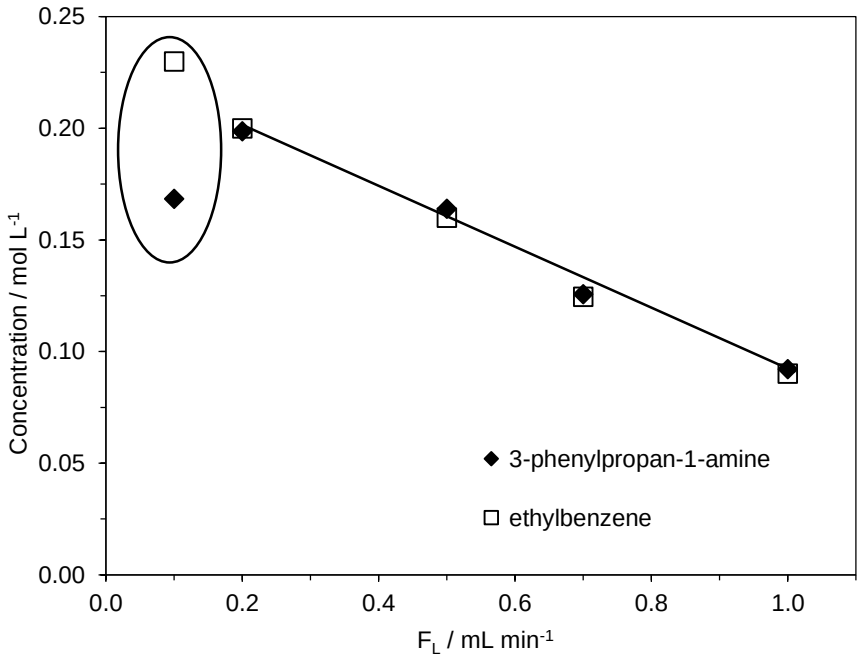

Figure 4.3. Influence of the liquid flow rate on the product concentration.
P_T = 8 bar, F_G = 21.0 mL (STP) min^{-1}, $C_{S,0}$ = 0.2 mol L^{-1}, T_1 = 298K, T_2= 393K.

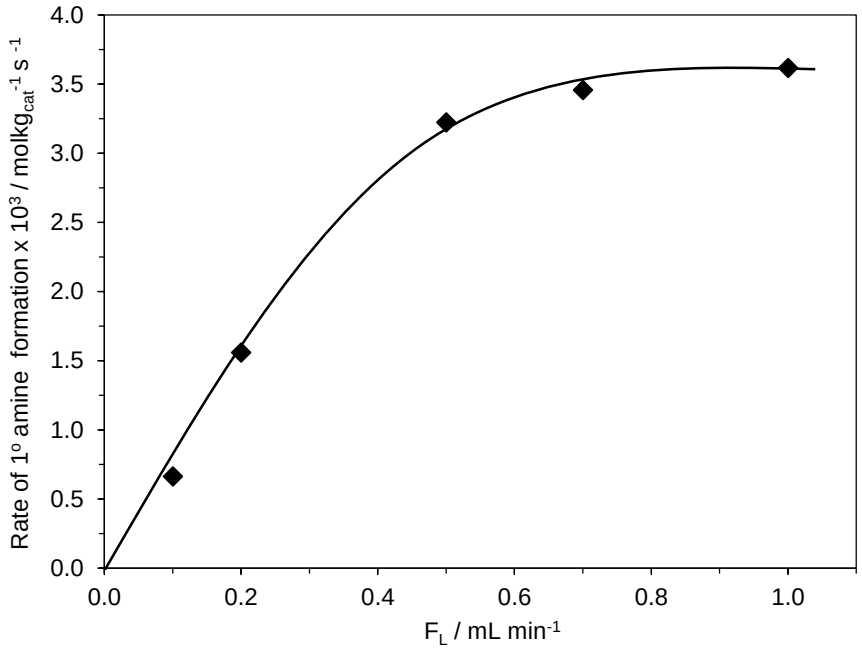

Figure 4.4. Influence of the liquid flow rate on the average rate of product formation.
P_T = 8 bar, F_G = 21.0 mL (STP) min^{-1}, $C_{S,0}$ = 0.2 mol L^{-1},T_1 = 298K, T_2 = 393K.

4.3.1.2. Effect of hydrogen flow rate

Figure 4.5 shows the desired product concentration as a function of the hydrogen flow rate. The results were obtained at 0.2 mol L^{-1} and 0.4 mol L^{-1} of initial substrate concentration at a 0.5 mL min^{-1} liquid flow rate, in order to neglect the mass transfer effect.

At low gas flow rates ($F_G \leq 10$ mL (STP) min^{-1}) the product concentration depends on the hydrogen flow rate and was limited by hydrogen supply. The hydrogen supply line presented in Figure 4.5 represents the theoretical stoichiometric volumetric flow rate of hydrogen for a given product concentration, calculated for both reactors. The product concentration was found to be almost independent for a higher range of gas flow rates ($F_G > 10$ mL (STP) min^{-1}). The independence of the product concentration on gas flow rate excludes the possibility of any influence of external mass transfer on the reaction.

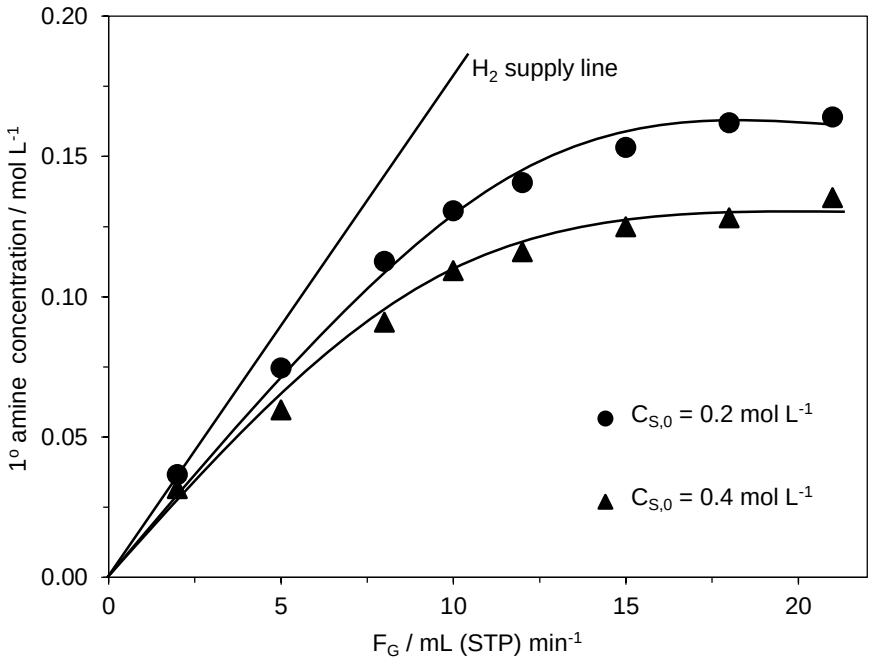

Figure 4.5. Influence of hydrogen flow rate on the product concentration.
P_T = 8 bar, F_L = 0.5 mL min^{-1}, T_1 = 298K, T_2 = 393K.

The increase in the gas flow rate decreases the liquid phase volumetric fraction and increases the superficial velocity of the liquid phase. According to the saturation value, β_L, is *ca.* five times higher at a hydrogen flow rate of 2.0 mL (STP) min^{-1} than at 21.0 mL (STP) min^{-1}. The contact time with the catalyst is therefore longer, which leads to the unwanted deamination step, resulting in a higher concentration of by-product (ethylbenzene) at the expense of the desired one (primary amine). A fuller explanation of these results requires further study of the 3-phenylpropan-1-amine hydrogenation reaction.

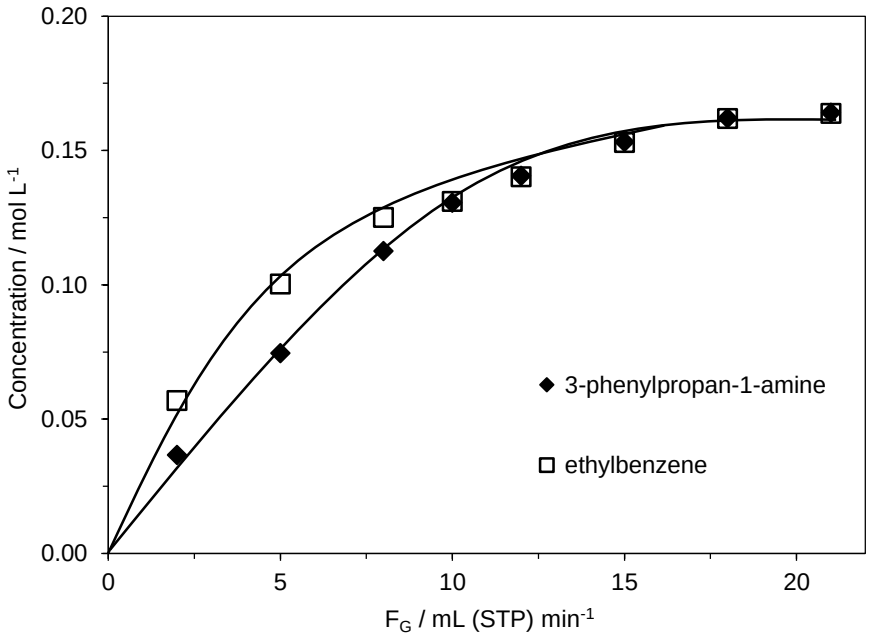

Figure 4.6. Influence of the hydrogen flow rate on product formation.
P_T = 8 bar, F_L = 0.5 mL min^{-1}, $C_{S,0}$ = 0.2 mol L^{-1}, T_1 = 298K, T_2 = 393K.

4.3.1.3. Effect of reaction temperature

The effect of the reaction temperature was measured using the 3 × 3 × 100 mm reaction channel. The results presented in Table 4.1 show how the selectivity of the reaction changes with the temperature in the second reactor. At lower temperatures, the selectivity towards the primary amine is only *ca.* 10%, but this increases by up to 100% as the temperature is increased to 393K. The desired primary amine concentration was in a 1:1 ratio to the reaction by-product (ethylbenzene) at all the reaction temperatures investigated.

Table 4.1. Influence of the second reactor temperature on the tandem reductive amination-hydrogenolysis process.

Temperature of the 2nd reactor (K)	**Selectivity (%)**		**C_1º amine (mol L^{-1})**
	2º amine	**1º amine**	
353	91	9	0.034
363	77	23	0.046
373	37	63	0.125
393	0	100	0.200

P_T = 8 bar, F_G = 21.0 mL (STP) min^{-1}, F_L = 0.2 mL min^{-1}, $C_{S,0}$ = 0.2 mol L^{-1}, T_1 = 298K.

4.3.1.4. Reactor efficiency with split injection of hydrogen

The microreactor system used in this study allows the split injection of hydrogen. This section investigates this to see if the efficiency of the reactor can be improved. The tandem process required two reactors. The arrangement of reactor channels for each step with different gas injection options is illustrated in Figure 4.7. Each of the reaction channels was loaded with 10% Pd/C catalyst (*ca.* 0.45g/channel). The initial concentration of hydrocinnamaldehyde and α-methylbenzylamine was 0.4 mol L^{-1}. The temperature of the first reactor was kept at 298K while the second one was at 393K. Previous studies have shown that at these temperatures the deamination of primary amine can be minimised. The results are presented in Figure 4.8.

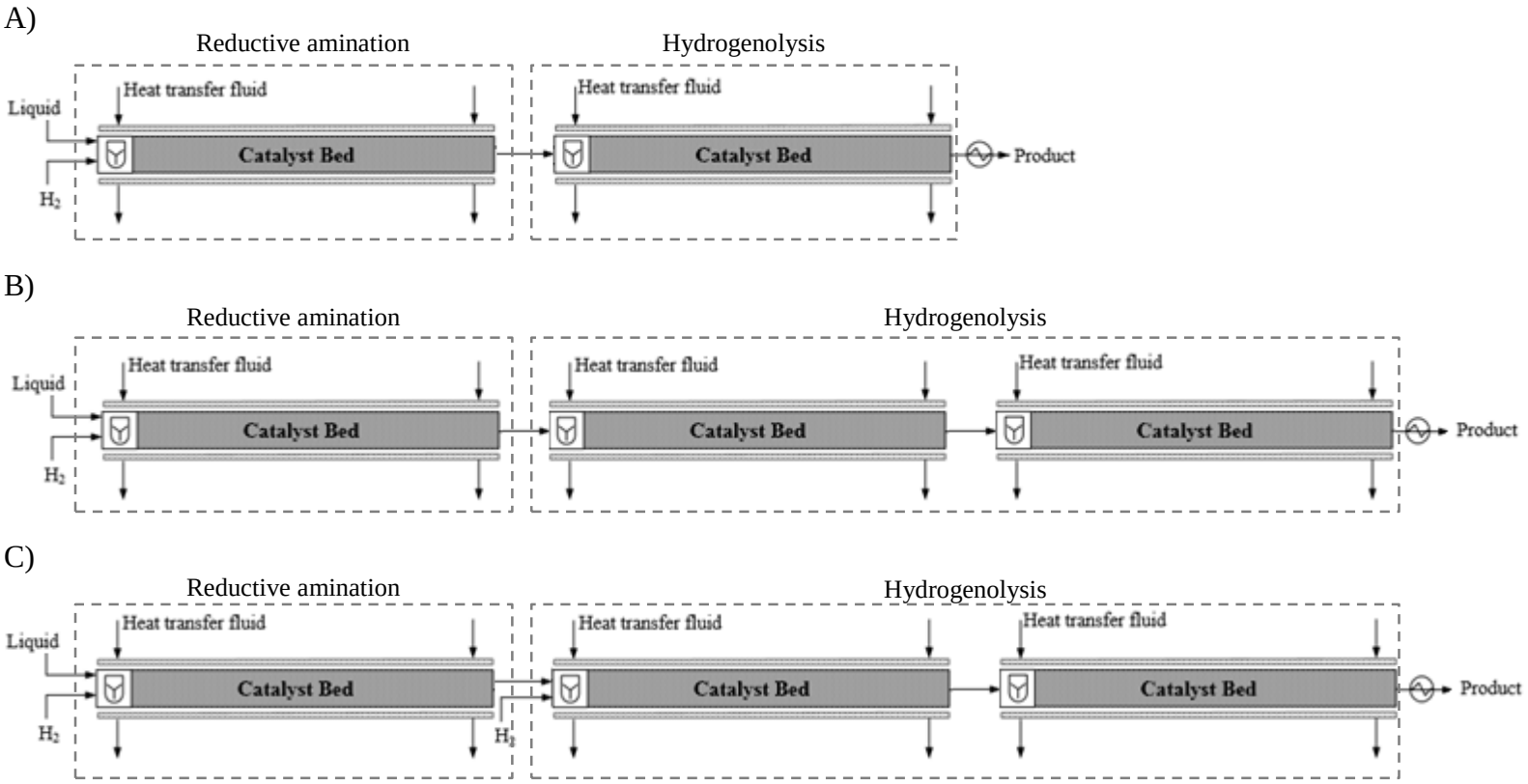

Figure 4.7. Reactor channel arrangement for split hydrogen injection experiments.

The product concentration increased from 0.21 mol L^{-1} to 0.28 mol L^{-1} using channel arrangements A and B, respectively at a hydrogen flow rate of 42.0 mL (STP) min^{-1}.

In arrangements A and B, up to F_G < 15 mL (STP) min^{-1}, the concentration of by-product (ethylbenzene) was *ca.* 12% higher than the desired product (primary amine). A fuller explanation of these o results requires further studies on the 3-phenylpropan-1-amine hydrogenation reaction.

For arrangement C, the primary amine concentration remained the same as the by-product (ethylbenzene) when the hydrogen flow rate was higher than 15.0 mL (STP) min^{-1} (Figure 4.9). The primary amine concentration, meanwhile, was *ca.* 0.34 mol L^{-1} at higher hydrogen flow rates, $F_G \geq 21.0$ mL (STP) min^{-1}.

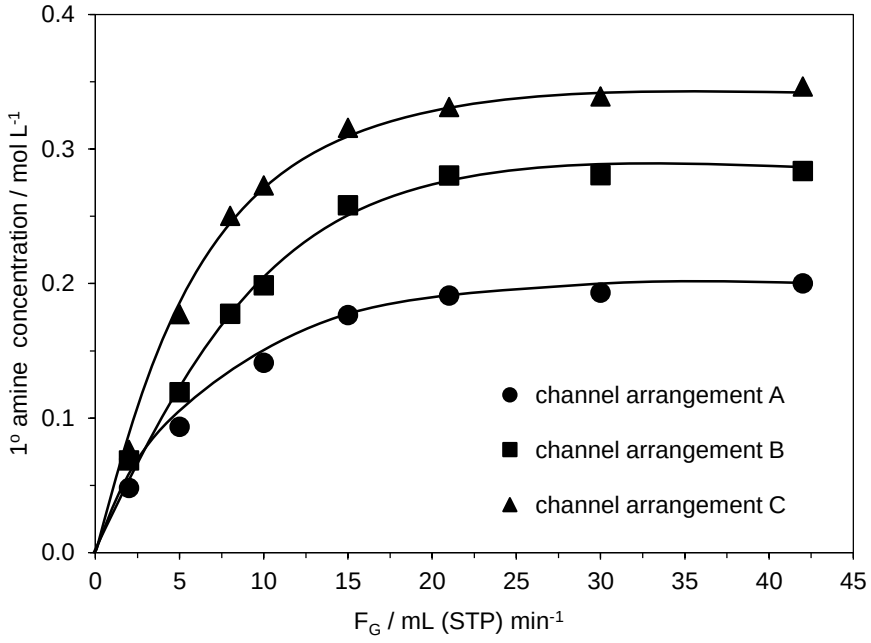

Figure 4.8. Product concentration vs gas flow rate for different hydrogen injection points. P_T = 8 bar, F_L = 0.5 mL min^{-1}, $C_{S,0}$ = 0.4 mol L^{-1}, T_1 = 298K, T_2 = 393K.

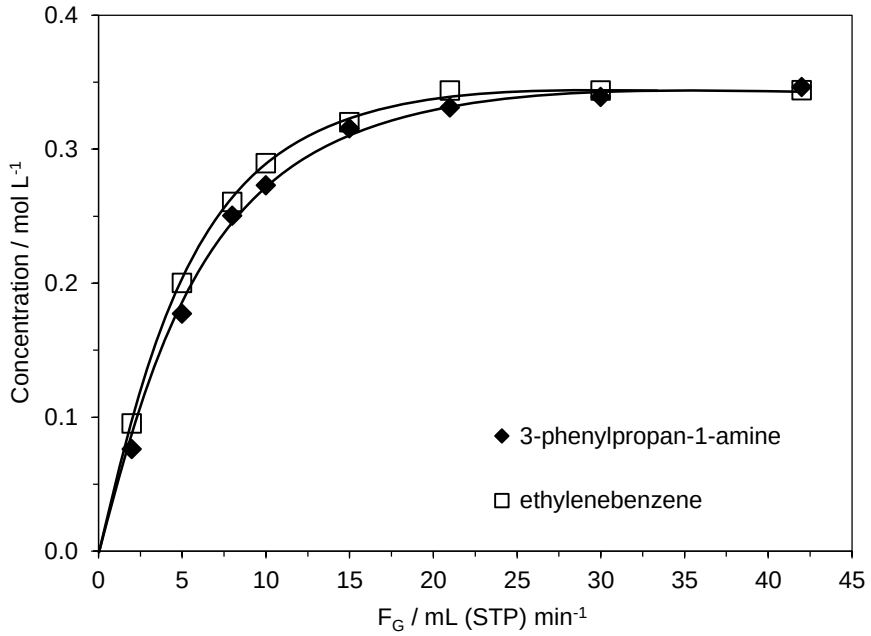

Figure 4.9. Influence of the hydrogen flow rate on the product concentration for channel arrangement C. P_T = 8 bar, F_L = 0.5 mL min^{-1}, $C_{S,0}$ = 0.4 mol L^{-1}, T_1 = 298K, T_2 = 393K.

This simple model of the split gas distribution along the length of the reaction channel resulted in a higher yield of the desired product for experiments performed with channel arrangement C. In continuous flow conditions using microreactors, the concept of dosing the required amount of gaseous reactant at different positions along the catalyst bed can be a flexible method for performing more complex reactions such as this tandem process.

4.3.1.5. Synthesis of selected primary amines by tandem reductive amination - hydrogenolysis reaction

A tandem reductive amination of aldehydes - hydrogenolysis of secondary amines was carried out in the multichannel packed-bed reactor for a range of aldehydes in order to demonstrate the generality of the process.

Aromatic, aliphatic and cyclic aldehydes were investigated and converted to primary amines with very good conversions and selectivities. Primary amines were synthesised and isolated as HCl salts with a good yield. The results are presented in Table 4.2.

Unsaturated cinnamaldehyde (Table 4.2, Entry 10) and citral (Table 4.2, Entry 11) were also converted to primary amine in good isolated yield. However, C-C double bond was also hydrogenated during the reaction.

The yield of butyraldehyde (Table 4.2, Entry 7) and isobutyraldehyde (Table 4.2, Entry 8) products was determined by GC analysis. Synthesised primary amines, butan-1-amine (Table 4.2, Entry 7) and 2-methylpropan-1-amine (Table 4.2, Entry 8) have boiling points very close to that of the solvent and therefore during evaporation of the solvent were removed from the reaction mixture as well. This is the most likely reason for the lack of isolated yield of these products, since the GC analysis of the reaction mixture, when compared with the standard samples analysis of butan-1-amine and 2-methylpropan-1-amine, confirmed that they were synthesised during the reaction.

Once the standard conditions for the tandem reductive amination of aldehydes - hydrogenolysis of secondary amines process were established the approach was extended to ketones. These results are presented in Table 4.3 and indicate that the reaction conditions for the tandem reductive amination of ketones - hydrogenolysis of secondary amine requires further optimisation to increase the yield of the desired product for the aromatic ketones. In the tandem process, 100% conversion was achieved for the 4-phenyl-2-butanone. However, the selectivity to the desired product, 4-phenylbutan-2-amine was only 45%, indicating that 55% of 4-phenyl-*N*-(1-phenylethyl)butan-2-amine remained unreacted.

Table 4.2. Primary amines synthesised by tandem reductive amination of aldehydes-hydrogenolysis of secondary amines in the packed-bed multichannel reactor over Pd/C catalyst.

Entry	Substrate	Product	Conversion[c]	Yield[d]
1[a]	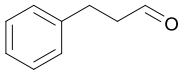	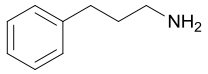	100	91
2[a]	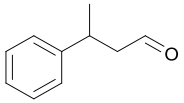	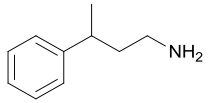	100	84
3[b]	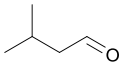	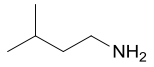	100	74
4[a]	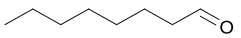	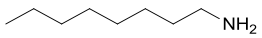	100	84
5[a]	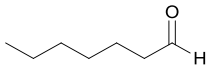	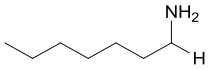	100	82
6[a]	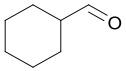	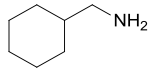	100	87

7[b]	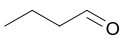	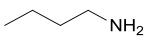	100	99[e]
8[b]		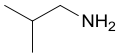	100	99[e]
9[a]	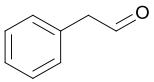	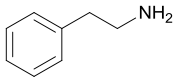	100	85
10[a]	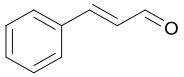	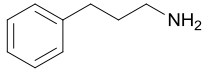	100	95
11[a]	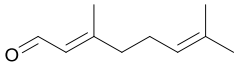	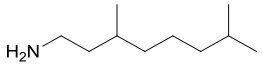	100	87

[a] Reaction conditions: P_T = 8 bar, F_G = 21.0 mL (STP) min^{-1}, F_L = 0.2 mL min^{-1}, $C_{S,0}$ = 0.2 mol L^{-1}, T_1 = 298K, T_2 = 393K, methanol as a solvent.

[b] Reaction conditions: P_T = 8 bar, F_G = 21.0 mL (STP) min^{-1}, F_L = 0.2 mL min^{-1}, $C_{S,0}$ = 0.4 mol L^{-1}, T_1 = 298K, T_2 = 373K, methanol as a solvent.

[c] Conversion was determined by GC analysis.

[d] Isolated as HCl salt.

[e] Yield was determined by GC analysis.

Table 4.3. Primary amines synthesised by tandem reductive amination of ketones - hydrogenolysis of secondary amines in the packed-bed multichannel reactor over Pd/C catalyst.

Entry	Substrate	Product	Conversion[c]	Yield[d]
1[a]	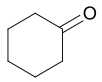	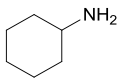	100	67
2[b]	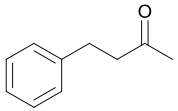	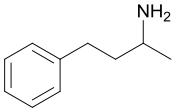	100	44

[a] Reaction conditions: P_T = 8 bar, F_G = 21.0 mL (STP) min^{-1}, F_L = 0.2 mL min^{-1}, $C_{S,0}$ = 0.2 mol L^{-1}, T_1 = 298K, T_2 = 393K, methanol as a solvent.

[b] Reaction conditions: P_T = 8 bar, F_G = 21.0 mL (STP) min^{-1}, F_L = 0.2.mL min^{-1}, $C_{S,0}$ = 0.2 mol L^{-1}, T_1 = 323K, T_2 =393K, methanol as a solvent.

[c] Conversion was determined by GC analysis.

[d] Isolated as HCl salt.

4.3.2. X-Cube^{TM} flow reactor

In this section the tandem reductive amination - deprotection process is investigated using the X-Cube^{TM} flow reactor. The optimisation of the process was studied by varying liquid flow rates, reaction pressure and temperature. As has been shown previously, the reductive amination of aldehydes (ketones) reaction (see Chapter 2) can be done at lower temperatures than the hydrogenolysis of secondary amine (see Chapter 3). Considering this fact, in this experiment, two channels loaded with 10% Pd/C catalyst were used to perform the tandem process. The results are presented in the following subsections.

4.3.2.1. Effect of liquid flow rate

Figure 4.10 shows the influence of the liquid flow rate on the primary amine concentration while performing the tandem reductive amination of hydrocinnamaldehyde and hydrogenolysis of (1-phenylethyl)(3-phenylpropyl)amine.

The 3-phenylpropan-1-amine was synthesised with 100% selectivity under the reaction conditions: P_T = 30 bar, T_1 = 298K and T_2 = 413K, $C_{S,0}$ = 0.2 mol L^{-1}. However, the deamination of primary amine was detected. The data presented in Figure 4.10 clearly indicates that the desired primary amine has decomposed, forming more by-product (ethylbenzene) and losing 15% of the primary amine. Due to this problem, another set of experiments was perform at a lower temperature, *i.e.* 403K, to see if the deamination step could be eliminated from the process.

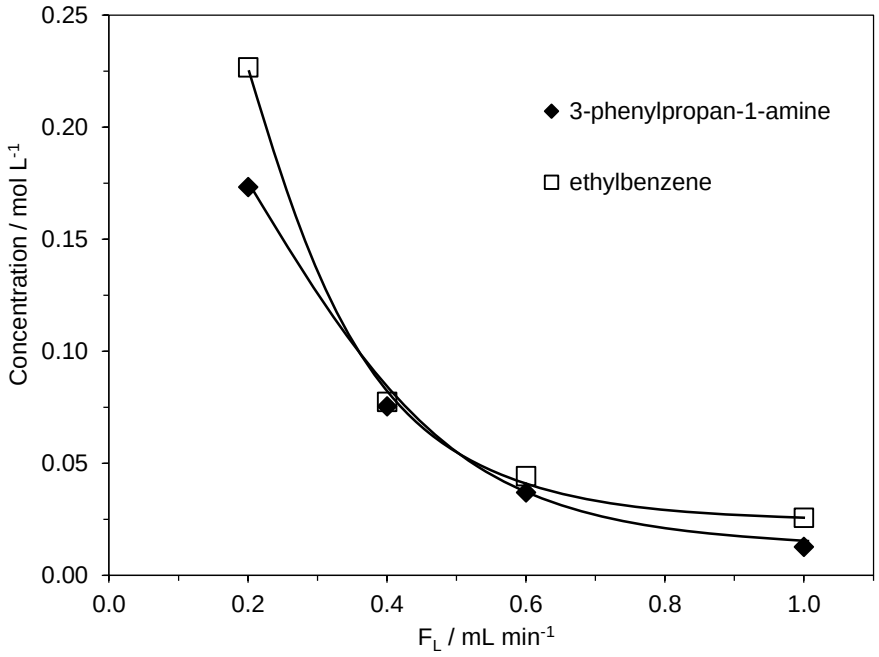

Figure 4.10. Influence of the liquid flow rate on the product concentration. P_T = 30 bar, $C_{S,0}$ = 0.2 mol L^{-1}, T_1 = 298K and T_2 = 413K.

Performing the experiments varying liquid flow rates at 403K (Figure 4.11) for the hydrogenolysis step, it was found that the desired primary amine can be formed without any loss. The unwanted deamination reaction to ethylbenzene was eliminated by decreasing the temperature from 413K to 403K. At a liquid flow rate of 0.2 mL min^{-1}, the 3-phenylpropan-1-amine was formed in 100%. Increasing the liquid flow rate up to 1.0 mL min^{-1} decreased the selectivity of the desired product.

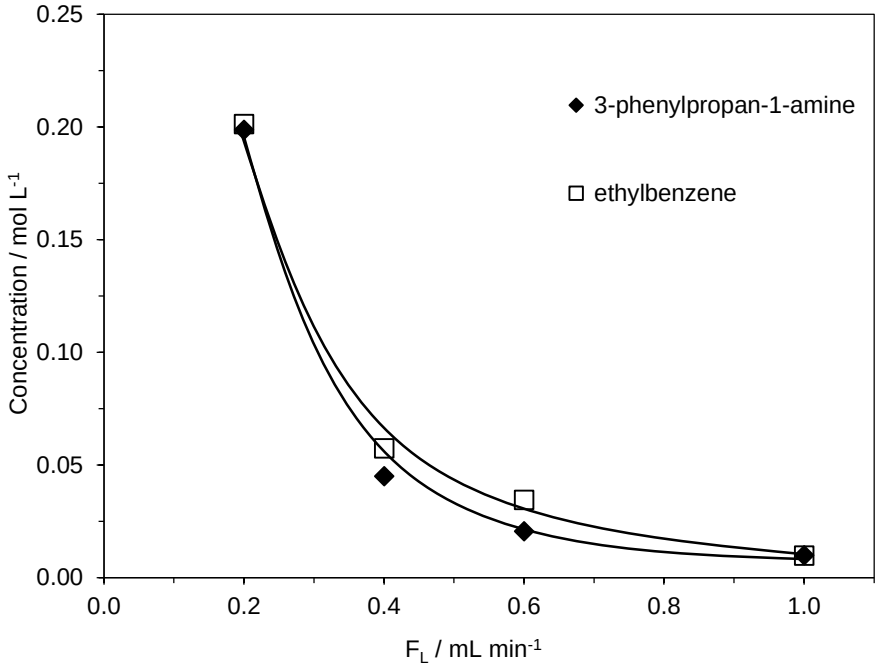

Figure 4.11. Influence of the liquid flow rate on the product concentration. P_T = 30 bar, $C_{S,0}$ = 0.2 mol L^{-1}, T_1 = 298K and T_2 = 403K.

Figure 4.12 presents the average rate of product formation (primary amine) as a function of liquid flow rate. The rate of product formation decreased as the liquid flow rate increased.

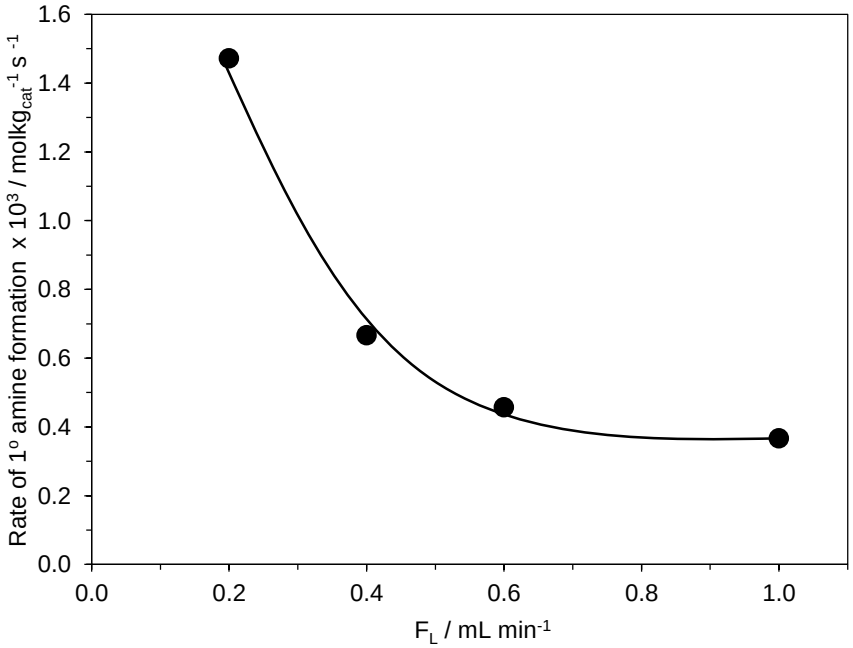

Figure 4.12. Influence of the liquid flow rate on the average rate of product formation. P_T = 30 bar, $C_{S,0}$ = 0.2 mol L^{-1}, T_1 = 298K,T_2 = 403K.

The increase in the liquid flow rate should increase the mass transfer. However, the data presented in Figure 4.12 is difficult to explain due to insufficient understanding of the hydrodynamic conditions in the X-Cube™ flow reactor. Furthermore, from visual observations while the system was running it could be assumed that some fluctuations in hydrogen availability in the system appeared. It was mentioned in Chapter 2, section 2.3.2.2 that the rate of gas bubbles in the liquid is regulated by the gas valve, and that it is independent of the applied pressure, and should be kept at a constant value of 5%. Nevertheless, it was noticed that the value fluctuated during experiments, varied from 0 up to 30%, depending on the chosen experimental conditions. Another indication of fluctuations in hydrogen availability could be the release of the gas from the product collecting line during the experiments, which was observed as sputtering.

A similar problem was described by Bryan *et al.* (2011) when evaluating the performance of the H-Cube® packed-bed flow hydrogenator. Bryan *et al.* (2011) found that the fluctuations in hydrogen availability in the H-Cube® flow hydrogenator are related to the design of the system, since this behaviour was observed in three H-Cube® reactors tested.

4.3.2.2. Effect of operating pressure

The effect of the hydrogen pressure on primary amine formation was studied at a liquid flow rate of 0.2 mL min^{-1} (Figure 4.13). It can be seen that, up to 30 bar of total pressure, the product concentration increased linearly. At 40 bar of total pressure, however, the product concentration decreased to 0.15 mol L^{-1}, suggesting that 30 bar of hydrogen pressure is optimal for the tandem process. 27% of the secondary amine remained unreacted under these reaction conditions. Furthermore, since sputtering of the hydrogen was also observed during the experiment, it was clear that at 40 bar of total pressure the flow became more turbulent than at lower pressures, which could also affect product formation.

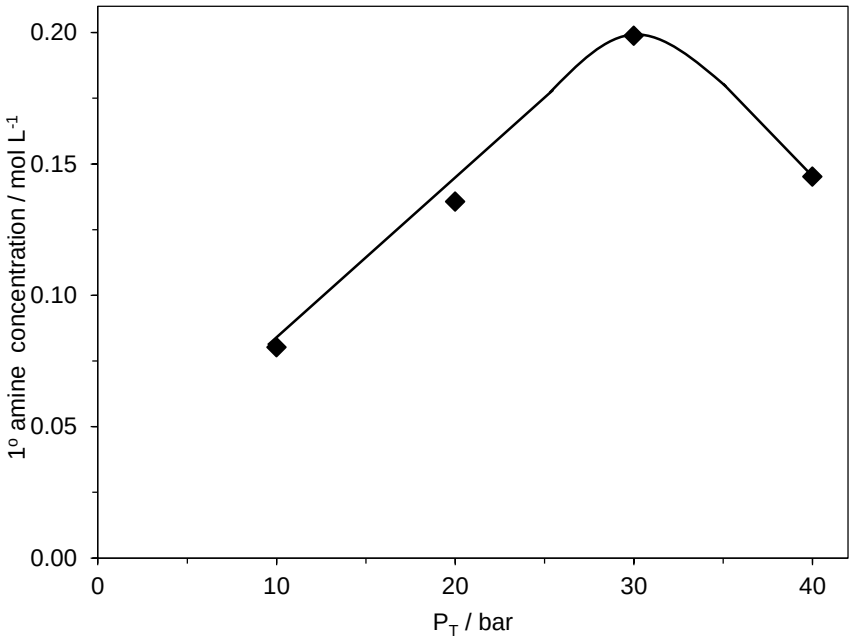

Figure 4.13. Influence of the pressure on the product concentration.
F_L = 0.2 mL min^{-1}, $C_{S,0}$ = 0.2 mol L^{-1},T_1 = 298K, T_2 = 403K.

4.3.2.3. Effect of reaction temperature

The effect of reaction temperature on product concentration is presented in Figure 4.14. It can be seen that the optimal temperatures for the tandem reductive amination - hydrogenolysis reaction are 298K and 403K. By varying the reaction temperature of the second reaction channel it is clear that 403K is the optimal temperature for the hydrogenolysis step, since, at 413K, the unwanted deamination reaction to ethylbenzene occurs. In the temperature range 323 - 403K the concentration of the desired product increased linearly from 0.0226 mol L^{-1} (at 323K) to 0.1988 mol L^{-1} (at 403K).

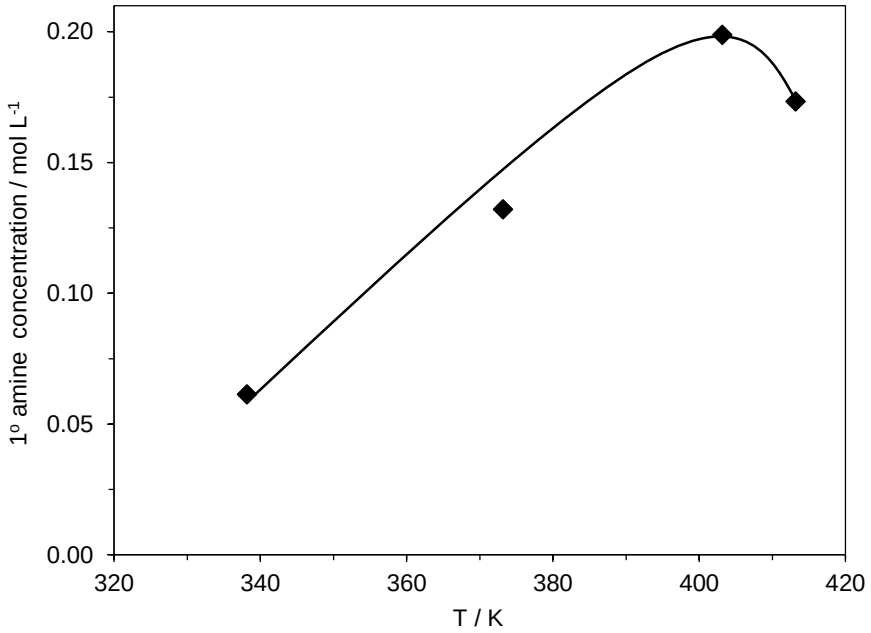

Figure 4.14. Influence of the reaction temperature on product concentration. P_T = 30 bar, F_L = 0.2 mL min^{-1}, $C_{S,0}$ = 0.2 mol L^{-1}, T_1 = 298K, T_2 = 403K.

4.3.2.4. Synthesis of selected primary amines by tandem reductive amination - hydrogenolysis reaction

A tandem reductive amination of aldehydes - hydrogenolysis of secondary amines was carried out in the commercially available X-Cube™ flow reactor for various aldehydes in order to demonstrate the generality of the process.

Various primary amines were synthesised and isolated as HCl salts with good yield. The results are presented in Table 4.4.

For butyraldehyde (Table 4.4, Entry 7) and isobutyraldehyde (Table 4.4, Entry 8), product yield was determined by GC analysis. Synthesised primary amines, butan-1-amine (Table 4.4, Entry 7) and 2-methylpropan-1-amine (Table 4.4, Entry 8) have boiling points very close to that of the solvent and it was therefore difficult to isolate them. Based on the results presented in Chapter 2, section 2.3.2.6, for the reductive amination of ketones using the X-Cube™ flow reactor, the tandem process performed for ketones did not give any good results (data are not presented):only very small amount of primary amines were achieved, indicating that further optimisation of the process is required.

Table 4.4. Primary amines[a] synthesised *via* tandem: reductive amination of aldehydes - hydrogenolysis of secondary amines in the X-Cube™ flow reactor over a Pd/C catalyst.

entry	substrate	product	Conversion[b]	Yield[c]
1	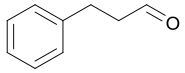	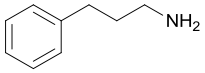	100	81
2	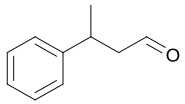	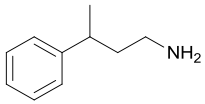	98	80
3	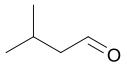	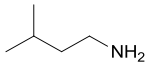	96	83
4	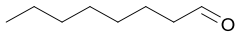	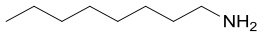	92	83
5	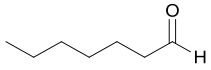	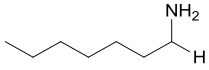	95	82

6	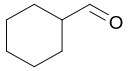	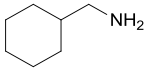	91	79
7	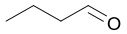	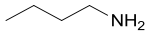	95	93 [d]
8		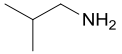	97	94[d]
9	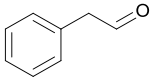	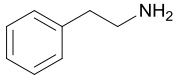	93	80

[a] Reaction conditions: P_T = 30 bar, F_L = 0.2 mL min^{-1}, $C_{S,0}$ = 0.2 mol L^{-1}, T_1 = 298K, T_2 = 403K, methanol as a solvent.

[b] Conversion was determined by GC analysis.

[c] Isolated as HCl salt.

[d] Yield was determined by GC analysis.

4.4. Conclusions

Tandem reductive amination of aldehydes - hydrogenolysis of protected primary amines was developed in two continuous flow systems. The tandem reductive amination of ketones - deprotection of secondary amine process, however, requires further studies to achieve higher conversion to the desired product.

Various aldehydes were investigated in this work to demonstrate that a compact multichannel packed-bed reactor and the X-Cube™ flow reactor are capable of performing the multi-step syntheses. Products were isolated with very good yield.

Obtained results show that these reactors might be a suitable alternative to the conventional batch processes. Nevertheless, the continuous catalytic rig showed better performance for the tandem process than the commercially available X-Cube™ (Table 4.5).

Table 4.5. Comparison of the reaction conditions for the tandem process.

	PBR	**X - Cube™**
P (bar)	8	30
T_1 / T_2 (K)	298/ 393	298/ 403
F_L (mL min^{-1})	0.2	0.2
F_G (mL min^{-1})	21.0	-
$C_{S,0}$ (mol L^{-1})	0.2	0.2
m_{cat} (g)	0.45	0.45
Productivity (mol h^{-1})	0.0024	0.0024

The hydrodynamic performance of the X-Cube™ flow reactor is not very well understood and the data obtained cannot, therefore, be analysed any further without a better knowledge of these hydrodynamic conditions.

Chapter 5

Reaction kinetics for the reductive amination of hydrocinnamaldehyde over a palladium on carbon catalyst

5.1. Introduction

Heterogeneous catalytic reactions involve more than one phase; the catalyst is in a solid form and the reactants/ products are in liquid and/or gas phase. In the multi-phase reaction system the overall process consists of several steps, *i.e.* external and/or internal mass transfer as well as gas absorption, together with the catalytic reaction. The reaction time, as well as selectivity and product yield, can be affected both by mass transfer resistance effects and by the chemical reaction itself. In order to obtain a true measure of the reaction kinetics, all of these factors need to be understood and quantified. The influence of heat and mass transfer limitations must be considered when analysing the overall rate of reaction and kinetic models for the intrinsic kinetics. In industry, multi-phase catalytic reactions are very often performed under mass transfer limited conditions. In order to develop an integral reactor design model, it is necessary to analyse the overall rate of reaction under different reaction conditions to distinguish the effects of various mass transfer steps (Mills and Chaudhari 1997; Fogler 1999).

Various mass transfer steps can be observed in three-phase (gas-liquid-solid) catalytic reactions, *i.e.* gas-liquid, liquid-solid and intraparticle mass transfer resistances.

Figure 5.1 shows all the steps involved in the three-phase (gas-liquid-solid) catalytic system where a solid phase is presented as a porous catalyst (Mills and Chaudhari 1997):

1. transport of the gas phase reactant from the bulk of gas phase to the liquid phase;
2. transport of a gas phase reactant and liquid reactant to the catalyst surface from the bulk liquid;
3. mass transfer (diffusion) of the reactant(s) from the bulk fluid to the external surface of the catalyst pellets;
4. diffusion of the reactant from the pore mouth through the catalyst pores to the internal catalytic surface;

5. catalytic reaction which can be broken into:
   a) chemisorption of the reactant onto the catalyst surface;
   b) reaction on the surface of the catalyst;
   c) desorption of products from the surface;

6. diffusion of products from the interior of the pellet to the pore mouth at the external surface.

Steps a, b and c involve making and breaking of chemical bonds and occur sequentially. Chemical reaction (step 5) and intra-partile diffusion (steps 4 and 6) occur simultaneously.

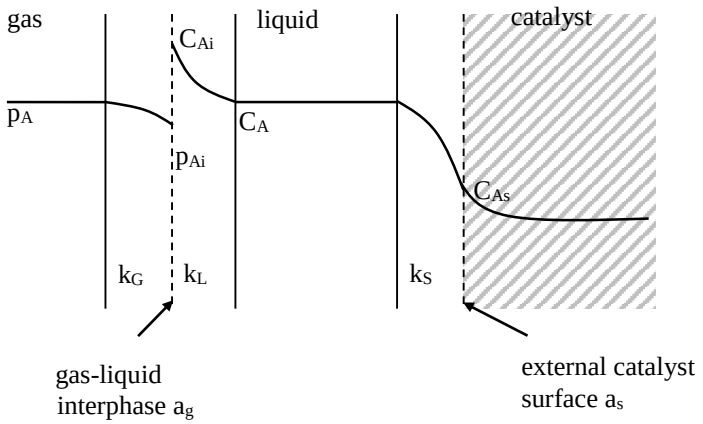

Figure 5.1. Schematic diagram of transport steps in multi-phase catalytic reactions (Hofmann 1978).

In multi-phase catalytic reactions it is important to analyse the impact of controlling regimes (*i.e.* the slowest step of the overall process), since heterogeneous catalysis is always associated with mass and heat transfer processes. For example, the overall reaction rate will be equal to the rate of the diffusion if the diffusion steps are the slowest, and the overall reaction rate will then be determined by the rate of physical processes. When the mass and heat transfer processes are fast enough, however, then they do not influence the catalytic process in any significant way. In multi-phase heterogeneous catalytic reactions, the rates of all consecutive steps should be equal to each another, and equal to the slowest one under steady state reaction conditions.

When performing kinetic experiments and data analysis, it is important to ensure that the resulting kinetic parameters correspond to the intrinsic kinetic regime, since the mass transfer processes can influence/ affect the progress of heterogeneous catalytic reactions (Satterfield 1981; Mills and Chaudhari 1997; Carberry 2001; Petrov 2002; Petrov *et al.* 2011).

Generally, the reductive amination reaction proceeds in three steps (Lehtonen *et al.* 1998):

1. an intermediate (carbinolamine) is formed through the reaction of the amino group with an aldehyde;
2. Schiff's base and water are formed due to the decomposition of the intermediate;
3. Schiff's base reacts with hydrogen on the active sites of the catalyst to form the product (secondary amine).

The formation of an intermediate (Scheme 5.1) is an endothermic reaction with the standard reaction enthalpy of 177 kJ mol^{-1}. This reaction is a homogeneous, non-catalytic reaction, and was previously described in Chapter 2, section 2.3.1.1).

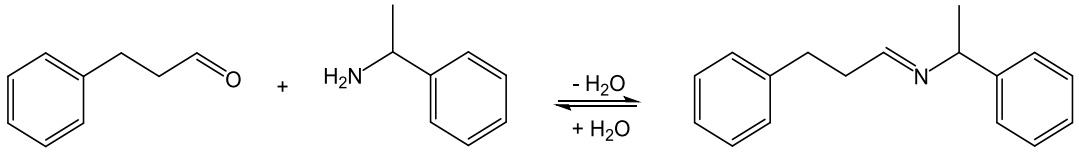

Scheme 5.1. Imine formation from hydrocinnamaldehyde and α-methylbenzylamine.

Hydrogenation of an imine (Scheme 5.2) is a mildly exothermic reaction with the standard reaction enthalpy of - 29 kJ mol^{-1} (thermodynamic properties of compounds involved in the reaction were obtained from ChemBioDraw Ultra 12.0). However, isothermal conditions were kept at all conversion levels, which were proven by temperature measurements during the experiments. Three thermocouples were used during all the studies (the first placed in the inlet, the second in the outlet of the heating liquid and the third at the top of the reaction channel).

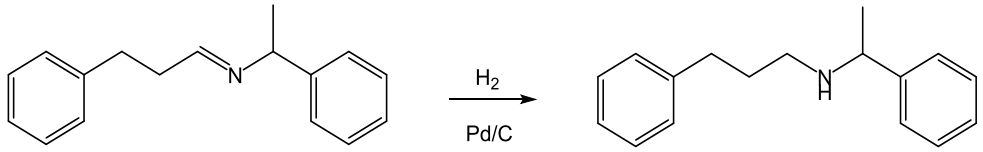

Scheme 5.2. Hydrogenation of an imine.

In the literature there are only a few reports of homogeneous-heterogeneous, noncatalytic-catalytic reactions. A semibatch slurry reactor model and a loop reactor model were described by Lehtonen *et al.* (1998) and Salmi *et al.* (1999) for the reductive alkylation reaction of aromatic amines with short-chain aldehydes (carbon chain length < 3) over a Pt/C catalyst. Another example of kinetic studies on the reductive alkylation reaction was presented by Roy *et al.* (2005). They report the reductive alkylation of aniline with acetone using a Pd/Al_2O_3 catalyst in a batch slurry reactor. They then extended their approach and investigated a more complex reaction system with *p*-phenylenediamine (PPDA) and methyl ethyl ketone (MEK), where two amine functionalities are available for the alkylation (Patil *et al.* 2007).

Lehtonen *et al.* (1998) developed a kinetic model for the reductive alkylation of aromatic amines for a semibatch reactor which is widely used on a laboratory and an industrial scale for the reductive alkylation reaction. This reaction involves both homogeneous (step 1 and 2) and heterogeneous (step 3) reactions. The authors combined a kinetic model with a reactor model for a three-phase system with mass transfer limitations at the gas-liquid interface, whereas the external and internal mass transfer resistances within the catalyst particles were assumed to be negligible due to the fact that very finely dispersed catalyst particles were used. It was previously mentioned that the reductive amination/alkylation reactions proceeded in three steps. In this work, the third step, *i.e.* the surface reaction was considered to be the rate-limiting step, assuming dissociative adsorption of hydrogen. The final rate expression for (step 3) was obtained as:

$$(-r_A) = \frac{k' C_{I2} C_{H_2}}{(1 + K_{I2} C_{I2} + \sqrt{K_{H_2} C_{H_2}} + \sum K_j C_j)^3} \qquad (5.1)$$

where:

$$k' = kK_{I2}K_{H_2}$$

C_{I2} intermediate 2 (imine) concentration;

C_{H_2} hydrogen concentration;

C_j any adsorbed species on the catalyst concentration;

k' lumped kinetic rate constant;

K_{I2} intermediate 2 adsorption equilibrium constant;

K_{H_2} hydrogen adsorption equilibrium constant;

K_j any adsorbed species on the catalyst equilibrium constant.

The authors stated, however, that it was difficult to judge whether this was the absolutely correct mechanism for the heterogeneous hydrogenation step. The mechanism proposed by Lehtonen *et al.* (1998) should, therefore, be considered as a good example rather than as an absolutely correct mechanism for the homogeneous-heterogeneous reaction system. The authors also mentioned that a non-competitive adsorption of the Shiff's base and hydrogen molecules could represent the data correctly to some extent, and that it was impossible to prove whether the adsorption of hydrogen takes place dissociatively, as proposed here, or non-dissociatively.

As an extension of this work, Salmi *et al.* (1999) developed the reductive alkylation reaction of aromatic amines with short-chain aldehydes over a Pt/C catalyst. They used a Langmuir-Hinshelwood rate equation for the hydrogenation step, assuming that the rate determining step was the surface reaction between Shiff's base and the dissociatively adsorbed hydrogen.

Roy *et al.* (2005) reported a kinetic study for the reductive alkylation of aniline with acetone using 3% Pd/Al_2O_3 as a catalyst in a batch slurry reactor. They reported that the imine formation from aniline and acetone (a homogeneous, noncatalytic equilibrium reaction) is the slowest step in the reaction sequence. A rate model based on the competitive adsorption of dissociatively adsorbed hydrogen, and other reactants, on the catalyst active centres was found to represent the experimental data satisfactorily.

Patil *et al.* (2007) reported a kinetic study of the reductive alkylation of *p*-phenylenediamine (PPDA) with methyl ethyl ketone (MEK) using a 3% Pt/Al_2O_3 catalyst in a semibatch slurry reactor. This involved a combination of parallel and consecutive reactions, *i.e.* equilibrium noncatalytic (homogeneous) and catalytic (heterogeneous) steps. In this case, the authors found that the experimental data can be represented satisfactorily by the rate models in which the catalytic reactions are assumed to be the rate-liming steps with dissociative adsorption of hydrogen.

For the partial hydrogenation of *(E)*-(1-phenylethyl)(3-phenylpropylidene)amine to (1-phenylethyl)(3-phenylpropyl)amine (Scheme 5.2) to take place in a three phase heterogeneous system, the following sequence must occur (Fogler 1999):

1. As almost pure hydrogen is in the gas phase ($p_{H_2} >> p_{MeOH}$), mass transfer resistance in the gas phase can be neglected. The interface hydrogen concentration in the liquid phase is in equilibrium with the hydrogen partial pressure (Henry's Law):

$$p_{H_2} = H\, x_{H_2} \tag{5.2}$$

where:

p_{H_2} partial pressure of hydrogen at gas-liquid interface (bar);
H Henry's constant (bar);
x_{H_2} mole fraction of the hydrogen in the liquid phase (-).

2. Transport of the dissolved gaseous hydrogen from the gas-liquid interface to the bulk liquid:

$$(-r_A) = k_{L,G} \cdot a_{G/L} \frac{1}{(1 - e_b)\rho_c} (C_{H_2,i} - C_{H_2,b}) \tag{5.3}$$

where:

$(-r_A)$ overall reaction rate (mol kg_{cat}^{-1} s^{-1});
$k_{L,G}$ gas-liquid mass transfer coefficient (m s^{-1});

$a_{G/L}$ gas-liquid interfacial area / volume of bed ($m^2\ m^{-3}$);

e_g bed porosity (-);

ρ_c density of catalyst pellet ($kg\ m^{-3}$);

$C_{H_2,i}$ hydrogen concentration in liquid at interface ($mol\ m^{-3}$);

$C_{H_2,b}$ hydrogen concentration in the bulk liquid ($mol\ m^{-3}$).

3. Transport of the dissolved gaseous hydrogen through the bulk liquid to the external surface of a catalyst particle:

$$(-r_A) = k_{L/S,\,H_2}\, a_s (C_{H_2,b} - C_{H_2,s}) \qquad (5.4)$$

where:

$(-r_A)$ overall reaction rate ($mol\ kg_{cat}^{-1}\ s^{-1}$);

$k_{L/S,H_2}$ liquid-solid mass transfer coefficient ($m\ s^{-1}$);

a_s external specific area of pellet ($m^2\ kg_{cat}^{-1}$);

$C_{H_2,b}$ hydrogen concentration in the bulk liquid ($mol\ m^{-3}$);

$C_{H_2,s}$ hydrogen concentration at the solid-liquid interface ($mol\ m^{-3}$).

4. Transport of the *(E)*-(1-phenylethyl)(3-phenylpropylidene)amine through the bulk liquid to the external surface of a catalyst particle:

$$(-r_A) = k_{L/S,\,imine}\ a_S (C_{imine,b} - C_{imine,s}) \qquad (5.5)$$

where:

$(-r_A)$ overall reaction rate ($mol\ kg_{cat}^{-1}\ s^{-1}$);

$k_{L/S,imine}$ liquid-solid mass transfer coefficient ($m\ s^{-1}$);

a_S external specific area of pellet ($m^2\ kg_{cat}^{-1}$);

$C_{imine,b}$ *(E)*-(1-phenylethyl)(3-phenylpropylidene)amine concentration in the bulk liquid ($mol\ m^{-3}$);

$C_{imine,s}$ *(E)*-(1-phenylethyl)(3-phenylpropylidene)amine concentration at the solid-liquid interface ($mol\ m^{-3}$).

5. Diffusion and reaction in the catalyst:

$$(-r_A) = \eta \cdot k C_{H_2,s} C_{imine,s} \qquad (5.6)$$

where:

$(-r_A)$	overall reaction rate (mol kg_{cat}^{-1} s^{-1});
η	effectiveness factor (-);
k	specific reaction constant / m^3 of liquid (mol^{-1} $kg_{cat}^{-1}s^{-1}$);
$C_{H_2,s}$	surface concentration of hydrogen at solid-liquid interface (mol m^{-3});
$C_{imine,s}$	surface concentration of *(E)*-(1-phenylethyl)(3-phenylpropylidene) amine at the solid-liquid interface (mol m^{-3}).

The work presented in this chapter focuses on the investigation of the global kinetics for the reductive amination of hydrocinnamaldehyde with α-methylbenzylamine. Experiments were performed with a palladium catalyst supported on an activated carbon kindly supplied by Mast Carbon Ltd. (UK) (see Chapter 2, section 2.2.1). In a set of experiments, appropriate experimental conditions were established to achieve a better understanding of the effect of the key variables. The work aimed at individuating the main factors that influence the reaction, *i.e.* liquid and gas flow rates, hydrogen partial pressures, temperatures and reactant concentrations. A possible reaction mechanism was proposed and the rate equations that describe the reactions involved in the process were developed and used to obtain the necessary kinetic parameters. The equations were used to fit experimental data obtained using Matlab software. The experimental conditions tested were chosen so that the effect of all the main influencing parameters could be investigated and the validity of the assumptions made tested.

5.2. Experimental

5.2.1. Pd/C catalyst and reagents

The Pd/C catalyst (Pd 10% by weight) was prepared by impregnation of the mesoporous microspherical (125-250 μm) synthetic carbon support supplied by Mast Carbon Ltd., Guildford, UK (see Chapter 2, section 2.2.1).

The loading capacity of the compact reactor is *ca.* 0.45 g of catalyst. For kinetic studies, the catalyst (total amount Pd/C = 0.085 g) was diluted with the pure carbon particles.

All chemicals used in this study were purchased from Acros Organics, Sigma-Aldrich, Fluka or Lancaster and used without further purification

5.2.2. Analytical technique

During the kinetic experiments, samples of the liquid were taken via the 6-way valve and were analysed with a GC (Varian CP-3800). The GC was equipped with a CP Sil-8CB column.

5.2.3. Structured compact reactor and continuous catalytic rig

Details of the structured multichannel packed-bed reactor and of the continuous catalytic system used in these studies are presented in Chapter 2, section 2.2.2 and 2.2.3, respectively.

All concentrations were measured under steady state reaction conditions. Based on previous "optimisation studies'' (see Chapter 2, section 2.3.1.2) the steady state was achieved in the reaction system 12 minutes after introducing the reagents and the same behaviour was observed during the kinetic studies.

5.3. Results and discussion

5.3.1. Effect of external and internal mass transfer

In the three-phase reaction system the overall process may be limited/ influenced by external or internal mass transfer or by the chemical reaction. The overall reaction rate in heterogeneous catalysis is determined by the slowest reaction step, *i.e.* adsorption, surface reaction or desorption, and is known as the rate-limiting (rate-controlling) step (Fogler 1999). In heterogeneous catalysis different regimes may be observed (Petrov 2002):

- a kinetic regime, in which the overall reaction rate is determined by the surface reaction;
- an external mass transfer regime, in which the overall reaction rate is determined by the processes of mass transfer of the substrates and product of the reaction to and from the external catalyst surface;
- an internal diffusion regime, in which the overall reaction rate is determined by the internal diffusion of the substrates and product of the reaction within the pores of catalyst particles.

Various combinations of the above regimes are possible. A transition regime, in which the overall reaction rate is determined by the surface reaction and diffusion, may exist where the chemical and mass transfer processes have approximately equal rates.

5.3.1.1. Effect of liquid phase flow rate

In order to determine the kinetics of the catalytic process, the reactor was operated as a differential flow reactor considering that the overall rate of the reaction is constant at all points within the reactor. Based on this assumption and the fact that the reaction rate is concentration-dependent, the reactor was operated only for small conversions (Levenspiel 1972).

The average reaction rate was calculated using the following equation:

$$(-r_A) = \frac{F_L\, C_p}{m_{cat}} \tag{5.7}$$

where:

$(-r_A)$	overall reaction rate (mol kg_{cat}^{-1} s^{-1});
F_L	volumetric flow rate of liquid phase (L s^{-1});
C_p	exit concentration of product (mol L^{-1});
m_{cat}	mass of catalyst (Pd/C) in an individual channel (kg).

Figure 5.2 shows how the overall rate of reaction varies with the liquid flow rate at a hydrogen partial pressure of 7.8 bar. Based on these results, two mass transfer regimes can be identified. The first regime (F_L < 1.0 mL min^{-1}) depends on the liquid flow rate and, therefore, on the convective mass transfer. The second regime ($F_L \geq$ 1.0 mL min^{-1}) is independent of the convective mass transfer and is likely to be kinetic, where the catalytic process is limited by chemical reaction itself and/ or by internal diffusion.

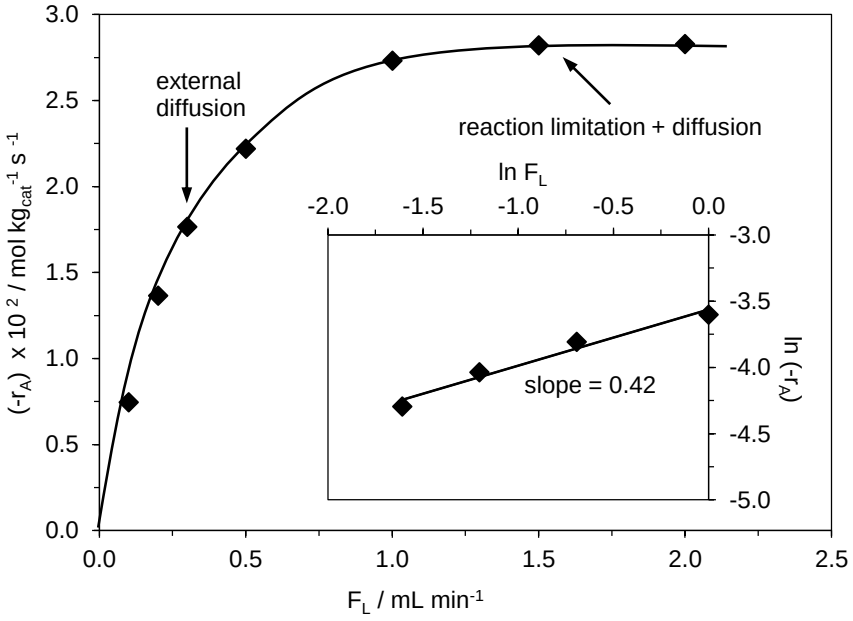

Figure 5.2. Influence of the liquid flow rate on the average reaction rate. P_{H_2} = 7.8 bar, F_G = 21.0 mL (STP) min^{-1}, $C_{S,0}$ = 0.4 mol L^{-1}, T = 298K.

By varying the liquid flow rate it is possible to distinguish between various limitations of the catalytic process (either in mass transfer or kinetic regimes). The results are shown in Figure 5.2. It is clear that when the liquid flow rate is $\geq$ 1 mL min^{-1}, the reaction is independent of the liquid flow rate and is likely to be in the kinetic regime. External mass transfer limitations are absent in the compact reactor at liquid flow rates $\geq$ 1.0 mL min^{-1}.

The mass transfer can be characterised by the Sherwood number, *Sh*, which represents the ratio of convective to diffusive mass transport, and is defined as:

$$Sh = \frac{k_c d_p}{D_{AB}} \tag{5.8}$$

where:

Sh	Sherwood number (-);
k_c	mass transfer coefficient (m s^{-1});
d_p	diameter of catalyst pellet (m);
D_{AB}	diffusivity (m^2 s^{-1}).

Sherwod number, *Sh*, is a function of Reynolds (*Re*) number:

$$Sh = f(Re)^n \tag{5.9}$$

where:

n	exponential factor (-).

The Reynolds number of the liquid phase (Trambouze *et al.* 1988) was calculated based on Equation 5.10 and was found to be Re_L= 0.43 at a liquid flow rate of 1.0 mL min^{-1}, which corresponds to laminar flow.

$$Re_L = \frac{\rho_L U_L d_p}{\mu_L} \tag{5.10}$$

where:

Re_L Reynolds number of the liquid phase (-);

ρ_L liquid density (kg m^{-3});

U_L superficial liquid velocity (m s^{-1});

d_p diameter of pellet (m);

μ_L liquid viscosity (Pa · s).

The Reynolds number depends on the superficial liquid velocity (U_L), which depends on the volumetric flow rate of the liquid phase:

$$U_L = \frac{F_L}{A} \tag{5.11}$$

where:

U_L superficial liquid velocity (m s^{-1});

F_L volumetric flow rate of liquid phase (m^3 s^{-1});

A channel cross-section area (m^2).

The Reynolds number defines the flow region in the reactor, whereas the exponential factor of the Reynolds number defines how the volumetric flow rate influences the mass transfer coefficient. The overall catalytic reaction is in the mass transfer regime if it is a function of the Reynolds number.

According to the insert in Figure 5.2 (the Reynolds number versus F_L) it was found that the overall rate of reaction depends on the $Re^{0.42}$ for low liquid flow rates (F_L<1.0 mL min^{-1}). The exponential factor was found experimentally and is very similar to the ones reported in the literature, for example Delaunay *et al.* (1982) found the exponential factor to be equal 0.48, whereas Chou *et al.* (1979) found it to be 0.54

and Lakota and Levec (1990) found it to be 0.495, indicating that the reaction is in the mass transfer regime.

5.3.1.2. Effect of gas phase flow rate

Figure 5.3 shows the overall rate of reaction as a function of hydrogen flow rate at 298K and 7.8 bar of hydrogen partial pressure. At low gas flow rates (F_G < 18 mL (STP) min^{-1}), the overall reaction rate depended on the hydrogen flow rate. The reaction rate was found to be almost independent of the gas flow rate for higher flow rates ($F_G \geq$ 18 mL (STP) min^{-1}). In almost all the experiments, hydrogen was supplied to the reactor in excess, except one performed at 2.0 mL (STP) min^{-1} of hydrogen flow rate (straight line in Figure 5.3).

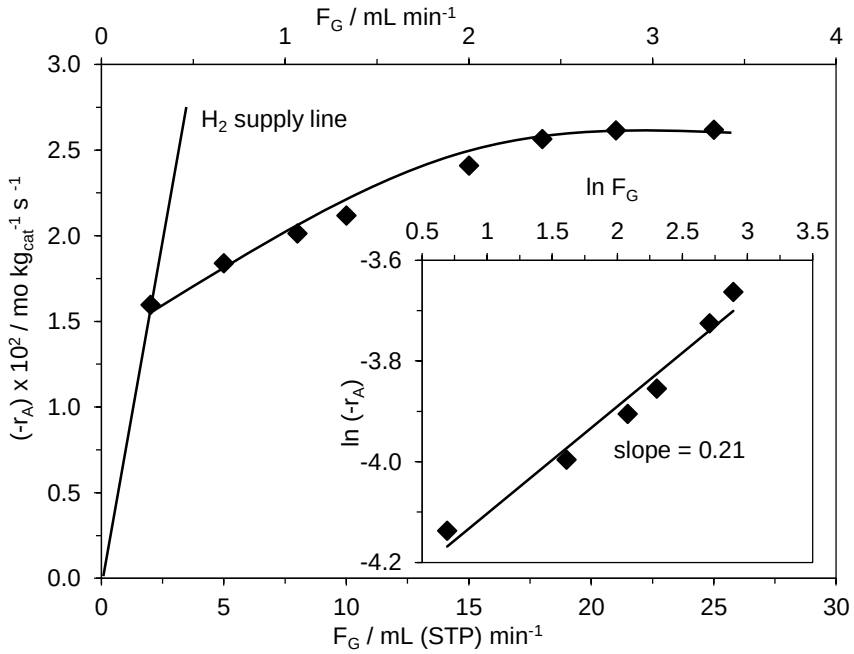

Figure 5.3. Influence of the gas flow rate on the average reaction rate.
P_{H_2} = 7.8 bar, F_L = 1.0 mL min^{-1}, $C_{S,0}$ = 0.4 mol L^{-1}, T = 298 K.

The Reynolds number of the gas phase was calculated based on Equation 5.12 and was found to be 0.45 at a gas flow rate of 21.0 mL (STP) min^{-1}.

$$Re_G = \frac{\rho_G U_G d_p}{\mu_G} \tag{5.12}$$

where:

Re_G Reynolds number of the gas phase (-);

ρ_G gas density (kg m^{-3});

U_G superficial gas velocity (m s^{-1});

d_p diameter of pellet (m);

μ_G gas viscosity (Pa · s).

The Reynolds number depends on the superficial gas phase velocity (U_G) which depends on the volumetric flow rate of gas phase:

$$U_G = \frac{F_G}{A} \tag{5.13}$$

where:

U_G superficial gas velocity (m s^{-1});

F_G volumetric flow rate of gas phase (m^3 s^{-1});

A channel cross-section area (m^2).

The Reynolds number defines the flow pattern of the gas phase in the reactor whereas the exponential factor of the Reynolds number defines how the volumetric flow rate influences the mass transfer coefficient.

According to the insert in Figure 5.3 (the Reynolds number versus F_G) it was found that the rate of reaction depends on the $Re^{0.21}$ for low gas flow rates (F_G<15.0 mL (STP) min^{-1}). The exponential factor was found experimentally and it is very similar to the ones reported in the literature, for example Chou *et al.* (1979) found

it to be equal to 0.16, indicating that the reaction is in the mass transfer regime, however the influence of the gas flow rate on the overall reaction rate is a weak one.

It is worth mentioning that the exponential factor found experimentally for the gas and liquid phases is $n_G < n_L$, indicating that the mass transfer limitation on the overall rate of reaction in the gas phase is lower than the one in the liquid phase.

The independence between the overall reaction rate and the gas phase flow rate for higher hydrogen flow rates excludes the possibility of external mass transfer limitations on the overall process. The catalytic process could be limited either by the chemical reaction itself or by internal diffusion.

5.3.1.3. Effect of internal diffusion

The Weisz-Prater criterion (Equation 5.14) was used to evaluate the importance of internal diffusion in the overall process. In this case the threshold value is 1. If $C_{WP} \ll 1$ internal diffusion is considered negligible; if $C_{WP} \gg 1$ than the phenomenon should be further investigated and accounted for (Weisz and Prater 1954; Fogler 1999; Vannice and Joyce 2005).

Since an investigation of the catalyst porosity effects on the overall kinetics (influencing internal diffusion) was not possible, the influence of the phenomena was estimated by applying the Weisz-Prater criterion:

$$C_{WP} = \eta\phi^2 = \frac{-r_A^{'}(obs)\rho_c R^2}{D_e C_{AS}} \qquad (5.14)$$

where:

$-r_A^{'}(obs)$	observed reaction rate per volume of the catalyst (mol kg_{cat}^{-1} s^{-1});
ρ_c	catalyst density (kg m^{-3});
R	catalyst particle radius (m);
C_{AS}	reactant concentration at the particle surface (mol m^{-3});
D_e	effective diffusivity (m^2 s^{-1}).

The effective diffusivity (Equation 5.15) was calculated starting from Wilke-Chang correlation (Equation 5.16) and the diffusion coefficient was corrected for estimated values of porosity, constriction factor and tortuosity (0.42, 1 and 3, respectively) (Fogler 1999; Cussler 2009)

$$D_e = \frac{D_{AB}\phi_p\sigma_c}{\tilde{\tau}} \tag{5.15}$$

where:

D_{AB} binary diffusion coefficient of A in B ($cm^2\ s^{-1}$);

$\tilde{\tau}$ tortuosity (-);

ϕ_p pellet porosity (-);

σ_c constriction factor (-).

$$D_{AB} = \frac{7.4 \cdot 10^{-8}\left(\chi M_B\right)^{1/2} T}{\mu \upsilon_A^{0.6}} \tag{5.16}$$

where:

D_{AB} diffusion coefficient of A in B ($cm^2\ s^{-1}$);

χ association factor of solvent B;

M_B molecular weight of solvent B ($g\ mol^{-1}$);

T temperature (K);

μ viscosity of solvent B (cP);

υ_A molar volume of A ($cm^3\ mol^{-1}$).

The diffusion coefficient was estimated to be $6.63 \cdot 10^{-5}$ $cm^2\ s^{-1}$ (Equation 5.16) and the effective diffusivity of hydrogen in MeOH is equal to $9.19 \cdot 10^{-6}$ $cm^2\ s^{-1}$ (Equation 5.15). The Weisz-Prater criterion was found to be 0.063 (Equation 5.14) which excluded the possibility of internal diffusion being a rate limiting step. It could, therefore, be confirmed that the reaction in a compact packed-bed reactor is limited by the catalytic reaction itself and the influence of the internal diffusion on the overall process can be considered negligible.

5.3.2. Effect of hydrogen partial pressure

The influence of the hydrogen partial pressure on the overall reaction rate was studied at two temperatures: 298K and 323K (Figure 5.4). The overall reaction rate is almost independent of the hydrogen partial pressure at 298K. Increasing hydrogen partial pressure by *ca.* 9 times increased the rate of the reaction only by *ca.* two times (Figure 5.4). At higher temperatures (323K) the overall rate of reaction increased *ca.* 30% at 0.5 and 4.5 bar of hydrogen partial pressure. Further increases in the hydrogen partial pressure had no significant effect on the overall reaction rate. The reaction rate is almost independent of the hydrogen partial pressure for $p_{H_2} > 6\,bar$ at 298K and for $p_{H_2} > 4.5\,bar$ at 323K, *i.e.* almost independent of the hydrogen concentration. The asymptotic approach of the overall reaction rate as a function of hydrogen partial pressure (Figure 5.4) indicates that the liquid phase is saturated with hydrogen and represents a Langmuir-Hinshelwood type of isotherm.
The reactor can therefore be operated in a purely kinetic regime by increasing the hydrogen partial pressure and by saturating the liquid phase with hydrogen prior to entering the reaction channel.

Data presented in Figure 5.4 also confirms the lack of influence of hydrogen partial pressure on the "optimisation studies'' (see Chapter 2, section 2.3.1.4).

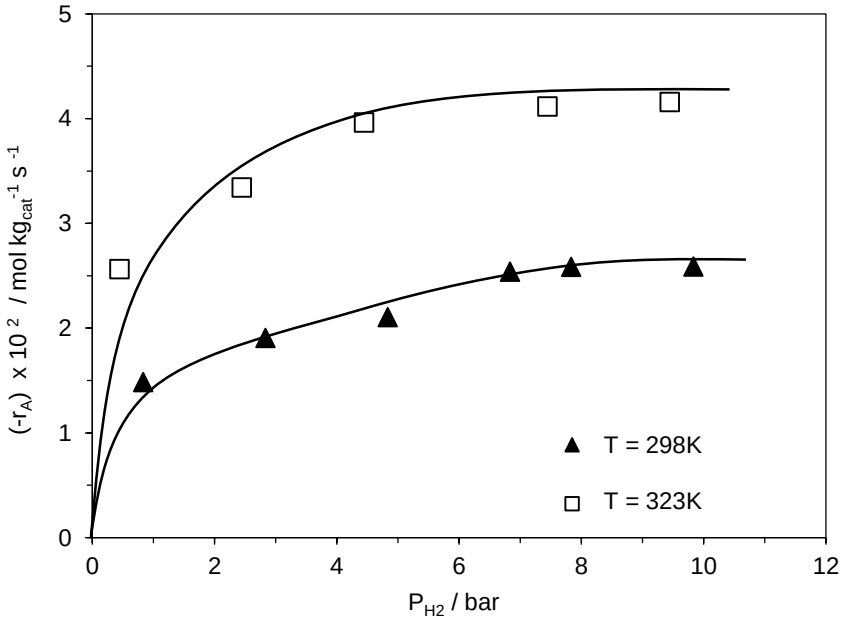

Figure 5.4. Effect of the hydrogen partial pressure on the average reaction rate.
F_G = 21.0 mL (STP) min^{-1}, F_L = 1.0 mL min^{-1}, $C_{S,0}$ = 0.4 mol L^{-1}.

The hydrogen partial pressure was calculated according to Equation 5.17:

$$p_{H_2} = p_T - p_{MeOH}^{sat} \quad (5.17)$$

where:

p_{H_2} hydrogen partial pressure (bar);

p_T total pressure (measured) (bar);

p_{MeOH}^{sat} saturated vapour pressure (calculated) (bar).

In Equation 5.17 the partial pressure of the reactant (imine) was neglected due to the high boiling point of liquid, *ca.* 423K (www.reaxys.com).

The *Antoine Equation* (Perry *et al.* 1984) was used to calculate the saturated vapour pressure:

$$log_{10}\, p_{MeOH}^{sat} = A - \frac{B}{C+T} \quad (5.18)$$

where:

A, B, C *Antoine* coefficients (-);

p_{MeOH}^{sat} saturated vapour pressure (bar);

T temperature (K).

Antoine coefficients for methanol at the desired temperature were taken from the National Institute of Standard Technology database (www.nist.gov).

The mole fraction of hydrogen in the liquid phase was calculated using *Henry's Law*:

$$p_{H_2} = H\, x_{H_2} \tag{5.19}$$

where:

p_{H_2} partial pressure of hydrogen (bar);

H Henry's constant (bar);

x_{H_2} mole fraction of hydrogen in the liquid phase (-).

Henry's constant was calculated from the following correlation (Liu *et al.* 1996):

$$ln(H) = 122.3 - \frac{4815.6}{T} - 17.5\, ln(T) + 1.4 \cdot 10^{-7} P \tag{5. 20}$$

where:

H Henry's constant (MPa);

T temperature (K);

P pressure (Pa).

Then the concentration of hydrogen in methanol was calculated by:

$$x_{H_2} = \frac{n_{H_2}}{n_{H_2} + n_{MeOH}} \approx \frac{n_{H_2}}{n_{MeOH}}$$

$$n_{H_2} << n_{MeOH} \tag{5.21}$$

$$C_{H_2} = C_{MeOH}\, x_{H_2}$$

According to the data presented in Figure 5.5 it can be seen that the concentration of hydrogen changes linearly with an increase in the hydrogen partial pressure at 298 and 323K. It can also be seen, however, that at the desired hydrogen partial pressure, the concentration of hydrogen in the liquid phase remains almost constant ($P_{H_2} \leq 5$ bar) and changes only by *ca.* 10% at higher hydrogen partial pressures ($P_{H_2} \geq 7$ bar) as the temperature increases from 298K to 323K.

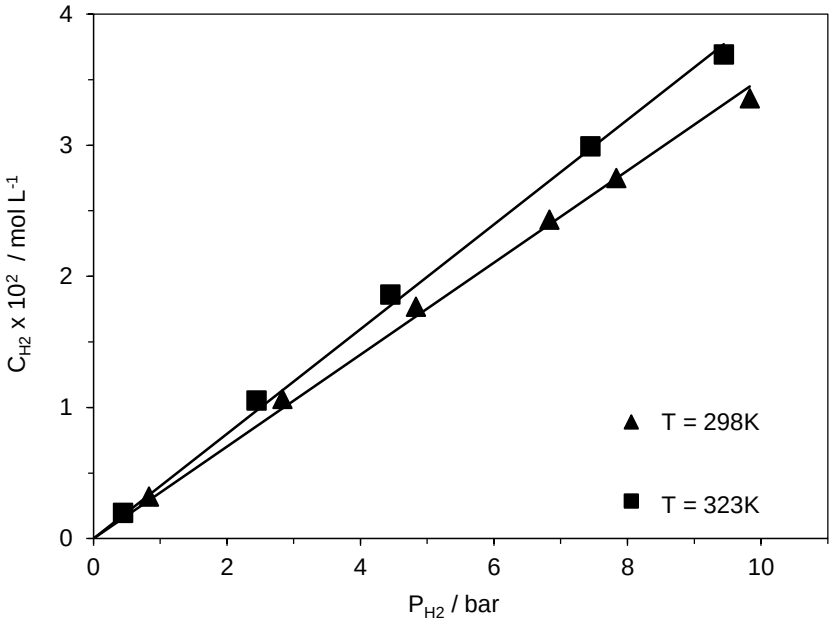

Figure 5.5. Hydrogen solubility in methanol at different temperatures and partial pressures of hydrogen.

5.3.3. Effect of reagent concentration

Figure 5.6 shows the dependence of the overall reaction rate, measured at 7.8 bar of hydrogen partial pressure, and at 298K and 323K on the initial reagent concentration. First, especially for the experiments carried out at 323K, a strong increase in the initial activity of the catalyst with the increase of the reagent concentration was observed for $C_{S,0} < 0.4$ mol L^{-1}. Then, for higher concentrations ($C_{S,0} \geq 0.4$ mol L^{-1}), the overall reaction rate was constant. This, finding supports a Langmuir-Hinshelwood type of rate law expression. At low reactant concentrations, the fractional occupancy of the catalyst surface increases linearly with the concentration in the solution and, with this, the activity. At higher reactant concentrations, however, the surface is almost fully saturated and the activity becomes independent of the reactant's concentration (Toebes *et al.* 2005).

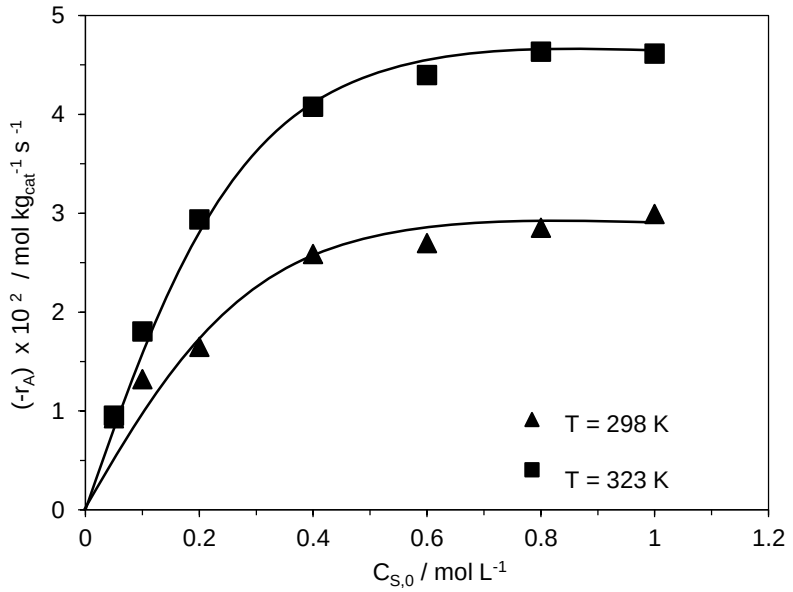

Figure 5.6. Influence of the initial reagent concentration on the overall rate of reaction. P_{H_2} = 7.8 bar, F_G = 21.0 mL (STP) min^{-1}, F_L = 1.0 mL min^{-1}.

5.3.4. Effect of reaction temperature

The effect of reaction temperature was studied for the conditions in which the reaction is in the kinetic regime, *i.e.*, P_{H_2} = 7.8 bar, F_{Gas} = 21.0 mL (STP) min^{-1}, F_L = 1.0 mL min^{-1} (see previous results). The overall reaction rate depends on the temperature (Figure 5.7). An increase in the reaction temperature resulted in a higher reaction rate and had no influence on the selectivity.

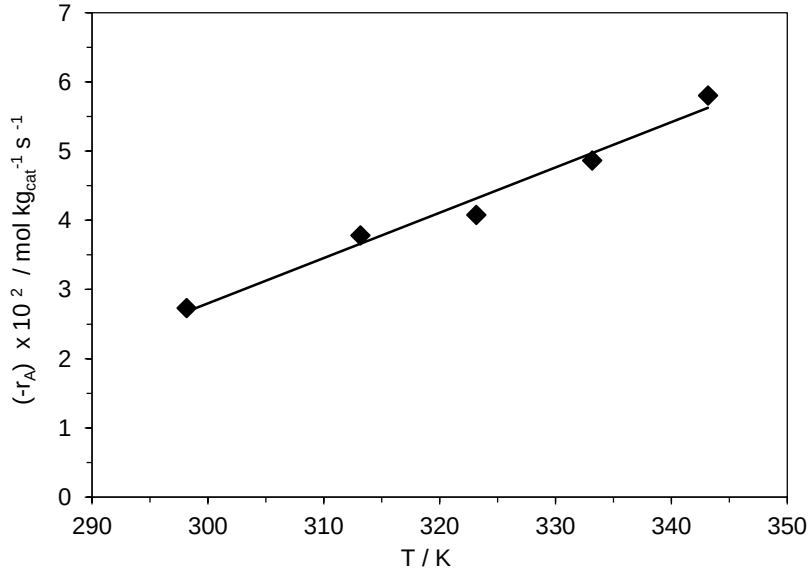

Figure 5.7. Influence of the reaction temperature on the overall rate of reaction. F_G = 21.0 mL (STP) min^{-1}, F_L = 1.0 mL min^{-1}, $C_{S,0}$ = 0.4 mol L^{-1}.

According to the data presented in Figure 5.8 the reductive amination of aldehyde has very low apparent activation energy. The apparent activation energy was calculated from the Arrhenius plot and was found to be 15 kJ mol^{-1}.

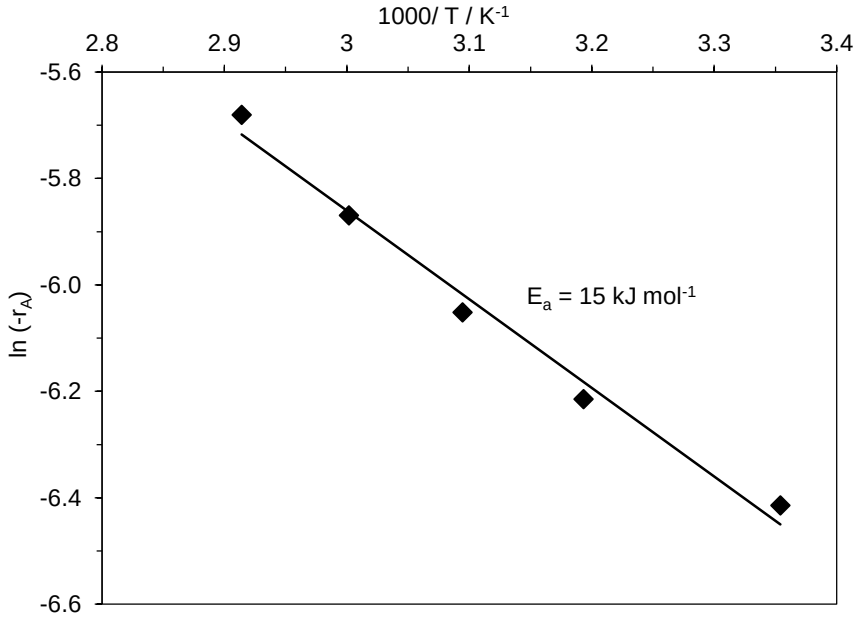

Figure 5.8. Influence of temperature on the overall reaction rate (in Arrhenius coordinates). F_G = 21.0 mL (STP) min^{-1}, F_L = 1.0 mL min^{-1}, $C_{S,0}$ = 0.4 mol L^{-1}.

The increase of the reaction temperature affects the partial pressure and solubility of hydrogen, and is considered to be negligible (Figure 5.9). The hydrogen concentration increased only by *ca.* 15% with the increase in temperature resulting from a decrease in the hydrogen partial pressure due to the vaporization of methanol. This indicates that the reaction is in the kinetic regime and the rate of the reductive amination depends on the temperature.

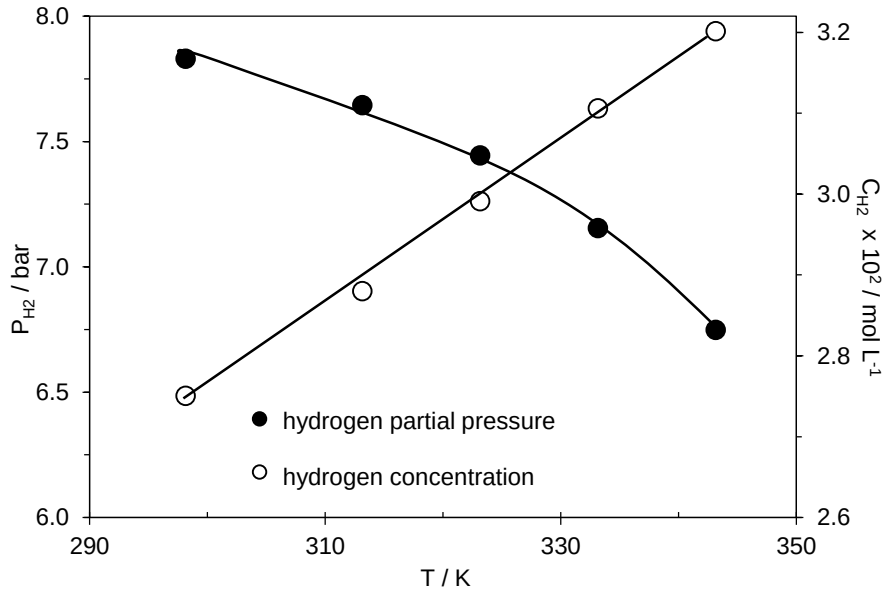

Figure 5.9. Hydrogen solubility in methanol and partial pressure at different temperatures.

Considering the surface-reaction as the limiting step in which both *A* and *B* adsorbed on the catalyst surface, the general expression for the Langmuir-Hinshelwood type of rate law can be written as follows:

$$(-r_A) = \frac{k^* K_A K_B C_A C_B}{(1 + K_A C_A + K_B C_B)^n} \tag{5.22}$$

The kinetic reaction rate constant k^*, follows Arrhenius temperature dependence and increases exponentially with temperature (Equation 5.23):

$$k^*(T) = A e^{-E/RT} \tag{5.23}$$

where:

k^* reaction rate constant;

A pre-exponential factor or frequency factor;

E_a activation energy (kJ mol^{-1});

R gas constant (8.314 J mol^{-1} K^{-1})

T absolute temperature (K).

The adsorption equilibrium constants, K_A and K_B, decrease with an increase in temperature, since adsorption is an exothermic process resulting in lower coverage of the catalyst surface by the reactants. Consequently, an increase in reaction temperature increases the reaction rate constant (k^*), decreases the equilibrium constants (K_A and K_B), changes the hydrogen concentration in the liquid phase, as well as the hydrogen partial pressure. Taking all these factors into account, it can be seen that the influence of the reaction temperature is very complex. To explain all these influences, rigorous mathematical modelling is needed.

5.3.5. Kinetic model and reaction mechanism

The Langmuir-Hinshelwood approach is widely used in the literature to describe the kinetic models for hydrogenation reactions. This approach assumes that the adsorption of organic and hydrogen molecules is in an equilibrium. Competitive or non-competitive adsorption of both reactants is also considered in the literature, however. The non-competitive approach assumes that the differences in sizes of hydrogen and other reacting species is sufficiently large for hydrogen to be able to adsorb in voids on the surface between bulky organic molecules (Simakova *et al.* 2009).

Based on the obtained results, Langmuir-Hinshelwood rate expressions for either competitive or non-competitive adsorption of organic and hydrogen molecules were developed, assuming molecular or dissociative adsorption of hydrogen. The following assumptions were made (Carrara *et al.* 2014):

- only one reaction mechanism acts over the whole range of conditions used;
- the adsorption of gaseous reactant can either be dissociative or non-dissociative;
- the liquid phase is saturated with hydrogen;
- adsorption and desorption of all species are at equilibrium;
- the adsorption of the reaction solvent (MeOH) and H_2O are considered to be negligible;
- adsorption of the reaction product is considered to be negligible.

Four possible mechanisms of hydrogenation are considered:

1. competitive molecular adsorption of hydrogen;
2. non-competitive molecular adsorption of hydrogen;
3. competitive dissociative adsorption of hydrogen;
4. non-competitive dissociative adsorption of hydrogen.

The overall process can be schematically represented by:

$$A_{(Liquid)} + B_{(Gas)} \rightarrow C_{(Liquid)}$$

Competitive molecular adsorption of hydrogen

Considering the above assumptions, the elementary steps of the catalytic process (adsorption, surface reaction, desorption) can be analysed so that the rate limiting ones can be individuated. For the reversible adsorption of A and B onto active sites, the rate equations can be written as the sum of the forward reaction (adsorption onto the site) and backward reaction (desorption), each with its own rate constant: k_A for the forward adsorption reaction and k_D for the backward reaction (desorption).

The adsorption of A onto an active site S is represented by:

$$A + S \rightleftarrows AS$$

The corresponding rate of adsorption of A can be expressed as:

$$r_{A,A} = (-r_A) = k_{A,A} \cdot C_A C_S - k_{D,A} \cdot C_{AS} \qquad (5.24)$$

The adsorption of B onto an active site S is represented by:

$$B + S \rightleftarrows BS$$

The corresponding rate of adsorption of B can be expressed as:

$$r_{A,B} = (-r_A) = k_{A,B} \cdot C_B C_S - k_{D,B} \cdot C_{BS} \qquad (5.25)$$

For the surface reaction step it is assumed that both reactants A and B adsorb on the same active site of the catalyst. The surface reaction is represented by:

$$AS + BS \rightleftarrows CS + S$$

The corresponding rate of surface reaction can be expressed as:

$$r_R = (-r_A) = k_R \cdot C_{AS}\, C_{BS} - k_{-R} \cdot C_{CS} C_S \tag{5.26}$$

For low conversion (differential reactor), the concentration of the product is very low and the negative term of Equation 5.26 can be neglected. Assuming irreversibility, the corresponding rate of surface reaction can be written as:

$$r_R = (-r_A) = k_R \cdot C_{AS}\, C_{BS} \tag{5.27}$$

Finally, desorption of product C from an active site S is represented by:

$$CS \rightleftarrows C + S$$

The corresponding rate of desorption of C can be expressed as:

$$r_{D,C} = (-r_A) = k_{D,C} \cdot C_{CS} - k_{A,C} \cdot C_C\, C_S \tag{5.28}$$

Since the equilibrium constants are defined as $K_{eq} = \frac{k_A}{k_D}$, we can then write for adsorption and desorption steps:

$$K_{A,A} = \frac{k_{A,A}}{k_{D,A}} \tag{5.29a}$$

$$K_{A,B} = \frac{k_{A,B}}{k_{D,B}} \tag{5.29b}$$

$$K_{D,C} = \frac{k_{D,C}}{k_{A,C}} \tag{5.29c}$$

At equilibrium, the net rate of adsorption equals zero. Setting the left-hand side of Equation 5.24 equal to zero and solving for the concentration of A adsorbed onto an active site S, we get:

$$\frac{(-r_A)}{k_{A,A}} = \left(C_A C_S - \frac{C_{AS}}{K_{A,A}} \right) \downarrow 0$$

$$C_{AS} = K_{A,A} C_A C_S \tag{5.30}$$

Similarly for component B at equilibrium, the net rate of adsorption equals zero. Setting the left-hand side of Equation 5.25 equal to zero and solving for the concentration of B adsorbed onto an active site S, we get:

$$\frac{(-r_A)}{k_{A,B}} = \left(C_B C_S - \frac{C_{BS}}{K_{A,B}} \right) \downarrow 0$$

$$C_{BS} = K_{A,B} C_B C_S \tag{5.31}$$

As previously, at equilibrium, the net rate of adsorption equals zero. Setting the left-hand side of Equation 5.28 equal to zero and solving for the concentration of C adsorbed onto an active site S, we get:

$$\frac{(-r_A)}{k_{D,C}} = \left(C_{CS} - \frac{C_C C_S}{K_{D,C}} \right) \downarrow 0$$

$$C_{CS} = \frac{C_C C_S}{K_{D,C}} \tag{5.32}$$

Because A, B and C are adsorbed on the surface, the concentration of occupied sites is $\left(C_{AS} + C_{BS} + C_{CS}\right)$. A catalytic site balance can now be written as:

$$C_T = C_S + C_{AS} + C_{BS} + C_{CS} \tag{5.33}$$

Taking into account Equations 5.30 - 5.32 the concentration of the vacant sites, C_S, can now be calculated as follow:

$$C_T = C_S + K_{A,A}C_A C_S + K_{A,B}C_B C_S + \frac{C_C C_S}{K_{D,C}}$$

$$C_T = C_S\left(1 + K_{A,A}C_A + K_{A,B}C_B + \frac{C_C}{K_{D,C}}\right)$$

$$C_S = \frac{C_T}{1 + K_{A,A}C_A + K_{A,B}C_B + \frac{C_C}{K_{D,C}}} \tag{5.34}$$

The final rate equation for the hydrogenation step assuming competitive molecular adsorption of B can now be obtained by substituting Eqs. 5.30 - 5.34 into Eq. 5.27. This last operation leads to the general rate equation that can be further simplified and/ or linearized to obtain the kinetic parameters of the surface reaction step:

$$r_R = (-r_A) = k_R \cdot K_{A,A}C_A C_S \cdot K_{A,B}C_B C_S$$

$$r_R = (-r_A) = k_R \cdot K_{A,A}C_A \cdot K_{A,B}C_B \cdot C_S^2$$

$$r_R = (-r_A) = \frac{k_R C_T^2 \cdot K_{A,A}C_A \cdot K_{A,B}C_B}{\left(1 + K_{A,A}C_A + K_{A,B}C_B\right)^2}$$

$$r_R = (-r_A) = \frac{k_R^* K_{A,A}C_A K_{A,B}p_B}{(1 + K_{A,A}C_A + K_{A,B}p_B)^2} \tag{5.35}$$

where: $k_R^* = k_R C_T^2$

Non-competitive molecular adsorption of hydrogen

The model of non-competitive molecular adsorption of B leads to the following equations, which can be easily derived based on the previous assumptions.

The adsorption of A onto an active site S is represented by:

$$A + S \rightleftarrows AS$$

The corresponding rate of adsorption of A can be expressed as:

$$r_{A,A} = (-r_A) = k_{A,A} \cdot C_A C_S - k_{D,A} \cdot C_{AS} \tag{5.36}$$

The adsorption of B onto an active site S^* is represented by:

$$B + S^* \rightleftarrows BS^*$$

The corresponding rate of adsorption of B can be expressed as:

$$r_{A,B} = (-r_A) = k_{A,B} \cdot C_B C_{S^*} - k_{D,B} \cdot C_{BS^*} \tag{5.37}$$

For the surface reaction step it is assumed that reactants A and B adsorb on the different active sites of the catalyst. The surface reaction is represented by:

$$AS + BS^* \rightleftarrows CS + S^*$$

The corresponding rate of surface reaction can be expressed as:

$$r_R = (-r_A) = k_R \cdot C_{AS}\, C_{BS^*} - k_{-R} \cdot C_{CS} C_{S^*} \tag{5.38}$$

For low conversion (differential reactor), the concentration of the product is very low and the negative term of Equation 5.38 can therefore be neglected. Assuming irreversibility, the corresponding rate of surface reaction can be written as:

$$r_R = (-r_A) = k_R \cdot C_{AS} C_{BS^*} \tag{5.39}$$

Finally, desorption of C from an active site S is represented by:

$$CS \rightleftarrows C + S$$

The corresponding rate of desorption of C can be expressed as:

$$r_{D,C} = (-r_A) = k_{D,C} \cdot C_{CS} - k_{A,C} \cdot C_C C_S \tag{5.40}$$

Since equilibrium constants are defined as $K_{eq} = \frac{k_A}{k_D}$, the following can be written for adsorption and desorption steps:

$$K_{A,A} = \frac{k_{A,A}}{k_{D,A}} \tag{5.41a}$$

$$K_{A,B} = \frac{k_{A,B}}{k_{D,B}} \tag{5.41b}$$

$$K_{D,C} = \frac{k_{D,C}}{k_{A,C}} \tag{5.41c}$$

At equilibrium, the net rate of adsorption equals zero. Setting the left-hand side of Equation 5.36 equal to zero and solving for the concentration of A adsorbed onto an active site S, we get:

$$\frac{(-r_A)}{k_{A,A}} = \left(C_A C_S - \frac{C_{AS}}{K_{A,A}} \right) \downarrow 0$$

$$C_{AS} = K_{A,A} C_A C_S \tag{5.42}$$

Similarly for B, at equilibrium, the net rate of adsorption equals zero. Setting the left-hand side of Equation 5.37 equal to zero and solving for the concentration of B adsorbed onto an active site S^*, we get:

$$\frac{(-r_A)}{k_{A,B}} = \left(C_B C_S - \frac{C_{BS^*}}{K_{A,B}} \right) \downarrow 0$$

$$C_{BS^*} = K_{A,B} C_B C_{S^*} \tag{5.43}$$

As previously, at equilibrium, the net rate of adsorption equals zero. Setting the left-hand side of Equation 5.40 equal to zero and solving for the concentration of C adsorbed onto an active site S, we get:

$$\frac{(-r_A)}{k_{D,C}} = \left(C_{CS} - \frac{C_C C_S}{K_{D,C}} \right) \downarrow 0$$

$$C_{CS} = \frac{C_C C_S}{K_{D,C}} \tag{5.44}$$

Because A, B and C are adsorbed on the surface the concentration of occupied sites is $\left(C_{AS} + C_{BS^*} + C_{CS}\right)$. A catalytic sites balance can now be written as:

$$C_T = C_S + C_{AS} + C_{CS}$$
$$C_T = C_S + K_{A,A} C_A C_S + \frac{C_C C_S}{K_{D,C}}$$
$$C_T = C_S \left(1 + K_{A,A} C_A + \frac{C_C}{K_{D,C}} \right)$$

$$C_S = \frac{C_T}{1 + K_{A,A} C_A + \frac{C_C}{K_{D,C}}} \tag{5.45}$$

and:

$$C_{T^*} = C_{S^*} + C_{BS^*}$$
$$C_{T^*} = C_{S^*} + K_{A,B} C_B C_{S^*}$$
$$C_{T^*} = C_{S^*} \left(1 + K_{A,B} C_B\right)$$

$$C_{S^*} = \frac{C_{T^*}}{1 + K_{A,B} C_B} \tag{5.46}$$

The final rate expression for the hydrogenation step, assuming non-competitive molecular adsorption of B can now be obtained by substituting Eqs. 5.42-5.46 into Eq. 5.39. This last operation leads us to the general rate equation that can be further simplified and/ or linearized to obtain the kinetic parameters of the surface reaction step:

$$r_R = (-r_A) = k_R \cdot K_{A,A} C_A C_S \cdot K_{A,B} C_B C_{S^*}$$

$$r_R = (-r_A) = k_R \cdot K_{A,A} C_A \cdot K_{A,B} C_B \cdot C_S \cdot C_{S^*}$$

$$r_R = (-r_A) = \frac{k_R \cdot C_T C_{T^*} \cdot K_{A,A} C_A \cdot K_{A,B} C_B}{\left(1 + K_{A,A} C_A + \frac{C_C}{K_{D,C}}\right)\left(1 + K_{A,B} C_B\right)}$$

$$r_R = (-r_A) = \frac{k_R^* K_{A,A} C_A K_{A,B} p_B}{(1 + K_{A,A} C_A)(1 + K_{A,B} p_B)} \tag{5.47}$$

where: $k_R^* = k_R C_T C_{T^*}$

Competitive dissociative adsorption of hydrogen

Considering the former hypotheses, the elementary steps in the reaction can be written as follows:

The adsorption of A onto an active site S is represented by:

$A + S \rightleftarrows AS$

The corresponding rate of adsorption of A can be expressed as:

$$r_{A,A} = (-r_A) = k_{A,A} \cdot C_A C_S - k_{D,A} \cdot C_{AS} \tag{5.48}$$

The adsorption of B onto an active site S is represented by:

$B + 2S \rightleftarrows 2BS$

The corresponding rate of adsorption of B can be expressed as:

$$r_{A,B} = (-r_A) = k_{A,B} \cdot C_B C_S^2 - k_{D,B} \cdot (C_{BS})^2 \tag{5.49}$$

For the surface reaction step it is assumed that both reactants A and B adsorb on the same active site of the catalyst. The surface reaction is represented by:

$AS + 2BS \rightleftarrows CS + 2S$

The corresponding rate of surface reaction can be expressed as:

$$r_R = (-r_A) = k_R \cdot C_{AS} (C_{BS})^2 - k_{-R} \cdot C_{CS} C_S^2 \tag{5.50}$$

For low conversion (differential reactor), the concentration of the product is very low and the negative term of Equation 5.50 can therefore be neglected. Assuming irreversibility, the corresponding rate of surface reaction can be written as:

$$r_R = (-r_A) = k_R \cdot C_{AS} \left(C_{BS}\right)^2 \tag{5.51}$$

Finally, desorption of C from an active site S is represented by:

$$CS \rightleftarrows C + S$$

The corresponding rate of desorption of C can be expressed as:

$$r_{D,C} = (-r_A) = k_{D,C} \cdot C_{CS} - k_{A,C} \cdot C_C C_S \tag{5.52}$$

Since equilibrium constants are defined as $K_{eq} = \frac{k_A}{k_D}$, we can then write for adsorption and desorption steps:

$$K_{A,A} = \frac{k_{A,A}}{k_{D,A}} \tag{5.53a}$$

$$K_{A,B} = \frac{k_{A,B}}{k_{D,B}} \tag{5.53b}$$

$$K_{D,C} = \frac{k_{D,C}}{k_{A,C}} \tag{5.53c}$$

At equilibrium, the net rate of adsorption equals zero. Setting the left-hand side of Equation 5.48 equal to zero and solving for the concentration of A adsorbed onto an active site S, we get:

$$\frac{(-r_A)}{k_{A,A}} = \left(C_A C_S - \frac{C_{AS}}{K_{A,A}} \right) \downarrow 0$$

$$C_{AS} = K_{A,A} C_A C_S \tag{5.54}$$

Similarly for B, at equilibrium, the net rate of adsorption equals zero. Setting the left-hand side of Equation 5.49 equal to zero and solving for the concentration of B adsorbed onto an active site S, we get:

$$\frac{(-r_A)}{k_{A,B}} = \left(C_B\, C_S^2 - \frac{(C_{BS})^2}{K_{A,B}} \right) \downarrow 0$$

$$C_{BS} = \sqrt{K_{A,B} C_B} \cdot C_S \qquad (5.55)$$

As previously, at equilibrium, the net rate of adsorption equals zero. Setting the left-hand side of Equation 5.52 equal to zero and solving for the concentration of C adsorbed onto an active site S, we get:

$$\frac{(-r_A)}{k_{D,C}} = \left(C_{CS} - \frac{C_C C_S}{K_{D,C}} \right) \downarrow 0$$

$$C_{CS} = \frac{C_C C_S}{K_{D,C}} \qquad (5.56)$$

Because A, B and C are adsorbed on the surface, the concentration of occupied sites is $(C_{AS} + C_{BS} + C_{CS})$. A catalytic site balance can now be written as:

$$C_T = C_S + C_{AS} + C_{BS} + C_{CS}$$

Taking into account Equations 5.54 – 5.56, the concentration of the vacant sites, C_S, can now be calculated as follows:

$$C_T = C_S + K_{A,A} C_A C_S + \sqrt{K_{A,B} C_B} C_S + \frac{C_C C_S}{K_{D,C}}$$

$$C_T = C_S \left(1 + K_{A,A} C_A + \sqrt{K_{A,B} C_B} + \frac{C_C}{K_{D,C}} \right)$$

$$C_S = \frac{C_T}{1 + K_{A,A} C_A + \sqrt{K_{A,B} C_B}} \qquad (5.57)$$

The final rate expression for the hydrogenation step, assuming competitive dissociative adsorption of B, can now be obtained by substituting Eqs. 5.54 - 5.57 into Eq. 5.51. This last operation leads us to the general rate equation that can be further

simplified and/ or linearized to obtain the kinetic parameters of the surface reaction step:

$$r_R = (-r_A) = k_R \cdot K_{A,A} C_A C_S \cdot K_{A,B} C_B C_S^2$$
$$r_R = (-r_A) = k_R \cdot K_{A,A} C_A \cdot K_{A,B} C_B \cdot C_S^3$$
$$r_R = (-r_A) = \frac{k_R \cdot K_{A,A} K_{A,B} \cdot C_T^3 C_A C_B}{\left(1 + K_{A,A} C_A + \sqrt{K_{A,B} C_B}\right)^3}$$

$$r_R = (-r_A) = \frac{k_R^* K_{A,A} C_A K_{A,B} p_B}{\left(1 + K_{A,A} C_A + \sqrt{K_{A,B} p_B}\right)^3} \quad (5.58)$$

where: $k_R^* = k_R C_T^3$

Non-competitive dissociative adsorption of hydrogen

The model of non-competitive dissociative adsorption of B leads to the following equations, which can be easily derived based on the previous assumptions.

The adsorption of A onto an active site S is represented by:

$A + S \rightleftarrows AS$

The corresponding rate of adsorption of A can be expressed as:

$$r_{A,A} = (-r_A) = k_{A,A} \cdot C_A C_S - k_{D,A} \cdot C_{AS} \quad (5.59)$$

The adsorption of B onto an active site S^* is represented by:

$B + 2S^* \rightleftarrows 2BS^*$

The corresponding rate of adsorption of B can be expressed as:

$$r_{A,B} = (-r_A) = k_{A,B} \cdot C_B C_{S^*}^2 - k_{D,B} \cdot \left(C_{BS^*}\right)^2 \quad (5.60)$$

For the surface reaction step it is assumed that reactants A and B adsorb on the different active sites of the catalyst. The surface reaction is represented by:

$AS + 2BS^* \rightleftarrows CS + 2S^*$

The corresponding rate of surface reaction can be expressed as:

$$r_R = (-r_A) = k_R \cdot C_{AS} \left(C_{BS^*}\right)^2 - k_{-R} \cdot C_{CS} \left(C_{S^*}\right)^2 \quad (5.61)$$

For low conversion (differential reactor), the concentration of the product is very low and the negative term of Equation 5.61 can therefore be neglected. Assuming irreversibility, the corresponding rate of surface reaction can be written as:

$$r_R = (-r_A) = k_R \cdot C_{AS} \left(C_{BS^*}\right)^2 \quad (5.62)$$

Finally, desorption of C from an active site S is represented by:

$$CS \rightleftarrows C + S$$

The corresponding rate of desorption of C can be expressed as:

$$r_{D,C} = (-r_A) = k_{D,C} \cdot C_{CS} - k_{A,C} \cdot C_C C_S \quad (5.63)$$

Since equilibrium constants are defined as $K_{eq} = \frac{k_A}{k_D}$, it can be written for the adsorption and desorption steps as follow:

$$K_{A,A} = \frac{k_{A,A}}{k_{D,A}} \quad (5.64a)$$

$$K_{A,B} = \frac{k_{A,B}}{k_{D,B}} \quad (5.64b)$$

$$K_{D,C} = \frac{k_{D,C}}{k_{A,C}} \quad (5.64c)$$

At equilibrium, the net rate of adsorption equals zero. Setting the left-hand side of Equation 5.59 equal to zero and solving for the concentration of A adsorbed onto an active site S, we get:

$$\frac{(-r_A)}{k_{A,A}} = \left(C_A C_S - \frac{C_{AS}}{K_{A,A}} \right) \downarrow 0$$

$$C_{AS} = K_{A,A} C_A C_S \quad (5.65)$$

Similarly for B, at equilibrium, the net rate of adsorption equals zero. Setting the left-hand side of Equation 5.60 equal to zero and solving for the concentration of B adsorbed onto an active site S, we get:

$$\frac{(-r_A)}{k_{A,B}} = \left(C_B \, C_{S^*}^2 - \frac{\left(C_{BS^*}\right)^2}{K_{A,B}} \right) \downarrow 0$$

$$C_{BS*} = \sqrt{K_{A,B} C_B} \cdot C_{S^*} \tag{5.66}$$

As previously, at equilibrium, the net rate of adsorption equals zero. Setting the left-hand side of Equation 5.63 equal to zero and solving for the concentration of C adsorbed onto an active site S, we get:

$$\frac{(-r_A)}{k_{D,C}} = \left(C_{CS} - \frac{C_C C_S}{K_{D,C}} \right) \downarrow 0$$

$$C_{CS} = \frac{C_C C_S}{K_{D,C}} \tag{5.67}$$

Because A, B and C are adsorbed on the surface the concentration of occupied sites is $\left(C_{AS} + C_{BS^*} + C_{CS}\right)$. A catalytic sites balance can now be written as:

$$C_T = C_S + C_{AS} + C_{CS}$$

$$C_T = C_S + K_{A,A} C_A C_S + \frac{C_C C_S}{K_{D,C}}$$

$$C_T = C_S \left(1 + K_{A,A} C_A + \frac{C_C}{K_{D,C}} \right)$$

$$C_S = \frac{C_T}{1 + K_{A,A} C_A + \frac{C_C}{K_{D,C}}} \tag{5.68}$$

and:

$$C_{T^*} = C_{S^*} + C_{BS^*}$$
$$C_{T^*} = C_{S^*} + \sqrt{K_{A,B}C_B}\,C_{S^*}$$
$$C_{T^*} = C_{S^*}\left(1 + \sqrt{K_{A,B}C_B}\right)$$

$$C_{S^*} = \frac{C_{T^*}}{1 + \sqrt{K_{A,B}C_B}} \tag{5.69}$$

The final rate equation for the hydrogenation step, assuming non-competitive dissociative adsorption of hydrogen, can now be obtained by substituting Eqs. 5.65 - 5.69 into Eq. 5.62. This last operation leads us to the general rate equation that can be further simplified and/ or linearized to obtain the kinetic parameters of the surface reaction step:

$$r_R = (-r_A) = k_R \cdot K_{A,A}C_A C_S \cdot K_{A,B}C_B C_{S^*}^2$$
$$r_R = (-r_A) = k_R \cdot K_{A,A}C_A \cdot K_{A,B}C_B \cdot C_S \cdot C_{S^*}^2$$
$$r_R = (-r_A) = \frac{k_R^* \cdot K_{A,A}K_{A,B} \cdot C_S C_{S^*}^2 \cdot C_A C_B}{\left(1 + K_{A,A}C_A + \dfrac{C_C}{K_{D,C}}\right)\left(1 + \sqrt{K_{A,B}C_B}\right)}$$

$$r_R = (-r_A) = \frac{k_R^* K_{A,A}C_A K_{A,B}p_B}{(1 + K_{A,A}C_A)(1 + \sqrt{K_{A,B}p_B})^2} \tag{5.70}$$

where: $k_R^* = k_R C_T C_{T^*}^2$

All four final rate equations (5.35, 5.47, 5.58, 5.70) for the hydrogenation step were linearized to facilitate the data fitting procedure and to evaluate graphically the quality of the assumptions made so far (Table 5.1).

The fit was performed using the LSCRUVE FIT optimisation function of Matlab (Higham and Higham 2005). This function uses a least square refinement method to find a solution for the selected equation that will fit the experimental data. The model equation includes one or more parameters (*e.g* k_R^*, K_A and K_B) that the

Matlab function will manipulate in order to obtain the best fit for the experimental data provided. The least square refinement method fits the data by minimising the sum of the square of the residuals S (Chapra and Canale 2010).

Given a set of n data points (x_i, y_i) and a model function $f(x_i, a_1, a_2, ..., a_n)$, where x_i is the independent variable, y_i is the dependent vatriable and $a_1, a_2, ..., a_n$ are the adjustable parameters, the least square method finds the optimum values for all a_i when the sum of squared residuals S is a minimum:

$$S = \sum_{i=1}^{n} [y_i - f(x_i, a_1, a_2, ..., a_n)]^2 \qquad (5.71)$$

where the residual is defined as the difference between the experimental value, x_i, and the value predicted by the model equation, $f(x_i, a_1, a_2, ..., a_n)$. The condition for S to be a minimum is that $\frac{\partial S}{\partial a_i} = 0.$

At the end of the fitting routine Matlab also provides the necessary statistical parameters, such as, R^2, 95% confidence intervals for the fitted parameters and an estimate of multicollinearity.

The values of R^2 obtained for the experiments performed at 298K and 323K are presented in (Table 5.1). Two models, *i.e.* competitive and non-competitive molecular adsorption of hydrogen, were excluded from further consideration since they had the lowest R^2, very high error and multicollinearity of estimated values.

The models of competitive and non-competitive dissociative adsorption of hydrogen had the highest R^2 and showed no problem with correlation or multicollinearity of the estimated values, with a 95 % Confidence Interval (CI).

The estimated values of the reaction rate constant k_R^*, adsorption equilibrium constant of imine (K_A) and adsorption equilibrium constant of hydrogen (K_B) for experiments performed at 298 and 323K are presented in Table 5.2 and Table 5.3.

Table 5.1. Various models for Reductive Amination of hydrocinnamaldehyde with α-methylbenzylamine over 10% Pd/C catalyst.

Mechanism	Rate equation	Linearized rate equation	R^2	
			T =298K	T =323K
Competitive molecular adsorption of H_2	$r_R = (-r_A) = \frac{k_R^* K_A C_A K_B p_B}{(1 + K_A C_A + K_B p_B)^2}$	$\sqrt{\frac{C_A p_B}{(-r_A)}} = \frac{1}{\sqrt{k_R^* K_A K_B}} + \frac{K_A}{\sqrt{k_R^* K_A K_B}} \cdot C_A + \frac{K_B}{\sqrt{k_R^* K_A K_B}} \cdot p_B$	0.9764	0.9832
Non-competitive molecular adsorption of H_2	$r_R = (-r_A) = \frac{k_R^* K_A C_A K_B p_B}{(1 + K_A C_A)(1 + K_B p_B)}$	$\frac{C_A p_B}{(-r_A)} = \frac{1}{k_R^* K_A K_B} + \frac{p_B}{k_R^* K_A} + \frac{C_A}{k_R^* K_B} + \frac{C_A p_B}{k_R^*}$	0.9874	0.9917
Competitive dissociative adsorption of H_2	$r_R = (-r_A) = \frac{k_R^* K_A C_A K_B p_B}{(1 + K_A C_A + \sqrt{K_B p_B})^3}$	$\sqrt[3]{\frac{C_A p_B}{(-r_A)}} = \frac{1}{\sqrt[3]{k_R^* K_A K_B}} + \frac{K_A}{\sqrt[3]{k_R^* K_A K_B}} \cdot C_A + \frac{\sqrt{K_B}}{\sqrt[3]{k_R^* K_A K_B}} \cdot \sqrt{p_B}$	0.9942	0.9979
Non-competitive dissociative adsorption of H_2	$r_R = (-r_A) = \frac{k_R^* K_A C_A K_B p_B}{(1 + K_A C_A)(1 + \sqrt{K_B p_B})^2}$	$\frac{C_A p_B}{(-r_A)} = \frac{(1 + K_A C_A)(1 + \sqrt{K_B p_B})^2}{k_R^* K_A K_B}$	0.9941	0.9962

Table 5.2. Kinetic and adsorption parameters for reductive amination at 298K.

Mechanism	k_R^* (mol kg_{cat}^{-1} s^{-1})	K_A ($L\ mol^{-1}$)	K_B (bar^{-1})
Competitive dissociative adsorption of H_2	0.45 ± 0.10	1.80 ± 0.45	0.52 ± 0.35
Non-competitive dissociative adsorption of H_2	0.05 ± 0.01	5.60 ± 1.12	2.51 ± 2.98

Table 5.3. Kinetic and adsorption parameters for reductive amination at 323K.

Mechanism	k_R^* (mol kg_{cat}^{-1} s^{-1})	K_A ($L\ mol^{-1}$)	K_B (bar^{-1})
Competitive dissociative adsorption of H_2	0.51 ± 0.06	3.09 ± 0.60	1.72 ± 0.81
Non-competitive dissociative adsorption of H_2	0.07 ± 0.01	5.12 ± 1.18	11.52 ± 21.00

Some of the estimated values were obtained with very large errors, however (Table 5.2 and Table 5.3). This could be attributed to an insufficient amount of experimentally obtained data that could be used for fitting. It was also impossible to distinguish which of the two mechanisms describe the obtained results better. In order to distinguish between competitive and non-competitive dissociative adsorption of hydrogen as well as improve the estimated reaction parameters further studies are therefore required. Figures 5.11 and 5.12 present the overall rate of reaction calculated based on the Equations 5.58 and 5.70, with estimated values of k_R^*, K_A, and K_B. It can be seen that even though some of the estimated parameters were obtained with

large errors, they nonetheless proved to be a good fit for the experimental data (Figure 5.10 and Figure 5.11). The lines on both graphs (Figure 5.10 and Figure 5.11) show how these two models would behave at higher hydrogen partial pressures and initial substrate concentrations. It can be seen from Figure 5.10 that, in order to distinguish between the competitive and non-competitive dissociative adsorption of hydrogen models, the hydrogen partial pressure investigated would have to be *ca.* 50 - 100 bar. For health and safety reasons these experiments could not be performed with the equipment available. Experiments with higher initial reactant concentration (Figure 5.12) were therefore performed in order to distinguish between the competitive and non-competitive dissociative adsorption of hydrogen models.

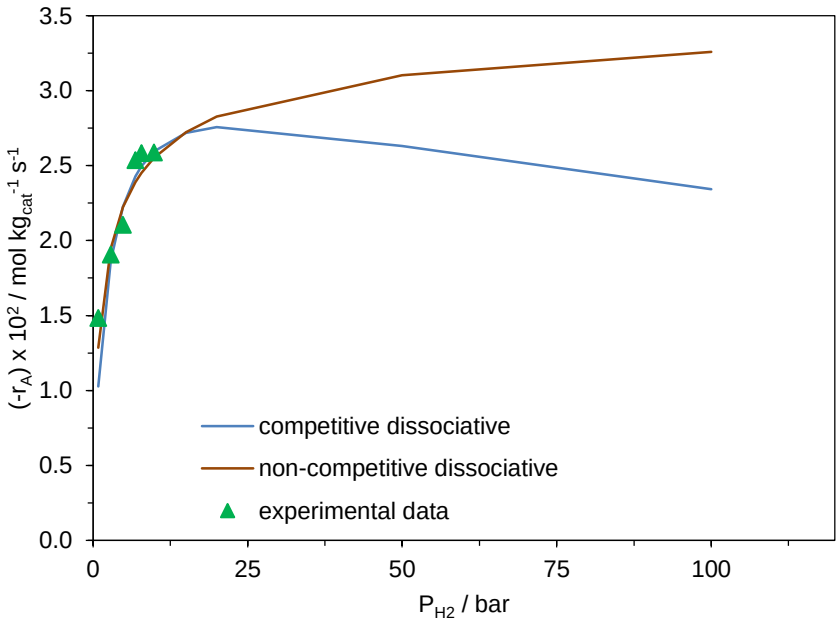

Figure 5.10. Fits of the competitive and non-competitive dissociative adsorption of hydrogen models. Experimental data obtained at 298K. Lines give the model prediction at higher hydrogen partial pressures.

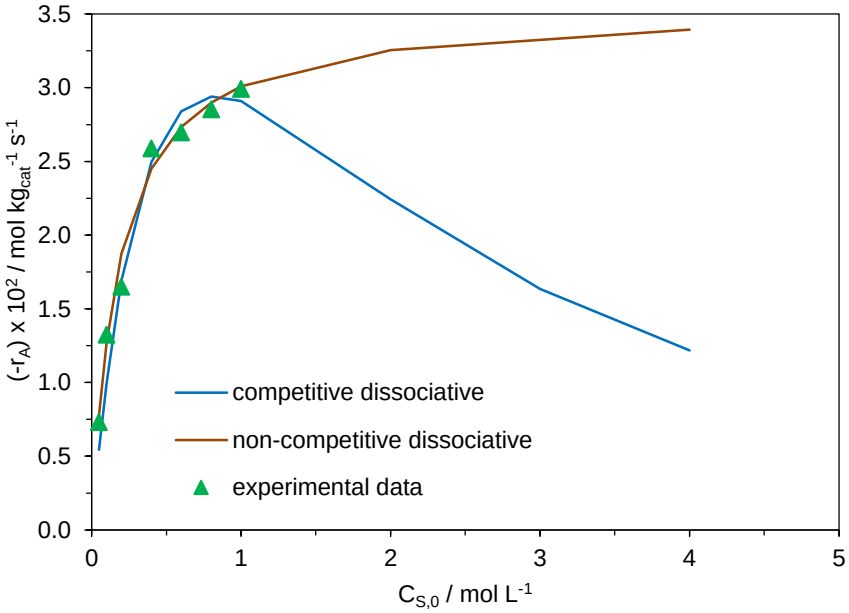

Figure 5.11. Fits of the competitive and non-competitive dissociative adsorption of hydrogen models. Experimental data obtained at 298K. Lines give the model prediction at higher reagent concentrations.

As can be seen from Figure 5.12, the competitive dissociative adsorption of hydrogen model represents the experimental data very well. The linearized version of the rate equation for competitive dissociative adsorption of hydrogen was used again to facilitate the data fitting procedure and to evaluate graphically the quality of the assumptions made. The fit was performed using a least square refinement routine programmed in Matlab. The estimated values of the reaction rate constant, k_R^*, adsorption equilibrium constant of imine (K_A) and adsorption equilibrium constant of hydrogen (K_B) for experiments performed at 298 and 323K using an extended range of experimental results obtained for higher initial reagent concentrations are presented in Table 5.4 and Table 5.5.

The estimated values for the adsorption equilibrium constant of hydrogen, K_B, were still obtained with a very large error, however (Table 5.4 and Table 5.5), which could be attributed to an insufficient amount of experimentally obtained data that could be used for fitting. According to the thermodynamic van't Hoff Law, the adsorption equilibrium constants should decrease with an increase in the reaction temperature. It can be seen from the data presented in Table 5.4 and Table 5.5, however, that the adsorption equilibrium constants increased with an increase in temperature, which

could indicate a possibility of endothermic chemisorption. The same behaviour was also observed by Roy *et al.* (2005) and Patil *et al.* (2007).

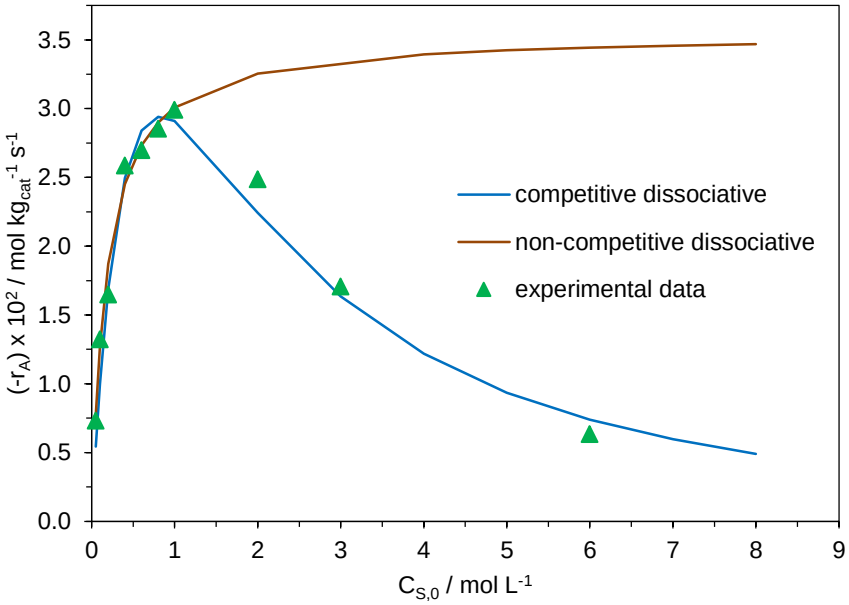

Figure 5.12. Fits of the competitive and non-competitive dissociative adsorption of hydrogen models. Experimental data obtained at 298K.

Table 5.4. Kinetic and adsorption parameters for reductive amination at 298K.

Mechanism	k_R^* *(mol kg_{cat}^{-1} s^{-1})*	K_A *(L mol^{-1})*	K_B *(bar^{-1})*
Competitive dissociative adsorption of H_2	0.39 ± 0.11	2.26 ± 0.86	0.98 ± 1.02

Table 5.5. Kinetic and adsorption parameters for reductive amination at 323K.

Mechanism	k_R^* *(mol kg_{cat}^{-1} s^{-1})*	K_A *(L mol^{-1})*	K_B *(bar^{-1})*
Competitive dissociative adsorption of H_2	0.52 ± 0.10	3.05 ± 1.30	3.02 ± 3.14

5.4. Conclusions

The kinetic study on the reductive amination of hydrocinnamaldehyde with α-methylbenzylamine over a Pd/C catalyst in the continuous flow system was demonstrated using the packed-bed structured compact multifunctional reactor.

It was possible to find operating conditions for which mass transport limitations could be eliminated, thereby ensuring that the reaction is in the reaction-limited regime. Performing the reaction in this regime is important for studying the reaction kinetics.

Apparent activation energy was determined to be 15 kJ mol^{-1}.

Calculation of the Weisz-Prater criterion excluded the possibility of the intra-particle diffusion limitation on the reaction, $C_{WP} << 1$.

The model of competitive dissociative adsorption of hydrogen was found to represent the mechanism of the reaction and to fit the experimental data very well. The estimated values of the reaction rate constant, k_R^*, adsorption equilibrium constant of imine (K_A) and adsorption equilibrium constant of hydrogen (K_B) for experiments performed at 298 and 323K are presented in Table 5.6.

Table 5.6. Kinetic and adsorption parameters for reductive amination at 298 and 323K.

T (K)	k_R^* (mol kg_{cat}^{-1} s^{-1})	K_A (L mol^{-1})	K_B (bar^{-1})
298	0.39 ± 0.11	2.26 ± 0.86	0.98 ± 1.02
323	0.52 ± 0.10	3.05 ± 1.30	3.02 ± 3.14

Chapter 6

Reaction kinetics for the deprotection of (1-phenylethyl)(3-phenylpropyl) amine over a palladium on carbon catalyst

6.1. Introduction

In multi-phase catalytic reactions it is important to analyse the impact of controlling regimes, since heterogeneous catalysis is always associated with the mass and heat transfer processes. In three-phase (gas-liquid-solid) catalytic reactions various mass transfer steps can be observed, *i.e.* gas-liquid, liquid-solid and intraparticle mass transfer resistances, in addition to the catalytic reaction.

Figure 6.1 shows concentration profiles of hydrogen in three-phase (gas-liquid-solid) catalytic reaction system for the deprotection of secondary amine (Mills and Chaudhari 1997):

1. transport of the gas phase reactant (H_2) from the gas phase to the bulk of the liquid phase;
2. transport of a gas phase and liquid reactants from the bulk of the liquid phase to the external catalyst surface;
3. intraparticle diffusion of gas and liquid reactants into the pores of the catalyst followed by a chemical reaction at the catalyst surface;

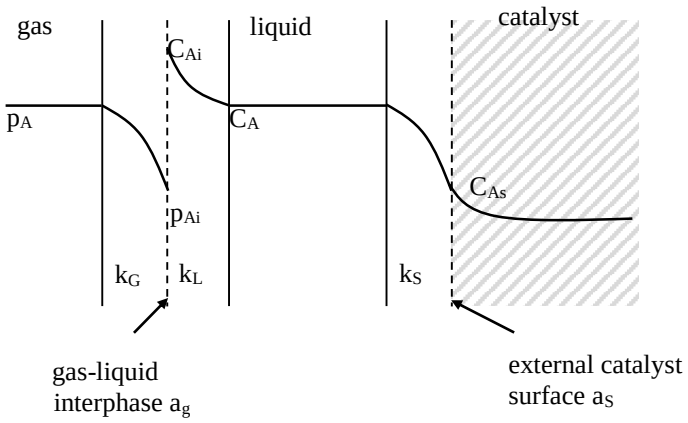

Figure 6.1. Schematic diagram of transport steps in multi-phase catalytic reactions (Hofmann 1978).

No data on kinetic studies of the deprotection of secondary amines have been reported in the literature to the best of the author's knowledge.

For the partial deprotection of (1-phenylethyl)(3-phenylpropyl)amine to 3-phenylpropan-1-amine) in a three phase heterogeneous system, the following sequence must occur:

1. Mass transfer of hydrogen from the bulk of the gas phase to the gas-liquid interface:

$$(-r_A) = k_{G,H_2} a_{G/L} \frac{1}{(1-e_b)\rho_c}\left(C_{H_2,b} - C_{H_2,i}\right) \qquad (6.1)$$

where:

$(-r_A)$ overall reaction rate (mol kg_{cat}^{-1} s^{-1});

k_{G/H_2} gas phase mass transfer coefficient (m s^{-1});

$a_{G/L}$ gas-liquid interfacial area/ volume of bed (m^2 m^{-3});

ρ_c density of catalyst pellet (kg m^{-3});

e_b bed porosity (-);

$C_{H_2,b}$ bulk gas-phase concentration of hydrogen (mol m^{-3});

$C_{H_2,i}$ interfacial concentration of hydrogen (mol m^{-3}).

Under the reaction conditions investigated in this study $p_{MeOH} > p_{H_2}$ due to methanol vaporization, so mass transfer resistance of hydrogen in the gas phase may exist.

2. Equilibrium at the gas-liquid interface (Henry's law):

$$p_{H_2} = Hx_{H_2} \qquad (6.2)$$

where:

p_{H_2} partial pressure of hydrogen (bar);

H Henry's constant of hydrogen in the reaction mixture (bar);

x_{H_2} mole fraction of the hydrogen in the liquid phase (-).

3. Mass transfer of hydrogen away from the gas-liquid interface:

$$(-r_A) = k_{L,G} \cdot a_{G/L} \frac{1}{(1 - e_b)\rho_c}(C_{H_2,i} - C_{H_2,b}) \qquad (6.3)$$

where:

$(-r_A)$ overall reaction rate (mol kg_{cat}^{-1} s^{-1});

$k_{L,G}$ gas-liquid mass transfer coefficient (m s^{-1});

$a_{G/L}$ gas-liquid interfacial area / volume of bed (m^2 m^{-3});

e_g bed porosity (-);

ρ_c density of catalyst pellet (kg m^{-3});

$C_{H_2,i}$ hydrogen concentration in liquid at interface (mol m^{-3});

4. Transport of the dissolved gaseous hydrogen through the bulk of the liquid to the external surface of a catalyst particle:

$$(-r_A) = k_{L/S,H_2} a_s (C_{H_2,b} - C_{H_2,s}) \qquad (6.4)$$

where:

$(-r_A)$ overall reaction rate (mol kg_{cat}^{-1} s^{-1});

k_{LH_2} liquid-solid mass transfer coefficient (m s^{-1});

a_s external specific area of pellet (m^2 kg_{cat}^{-1});

$C_{H_2,b}$ hydrogen concentration in the bulk liquid (mol m^{-3});

$C_{H_2,s}$ hydrogen concentration at the solid-liquid interface (mol m^{-3}).

5. Transport of the (1-phenylethyl)(3-phenylpropyl)amine through the bulk of the liquid to the surface of a catalyst particle:

$$(-r_A) = k_{L/S,2^o\ amine}\, a_S\, (C_{2^o\ amine,b} - C_{2^o\ amine,s}) \qquad (6.5)$$

where:

$(-r_A)$	overall reaction rate (mol kg_{cat}^{-1} s^{-1});
$k_{L/S,2^o\ amine}$	liquid-solid mass transfer coefficient (m s^{-1});
a_s	external specific area of pellet (m^2 kg_{cat}^{-1});
$C_{2^o\ amine,b}$	(1-phenylethyl)(3-phenylpropyl)amine concentration in the bulk liquid (mol m^{-3});
$C_{2^o\ amine,s}$	(1-phenylethyl)(3-phenylpropyl)amine concentration at the solid-liquid interface (mol m^{-3}).

6. Diffusion and reaction in the porous catalyst:

$$(-r_A) = \eta \cdot kC_{H_2,s}\, C_{2^o\ amine,s} \qquad (6.6)$$

where:

$(-r_A)$	overall reaction rate (mol kg_{cat}^{-1} s^{-1});
η	effectiveness factor (-);
k	specific reaction constant / m^3 of liquid (mol^{-1} $kg_{cat}^{-1}s^{-1}$);
$C_{H_2,s}$	surface concentration of hydrogen at solid-liquid interface (mol m^{-3});
$C_{2^o\ amine,s}$	surface concentration of (1-phenylethyl)(3-phenylpropyl)amine at the solid-liquid interface (mol m^{-3}).

This chapter reports kinetic experiments on the hydrogenolysis of (1-phenylethyl)(3-phenylpropyl)amine using a structured multichannel packed-bed reactor. Experiments were performed with a palladium catalyst supported on activated carbon and provided a better understanding of the effect of the key variables on the process. The work aimed at individuating the main factors that influence the reaction, *i.e.* liquid and gas flow rates, hydrogen partial pressures, temperatures and reactant concentrations. A possible reaction mechanism was proposed and the rate equations that describe the reactions involved in the process were developed and used to obtain the necessary kinetic parameters. The equations were used to fit the experimental data obtained using Matlab software. The experimental conditions tested were chosen so that the effect of all the main influencing parameters could be investigated and the validity of the assumptions made tested.

6.2. Experimental

6.2.1. Pd/C catalyst and reagents

The Pd/C catalyst (Pd 10% by weight) was prepared by impregnation of the mesoporous microspherical (125-250 μm) synthetic carbon support supplied by Mast Carbon Ltd., Guildford, UK.

The loading capacity of the reactor channel is *ca.* 0.45 g of catalyst. For kinetic studies the catalyst (total amount = 0.085 g) was diluted with the carbon support *ca.* five times.

All chemicals used in this study were purchased from Acros Organics, Sigma-Aldrich, Fluka or Lancaster and used without further purification

6.2.2. Analytical technique

During the kinetic experiments, samples of the liquid were taken via the 6-way valve and were analysed with a GC (Varian CP-3800). The GC was equipped with a CP Sil-8CB column.

6.2.3. Structured compact reactor and continuous catalytic rig

Details of the structured multichannel packed-bed reactor and of the continuous catalytic system used in these studies are presented in Chapter 2 section 2.2.2 and 2.2.3, respectively.

6.3. Results and discussion

6.3.1. Effect of external and internal mass transfer

In Chapter 5, the different regimes observed in heterogeneous catalysis were described, *i.e.* kinetic regime, the external and internal diffusion regimes and the transition regime (see Chapter 5, section 5.3.1). It was also mentioned previously that, in order to obtain reliable quantitative kinetic data, all transport limitations, *i.e.* gas-liquid, liquid-solid, must be understood and evaluated (Pakdehi *et al.* 2010).

6.3.1.1. Effect of liquid phase flow rate

In order to determine the significance of the external mass transfer resistances, the effect of the liquid flow rate on the rate of reaction was studied in the range of 0.2 - 1.5 mL min^{-1} at 393 K. The results presented in Figure 6.2 indicate that the rate of deprotection is independent of the liquid flow rate at $F_L \geq 0.5$ mL min^{-1} and is not controlled by the external mass transfer. These results may indicate that the data obtained within the range of 0.5 - 1.5 mL min^{-1} liquid flow rate reflect the kinetic control model with possible internal diffusion. The Reynolds liquid number was found to be 0.63 at a liquid flow rate of 0.5 mL min^{-1}.

Further experiments were, therefore, carried out at a liquid flow rate of 0.5 mL min^{-1} in order to neglect the mass transfer limitations.

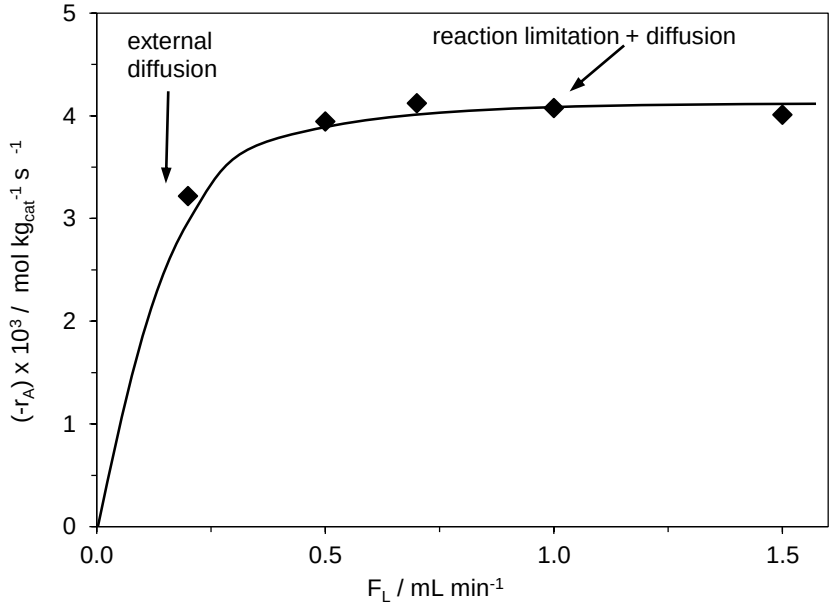

Figure 6.2. Influence of the liquid flow rate on the average rate of reaction.
P_{H_2} = 2 bar, F_G = 21.0 mL (STP) min^{-1}, $C_{S,0}$ = 0.2 mol L^{-1}, T = 393K.

The average reaction rate was calculated using Equation 5.7 (see Chapter 5) and the liquid Reynolds number was calculated based on Equation 5.10 (see Chapter 5).

6.3.1.2. Effect of gas phase flow rate

The effect of the hydrogen flow rate on the overall rate of reaction is presented in Figure 6.3. At low gas flow rates (F_G < 10 mL (STP) min^{-1}), the rate of reaction depends strongly on the hydrogen flow rate and is limited by its supply. Further increases in the gas flow rate, however (F_G > 10 mL (STP) min^{-1}), did not have a pronounced influence on the rate of the reaction. This could be explained by two effects:

1. a slight change in the gas-liquid interfacial areas;
2. a change in the liquid saturation of the catalytic channel (β_L).

These results may indicate that the data obtained for a hydrogen flow rate of F_G > 10 mL (STP) min^{-1} reflect kinetic control of the catalytic process.

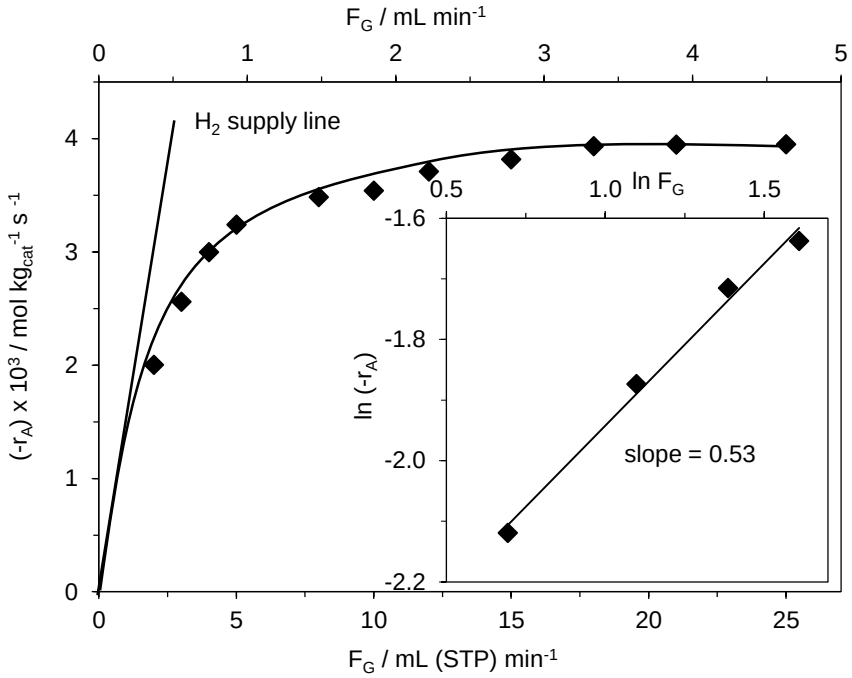

Figure 6.3. Influence of hydrogen flow rate on the average rate of reaction. P_{H_2} = 2 bar, F_L = 0.5 mL min^{-1}, $C_{S,0}$ = 0.2 mol L^{-1}, T = 393K.

The Reynolds number was calculated based on Equation 5.12 (see Chapter 5) and was found to be 0.03 at 21.0 mL (STP) min^{-1} of hydrogen flow rate.

6.3.1.3. Effect of internal diffusion

The Weisz-Prater criterion (Equation 5.14, see Chapter 5) was used to evaluate the importance of internal diffusion in the overall process. In this case, the threshold value is 1. If $C_{WP} \ll 1$ internal diffusion is considered negligible; if $C_{WP} \gg 1$ than the phenomenon should be further investigated and accounted for (Weisz and Prater 1954; Fogler 1999; Vannice and Joyce 2005).

Since an investigation of the catalyst porosity effects on the kinetics (influencing internal diffusion) was not possible, the influence of the phenomena was estimated by applying the Weisz-Prater criterion.

The diffusion coefficient (D_{AB}) was calculated based on Equation 5.14 (see Chapter 5) and was estimated to be $8.75 \cdot 10^{-5}$ cm^2 s^{-1}, whereas the effective diffusivity (D_e) calculated using Equation 5.15 (see Chapter 5) is equal to $1.21 \cdot 10^{-5}$ cm^2 s^{-1}. The Weisz-Prater criterion was found to be 0.02, which excluded the possibility of internal diffusion being a rate limiting step.

It could therefore be confirmed that the reaction in a compact packed-bed reactor is limited by the catalytic reaction itself.

6.3.2. Effect of hydrogen partial pressure

The effect of hydrogen pressure on the rate of product formation was investigated in a range of 1 - 4 bar of hydrogen partial pressure at 393K. The results presented in Figure 6.4 show that the overall rate of reaction is almost independent of the hydrogen partial pressure investigated. The methodology of the calculation of the partial pressure of hydrogen was shown in Chapter 5, section 5.3.3.

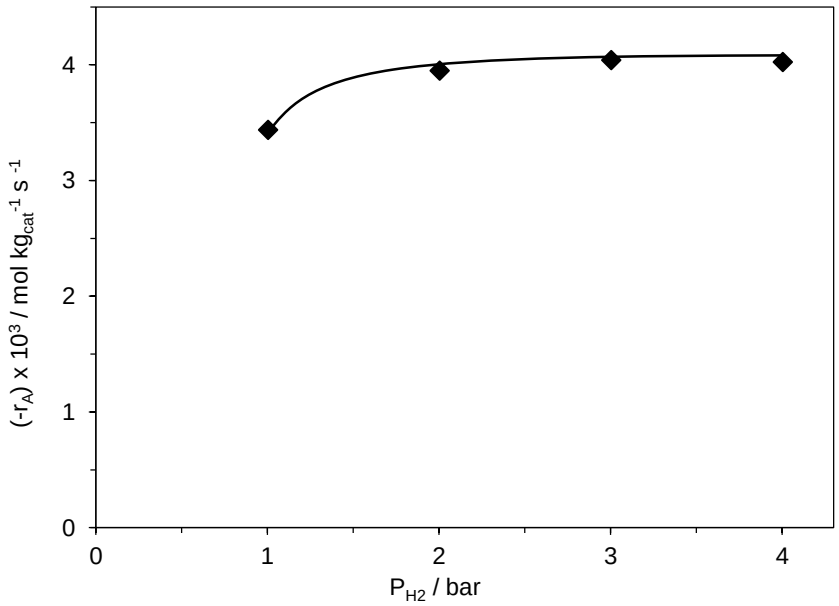

Figure 6.4. Influence of the hydrogen partial pressure on the overall reaction rate. F_G =21.0 mL (STP) min^{-1}, F_L = 0.5 mL min^{-1}, $C_{S,0}$ = 0.2 mol L^{-1}, T= 393K.

The average rate of the reaction is independent of hydrogen partial pressure (Figure 6.4), *i.e.* independent of the hydrogen concentration in the liquid phase. This means that the deprotection of (1-phenylethyl)(3-phenylpropyl)amine on a Pd/C catalyst was zero order with respect to hydrogen. Furthermore, it could be suggested that the reaction was in the kinetic regime, and was not affected by liquid phase mass transfer resistances (g/l and l/s). Figure 6.5 presents the influence of hydrogen partial pressure on the hydrogen solubility in the liquid phase at 393K. Increasing the hydrogen partial pressure from 1 to 4 bar increased the hydrogen concentration *ca.* 4 times.

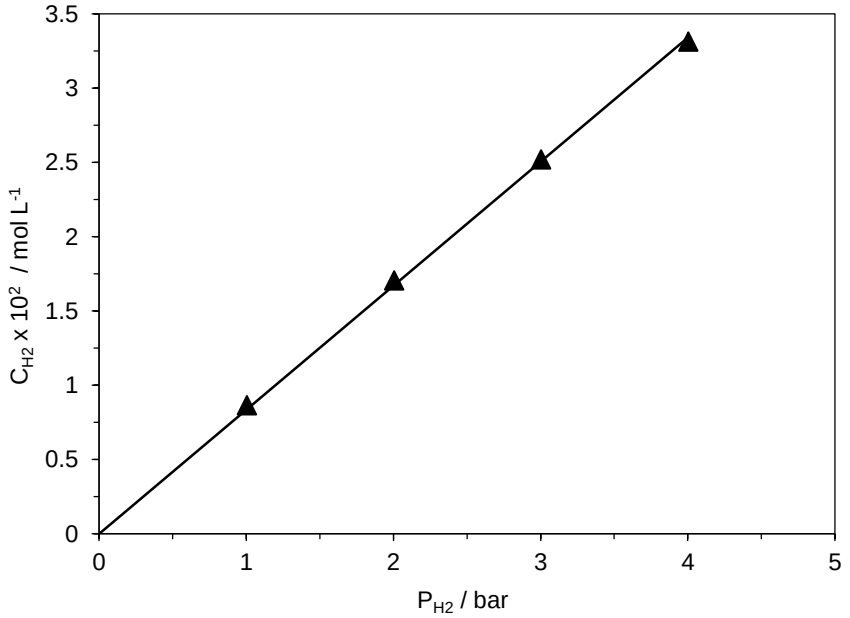

Figure 6.5. Hydrogen solubility in methanol at 393K.

6.3.3. Effect of reagent concentration

The influence of initial concentration of the secondary amine on the rate of product formation is presented in Figure 6.6. An increase of the substrate concentration increased the rate of the reaction up to $C_{S,0}$ = 0.4 mol L^{-1}; for higher concentrations the rate of reaction was concentration independent. The asymptotic approach at higher concentrations implies a Langmuir-Hinshelwood type of secondary amine deprotection catalytic mechanism.

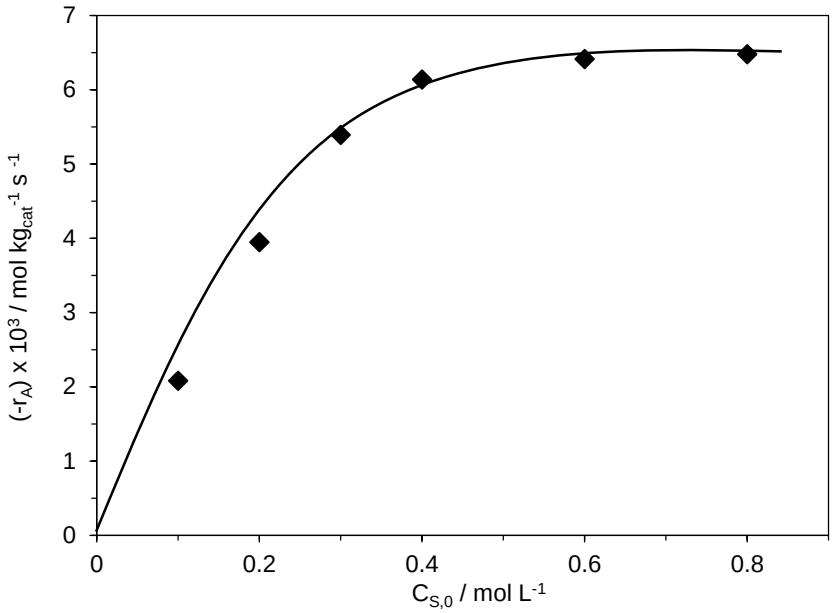

Figure 6.6. Influence of the initial concentration of (1-phenylethyl)(3-phenylpropyl) amine on the average rate of reaction. P_{H_2} = 2 bar, F_G = 21.0 mL (STP) min^{-1}, F_L = 0.5 mL min^{-1}, T = 393K.

6.3.4. Effect of reaction temperature

The hydrogenolysis of (1-phenylethyl)(3-phenylpropyl)amine (Scheme 6.1) is an exothermic reaction with the standard reaction enthalpy of - 86 kJ mol^{-1} (thermodynamic properties of compounds involved in the reaction were obtained from ChemBioDraw Ultra 12.0).

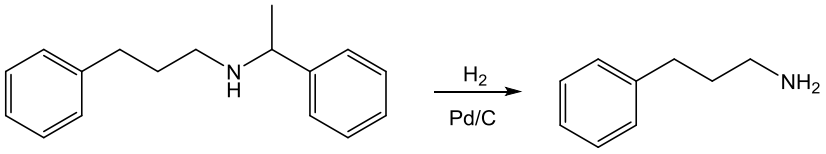

$\Delta H_{R,0}$ = - 86 kJ mol^{-1}

Scheme 6.1. Deprotection of (1-phenylethyl)(3-phenylpropyl)amine.

The effect of reaction temperature was studied for the conditions in which the reaction is in the kinetic regime, *i.e.*, P_{H_2} = 2 bar, F_G = 21.0 mL (STP) min^{-1}, F_L = 0.5 mL min^{-1}. The overall reaction rate strongly depends on the temperature (Figure 6.7). An increase in the reaction temperature resulted in a higher reaction rate but had no influence on the selectivity.

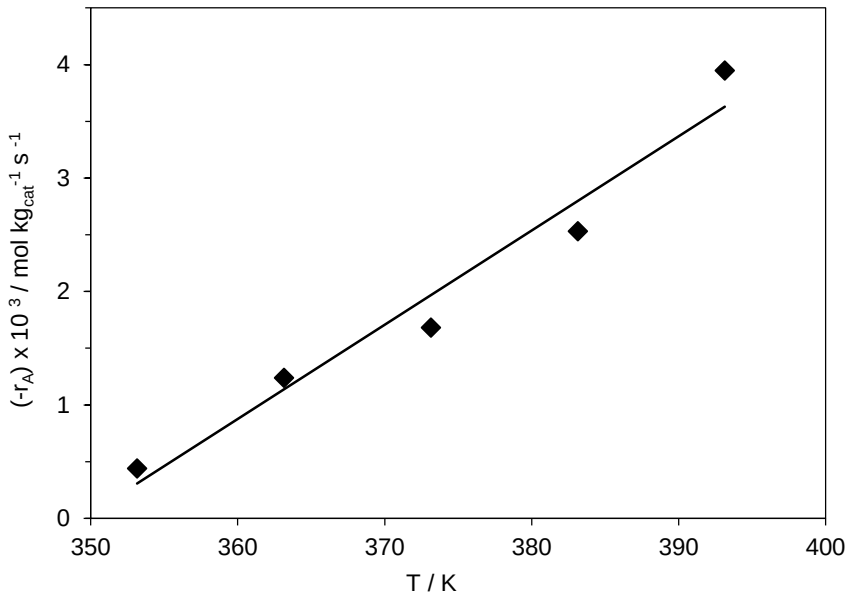

Figure 6.7. Influence of the reaction temperature on the overall rate of reaction. F_G = 21.0 mL (STP) min^{-1}, F_L = 0.5 mL min^{-1}, $C_{S,0}$ = 0.2 mol L^{-1}.

The corresponding Arrhenius plot (Figure 6.8) from the experiments performed at a liquid flow rate of 0.5 mL min^{-1} allowed the determination of the value of apparent activation energy as 80 kJ mol^{-1}. This suggests that the overall rate of reaction may be limited by the surface reaction step, since mass transfer processes are usually less dependent on temperature than chemical reactions.

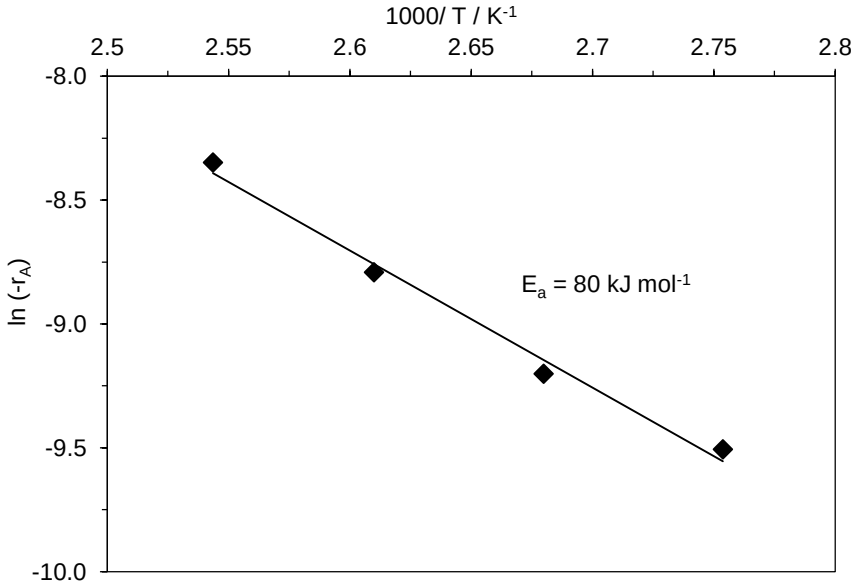

Figure 6.8. Arrhenius plot for apparent activation energy.

It is worth noting that the apparent activation energy determined from the experimental results, includes the temperature dependence of following processes: (*i*) surface reaction itself (Arrhenius Law), (*ii*) adsorption equilibrium (van't Hoff's Law), and (*iii*) the change of the hydrogen solubility with the temperature (Henry's Law). The latter depends also on the change of the methanol saturation vapour pressure with temperature (Antoine Equation).

An increase in the reaction temperature affects the partial pressure and solubility of hydrogen in methanol (Figure 6.9). The hydrogen concentration decreased with an increase in the reaction temperature resulting from a decrease in the hydrogen partial pressure in the reactor due to the vaporization of methanol.This indicates that the reaction is in the kinetic regime and the rate of the hydrogenolysis of secondary amines depends on the temperature.

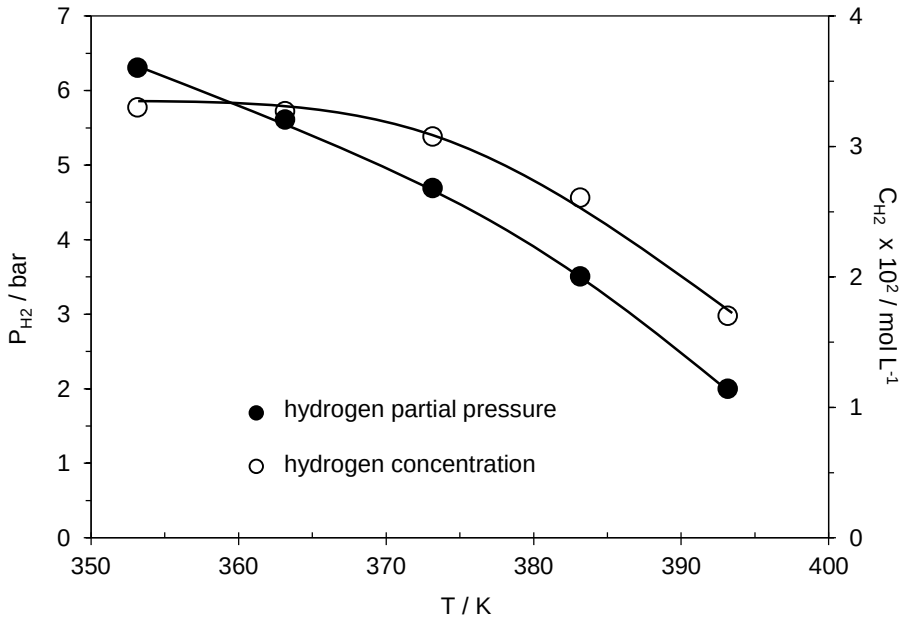

Figure 6.9. Hydrogen solubility in methanol and partial pressure at different temperatures.

6.3.5. Kinetic model and reaction mechanism

As presented in Chapter 5 (see section 5.3.5), in the literature the Langmuir-Hinshelwood approach is widely used to describe the kinetic models for hydrogenation reactions. This approach assumes that the adsorption of organic and hydrogen molecules at the surface of catalyst is in an equilibrium. Competitive or non-competitive adsorption of both reactants is also considered in the literature. The non-competitive approach assumes that the differences in sizes of hydrogen and other reacting species is sufficiently large for hydrogen to be able to adsorb in voids on the surface between bulky organic molecules (Simakova *et al.* 2009).

Based on the obtained results, Langmuir-Hinshelwood models were developed for competitive and non-competitive adsorption of organic and hydrogen molecules, assuming molecular and dissociative adsorption of hydrogen. The following assumptions were made, however:

- only one reaction mechanism is acting over the whole range of conditions used;
- the adsorption of gaseous reactant can either be dissociative or non-dissociative;
- the liquid phase is saturated with the gas phase;
- product adsorption and desorption are reversible equilibrium steps;
- the adsorption of the reaction solvent (MeOH) is considered to be negligible;
- adsorption of the reaction product is considered to be negligible.

In Chapter 5, section 5.3.5, rate equations were developed for competitive and non-competitive molecular adsorption of hydrogen, as well as for competitive and non-competitive dissociative adsorption of hydrogen. The following equations were obtained:

- competitive molecular adsorption of hydrogen:

$$r_R = (-r_A) = \frac{k_R^* K_{A,A} K_{A,B} C_A p_B}{\left(1 + K_{A,A} C_A + K_{A,B} p_B\right)^2} \qquad (6.7)$$

where: $k_R^* = k_R C_T^2$

- non-competitive molecular adsorption of hydrogen:

$$r_R = (-r_A) = \frac{k_R^* K_{A,A} C_A K_{A,B} p_B}{\left(1 + K_{A,A} C_A\right)\left(1 + K_{A,B} p_B\right)} \qquad (6.8)$$

where: $k_R^* = k_R C_T C_{T^*}$

- competitive dissociative adsorption of hydrogen:

$$r_R = (-r_A) = \frac{k_R^* K_{A,A} C_A K_{A,B} p_B}{\left(1 + K_{A,A} C_A + \sqrt{K_{A,B} p_B}\right)^3} \qquad (6.9)$$

where: $k_R^* = k_R C_T^3$

- non-competitive dissociative adsorption of hydrogen:

$$r_R = (-r_A) = \frac{k_R^* K_{A,A} C_A K_{A,B} p_B}{\left(1 + K_{A,A} C_A\right)\left(1 + \sqrt{K_{A,B} p_B}\right)^2} \qquad (6.10)$$

where: $k_R^* = k_R C_T C_{T^*}^2$

All four final rate equations (6.7, 6.8, 6.9 and 6.10) for the hydrogenation step were linearized to facilitate the data fitting procedure to evaluate graphically the quality of the assumptions made so far (Table 6.1).

The fit was performed using a least square refinement routine programmed in Matlab. The values of R^2 obtained for the experiments performed at 393K are presented in (Table 6.1).

Two models, *i.e.* competitive and non-competitive molecular adsorption of hydrogen, were excluded from further consideration since they had the lowest R^2, very high error and multicollinearity of estimated values.

The models of competitive and non-competitive dissociative adsorption of hydrogen had the highest R^2 and showed no problem with correlation or multicollinearity of the estimated values, with a 95 % Confidence Interval (CI).

The estimated values of the reaction rate constant, $\left(k_R^*\right)$, adsorption equilibrium constant of secondary amine (K_A) and adsorption equilibrium constant of hydrogen (K_B) for experiments performed at 393K are presented in Table 6.2.

Table 6.1. Various models for the hydrogenolysis of secondary (1-phenylethyl)(3-phenylpropyl)amine over 10% Pd/C catalyst at 393K.

Mechanism	Rate equation	Linearized rate equation	R^2
Competitive molecular adsorption of H_2	$r_R = (-r_A) = \frac{k_R^* K_A C_A K_B p_B}{(1 + K_A C_A + K_B p_B)^2}$	$\sqrt{\frac{C_A p_B}{(-r_A)}} = \frac{1}{\sqrt{k_R^* K_A K_B}} + \frac{K_A}{\sqrt{k_R^* K_A K_B}} \cdot C_A + \frac{K_B}{\sqrt{k_R^* K_A K_B}} \cdot p_B$	0.9740
Non-competitive molecular adsorption of H_2	$r_R = (-r_A) = \frac{k_R^* K_A C_A K_B p_B}{(1 + K_A C_A)(1 + K_B p_B)}$	$\frac{C_A p_B}{(-r_A)} = \frac{1}{k_R^* K_A K_B} + \frac{p_B}{k_R^* K_A} + \frac{C_A}{k_R^* K_B} + \frac{C_A p_B}{k_R^*}$	0.9670
Competitive dissociative adsorption of H_2	$r_R = (-r_A) = \frac{k_R^* K_A C_A K_B p_B}{(1 + K_A C_A + \sqrt{K_B p_B})^3}$	$\sqrt[3]{\frac{C_A p_B}{(-r_A)}} = \frac{1}{\sqrt[3]{k_R^* K_A K_B}} + \frac{K_A}{\sqrt[3]{k_R^* K_A K_B}} \cdot C_A + \frac{\sqrt{K_B}}{\sqrt[3]{k_R^* K_A K_B}} \cdot \sqrt{p_B}$	0.9994
Non-competitive dissociative adsorption of H_2	$r_R = (-r_A) = \frac{k_R^* K_A C_A K_B p_B}{(1 + K_A C_A)(1 + \sqrt{K_B p_B})^2}$	$\frac{C_A p_B}{(-r_A)} = \frac{(1 + K_A C_A)(1 + \sqrt{K_B p_B})^2}{k_R^* K_A K_B}$	0.9979

Table 6.2. Kinetic and adsorption parameters for hydrogenolysis of (1-phenylethyl)(3-phenylpropyl)amine at 393K.

Mechanism	k_R^* ***(mol kg_{cat}^{-1} s^{-1})***	K_A ***(L mol^{-1})***	K_B ***(bar $^{-1}$)***
Competitive dissociative adsorption of H_2	0.15 ± 0.02	1.08 ± 0.18	1.59 ± 0.28
Non-competitive dissociative adsorption of H_2	0.02 ± 0.01	1.23 ± 0.40	56.15 ± 79.84

Some of the estimated values, *(K_B)*, have been obtained with very large errors; however (Table 6.2), which could be attributed to an insufficient amount of experimentally obtained data being available for fitting. It was also impossible to distinguish which of the two mechanisms describe the obtained results better. In order to distinguish between competitive and non-competitive dissociative adsorption of hydrogen, as well as improve the estimated reaction parameters further studies are therefore required. Figure 6.10 and Figure 6.11 present the overall rate of reaction calculated based on Equations 6.9 and 6.10, with estimated values of k_R^*, K_A and K_B. It can be seen that even though some of the estimated parameters were obtained with large errors they nonetheless proved to be a good fit for the experimental data (Figure 6.10 and Figure 6.11). The lines on both graphs (Figure 6.10 and Figure 6.11) show how these two models would behave at higher hydrogen partial pressures and initial substrate concentrations. It can be seen from Figure 6.10 that, in order to distinguish between the competitive and non-competitive dissociative adsorption of hydrogen models, the hydrogen partial pressure investigated would have to be *ca.* 20 - 100 bar. For Health and Safety reasons these experiments could not be done with the equipment available. Experiments with higher initial reactant concentrations (Figure 6.12) were, therefore, performed in order to distinguish between the competitive and non-competitive dissociative adsorption of hydrogen models.

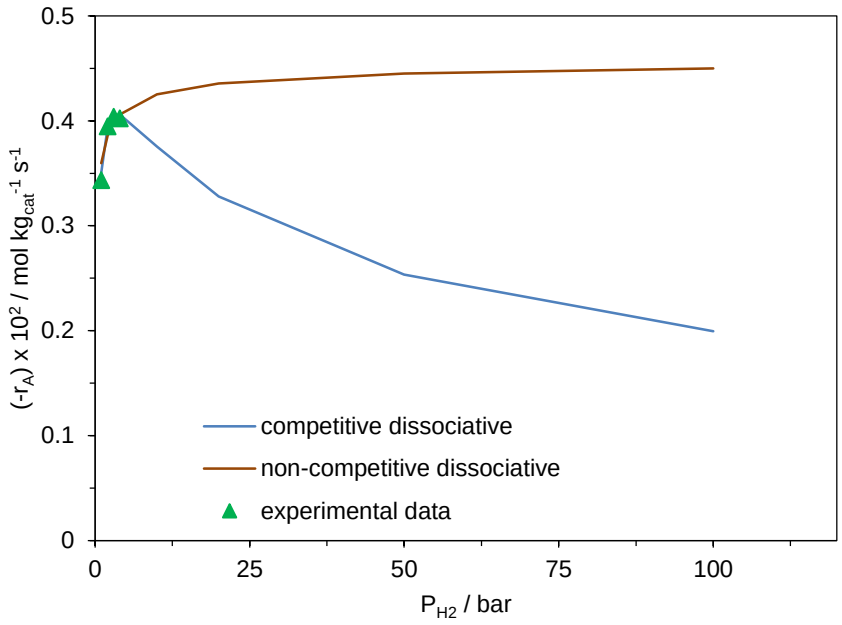

Figure 6.10. Fits of the competitive and non-competitive dissociative adsorption of hydrogen models. Experimental data obtained at 393K. Lines give the model prediction at higher hydrogen partial pressure.

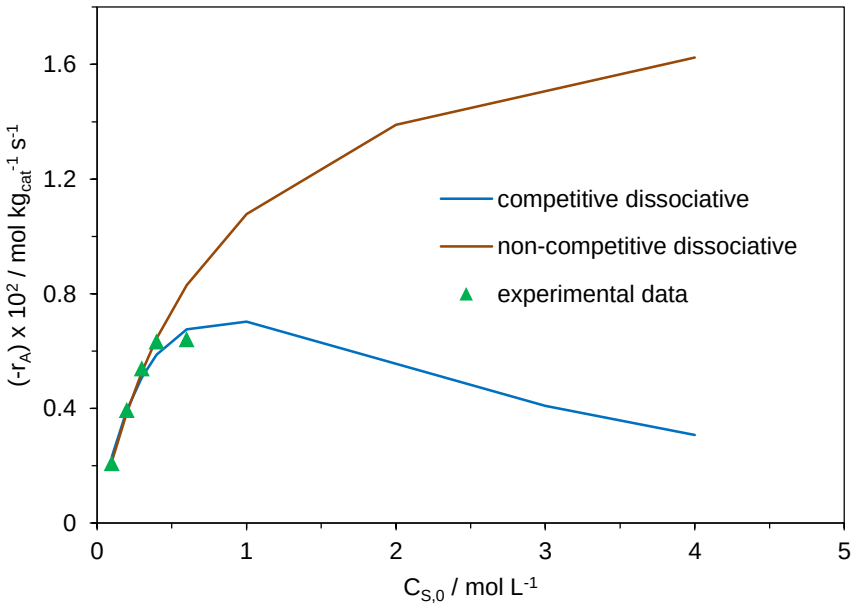

Figure 6.11. Fits of the competitive and non-competitive dissociative adsorption of hydrogen models. Experimental data obtained at 393K. Lines give the model prediction at higher reagent concentration.

As can be seen from Figure 6.12, the competitive dissociative adsorption of hydrogen model represents the experimental data very well. The linearized version of the rate equation for competitive dissociative adsorption of hydrogen was also used to

facilitate the data fitting procedure and to evaluate graphically the quality of the assumptions made. The fit was performed using a least square refinement routine programmed in Matlab. The estimated values of the reaction rate constant (k_R^*) adsorption equilibrium constant of secondary amine (K_A) and adsorption equilibrium constant of hydrogen (K_B) for experiments performed at 393K using an extended range of experimental results obtained for higher initial reagent concentrations are presented in Table 6.3. The estimated values for the adsorption equilibrium constant of hydrogen, K_B, however, was still obtained with very large errors, which could be attributed to an insufficient amount of experimentally obtained data being available for fitting.

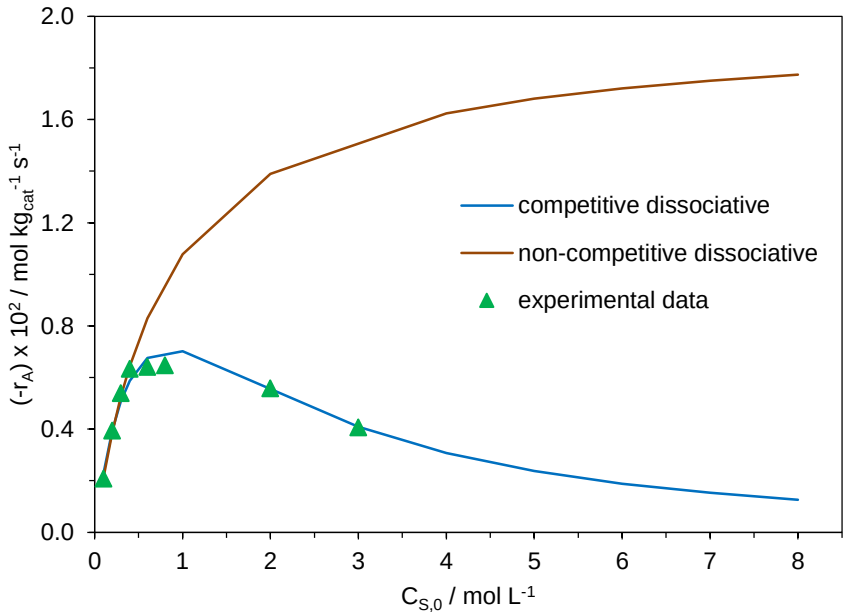

Figure 6.12. Fits of the competitive and non-competitive dissociative adsorption of hydrogen models. Experimental data obtained at 393K.

Table 6.3. Kinetic and adsorption parameters for reductive amination at 393K.

Mechanism	k_R^* **(mol kg$_{cat}^{-1}$ s^{-1})**	K_A **(L mol^{-1})**	K_B **(bar^{-1})**
Competitive dissociative adsorption of H_2	0.11 ± 0.02	1.70 ± 0.39	1.96 ± 1.29

6.4. Conclusions

The kinetic study on the deprotection of secondary amine over a Pd/C catalyst in the continuous flow system was demonstrated using the structured compact packed-bed reactor.

It was possible to neglect the mass transport limitations and to ensure the reaction remained within the reaction-limited regime. Performing the reaction in this regime is important for studying the reaction kinetics.

Apparent activation energy was determined to be 80 kJ mol^{-1}.

Calculation of the Weisz-Prater criterion excluded the possibility of the intra-particle diffusion limitation of the reaction, $C_{WP} << 1$.

The model of competitive molecular adsorption of hydrogen was found to represent the mechanism of the reaction and fitted the experimental data very well. The estimated values of the reaction rate constant $\left(k_R^*\right)$, adsorption equilibrium constant of secondary amine *(K_A)* and adsorption equilibrium constant of hydrogen *(K_B)* for experiments performed at 393K are presented in Table 6.4.

Table 6.4. Kinetic and adsorption parameters for hydrogenolysis reaction at 393K.

k_R^* *(mol kg_{cat}^{-1} s^{-1})*	K_A *(L mol^{-1})*	K_B *(bar $^{-1}$)*
0.11 ± 0.02	1.70 ± 0.39	1.96 ± 1.29

Chapter 7

Final conclusions and recommendations for further work

7.1. Conclusions

In this work, a structured compact multifunctional reactor with mm-scale packed-bed reaction channels and a commercially available X-Cube™ flow reactor developed by ThalesNano were presented, and their application for the synthesis of primary amines in continuous-flow tandem process was studied.

It has been shown that a variety of primary amines can be synthesised under continuous flow reaction conditions *via* a tandem reductive amination of aldehydes - hydrogenolysis of secondary amine process.

Primary amines were synthesised using the tandem reductive amination - deprotection process in the multichannel packed-bed reactor and X-Cube™ flow reactor with very high conversion, selectivity and isolated as HCl salts with a yield ranging from 74 to 99%. Comparison of the results obtained from both reactors showed that the packed-bed multichannel reactor was more efficient than the commercially available X-Cube™ flow reactor. In this work, two consecutive structured multichannel reactors, or two CatCarts at different temperatures, were used to ensure high selectivity towards the desired product. The desired primary amines were obtained with high selectivity and conversion and a yield of product of *ca.* 0.0024 mol h^{-1} was achieved in both reactors under optimal reaction conditions (Table 7.1). The X-Cube™ flow reactor, however, required higher pressures and temperatures *i.e.* 30 bar and 298/ 403K (1^{st}/ 2^{nd} CatCart) while the mutichannel packed-bed reactor was operated at 8 bar and 298/ 393K (1^{st}/ 2^{nd} reactor). In the case of multichannel packed-bed reactor, however, the split injection of hydrogen along the length of the reaction channels proved to be beneficial, and increased the reactor's efficiency. Furthermore, compared with the conventional "one-pot" synthesis in a batch reactor (which takes several hours to attain a similar yield), the compact reactor promoted a more intensified reductive amination of aldehydes and deprotection of secondary amines, *i.e.* the target product was synthesised in both reactors with a residence time of just minutes. The tandem synthesis under continuous flow conditions demonstrated here showed that both reactors might be a suitable alternative to conventional batch reactors for laboratory-scale multi-step synthesis.

Table 7.1. Optimal reaction conditions for the tandem reductive amination-hydrogenolysis reaction for both reactors.

	PBR	**X-Cube™**
P_T (bar)	8	30
T_1/ T_2 (K)	298/ 393	298/ 403
F_L (mL min^{-1})	0.2	0.2
F_G (mL min^{-1})	21.0	-
$C_{S,0}$ (mol L^{-1})	0.2	0.2
m_{cat} (g)	0.45	0.45
Productivity (mol h^{-1})	0.0024	0.0024

Reductive amination of aldehydes and deprotection of secondary amines, which are regarded as an important class of reactions due to their various applications in the synthesis of fine chemicals and pharmaceuticals, were used as model reactions in this study for evaluating the performance of both reactors.

The reductive amination of hydrocinnamaldehyde with α-methylbenzylamine was demonstrated by using a stuctured compact reactor and a commercially available X-Cube™ flow reactor. A variety of secondary amines, which are either commercially unavailable or very expensive compounds, were synthesised with high yield in a continuous process. Comparison of the results obtained from both reactors showed that the packed-bed multichannel reactor was more efficient than the X-Cube™ . 0.012 mol h^{-1} of product can be obtained in a single pass through the reaction channel (3×3×100 mm) using the continuous catalytic rig while the X-Cube™ flow reactor can only produce 0.006 mol h^{-1} using a single CatCart (70×4 mm) under optimal reaction conditions (Table 7.2).

Table 7.2. Optimal reaction conditions for reaductive amination of aldehydes reaction for both reactors at 298 K.

	PBR	**X-Cube™**
P_T (bar)	8	30
T (K)	298	298
F_L (mL min^{-1})	0.5	0.5
F_G (mL min^{-1})	21.0	-
$C_{S,0}$ (mol L^{-1})	0.4	0.2
m_{cat} (g)	0.45	0.45
Productivity (mol h^{-1})	0.012	0.006

For the model reaction, it was also shown that the productivity of each reactor can be increased by increasing the reaction temperature (Table 7.3). At 323K the productivity increased up to 0.048 mol h^{-1} and 0.012 mol h^{-1} for the multichannel packed-bed reactor and X-Cube™ reactor, respectively. At higher temperatures ($T \geq 363K$) the selectivity of the reaction decreased, giving a mixture of primary, secondary and tertiary amines, indicating that for the chosen reaction condition, the temperature of 333K was optimal to perform the reaction with 100% selectivity. In the case of the multichannel packed-bed reactor, split injection of hydrogen along the length of the reaction channels proved to be beneficial and increased the efficiency of the reactor.

Table 7.3. Optimal reaction conditions for reaductive amination of aldehydes reaction for both reactors at higher temperature.

	PBR	**X-Cube™**
P_T (bar)	8	30
T (K)	323	343
F_L (mL min^{-1})	2.0	0.5
F_G (mL min^{-1})	21.0	-
$C_{S,0}$ (mol L^{-1})	0.4	0.4
m_{cat} (g)	0.45	0.45
Productivity (mol h^{-1})	0.048	0.012

The deprotection of (1-phenylethyl)(3-phenylpropyl)amine was demonstrated using the same two types of reactor. This secondary amine was synthesised *via* reductive amination of hydrocynnamaldehyde (see Chapter 2). Comparison of the results obtained from both reactors showed that the packed-bed multichannel reactor was again more efficient than the X-Cube™ . 0.0024 mol h^{-1} of product could be obtained in a single pass through the reaction channel (3×3×100 mm) using the continuous catalytic rig, while the X - Cube™ flow reactor could only produce 0.0012 mol h^{-1} using a single CatCart (70×4 mm) under optimal reaction conditions (Table 7.4). The results obtained using the X-Cube™ flow reactor showed that the mass transfer is very slow and the rate of product formation decreased with an increase in the liquid flow rate. The results obtained also showed that the desired product (primary amine) can undergo an unwanted deamination reaction under certain reaction conditions (low flow rates of gas and liquid phases, high temperature), indicating that the temperature of the reaction is crucial.

Table 7.4. Optimal reaction conditions for the hydrogenolysis reaction for both reactors.

	PBR	**X-Cube™**
P_T (bar)	8	30
T (K)	393	413
F_L (mL min^{-1})	0.2	0.2
F_G (mL min^{-1})	21.0	-
$C_{S,0}$ (mol L^{-1})	0.2	0.1
m_{cat} (g)	0.45	0.45
Productivity (mol h^{-1})	0.0024	0.0012

Preliminary kinetic studies on the reductive amination of aldehydes using multichannel packed-bed reactor were presented. The reductive amination of hydrocinnamaldehyde with α-methylbenzylamine over a Pd/C catalyst was chosen as a model reaction. It was possible to find operating conditions for which mass transport limitations could be eliminated, thereby ensuring the reaction remained in the kinetic (reaction-limited) regime. Performing the reaction in this regime was important for studying the reaction kinetics. The calculation of the Weisz-Prater criterion excluded the possibility of the intra-particle diffusion limitation on the reaction, $C_{WP} << 1$. The apparent activation energy was determined to be 15 kJ mol^{-1}. Based on the obtained results, kinetic models based on the Langmuir-Hinshelwood approach were proposed. The model of competitive dissociative adsorption of hydrogen, resulting with following rate expression:

$$r_R = (-r_A) = \frac{k_R^* K_{A,A} C_A K_{A,B} p_B}{\left(1 + K_{A,A} C_A + \sqrt{K_{A,B} p_B}\right)^3} \qquad (7.1)$$

where: $k_R^* = k_R C_T^3$

was found to represent the mechanism of the reaction and fitted the experimental data very well. The estimated values of the reaction rate constant (k_R^*), adsorption equilibrium constant of imine (K_A) and adsorption equilibrium constant of hydrogen (K_B) for experiments performed at 298 and 323K are presented in Table 7.5.

Table 7.5. Kinetic and adsorption parameters for reductive amination at 298 and 323K.

T (K)	k_R^* (mol kg_{cat}^{-1} s^{-1})	K_A (L mol^{-1})	K_B (bar^{-1})
298	0.39 ± 0.11	2.26 ± 0.86	0.98 ± 1.02
323	0.52 ± 0.10	3.05 ± 1.30	3.02 ± 3.14

Kinetic studies were also performed for the hydrogenolysis of secondary amines, *i.e.* hydrogenolysis of (1-phenylethyl)(3-phenylpropyl)amine as a model reaction using a multichannel packed-bed reactor. It was possible to neglect the mass transport limitations and to ensure that the reaction remained in the reaction-limited regime. Calculation of the Weisz-Prater criterion excluded the possibility of the intra-particle diffusion limitation of the reaction, $C_{WP} << 1$. Apparent activation energy was determined to be 80 kJ mol^{-1}. From the obtained results kinetic models based on Langmuir-Hinshelwood approach were proposed. The model of competitive dissociative adsorption of hydrogen was found to represent the mechanism of the reaction and fitted the experimental data very well. The resulting rate expression is given below:

$$r_R = (-r_A) = \frac{k_R^* K_{A,A} C_A K_{A,B} p_B}{\left(1 + K_{A,A} C_A + \sqrt{K_{A,B} p_B}\right)^3} \qquad (7.2)$$

where: $k_R^* = k_R C_T^3$

The estimated values of the reaction rate constant (k_R^*), adsorption equilibrium constant of secondary amine (K_A) and adsorption equilibrium constant of hydrogen (K_B) for experiments performed at 393K are presented in Table 7.6.

Table 7.6. Kinetic and adsorption parameters for hydrogenolysis reaction at 393K.

k_R^* (mol kg_{cat}^{-1} s^{-1})	K_A (L mol^{-1})	K_B (bar^{-1})
0.11 ± 0.02	1.70 ± 0.39	1.96 ± 1.29

7.2. Recommendations for further work

The results of this investigation have shown that further research within this area is still required in order to optimise the continuous-flow reactor technology and extend its applicability for different processes.

The structured compact reactor and X-Cube™ flow reactor showed how efficient it is to transfer some conventional heterogeneous catalytic processes to a continuous flow approach. When considering the multi-phase systems in micro and compact reactors, a full understanding of the hydrodynamics of individual phases and the interfacial transport phenomena in the microreaction system is necessary to further optimise the present design or to develop new types of micro and compact reactors. Subsequently, further experimental work, together with mathematical modelling (*e.g.* Computational Fluid Dynamics (CFD) studies) on these two aspects, is recommended.

In Chapters 2, 3 and 4, where the reductive amination of aldehydes, hydrogenolysis of secondary amines and tandem process were investigated from the optimisation point of view, further studies are required, especially where ketones are to be used as a starting material. In the case of the reductive amination of ketones, a lower conversion

and product yield were achieved. This can be attributed to the reactivity of carbonyl compounds which follows the order aldehyde > cyclic ketones > acyclic ketones. Reductive amination of ketones can require harsher reaction conditions due to their lower reactivity in comparison with aldehydes. The reaction may require a longer reaction time or more than one cycle of the process for adequate results. Further studies are required for the reductive amination of ketones in order to increase the conversion and product yield. At this point, longer residence time may be suggested rather than a temperature increase since this may lead to a mixture of products. It is very likely that once the reductive amination of ketones is optimised, the second step of the tandem process (deprotection of secondary amines) will give the desired primary amine with high conversion, selectivity and isolated yield.

The hydrogenolysis of the secondary amine reaction presented in Chapter 3 also requires more attention. It has been shown that, under certain reaction conditions, the desired product (primary amine) can undergo an unwanted deamination reaction resulting in a lower yield of the desired product. Detailed studies on the hydrogenation of 3-phenylpropan-1-amine are required to fully understand and eliminate the deamination step. In the investigation described here, a high vapour pressure of methanol was achieved in the reaction channel. From the research point of view it would be interesting to investigate the reaction under conditions where the solvent (MeOH) is mostly in the liquid phase; meaning that at the temperature investigated, *i.e.* 393K the total pressure of the system should be kept at 15 bar. Further, in order to investigate lower partial pressures of hydrogen a mixture of hydrogen and nitrogen would be required to keep the methanol in a liquid phase.

Both reactions, the reductive amination of aldehydes and hydrogenolysis of secondary amines, require more detailed kinetic studies as only preliminary experiments were performed and results were presented in Chapter 5 and 6. Fuller explanation of reaction mechanisms as well as the influence of different parameters would require rigorous mathematical modelling of each process. The apparent activation energies were determined, however further studies are required to determine how the reaction rate constant and equilibrium constants are affected by the changes in temperatures.

The deprotection of the secondary amine reaction could also be performed under higher total pressures to prevent the vaporization of methanol. Since under the reaction conditions described in Chapter 6, the vapour pressure of methanol is much higher than the partial pressure of hydrogen, it would be also interesting to investigate the hydrogenolysis reaction under solvent-less reaction conditions.

Further, studies using different Pd content, as well as various catalyst sizes, could additionally confirm the absence of the intra-particle diffusion limitation on the reactions performed.

References

Abdel-Magid, A.F., Carson, K.G., Harris, B.D., Maryanoff, C.A. & Shah, R.D., 1996. Reductive Amination of Aldehydes and Ketones with Sodium Triacetoxyborohydride. Studies on Direct and Indirect Reductive Amination Procedures1. *The Journal of Organic Chemistry,* 61(11), pp. 3849-3862.

Abdel-Magid, A.F. & Mehrman, S.J., 2006. A review on the use of sodium triacetoxyborohydride in the reductive amination of ketones and aldehydes. *Organic Process Research & Development,* 10(5), pp. 971-1031.

Acke, D.R.J., Orru, R.V.A. & Stevens, C.V., 2006. Continuous Synthesis of Tri and Tetrasubstituted Imidazoles *via* a Multicomponent Reaction under Microreactor Conditions. *QSAR & Combinatorial Science,* 25(5 6), pp. 474-483.

Adam, W. & Prein, M., 1996. P-Facial Diastereoselectivity in the [4+ 2] Cycloaddition of Singlet Oxygen as a Mechanistic Probe. *Accounts of Chemical Research,* 29(6), pp. 275-283.

Adamschik, M., Hinz, M., Maier, C., Schmid, P., Seliger, H., Hofer, E.P. & Kohn, E., 2001. Diamond micro system for bio-chemistry. *Diamond and Related Materials,* 10(3–7), pp. 722-730.

Ajmera, S.K., Losey, M.W., Jensen, K.F. & Schmidt, M.A., 2001. Microfabricated packed-bed reactor for phosgene synthesis. *American Institute of Chemical Engineers Journal,* 47(7), pp. 1639-1647.

Al-Dahhan, M., Larachi, F., Dudukovic, M. & Laurents, A., 1997. High-pressure trickle-bed reactors: A review. *Industrial & Engineering Chemistry Research,* 36(8), pp. 3292-3314.

Albericio, F., 2000. *Solid-Phase Synthesis: A Practical Guide.* Marcel Dekker, Inc., New York.

Alonso-Amigo, M.G., 2000. Polymer Microfabrication for Microarrays, Microreactors and Microfluidics. *Journal of the Association for Laboratory Automation,* 5(6), pp. 96-101.

Anastas, P. & Kirchhoff, M., 2002. Origins, Current Status, and Future Challenges of Green Chemistry. *Accounts of Chemical Research,* 35(9), pp. 686-694.

Ashish, V.P. & Mayuresh, V.K., 2003. Novel microfluidic interconnectors for high temperature and pressure applications. *Journal of Micromechanics and Microengineering,* 13(2), p. 337.

Attia, U., Marson, S. & Alcock, J., 2009. Micro-injection moulding of polymer microfluidic devices. *Microfluid Nanofluid,* 7(1), pp. 1-28.

Ayedi, M.A., Le Bigot, Y., Ammar, H., Abid, S., Gharbi, R.E. & Delmas, M., 2013. Synthesis of Primary Amines by One-Pot Reductive Amination of Aldehydes. *Synthetic Communications,* 43(16), pp. 2127-2133.

Balkenhohl, F., von dem Bussche-Hünnefeld, C., Lansky, A. & Zechel, C., 1996. Combinatorial synthesis of small organic molecules. *Angewandte Chemie International Edition in English,* 35(20), pp. 2288-2337.

Bart, J., Kolkman, A.J., Oosthoek-de Vries, A.J., Koch, K., Nieuwland, P.J., Janssen, H., van Bentum, J., Ampt, K.A.M., Rutjes, F.P.J.T., Wijmenga, S.S., Gardeniers, H. & Kentgens, A.P.M., 2009. A Microfluidic High-Resolution NMR Flow Probe. *Journal of the American Chemical Society,* 131(14), pp. 5014-5015.

Basu, B., Bhuiyan, M.M.H., Das, P. & Hossain, I., 2003. Catalytic transfer reduction of conjugated alkenes and an imine using polymer-supported formates. *Tetrahedron Letters,* 44(50), pp. 8931-8934.

Baumann, M., Baxendale, I., Ley, S., Nikbin, N., Smith, C. & Tierney, J., 2008. A modular flow reactor for performing Curtius rearrangements as a continuous flow process. *Organic & Biomolecular Chemistry,* 6(9), pp. 1577-1586.

Baumann, M., Baxendale, I.R. & Ley, S.V., 2010. Synthesis of 3-nitropyrrolidines via dipolar cycloaddition reactions using a modular flow reactor. *Synlett,* 2010(05), pp. 749-752.

Bavykin, D., Lapkin, A., Kolaczkowski, S. & Plucinski, P., 2005. Selective oxidation of alcohols in a continuous multifunctional reactor: Ruthenium oxide catalysed oxidation of benzyl alcohol. *Applied Catalysis A: General,* 288(1-2), pp. 175-184.

Baxendale, I.R., Carter, C.F., O'Brien, M., Pavey, J.B.J. & Ley, S.V., 2009. Synthesis of acetal protected building blocks using flow chemistry with flow I.R. analysis: preparation of butane-2,3-diacetal tartrates. *Organic & Biomolecular Chemistry,* 7(22), pp. 4594-4597.

Baxendale, I.R., Deeley, J., Griffiths-Jones, C.M., Ley, S.V., Saaby, S. & Tranmer, G.K., 2006a. A flow process for the multi-step synthesis of the alkaloid natural product oxomaritidine: a new paradigm for molecular assembly. *Chemical Communications,* (24), pp. 2566-2568.

Baxendale, I.R., Ley, S.V., Smith, C.D. & Tranmer, G.K., 2006b. A flow reactor process for the synthesis of peptides utilizing immobilized reagents, scavengers and catch and release protocols. *Chemical Communications,* (46), pp. 4835-4837.

Beato, P., Kraehnert, R., Engelschalt, S., Frank, T. & Schlögl, R., 2008. A micro-structured quartz reactor for kinetic and in situ spectroscopic studies in heterogeneous catalysis. *Chemical Engineering Journal,* 135, Supplement 1(0), pp. S247-S253.

Becker, H. & Gärtner, C., 2001. Polymer based micro-reactors. *Reviews in Molecular Biotechnology,* 82(2), pp. 89-99.

Benito-Lopez, F., Verboom, W., Kakuta, M., Gardeniers, J.G.E., Egberink, R.J.M., Oosterbroek, E.R., van den Berg, A. & Reinhoudt, D.N., 2005. Optical fiber-based on-line UV/Vis spectroscopic monitoring of chemical reaction kinetics under high pressure in a capillary microreactor. *Chemical Communications,* (22), pp. 2857-2859.

Bhattacharyya, S., 1994. Titanium (IV) isopropoxide and sodium borohydride: a reagent of choice for reductive amination. *Tetrahedron Letters,* 35(15), pp. 2401-2404.

Bogdan, A.R. & James, K., 2010. Efficient Access to New Chemical Space Through Flow—Construction of Druglike Macrocycles Through Copper-Surface-Catalyzed Azide–Alkyne Cycloaddition Reactions. *Chemistry-A European Journal,* 16(48), pp. 14506-14512.

Bogdan, A.R., Mason, B.P., Sylvester, K.T. & McQuade, D.T., 2007. Improving Solid-Supported Catalyst Productivity by Using Simplified Packed-Bed Microreactors. *Angewandte Chemie International Edition,* 46(10), pp. 1698-1701.

Bökenkamp, D., Desai, A., Yang, X., Tai, Y., Marzluff, E. & Mayo, S., 1998. Microfabricated silicon mixers for submillisecond quench-flow analysis. *Analytical Chemistry,* 70(2), pp. 232-236.

Bomann, M., Guch, I. & DiMare, M., 1995. A mild, pyridine-borane-based reductive amination protocol. *The Journal of Organic Chemistry,* 60(18), pp. 5995-5996.

Borch, R., Bernstein, M. & Durst, H., 1971. Cyanohydridoborate anion as a selective reducing agent. *Journal of the American Chemical Society,* 93(12), pp. 2897-2904.

Brandt, J.C. & Wirth, T., 2009. Controlling hazardous chemicals in microreactors: Synthesis with iodine azide. *Beilstein Journal of Organic Chemistry,* 5(1), p. 30.

Braune, S., Pöchlauer, P., Reintjens, R., Steinhofer, S., Winter, M., Lobet, O., Guidat, R., Woehl, P. & Guermeur, C., 2009. Selective nitration in a microreactor for pharmaceutical production under cGMP conditions. *Chemistry Today,* 27(1), pp. 26-29.

Brivio, M., Oosterbroek, R., Verboom, W., Goedbloed, M., Berg, A. & Reinhoudt, D., 2003. Surface effects in the esterification of 9-pyrenebutyric acid within a glass micro reactor. *Chemical Communications,* 2003(15), pp. 1924-1925.

Brivio, M., Verboom, W. & Reinhoudt, D., 2006. Miniaturized continuous flow reaction vessels: influence on chemical reactions. *Lab on a Chip,* 6(3), pp. 329-344.

Brown, B.R., 1994. *The Organic Chemistry of Aliphatic Nitrogen Compounds.* Oxford: Clarendon Press.

Brown, H.C. & Heim, P., 1973. Selective reductions. XVIII. Fast reaction of primary, secondary, and tertiary amides with diborane. Simple, convenient procedure for the conversion of amides to the corresponding amines. *The Journal of Organic Chemistry,* 38(5), pp. 912-916.

Brussee, J., van Benthem, R., Kruse, C. & van der Gen, A., 1990. Magnesium ion mediated stereospecific formation of N-substituted ethanolamines during reductive amination. *Tetrahedron: Asymmetry,* 1(3), pp. 163-166.

Bryan, M.C., Dillon, B., Hamann, L.G., Hughes, G.J., Kopach, M.E., Peterson, E.A., Pourashraf, M., Raheem, I., Richardson, P. & Richter, D., 2013. Sustainable Practices in Medicinal Chemistry: Current State and Future Directions. *Journal of Medicinal Chemistry*.

Bryan, M.C., Wernick, D., Hein, C.D., Petersen, J.V., Eschelbach, J.W. & Doherty, E.M., 2011. Evaluation of a commercial packed bed flow hydrogenator for reaction screening, optimization, and synthesis. *Beilstein Journal of Organic Chemistry,* 7(1), pp. 1141-1149.

Burkhardt, E. & Coleridge, B., 2008. Reductive amination with 5-ethyl-2-methylpyridine borane. *Tetrahedron Letters,* 49(35), pp. 5152-5155.

Burns, J. & Ramshaw, C., 1999. Development of a microreactor for chemical production. *Chemical Engineering Research and Design,* 77(3), pp. 206-211.

Burns, J.R. & Ramshaw, C., 2002. A microreactor for the nitration of benzene and toluene. *Chemical Engineering Communications,* 189(12), pp. 1611-1628.

Byun, E., Hong, B., De Castro, K.A., Lim, M. & Rhee, H., 2007. One-pot reductive mono-N-alkylation of aniline and nitroarene derivatives using aldehydes. *The Journal of Organic Chemistry,* 72(25), pp. 9815-9817.

Calabrese, G.S. & Pissavini, S., 2011. From batch to continuous flow processing in chemicals manufacturing. *American Institute of Chemical Engineers Journal,* 57(4), pp. 828-834.

Cao, E., Sankar, M., Firth, S., Lam, K.F., Bethell, D., Knight, D.K., Hutchings, G.J., McMillan, P.F. & Gavriilidis, A., 2011. Reaction and Raman spectroscopic studies of alcohol oxidation on gold–palladium catalysts in microstructured reactors. *Chemical Engineering Journal,* 167(2), pp. 734-743.

Carberry, J.J., 2001. *Chemical and catalytic reaction engineering.* Mineola, N.Y.: Courier Dover Publications.

Carrara, N., Badano, J., Bertero, N., Torres, G., Betti, C., Martínez-Bovier, L., Quiroga, M. & Vera, C., 2014. Kinetics of the liquid phase selective hydrogenation of 2, 3-butanedione over new composite supported Pd catalysts. *Journal of Chemical Technology and Biotechnology,* 89(2), pp. 265-275.

Chambers, R., Fox, M. & Sandford, G., 2005. Elemental fluorine. Part 18. Selective direct fluorination of 1, 3-ketoesters and 1, 3-diketones using gas/liquid microreactor technology. *Lab Chip,* 5(10), pp. 1132-1139.

Chambers, R., Holling, D., Spink, R. & Sandford, G., 2001. Elemental fluorinePart 13. Gas–liquid thin film microreactors for selective direct fluorination. *Lab on a Chip,* 1(2), pp. 132-137.

Chambers, R. & Spink, R., 1999. Microreactors for elemental fluorine. *Chemical Communications,* 1999(10), pp. 883-884.

Chapra, S.C. & Canale, R.P., 2010. *Numerical methods for engineers.* McGraw-Hill Higher Education, New York.

Cheng, C., Sun, J., Xing, L., Xu, J., Wang, X. & Hu, Y., 2009. Highly Chemoselective Pd- C Catalytic Hydrodechlorination Leading to the Highly Efficient N-Debenzylation of Benzylamines. *The Journal of Organic Chemistry,* 74(15), pp. 5671-5674.

Cho, K., Ando, M., Kobayashi, K., Miyazoe, H., Tsujino, T., Ito, S., Suzuki, T., Tanaka, T., Tokita, S. & Sato, N., 2009. Design, synthesis and evaluation of a novel cyclohexanamine class of neuropeptide Y Y1 receptor antagonists. *Bioorganic & Medicinal Chemistry Letters,* 19(16), pp. 4781-4785.

Chou, T.S., Worley Jr, F.L. & Luss, D., 1979. Local particle-liquid mass transfer fluctuations in mixed-phase cocurrent downflow through a fixed bed in the pulsing regime. *Industrial & Engineering Chemistry Fundamentals,* 18(3), pp. 279-283.

Clapham, B., Wilson, N.S., Michmerhuizen, M.J., Blanchard, D.P., Dingle, D.M., Nemcek, T.A., Pan, J.Y. & Sauer, D.R., 2007. Construction and validation of an automated flow hydrogenation instrument for application in high-throughput organic chemistry. *Journal of Combinatorial Chemistry,* 10(1), pp. 88-93.

Cooper, C.G., Lee, E.R., Silva, R.A., Bourque, A.J., Clark, S., Katti, S. & Nivorozhkin, V., 2011. Process Development of a Potent Glucosylceramide Synthase Inhibitor. *Organic Process Research & Development,* 16(5), pp. 1090-1097.

Costantini, F., Bula, W.P., Salvio, R., Huskens, J., Gardeniers, H.J., Reinhoudt, D.N. & Verboom, W., 2009. Nanostructure based on polymer brushes for efficient heterogeneous catalysis in microreactors. *Journal of the American Chemical Society,* 131(5), pp. 1650-1651.

Coyle, E.E. & Oelgemöller, M., 2008. Micro-photochemistry: photochemistry in microstructured reactors. The new photochemistry of the future? *Photochemical & Photobiological Sciences,* 7(11), pp. 1313-1322.

Cussler, E.L., 2009. *Diffusion: Mass Transfer in Fluid Systems.* Cambridge: Cambridge University Press.

Dangerfield, E.M., Plunkett, C.H., Win-Mason, A.L., Stocker, B.L. & Timmer, M.S., 2010. Protecting-Group-Free Synthesis of Amines: Synthesis of Primary Amines from Aldehydes via Reductive Amination. *The Journal of Organic Chemistry,* 75(16), pp. 5470-5477.

Darvas, F., Dorman, G., Lengyel, L., Kovacs, I., Jones, R. & Uerge, L., 2009. High pressure, high temperature reactions in continuous flow: merging discovery and process chemistry. *Chimica Oggi,* 27(3), pp. 40-43.

De Mas, N., Günther, A., Schmidt, M. & Jensen, K., 2003. Microfabricated multiphase reactors for the selective direct fluorination of aromatics. *Industrial & Engineering Chemistry Research,* 42(4), pp. 698-710.

De Mas, N., Günther, A., Schmidt, M.A. & Jensen, K.F., 2008. Increasing productivity of microreactors for fast gas− liquid reactions: The case of direct fluorination of toluene. *Industrial & Engineering Chemistry Research,* 48(3), pp. 1428-1434.

De Mas, N., Jackman, R.J., Schmidt, M.A. & Jensen, K.F., 2001. Microchemical systems for direct fluorination of aromatics. *Microreaction Technology.* Springer, pp. 60-67.

Delaunay, C.B., Storck, A., Laurent, A. & Charpentier, J., 1982. Electrochemical determination of liquid–solid mass transfer in a fixed-bed irrigated gas–liquid reactor with downward cocurrent flow. *Int. Chem. Eng,* 22, p. 244.

Desai, B., Dallinger, D. & Kappe, C.O., 2006. Microwave-assisted solution phase synthesis of dihydropyrimidine C5 amides and esters. *Tetrahedron,* 62(19), pp. 4651-4664.

Doku, G., Haswell, S., McCreedy, T. & Greenway, G., 2001. Electric field-induced mobilisation of multiphase solution systems based on the nitration of benzene in a micro reactor. *The Analyst,* 126(1), pp. 14-20.

Duan, J., Sun, L., Liang, Z., Zhang, J., Wang, H., Zhang, L., Zhang, W. & Zhang, Y., 2006. Rapid protein digestion and identification using monolithic enzymatic microreactor coupled with nano-liquid chromatography-electrospray ionization mass spectrometry. *Journal of Chromatography A,* 1106(1-2), pp. 165-174.

Duduković, M.P., Larachi, F. & Mills, P.L., 2002. Multiphase catalytic reactors: a perspective on current knowledge and future trends. *Catalysis Reviews,* 44(1), pp. 123-246.

Ebrahimi, F., Kolehmainen, E. & Turunen, I., 2009. Safety Advantages of On-Site Microprocesses. *Organic Process Research & Development,* 13(5), pp. 965-969.

Ehrfeld, W., Hessel, V. & Löwe, H., 2000. *Microreactors: New technology for modern chemistry.* Weinheim; Chichester: Wiley-VCH.

El Kadib, A., Chimenton, R., Sachse, A., Fajula, F., Galarneau, A. & Coq, B., 2009. Functionalized inorganic monolithic microreactors for high productivity in fine chemicals catalytic synthesis. *Angewandte Chemie,* 121(27), pp. 5069-5072.

Elvira, K.S., i Solvas, X.C. & Wootton, R.C., 2013. The past, present and potential for microfluidic reactor technology in chemical synthesis. *Nature chemistry*.

Falus, P., Boros, Z., Hornyánszky, G., Nagy, J., Darvas, F., Ürge, L. & Poppe, L., 2011. Reductive amination of ketones: novel one-step transfer hydrogenations in batch and continuous-flow mode. *Tetrahedron Letters,* 52(12), pp. 1310-1312.

Fan, X., Chen, H., Ding, Y., Plucinski, P. & Lapkin, A., 2008. Potential of 'nanofluids' to further intensify microreactors. *Green Chemistry,* 10(6), pp. 670-677.

Fan, X., Lapkin, A. & Plucinski, P., 2009. Liquid phase hydrogenation in a structured multichannel reactor. *Catalysis Today,* 147, pp. S313-S318.

Fernandez-Suarez, M., Wong, S. & Warrington, B., 2002. Synthesis of a three-member array of cycloadducts in a glass microchip under pressure driven flow. *Lab on a Chip,* 2(3), pp. 170-174.

Ferstl, W., Loebbecke, S., Antes, J., Krause, H., Haeberl, M., Schmalz, D., Muntermann, H., Grund, M., Steckenborn, A. & Lohf, A., 2004. Development of an automated microreaction system with integrated sensorics for process screening and production. *Chemical Engineering Journal,* 101(1), pp. 431-438.

Fichtner, M., Brandner, J., Lindner, G., Schygulla, U., Wenka, A. & Schubert, K., Year. Microstructure devices for applications in thermal and chemical process engineering. In., pp. 222-228.

Fletcher, P., Haswell, S. & Paunov, V., 1999. Theoretical considerations of chemical reactions in micro-reactors operating under electroosmotic and electrophoretic control. *The Analyst,* 124(9), pp. 1273-1282.

Fletcher, P.D., Haswell, S.J., Pombo-Villar, E., Warrington, B.H., Watts, P., Wong, S.Y. & Zhang, X., 2002. Micro reactors: principles and applications in organic synthesis. *Tetrahedron,* 58(24), pp. 4735-4757.

Fogler, H.S., 1999. *Elements of Chemical Reaction Engineering.* Upper Saddle River, N.J. ; London : Prentice-Hall

Fortt, R., Wootton, R.C.R. & de Mello, A.J., 2003. Continuous-Flow Generation of Anhydrous Diazonium Species: Monolithic Microfluidic Reactors for the Chemistry of Unstable Intermediates. *Organic Process Research & Development,* 7(5), pp. 762-768.

Franzen, R., 2000. The Suzuki, the Heck, and the Stille reaction-three versatile methods for the introduction of new CC bonds on solid support. *Canadian Journal of Chemistry,* 78(7), pp. 957-962.

Fredrickson, C.K. & Fan, Z.H., 2004. Macro-to-micro interfaces for microfluidic devices. *Lab on a Chip,* 4(6), pp. 526-533.

Freifelder, M., 1978. *Catalytic hydrogenation in organic synthesis : procedures and commentary.* New York, Chichester : Wiley.

Fuchs, M., Goessler, W., Pilger, C. & Kappe, C.O., 2010. Mechanistic Insights into Copper (I)-Catalyzed Azide-Alkyne Cycloadditions using Continuous Flow Conditions. *Advanced Synthesis & Catalysis,* 352(2-3), pp. 323-328.

Garcia-Egido, E., Spikmans, V., Wong, S. & Warrington, B., 2003. Synthesis and analysis of combinatorial libraries performed in an automated micro reactor system. *Lab on a Chip,* 3(2), pp. 73-76.

Garcia-Egido, E., Wong, S. & Warrington, B., 2002. A Hantzsch synthesis of 2-aminothiazoles performed in a heated microreactor system. *Lab on a Chip,* 2(1), pp. 31-33.

Gavriilidis, A., Angeli, P., Cao, E., Yeong, K. & Wan, Y., 2002. Technology and applications of microengineered reactors. *Chemical Engineering Research and Design,* 80(1), pp. 3-30.

Geyer, K., Codée, J. & Seeberger, P., 2006. Microreactors as Tools for Synthetic Chemists-The Chemists' Round Bottomed Flask of the 21st Century? *Chemistry–A European Journal,* 12(33), pp. 8434-8442.

Glasnov, T.N. & Kappe, C.O., 2007. Microwave-Assisted Synthesis under Continuous-Flow Conditions. *Macromolecular Rapid Communications,* 28(4), pp. 395-410.

Gomez, S., Peters, J. & Maschmeyer, T., 2002. The reductive amination of aldehydes and ketones and the hydrogenation of nitriles: mechanistic aspects and selectivity control. *Advanced Synthesis & Catalysis,* 344(10), pp. 1037-1057.

Greenway, G., Haswell, S., Morgan, D., Skelton, V. & Styring, P., 2000. The use of a novel microreactor for high throughput continuous flow organic synthesis. *Sensors and Actuators B: Chemical,* 63(3), pp. 153-158.

Gross, T., Seayad, A., Ahmad, M. & Beller, M., 2002. Synthesis of Primary Amines: First Homogeneously Catalyzed Reductive Amination with Ammonia. *Organic Letters,* 4(12), pp. 2055-2058.

Gunanathan, C. & Milstein, D., 2008. Selective synthesis of primary amines directly from alcohols and ammonia. *Angewandte Chemie International Edition,* 47(45), pp. 8661-8664.

Hallmark, B., Mackley, M.R. & Gadala-Maria, F., 2005. Hollow Microcapillary Arrays in Thin Plastic Films. *Advanced Engineering Materials,* 7(6), pp. 545-547.

Hartman, R. & Jensen, K., 2009. Microchemical systems for continuous-flow synthesis. *Lab on a Chip,* 9(17), pp. 2495-2507.

Haswell, S.J., O'Sullivan, B. & Styring, P., 2001. Kumada–Corriu reactions in a pressure-driven microflow reactor. *Lab on a Chip,* 1(2), pp. 164-166.

Heinen, A., Peters, J. & van Bekkum, H., 2000. The Reductive Amination of Benzaldehyde Over Pd/C Catalysts: Mechanism and Effect of Carbon Modifications on the Selectivity. *European Journal of Organic Chemistry,* 2000(13), pp. 2501-2506.

Hessel, V., 2009. Novel process windows-gate to maximizing process intensification via flow chemistry. *Chemical Engineering & Technology,* 32(11), pp. 1655-1681.

Hessel, V., Ehrfeld, W., Golbig, K., Hofmann, C., Löwe, H., Richter, T., Storz, M., Wolf, A., Wörz, O. & Breysse, J., 2000. High temperature HCN generation in an integrated Microreaction system. *Microreaction Technology: Industrial Prospects.* Springer, pp. 151-164.

Hessel, V., Hardt, S. & Löwe, H., 2004. *Chemical micro process engineering.* New York, Wiley-VCH.

Hessel, V., Hardt, S., Löwe, H. & Schönfeld, F., 2003. Laminar mixing in different interdigital micromixers: I. Experimental characterization. *American Institute of Chemical Engineers Journal,* 49(3), pp. 566-577.

Hessel, V., Kralisch, D. & Krtschil, U., 2008. Sustainability through green processing–novel process windows intensify micro and milli process technologies. *Energy & Environmental Science,* 1(4), pp. 467-478.

Hessel, V. & Löwe, H., 2003. Microchemical Engineering: Components, Plant Concepts, User Acceptance-Part II. *Chemical Engineering & Technology,* 26(4), pp. 391-408.

Hibara, A., Tokeshi, M., Uchiyama, K., Hisamoto, H. & Kitamori, T., 2001. Integrated Multilayer Flow System on a Microchip. *Analytical Sciences,* 17(1), pp. 89-93.

Higham, D.J. & Higham, N.J., 2005. *MATLAB guide.* Siam.

Hinchcliffe, A., Hughes, C., Pears, D. & Pitts, M., 2007. QuadraPure cartridges for removal of trace metal from reaction mixtures in flow. *Organic Process Research & Development,* 11(3), pp. 477-481.

Hisamoto, H., Saito, T., Tokeshi, M., Hibara, A. & Kitamori, T., 2001. Fast and high conversion phase-transfer synthesis exploiting the liquid–liquid interface formed in a microchannel chip. *Chemical Communications,* 2001(24), pp. 2662-2663.

Hofmann, H.P., 1978. Multiphase catalytic packed-bed reactors. *Catalysis Reviews Science and Engineering,* 17(1), pp. 71-117.

Hook, B.D., Dohle, W., Hirst, P.R., Pickworth, M., Berry, M.B. & Booker-Milburn, K.I., 2005. A practical flow reactor for continuous organic photochemistry. *The Journal of Organic Chemistry,* 70(19), pp. 7558-7564.

Hornung, C.H., Mackley, M.R., Baxendale, I.R. & Ley, S.V., 2007. A Microcapillary Flow Disc Reactor for Organic Synthesis. *Organic Process Research & Development,* 11(3), pp. 399-405.

Huang, H., Hutta, D.A., Rinker, J.M., Hu, H., Parsons, W.H., Schubert, C., DesJarlais, R.L., Crysler, C.S., Chaikin, M.A. & Donatelli, R.R., 2009. Pyrido [2, 3-d] pyrimidin-5-ones: A Novel Class of Antiinflammatory Macrophage Colony-Stimulating Factor-1 Receptor Inhibitors. *Journal of Medicinal Chemistry,* 52(4), pp. 1081-1099.

Hübner, S., Bentrup, U., Budde, U., Lovis, K., Dietrich, T., Freitag, A., Küpper, L. & Jähnisch, K., 2009. An Ozonolysis− Reduction Sequence for the Synthesis of Pharmaceutical Intermediates in Microstructured Devices. *Organic Process Research & Development,* 13(5), pp. 952-960.

Illg, T., Löb, P. & Hessel, V., 2010. Flow chemistry using milli-and microstructured reactors-From conventional to novel process windows. *Bioorganic & Medicinal Chemistry,* 18(11), pp. 3707-3719.

Insaf, S.S. & Witiak, D.T., 1999. Facile non-racemizing route for the N-alkylation of hindered secondary amines. *Synthesis,* 1999(03), pp. 435-440.

Irfan, M., Glasnov, T.N. & Kappe, C.O., 2011. Heterogeneous Catalytic Hydrogenation Reactions in Continuous-Flow Reactors. *ChemSusChem,* 4(3), pp. 300-316.

Jähnisch, K., Baerns, M., Hessel, V., Ehrfeld, W., Haverkamp, V., Löwe, H., Wille, C. & Guber, A., 2000. Direct fluorination of toluene using elemental fluorine in gas/liquid microreactors. *Journal of Fluorine Chemistry,* 105(1), pp. 117-128.

Jähnisch, K., Bentrup, U., Küpper, L., Budde, U. & Lovis, K., 2006. Mid-Infrared Monitoring of Gas-Liquid Reactions in Vitamin D Analogue Synthesis with a Novel Fiber Optical Diamond ATR Sensor. *Chemical Engineering & Technology,* 29(10), pp. 1216-1220.

Jähnisch, K., Hessel, V., Löwe, H. & Baerns, M., 2004. Chemistry in microstructured reactors. *Angewandte Chemie International Edition,* 43(4), pp. 406-446.

Jähnisch, K., Hübner, S., Bentrup, U., Budde, U., Lovis, K., Dietrich, T., Freitag, A. & Küpper, L., 2009. An Ozonolysis−Reduction Sequence for the Synthesis of Pharmaceutical Intermediates in Microstructured Devices. *Organic Process Research & Development,* 13(5), pp. 952-960.

Jain, K., Wu, C., Atre, S.V., Jovanovic, G., Narayanan, V., Kimura, S., Sprenkle, V., Canfield, N. & Roy, S., 2009. Synthesis of Nanoparticles in High Temperature

Ceramic Microreactors: Design, Fabrication and Testing. *International Journal of Applied Ceramic Technology,* 6(3), pp. 410-419.

Jas, G. & Kirschning, A., 2003. Continuous flow techniques in organic synthesis. *Chemistry–A European Journal,* 9(23), pp. 5708-5723.

Jensen, K., 1998. Chemical kinetics: smaller, faster chemistry. *Nature,* 393(6687), pp. 735-737.

Jensen, K., 2001. Microreaction engineering - is small better? *Chemical Engineering Science,* 56(2), pp. 293-303.

Jensen, K.F., 2006. Silicon-Based Microchemical Systems: Characteristics and Applications. *MRS Bulletin,* 31(02), pp. 101-107.

Jensen, K.F., de Mas, N., Günther, A., Kraus, T. & Schmidt, M.A., 2005. Scaled-Out Multilayer Gas−Liquid Microreactor with Integrated Velocimetry Sensors. *Industrial & Engineering Chemistry Research,* 44(24), pp. 8997-9013.

Jensen, K.F., Floyd, T.M., Losey, M.W., Firebaugh, S.L. & Schmidt, M.A., 2000. Novel liquid phase microreactors for safe production of hazardous specialty chemicals. *Microreaction technology: Industrial prospects.* Springer, pp. 171-180.

Jensen, K.F., Floyd, T.M. & Schmidt, M.A., 2004. Silicon Micromixers with Infrared Detection for Studies of Liquid-Phase Reactions. *Industrial & Engineering Chemistry Research,* 44(8), pp. 2351-2358.

Jensen, K.F., Losey, M.W. & Schmidt, M.A., 2001. Microfabricated multiphase packed-bed reactors: characterization of mass transfer and reactions. *Industrial & Engineering Chemistry Research,* 40(12), pp. 2555-2562.

Jiménez-González, C., Poechlauer, P., Broxterman, Q.B., Yang, B.-S., am Ende, D., Baird, J., Bertsch, C., Hannah, R.E., Dell'Orco, P. & Noorman, H., 2011. Key green engineering research areas for sustainable manufacturing: A perspective from pharmaceutical and fine chemicals manufacturers. *Organic Process Research & Development,* 15(4), pp. 900-911.

Kadyrov, R. & Riermeier, T., 2003. Highly enantioselective hydrogen-transfer reductive amination: catalytic asymmetric synthesis of primary amines. *Angewandte Chemie,* 115(44), pp. 5630-5632.

Kandlikar, S.G., 2002. Fundamental issues related to flow boiling in minichannels and microchannels. *Experimental Thermal and Fluid Science,* 26(2–4), pp. 389-407.

Kappe, C.O., Razzaq, T. & Glasnov, T.N., 2009. Continuous-Flow Microreactor Chemistry under High-Temperature/Pressure Conditions. *European Journal of Organic Chemistry,* 2009(9), pp. 1321-1325.

Katritzky, A.R., Meth-Cohn, O. & Rees, C.W., 1995. *Comprehensive organic functional group transformations.* Amsterdam; Boston: Elsevier.

Kaupp, G., 2006. Waste-free large-scale syntheses without auxiliaries for sustainable production omitting purifying workup. *CrystEngComm,* 8(11), pp. 794-804.

Kawaguchi, T., Miyata, H., Ataka, K., Mae, K. & Yoshida, J., 2005. Room Temperature Swern Oxidations by Using a Microscale Flow System. *Angewandte Chemie International Edition,* 44(16), pp. 2413-2416.

Kestenbaum, H., de Oliveira, A., Schmidt, W., Schüth, F., Ehrfeld, W., Gebauer, K., Löwe, H., Richter, T., Lebiedz, D. & Untiedt, I., 2002. Silver-catalyzed oxidation of ethylene to ethylene oxide in a microreaction system. *Industrial & Engineering Chemistry Research,* 41(4), pp. 710-719.

Kestenbaum, H., Lange de Oliveira, A., Schmidt, W., Schüth, F., Ehrfeld, W., Gebauer, K., Löwe, H. & Richter, T., 2000. Synthesis of ethylene oxide in a catalytic microreactor system. *Studies in Surface Science and Catalysis,* 130, pp. 2741-2746.

Kim, S., Oh, C.H., Ko, J.S., Ahn, K.H. & Kim, Y.J., 1985. Zinc-modified cyanoborohydride as a selective reducing agent. *The Journal Of Organic Chemistry,* 50(11), pp. 1927-1932.

Kirschning, A., Solodenko, W. & Mennecke, K., 2006. Combining enabling techniques in organic synthesis: continuous flow processes with heterogenized catalysts. *Chemistry–A European Journal,* 12(23), pp. 5972-5990.

Kirschning, A., Wegner, J. & Ceylan, S., 2012. Flow chemistry–a key enabling technology for (multistep) organic synthesis. *Advanced Synthesis & Catalysis,* 354(1), pp. 17-57.

Knitter, R., Göhring, D., Risthaus, P. & Haußelt, J., 2001. Microfabrication of ceramic microreactors. *Microsystem Technologies,* 7(3), pp. 85-90.

Kobayashi, J., Mori, Y. & Kobayashi, S., 2006. Multiphase organic synthesis in microchannel reactors. *Chemistry–An Asian Journal,* 1(1-2), pp. 22-35.

Kobayashi, J., Mori, Y., Okamoto, K., Akiyama, R., Ueno, M., Kitamori, T. & Kobayashi, S., 2004. A microfluidic device for conducting gas-liquid-solid hydrogenation reactions. *Science,* 304(5675), p. 1305.

Kolios, G., Frauhammer, J. & Eigenberger, G., 2000. Autothermal fixed-bed reactor concepts. *Chemical Engineering Science,* 55(24), pp. 5945-5967.

Kopach, M.E., Murray, M.M., Braden, T.M., Kobierski, M.E. & Williams, O.L., 2009. Improved synthesis of 1-(azidomethyl)-3, 5-bis-(trifluoromethyl) benzene: development of batch and microflow azide processes. *Organic Process Research & Development,* 13(2), pp. 152-160.

Kremsner, J.M. & Kappe, C.O., 2006. Silicon carbide passive heating elements in microwave-assisted organic synthesis. *The Journal of Organic Chemistry,* 71(12), pp. 4651-4658.

Kuehne, M.E. & Shannon, P.J., 1977. Reduction of amides and lactams to amines by reactions with phosphorus oxychloride and sodium borohydride. *The Journal of Organic Chemistry,* 42(12), pp. 2082-2087.

Kündig, P., 2007. The Future of Organic Synthesis. *Science Magazine,* 314(5798), pp. 430-431.

Kusakabe, K., Morooka, S. & Maeda, H., 2001. Development of a microchannel catalytic reactor system. *Korean J. Chem. Eng.*, 18(3), pp. 271-276.

Lakota, A. & Levec, J., 1990. Solid-liquid mass transfer in packed beds with cocurrent downward two-phase flow. *American Institute of Chemical Engineers Journal,* 36(9), pp. 1444-1448.

Lamb, G., Watson, A., Jolley, K., Maxwell, A. & Williams, J., 2009. Borrowing hydrogen methodology for the conversion of alcohols into N-protected primary amines and in situ deprotection. *Tetrahedron Letters,* 50(26), pp. 3374-3377.

LaPorte, T. & Wang, C., 2007. Continuous processes for the production of pharmaceutical intermediates and active pharmaceutical ingredients. *Current Opinion in Drug Discovery & Development,* 10(6), p. 738.

Larachi, F., Laurent, A., Midoux, N. & Wild, G., 1991a. Experimental study of a trickle-bed reactor operating at high pressure: two-phase pressure drop and liquid saturation. *Chemical Engineering Science,* 46(5–6), pp. 1233-1246.

Larachi, F., Laurent, A., Wild, G. & Midoux, N., 1991b. Some experimental liquid saturation results in fixed-bed reactors operated under elevated pressure in cocurrent upflow and downflow of the gas and the liquid. *Industrial & Engineering Chemistry Research,* 30(11), pp. 2404-2410.

Larock, R.C., 1999. *Comprehensive organic transformations : a guide to functional group preparations.* 2nd ed. ed.: New York, Chichester : Wiley-VCH.

Lau, W.N., Yeung, K.L. & Martin-Aranda, R., 2008. Knoevenagel condensation reaction between benzaldehyde and ethyl acetoacetate in microreactor and membrane microreactor. *Microporous and Mesoporous Materials,* 115(1–2), pp. 156-163.

Lawrence, S.A., 2004. *Amines: synthesis, properties and applications.* Cambridge: Cambridge University Press.

Leahy, D.K., Tucker, J.L., Mergelsberg, I., Dunn, P.J., Kopach, M.E. & Purohit, V.C., 2013. Seven Important Elements for an Effective Green Chemistry Program: An IQ Consortium Perspective. *Organic Process Research & Development,* 17(9), pp. 1099-1109.

Lee, D.-S., Yang, H., Chung, K.-H. & Pyo, H.-B., 2005. Wafer-Scale Fabrication of Polymer-Based Microdevices via Injection Molding and Photolithographic Micropatterning Protocols. *Analytical Chemistry,* 77(16), pp. 5414-5420.

Lee, J.N., Park, C. & Whitesides, G.M., 2003. Solvent Compatibility of Poly(dimethylsiloxane)-Based Microfluidic Devices. *Analytical Chemistry,* 75(23), pp. 6544-6554.

Lehtonen, J., Salmi, T., Vuori, A. & Tirronen, E., 1998. On the Principles of Modelling of Homogeneous-Heterogeneous Reactions in the Production of Fine Chemicals. A Case Study: Reductive Alkylation of Aromatic Amines. *Organic Process Research & Development,* 2(2), pp. 78-85.

Leonel, R.A., Nuria de, M., Raymond, S., Aleksander, J.F., Martin, A.S. & Klavs, F.J., 2007. Isotropic etching of silicon in fluorine gas for MEMS micromachining. *Journal of Micromechanics and Microengineering,* 17(2), p. 384.

Lerou, J.J., Tonkovich, A.L., Silva, L., Perry, S. & McDaniel, J., 2010. Microchannel reactor architecture enables greener processes. *Chemical Engineering Science,* 65(1), pp. 380-385.

Levenspiel, O., 1972. *Chemical Reaction Engineering.* New York, Chichester: Wiley

Lévesque, F. & Seeberger, P.H., 2012. Continuous-Flow Synthesis of the Anti-Malaria Drug Artemisinin. *Angewandte Chemie International Edition,* 51(7), pp. 1706-1709.

Ley, S.V., Carter, C.F., Lange, H., Baxendale, I.R., Wittkamp, B., Goode, J.G. & Gaunt, N.L., 2010. ReactIR Flow Cell: A New Analytical Tool for Continuous Flow Chemical Processing. *Organic Process Research & Development,* 14(2), pp. 393-404.

Ley, S.V., Franckevicius, V., Knudsen, K.R., Ladlow, M. & Longbottom, D.A., 2006. Practical Synthesis of (S)-Pyrrolidin-2-yl-1*H*-tetrazole, Incorporating Efficient Protecting Group Removal by Flow-reactor Hydrogenolysis. *Synlett,* 6, p. 889.

Ley, S.V., Knudsen, K.R., Holden, J. & Ladlow, M., 2007. Optimisation of Conditions for O-Benzyl and N-Benzyloxycarbonyl Protecting Group Removal using an Automated Flow Hydrogenator. *Advanced Synthesis & Catalysis,* 349(4-5), pp. 535-538.

Ley, S.V., Pastre, J.C. & Browne, D.L., 2013. Flow chemistry syntheses of natural products. *Chemical Society Reviews,* 42(23), pp. 8849-8869.

Lin, W.-Y., Wang, Y., Wang, S. & Tseng, H.-R., 2009. Integrated microfluidic reactors. *Nano Today,* 4(6), pp. 470-481.

Linden, J.J.v.d., Hilberink, P.W., Kronenburg, C.M. & Kemperman, G.J., 2008. Investigation of the Moffatt− Swern Oxidation in a Continuous Flow Microreactor System. *Organic Process Research & Development,* 12(5), pp. 911-920.

Lipshutz, B.H., Unger, J.B. & Taft, B.R., 2007. Copper-in-charcoal (Cu/C) promoted diaryl ether formation. *Organic Letters,* 9(6), pp. 1089-1092.

Liu, J., Fitzgerald, A. & Mani, N., 2012. Reductive Amination by Continuous-Flow Hydrogenation: Direct and Scalable Synthesis of a Benzylpiperazine. *Synthesis,* 44(15), pp. 2469-2473.

Liu, Q., Takemura, F. & Yabe, A., 1996. Solubility of hydrogen in liquid methanol and methyl formate at 20°C to 140°C. *Journal of Chemical & Engineering Data,* 41(5), pp. 1141-1143.

Liu, S., Fukuyama, T., Sato, M. & Ryu, I., 2004. Continuous Microflow Synthesis of Butyl Cinnamate by a Mizoroki- Heck Reaction Using a Low-Viscosity Ionic Liquid as the Recycling Reaction Medium. *Organic Process & Development,* 8(3), pp.477-481.

Losey, M.W., Schmidt, M.A. & Jensen, K.F., 2001. Microfabricated multiphase packed-bed reactors: Characterization of mass transfer and reactions. *Industrial & Engineering Chemistry Research,* 40(12), pp. 2555-2562.

Löwe, H. & Ehrfeld, W., 1999. State-of-the-art in microreaction technology: concepts, manufacturing and applications. *Electrochimica Acta,* 44(21-22), pp. 3679-3689.

Löwe, H., Hessel, V., Löb, P. & Hubbard, S., 2006. Addition of secondary amines to α, β-unsaturated carbonyl compounds and nitriles by using microstructured reactors. *Organic Process Research & Development,* 10(6), pp. 1144-1152.

Lu, H., Schmidt, M. & Jensen, K., 2001. Photochemical reactions and on-line UV detection in microfabricated reactors. *Lab on a Chip,* 1(1), pp. 22-28.

Luis, S.V. & García-Verdugo, E., 2010. *Chemical reactions and processes under flow conditions.* Cambridge: Royal Society of Chemistry.

Malhotra, G., 2005. Pharmaceutical processing - batch or a continuous process: a choice. *Pharmaceutical Processing*.

Manz, A., Harrison, D., Verpoorte, E., Fettinger, J., Ludi, H. & Widmer, H., 1991. Miniaturization of Chemical Analysis Systems A Look into Next Century's Technology or Just a Fashionable Craze? *CHIMIA International Journal for Chemistry,* 45(4), pp. 103-105.

March, J., 1997. *Advanced organic chemistry : reactions, mechanisms, and structure.* 4th ed. ed. New York, Chichester: Wiley-Interscience.

Marre, S., Adamo, A., Basak, S., Aymonier, C. & Jensen, K.F., 2010. Design and packaging of microreactors for high pressure and high temperature applications. *Industrial & Engineering Chemistry Research,* 49(22), pp. 11310-11320.

Maskill, K.G., Knowles, J.P., Elliott, L.D., Alder, R.W. & Booker-Milburn, K.I., 2013. Complexity from Simplicity: Tricyclic Aziridines from the Rearrangement of Pyrroles by Batch and Flow Photochemistry. *Angewandte Chemie,* 125(5), pp. 1539-1542.

Mason, B.P., Price, K.E., Steinbacher, J.L., Bogdan, A.R. & McQuade, D.T., 2007. Greener approaches to organic synthesis using microreactor technology. *Chemical Reviews-Columbus,* 107(6), pp. 2300-2318.

Matos, M.-C. & Murphy, P.V., 2007. Synthesis of macrolide-saccharide hybrids by ring-closing metathesis of precursors derived from glycitols and benzoic acids. *The Journal of Organic Chemistry,* 72(5), pp. 1803-1806.

McCreedy, T., 2000. Fabrication techniques and materials commonly used for the production of microreactors and micro total analytical systems. *Trends in Analytical Chemistry,* 19(6), pp. 396-401.

McCreedy, T., 2001. Rapid prototyping of glass and PDMS microstructures for micro total analytical systems and micro chemical reactors by microfabrication in the general laboratory. *Analytica Chimica Acta,* 427(1), pp. 39-43.

McGovern, S., Harish, G., Pai, C., Mansfield, W., Taylor, J., Pau, S. & Besser, R., 2008. Multiphase flow regimes for hydrogenation in a catalyst-trap microreactor. *Chemical Engineering Journal,* 135, pp. S229-S236.

McQuade, D.T. & Seeberger, P.H., 2013. Applying Flow Chemistry: Methods, Materials and Multi-Step Synthesis. *The Journal of Organic Chemistry,* 78, pp. 6384-6389.

Mello, A. & Wootton, R., 2002. FOCUSBut what is it good for? Applications of microreactor technology for the fine chemical industry. *Lab on a Chip,* 2(1), pp. 7-13.

Mićović, I.V., Ivanović, M.D., Piatak, D.M. & Bojić, V.D., 1991. A simple method for preparation of secondary aromatic amines. *Synthesis,* 1991(11), pp. 1043-1045.

Mikami, K., Yamanaka, M. & Islam, M., 2003. [] Fluorous nanoflow'system for the Mukaiyama aldol reaction catalyzed by the lowest concentration of the lanthanide complex with bis (perfluorooctanesulfonyl) amide ponytail. *Tetrahedron,* 59(52), pp. 10593-10597.

Mills, P. & Chaudhari, R., 1997. Multiphase catalytic reactor engineering and design for pharmaceuticals and fine chemicals. *Catalysis Today,* 37(4), pp. 367-404.

Min, K.-I., Lee, T.-H., Park, C.P., Wu, Z.-Y., Girault, H.H., Ryu, I., Fukuyama, T., Mukai, Y. & Kim, D.-P., 2010. Monolithic and Flexible Polyimide Film Microreactors

for Organic Microchemical Applications Fabricated by Laser Ablation. *Angewandte Chemie International Edition,* 49(39), pp. 7063-7067.

Moseley, J.D., Lenden, P., Lockwood, M., Ruda, K., Sherlock, J.-P., Thomson, A.D. & Gilday, J.P., 2007. A Comparison of Commercial Microwave Reactors for Scale-Up within Process Chemistry. *Organic Process Research & Development,* 12(1), pp. 30-40.

Müller, M., Bauer, W. & Kleissl, H., 2005. Low-pressure injection molding of ceramic micro devices using sub-micron and nano scaled powders. *Multi-material Micro Manufacture,* pp. 1-4.

Murphy, E.R., Inoue, T., Sahoo, H.R., Zaborenko, N. & Jensen, K.F., 2007. Solder-based chip-to-tube and chip-to-chip packaging for microfluidic devices. *Lab on a Chip,* 7(10), pp. 1309-1314.

Nicolaou, K., Hanko, R. & Hartwig, W., 2002. *Handbook of Combinatorial Chemistry-Drugs, Catalysts, Materials, Vol. 1.* Wiley-VCH, Weinheim.

Nugent, T.C., Negru, D.E., El-Shazly, M., Hu, D., Sadiq, A., Bibi, A. & Umar, M.N., 2011. Sequential Reductive Amination-Hydrogenolysis: A One-Pot Synthesis of Challenging Chiral Primary Amines. *Advanced Synthesis & Catalysis,* 353(11-12), pp. 2085-2092.

Okada, Y., Nitta, K., Tanaka, T. & Kudoh, S., 2012. Measurement of Concentration of Reaction Intermediate in Microreactors Using a Raman Microscope Spectrometer. *Journal of Chemical Engineering of Japan,* 45(7), pp. 539-543.

Okafor, O.C., Tadepalli, S., Tampy, G. & Lawal, A., 2010. Microreactor Performance Studies of the Cycloaddition of Isoamylene and α-Methylstyrene. *Industrial & Engineering Chemistry Research,* 49(12), pp. 5549-5560.

Oosterbroek, R.E., Hermes, D.C., Kakuta, M., Benito-Lopez, F., Gardeniers, J.G.E., Verboom, W., Reinhoudt, D.N. & Berg, A.v., 2006. Fabrication and mechanical testing of glass chips for high-pressure synthetic or analytical chemistry. *Microsystem Technologies,* 12(5), pp. 450-454.

Pakdehi, S., Sohrabi, M. & Moghaddam, A., 2010. Liquid phase hydrogenation of acethydrazone to N'-methyl acethydrazide over Pd/γ-Al_2O_3 catalyst. *Brazilian Journal of Chemical Engineering,* 27(1), pp. 145-152.

Panke, G., Schwalbe, T., Stirner, W., Taghavi-Moghadam, S. & Wille, G., 2003. A practical approach of continuous processing to high energetic nitration reactions in microreactors. *Synthesis,* (18), pp. 2827-2830.

Patai, S., 1968. The Chemistry of the Amino Group. Wiley, p. 37.

Patil, N.G., Roy, D., Chaudhari, A.S. & Chaudhari, R.V., 2007. Kinetics of reductive alkylation of *p*-phenylenediamine with methyl ethyl ketone using 3% Pt/Al_2O_3 catalyst

in a slurry reactor. *Industrial & Engineering Chemistry Research,* 46(10), pp. 3243-3254.

Patil, R.D. & Adimurthy, S., 2013. Catalytic Methods for Imine Synthesis. *Asian Journal of Organic Chemistry,* 2(9), pp. 726-744.

Pelter, A., Rosser, R.M. & Mills, S., 1984. Reductive aminations of ketones and aldehydes using borane–pyridine. *Journal of the Chemical Society, Perkin Transactions 1*, pp. 717-720.

Perry, R.H., Green, D.W. & Maloney, J.O., 1984. *Perry's Chemical Engineer's Handbook.* New York, London: McGraw-Hill

Petersen, T.P., Ritzén, A. & Ulven, T., 2009. A multistep continuous-flow system for rapid on-demand synthesis of receptor ligands. *Organic Letters,* 11(22), pp. 5134-5137.

Petrov, L., 2002. Problems and challenges about accelerated testing of the catalytic activity of catalysts. *Principles and Methods for Accelerated Catalyst Design and Testing.* Springer, pp. 13-69.

Petrov, L., Alhamed, Y., Al-Zahrani, A. & Daous, M., 2011. Role of Chemical Kinetics in the Heterogeneous Catalysis Studies. *Chinese Journal of Catalysis,* 32(6), pp. 1085-1112.

Piers, W.E., Blackwell, J.M., Sonmor, E.R. & Scoccitti, T., 2000. $B(C_6F_5)_3$-Catalyzed Hydrosilation of Imines via Silyliminium Intermediates. *Organic Letters,* 2(24), pp. 3921-3923.

Plucinski, P., Bavykin, D., Kolaczkowski, S. & Lapkin, A., 2005. Liquid-phase oxidation of organic feedstock in a compact multichannel reactor. *Industrial $ Engineering Chemistry Research,* 44(25), pp. 9683-9690.

Plumb, K., 2005. Continuous processing in the pharmaceutical industry: changing the mind set. *Chemical Engineering Research and Design,* 83(6), pp. 730-738.

Poe, S.L., Cummings, M.A., Haaf, M.P. & McQuade, D.T., 2006. Solving the Clogging Problem: Precipitate-Forming Reactions in Flow. *Angewandte Chemie International Edition,* 45(10), pp. 1544-1548.

Poechlauer, P., Colberg, J., Fisher, E., Jansen, M., Johnson, M.D., Koenig, S.G., Lawler, M.J., LaPorte, T., Manley, J.B. & Martin, B., 2013. Pharmaceutical roundtable study demonstrates value of continuous manufacturing in the design of greener processes. *Organic Process Research & Development*.

Ramani, A., M. Chanda, B., Velu, S. & Sivasanker, S., 1999. One-pot synthesis of coumarins . Catalysis by the solid base, calcined Mg-Al hydrotalcite. *Green Chemistry,* 1(3), pp. 163-165.

Razzaq, T., Glasnov, T.N. & Kappe, C.O., 2009a. Accessing Novel Process Windows in a High-Temperature/Pressure Capillary Flow Reactor. *Chemical Engineering & Technology,* 32(11), pp. 1702-1716.

Razzaq, T., Glasnov, T.N. & Kappe, C.O., 2009b. Continuous-Flow Microreactor Chemistry under High-Temperature/Pressure Conditions. *European Journal of Organic Chemistry,* 2009(9), pp. 1321-1325.

Rencurosi, A., Riva, E., Gagliardi, S., Martinelli, M., Passarella, D. & Vigo, D., 2010. Reaction of Grignard reagents with carbonyl compounds under continuous flow conditions. *Tetrahedron,* 66(17), pp. 3242-3247.

Renken, A., Hessel, V., Löb, P., Miszczuk, R., Uerdingen, M. & Kiwi-Minsker, L., 2007. Ionic liquid synthesis in a microstructured reactor for process intensification. *Chemical Engineering and Processing: Process Intensification,* 46(9), pp. 840-845.

Roberge, D.M., Ducry, L., Bieler, N., Cretton, P. & Zimmermann, B., 2005. Microreactor technology: a revolution for the fine chemical and pharmaceutical industries? *Chemical Engineering & Technology,* 28(3), pp. 318-323.

Roberge, D.M., Zimmermann, B., Rainone, F., Gottsponer, M., Eyholzer, M. & Kockmann, N., 2008. Microreactor technology and continuous processes in the fine chemical and pharmaceutical industry: Is the revolution underway? *Organic Process Research & Development,* 12(5), pp. 905-910.

Rodriguez, I., Spicar-Mihalic, P., Kuyper, C.L., Fiorini, G.S. & Chiu, D.T., 2003. Rapid prototyping of glass microchannels. *Analytica Chimica Acta,* 496(1–2), pp. 205-215.

Roe, A. & Montgomery, J.A., 1953. Kinetics of the Catalytic Hydrogenation of Certain Schiff Bases1. *Journal of the American Chemical Society,* 75(4), pp. 910-912.

Rouge, A., Spoetzl, B., Gebauer, K., Schenk, R. & Renken, A., 2001. Microchannel reactors for fast periodic operation: the catalytic dehydration of isopropanol. *Chemical Engineering Science,* 56(4), pp. 1419-1427.

Roy, D., Jaganathan, R. & Chaudhari, R.V., 2005. Kinetic modeling of reductive alkylation of aniline with acetone using Pd/Al2O3 catalyst in a batch slurry reactor. *Industrial & Engineering Chemistry Research,* 44(14), pp. 5388-5396.

Rylander, P.N., 1967. *Catalytic hydrogenation over platinum metals.* Academic Press.

Saaby, S., Knudsen, K.R., Ladlow, M. & Ley, S.V., 2005. The use of a continuous flow-reactor employing a mixed hydrogen-liquid flow stream for the efficient reduction of imines to amines. *Chemical Communications,* (23), pp. 2909-2911.

Salmi, T., Lehtonen, J., Kaplin, J., Vuori, A., Tirronen, E. & Haario, H., 1999. A homogeneous-heterogeneously catalysed reaction system in a loop reactor. *Catalysis Today,* 48(1), pp. 139-145.

Salvatore, R.N., Yoon, C.H. & Jung, K.W., 2001. Synthesis of secondary amines. *Tetrahedron,* 57(37), pp. 7785-7811.

Sands, M., Haswell, S., Kelly, S., Skelton, V., Morgan, D., Styring, P. & Warrington, B., 2001. The investigation of an equilibrium dependent reaction for the formation of enamines in a microchemical system. *Lab on a Chip,* 1(1), pp. 64-65.

Santamaría, J., de la Iglesia, O., Sebastián, V., Mallada, R., Nikolaidis, G., Coronas, J., Kolb, G., Zapf, R. & Hessel, V., 2007. Preparation of Pt/ZSM-5 films on stainless steel microreactors. *Catalysis Today,* 125(1–2), pp. 2-10.

Satterfield, C.N., 1981. *Mass transfer in heterogeneous catalysis.* RE Krieger Publishing Company.

Saunders, J., 2000. *Top drugs: top synthetic routes.* Oxford University Press.

Schaber, S.D., Gerogiorgis, D.I., Ramachandran, R., Evans, J.M., Barton, P.I. & Trout, B.L., 2011. Economic analysis of integrated continuous and batch pharmaceutical manufacturing: a case study. *Industrial & Engineering Chemistry Research,* 50(17), pp. 10083-10092.

Schaefer, M., Stach, E. & Foitzik, A., 2006. Computer Controlled Chemical Micro-Reactor. *Journal of Physics: Conference Series,* 28(1), p. 115.

Schubert, K., Bier, W., Linder, G. & Seidel, D., 1989. Production and Testing of Compact Micro Heat Exchangers. *Chem. Ing. Tech,* 61(2), pp. 172-173.

Schudel, B.R., Choi, C.J., Cunningham, B.T. & Kenis, P.J.A., 2009. Microfluidic chip for combinatorial mixing and screening of assays. *Lab on a Chip,* 9(12), pp. 1676-1680.

Schwalbe, T., Autze, V., Hohmann, M. & Stirner, W., 2004. Novel innovation systems for a cellular approach to continuous process chemistry from discovery to market. *Organic Process Research & Development,* 8(3), pp. 440-454.

Scott, J.L. & Raston, C.L., 2000. Solvent-free synthesis of 3-carboxycoumarins. *Green Chemistry,* 2(5), pp. 245-247.

Sedelmeier, J.r., Ley, S.V., Baxendale, I.R. & Baumann, M., 2010. $KMnO_4$-mediated oxidation as a continuous flow process. *Organic Letters,* 12(16), pp. 3618-3621.

Seeberger, P.H., Gustafsson, T. & Gilmour, R., 2008. Fluorination reactions in microreactors. *Chemical Communications,* (26), pp. 3022-3024.

Shen, J., Zhao, Y., Chen, G. & Yuan, Q., 2009. Investigation of Nitration Processes of *iso*-Octanol with Mixed Acid in a Microreactor. *Chinese Journal of Chemical Engineering,* 17(3), pp. 412-418.

Shintani, Y., Hirako, K., Motokawa, M., Takano, Y., Furuno, M., Minakuchi, H. & Ueda, M., 2004. Polydimethylsiloxane Connection for Quartz Microchips in a High-Pressure System. *Analytical Sciences,* 20(12), pp. 1721-1723.

Simakova, I.L., Solkina, Y., Deliy, I., Wärnå, J. & Murzin, D.Y., 2009. Modeling of kinetics and stereoselectivity in liquid-phase α-pinene hydrogenation over Pd/C. *Applied Catalysis A: General,* 356(2), pp. 216-224.

Simerska, P., Lu, H. & Toth, I., 2009. Synthesis of a *Streptococcus pyogenes* vaccine candidate based on the M protein PL1 epitope. *Bioorganic & Medicinal Chemistry Letters,* 19(3), pp. 821-824.

Singh, R.K., Sinha, N., Jain, S., Salman, M., Naqvi, F. & Anand, N., 2005. A convenient and new approach to the synthesis of w-heterocyclic amino acids from carboxy lactams through ring-chain-transformation. Part 2: Synthesis of (2*R*)-/(2*S*)-2-aminomethyl-3-(1-aryl-/1, 5-diaryl-1*H*-pyrazol-3-yl)-propionic acid. *Tetrahedron,* 61(37), pp. 8868-8874.

Skelton, V., Greenway, G., Haswell, S., Styring, P., Morgan, D., Warrington, B. & Wong, S., 2001a. The generation of concentration gradients using electroosmotic flow in micro reactors allowing stereoselective chemical synthesis. *The Analyst,* 126(1), pp. 11-13.

Skelton, V., Greenway, G., Haswell, S., Styring, P., Morgan, D., Warrington, B. & Wong, S., 2001b. The preparation of a series of nitrostilbene ester compounds using micro reactor technology. *The Analyst,* 126(1), pp. 7-10.

Solomons, T.W.G., 2000. *Organic chemistry.* 7th ed. ed. New York, Wiley

Stitt, E., 2002. Alternative multiphase reactors for fine chemicals: A world beyond stirred tanks? *Chemical Engineering Journal,* 90(1), pp. 47-60.

Szardenings, A.K., Burkoth, T.S., Look, G.C. & Campbell, D.A., 1996. A Reductive Alkylation Procedure Applicable to Both Solution- and Solid-Phase Syntheses of Secondary Amines. *The Journal of Organic Chemistry,* 61(19), pp. 6720-6722.

Tagawa, T., Isobe, M., Tanaka, M. & Yamada, H., 2011. Evaluation of catalyst prepared in microchannel with *in situ* FT-IR microscopy. *Chemical Engineering Journal,* 167(2), pp. 427-430.

Takasuga, M., Yabuki, Y. & Kato, Y., 2006. Pharmaceutical industrial experiments on continuous cryogenic reactions using mini-sized multi-stage reactors. *Journal of Chemical Engineering of Japan,* 39(7), pp. 772-776.

Tiggelaar, R.M., Benito-López, F., Hermes, D.C., Rathgen, H., Egberink, R.J.M., Mugele, F.G., Reinhoudt, D.N., van den Berg, A., Verboom, W. & Gardeniers, H.J.G.E., 2007. Fabrication, mechanical testing and application of high-pressure glass microreactor chips. *Chemical Engineering Journal,* 131(1–3), pp. 163-170.

Toebes, M.L., Alexander Nijhuis, T., Hájek, J., Bitter, J.H., Jos van Dillen, A., Murzin, D.Y. & de Jong, K.P., 2005. Support effects in hydrogenation of cinnamaldehyde over carbon nanofiber-supported platinum catalysts: Kinetic modeling. *Chemical Engineering Science,* 60(21), pp. 5682-5695.

Trachsel, F., Hutter, C. & von Rohr, P.R., 2008. Transparent silicon/glass microreactor for high-pressure and high-temperature reactions. *Chemical Engineering Journal,* 135, Supplement 1(0), pp. S309-S316.

Trambouze, P., Van Landeghem, H., Wauquier, J.-P. & Marshall, N., 1988. *Chemical reactors: Design, engineering, operation.* Editions Technip Paris, France.

Trost, B.M. & Fleming, I., 1991. *Comprehensive organic synthesis selectivity, strategy, and efficiency in modern organic chemistry.* 1st ed. ed. Oxford, England

Tucker, J.L., 2006. Green chemistry, a pharmaceutical perspective. *Organic Process Research & Development,* 10(2), pp. 315-319.

Ueno, K., Kim, H.-B. & Kitamura, N., 2003a. Characteristic Electrochemical Responses of Polymer Microchannel−Microelectrode Chips. *Analytical Chemistry,* 75(9), pp. 2086-2091.

Ueno, M., Hisamoto, H., Kitamori, T. & Kobayashi, S., 2003b. Phase-transfer alkylation reactions using microreactors. *Chemical Communications,* 2003(8), pp. 936-937.

Unnikrishnan, S., Jansen, H., Berenschot, E., Mogulkoc, B. & Elwenspoek, M., 2009. MEMS within a Swagelok[registered sign]: a new platform for microfluidic devices. *Lab on a Chip,* 9(13), pp. 1966-1969.

Vannice, M.A. & Joyce, W.H., 2005. *Kinetics of catalytic reactions.* Springer.

Verboom, W., 2009. Selected Examples of High-Pressure Reactions in Glass Microreactors. *Chemical Engineering & Technology,* 32(11), pp. 1695-1701.

Veser, G., 2001. Experimental and theoretical investigation of H2 oxidation in a high-temperature catalytic microreactor. *Chemical Engineering Science,* 56(4), pp. 1265-1273.

Wakchaure, V.N., Mohanty, R.R., Shaikh, A.J. & Nugent, T.C., 2007. A One-Pot Asymmetric Sequential Amination-Alkylation of Aldehydes: Expedient Synthesis of Aliphatic Chiral Amines. *European Journal of Organic Chemistry,* 2007(6), pp. 959-964.

Watanabe, Y., Yamashita, M., Mitsudo, T.-a., Tanaka, M. & Takegami, Y., 1974. The selective amination of carbonyl compounds using iron pentacarbonyl. *Tetrahedron Letters,* 15(22), pp. 1879-1880.

Watel, B., 2003. Review of saturated flow boiling in small passages of compact heat-exchangers. *International Journal of Thermal Sciences,* 42(2), pp. 107-140.

Watts, P. & Haswell, S., 2005. The application of micro reactors for organic synthesis. *Chemical Society Reviews,* 34(3), pp. 235-246.

Watts, P., Wiles, C., Haswell, S., Pombo-Villar, E. & Styring, P., 2001. The synthesis of peptides using micro reactors. *Chemical Communications,* 2001(11), pp. 990-991.

Watts, P., Wiles, C., Haswell, S.J. & Pombo-Villar, E., 2004. The application of microreactor technology for the synthesis of 1, 2-azoles. *Organic Process Research & Development,* 8(1), pp. 28-32.

Weisz, P. & Prater, C., 1954. Interpretation of measurements in experimental catalysis. *Advances in Catalysis,* 6, p. 143.

Welch, C.J., Gong, X., Cuff, J., Dolman, S., Nyrop, J., Lin, F. & Rogers, H., 2009. Online Analysis of Flowing Streams Using Microflow HPLC. *Organic Process Research & Development,* 13(5), pp. 1022-1025.

Wie, G. & Honicke, D., 1996. Heterogeneously Catalyzed Gas-Phase Hydrogenation of cis, trans, trans-1, 5, 9-Cyclododecatriene on Palladium Catalysts Having Regular Pore Systems. *Ind. Eng. Chem. Res,* 35(12), pp. 4412-4416.

Wießmeier, G. & Hönicke, D., 1996. Microfabricated components for heterogeneously catalysed reactions. *Journal of Micromechanics and Microengineering,* 6, p. 285.

Wiles, C. & Watts, P., 2011. *Micro reaction technology in organic synthesis.* CRC Press Llc.

Wiles, C. & Watts, P., 2012. Continuous flow reactors: a perspective. *Green Chemistry,* 14(1), pp. 38-54.

Wiles, C. & Watts, P., 2014. Continuous process technology: a tool for sustainable production. *Green Chemistry,* 16(1), pp. 55-62.

Wiles, C., Watts, P., Haswell, S. & Pombo-Villar, E., 2001. The aldol reaction of silyl enol ethers within a micro reactor. *Lab on a Chip,* 1(2), pp. 100-101.

Wiles, C., Watts, P., Haswell, S. & Pombo-Villar, E., 2002. 1, 4-Addition of enolates to , a, b-unsaturated ketones within a micro reactor. *Lab on a Chip,* 2(2), pp. 62-64.

Wiles, C., Watts, P. & Haswell, S.J., 2007. The use of electroosmotic flow as a pumping mechanism for semi-preparative scale continuous flow synthesis. *Chemical Communications,* (9), pp. 966-968.

Wilson, N. & McCreedy, T., 2000. On-chip catalysis using a lithographically fabricated glass microreactor—the dehydration of alcohols using sulfated zirconia. *Chemical Communications,* 2000(9), pp. 733-734.

Wirth, T., 2008. *Microreactors in organic synthesis and catalysis.* Wiley-VCH Verlag GmbH & co. KGaA, Weinheim.

Wirth, T., 2013. *Microreactors in Organic Chemistry and Catalysis.* Wiley. com.

Wootton, R., Fortt, R. & de Mello, A., 2002. A microfabricated nanoreactor for safe, continuous generation and use of singlet oxygen.

Wörz, O., Jäckel, K., Richter, T. & Wolf, A., 2001a. Microreactors-A new efficient tool for reactor development. *Chemical engineering & technology,* 24(2), pp. 138-142.

Wörz, O., Jäckel, K., Richter, T. & Wolf, A., 2001b. Microreactors, a new efficient tool for optimum reactor design. *Chemical Engineering Science,* 56(3), pp. 1029-1033.

Xing, L., Cheng, C., Zhu, R., Zhang, B., Wang, X. & Hu, Y., 2008. Self-modulated highly chemoselective direct-reductive-amination (DRA) of benzaldehydes straightforward to N-monosubstituted benzylamine hydrochlorides. *Tetrahedron,* 64(51), pp. 11783-11788.

Yoon, N., Kim, E., Son, H. & Choi, J., 1993. Borohydride exchange resin, a new reducing agent for reductive amination. *Synthetic Communications,* 23(11), pp. 1595-1599.

Yoon, T.-H., Park, S.-H., Min, K.-I., Zhang, X., Haswell, S.J. & Kim, D.-P., 2008. Novel inorganic polymer derived microreactors for organic microchemistry applications. *Lab on a Chip,* 8(9), pp. 1454-1459.

Yoshida, J.-i., 2008. *Flash chemistry: fast organic synthesis in microsystems.* New York: John Wiley & Sons, Ltd.

Yoshida, J.-i., Nagaki, A. & Yamada, D., 2013. Continuous flow synthesis. *Drug Discovery Today: Technologies,* 10(1), pp. 53-59.

Yoshida, J.i., Nagaki, A. & Yamada, T., 2008. Flash chemistry: fast chemical synthesis by using microreactors. *Chemistry-A European Journal,* 14(25), pp. 7450-7459.

Yoswathananont, N., Nitta, K., Nishiuchi, Y. & Sato, M., 2005. Continuous hydrogenation reactions in a tube reactor packed with Pd/C. *Chemical Communications,* (1), pp. 40-42.

Zhou, W.X. & Chan-Park, M.B., 2005. Large area UV casting using diverse polyacrylates of microchannels separated by high aspect ratio microwalls. *Lab on a Chip,* 5(5), pp. 512-518.

Appendix I

NMR and MS analysis of secondary amines

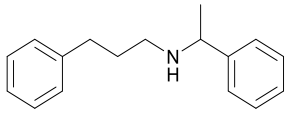

^{1}H NMR (400 MHz, $CDCl_3$): δ = 7.16-7.37 (10H, m, arom.), 3.77 (1H, q, *J* = 6.60 Hz), 2.47-2.71 (4H, m), 1.75-1.93 (2H, m), 1.37 (3H, d, *J* = 6.60 Hz). ^{13}C NMR (100 MHz, CDCl3): δ = 145.88, 142.24, 128.39, 128.36, 128.28, 126.83, 126.56, 125.70, 58.34, 47.39, 33.68, 31.94, 24.36. ESI-MS: calcd. for $C_{17}H_{21}NH^{+}$: 240.18. Found: 240.20 (MH^{+}).

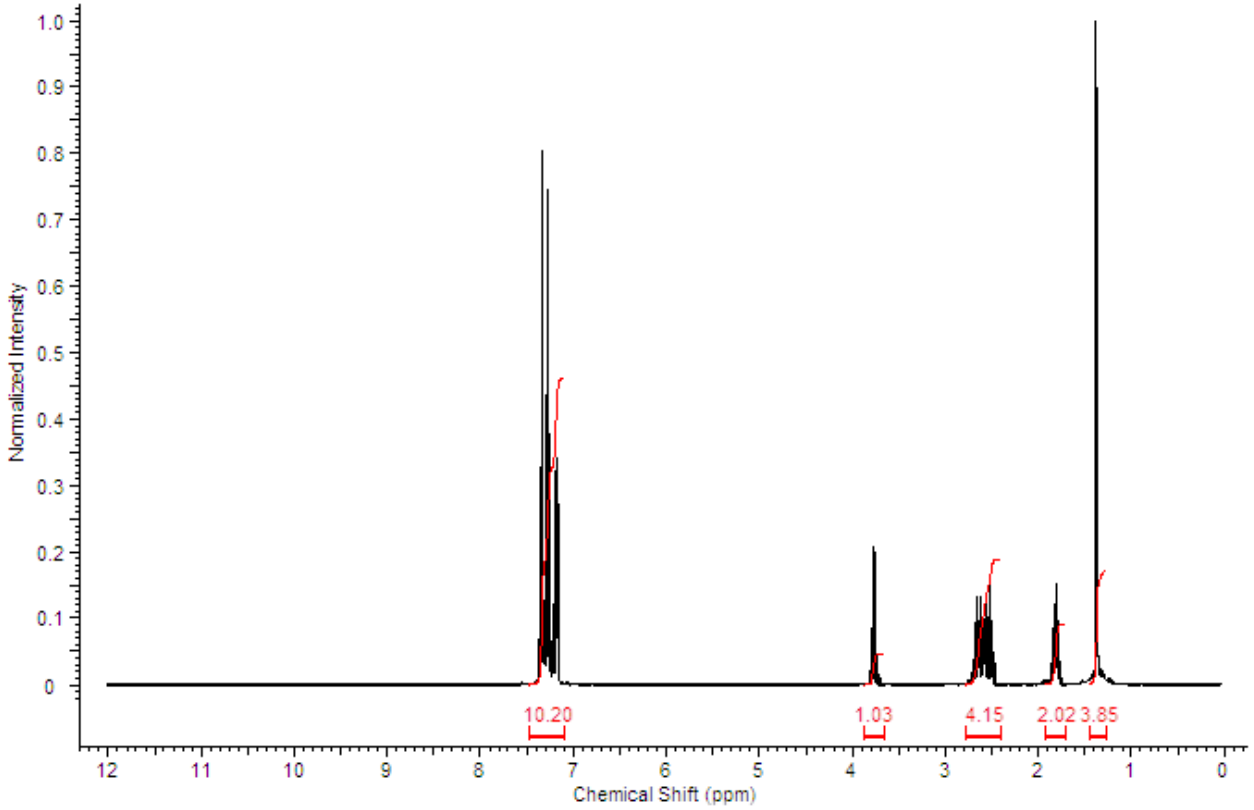

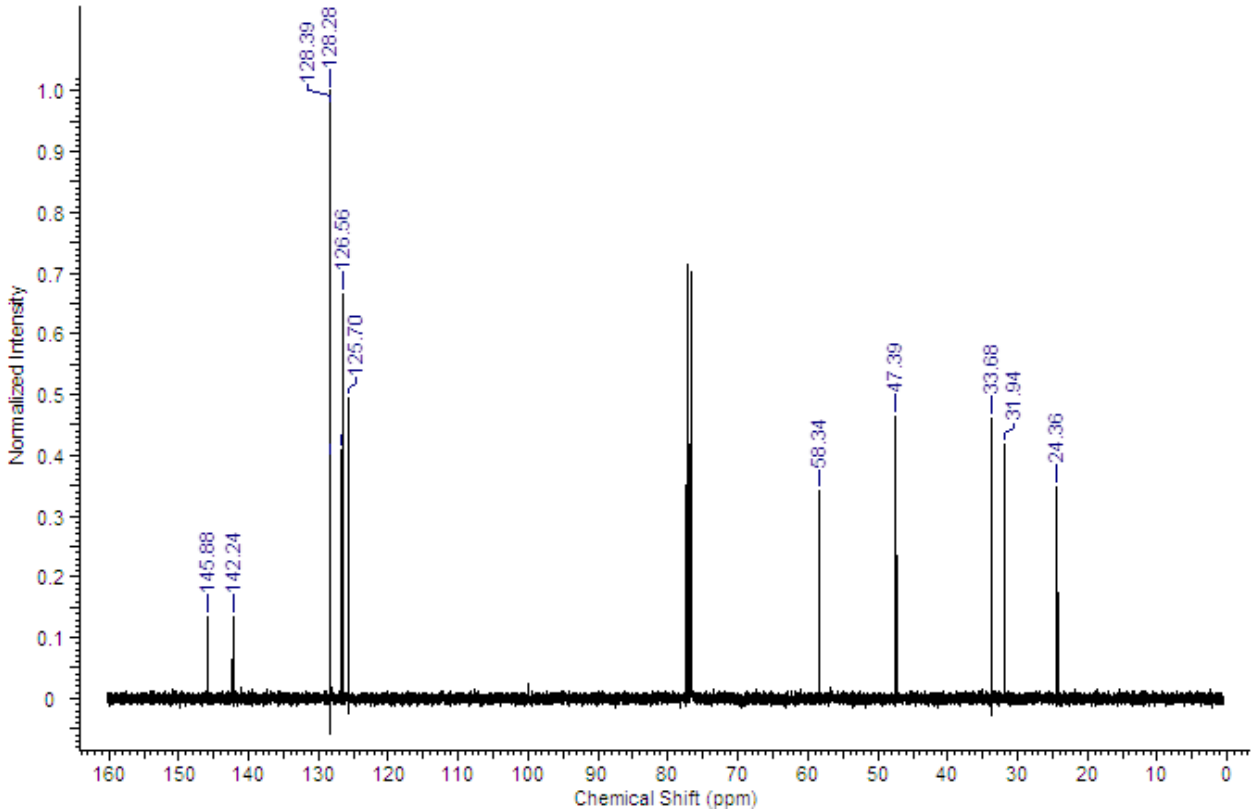
Normalized Intensity
Chemical Shift (ppm)
145.88
142.24
128.39
128.28
126.56
125.70
58.34
47.39
33.68
31.94
24.36

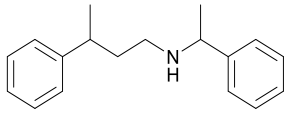

^{1}H NMR (400 MHz, $CDCl_3$): δ = 7.14-7.34 (10H, m, arom.), 3.69 (1H, q, *J* = 6.60 Hz), 2.34-2.59 (3H, m), 1.54-1.86 (2H, m), 1.20-1.51 (6H, m). ^{13}C NMR (100 MHz, $CDCl_3$): δ = 147.40, 145.91, 128.34, 128.32, 126.94, 126.88, 126.51, 125.91, 58.21, 46.10, 38.76, 24.36, 22.25. ESI-MS: calcd. for $C_{18}H_{23}NH^+$: 254.19. Found: 254.20 (MH^+).

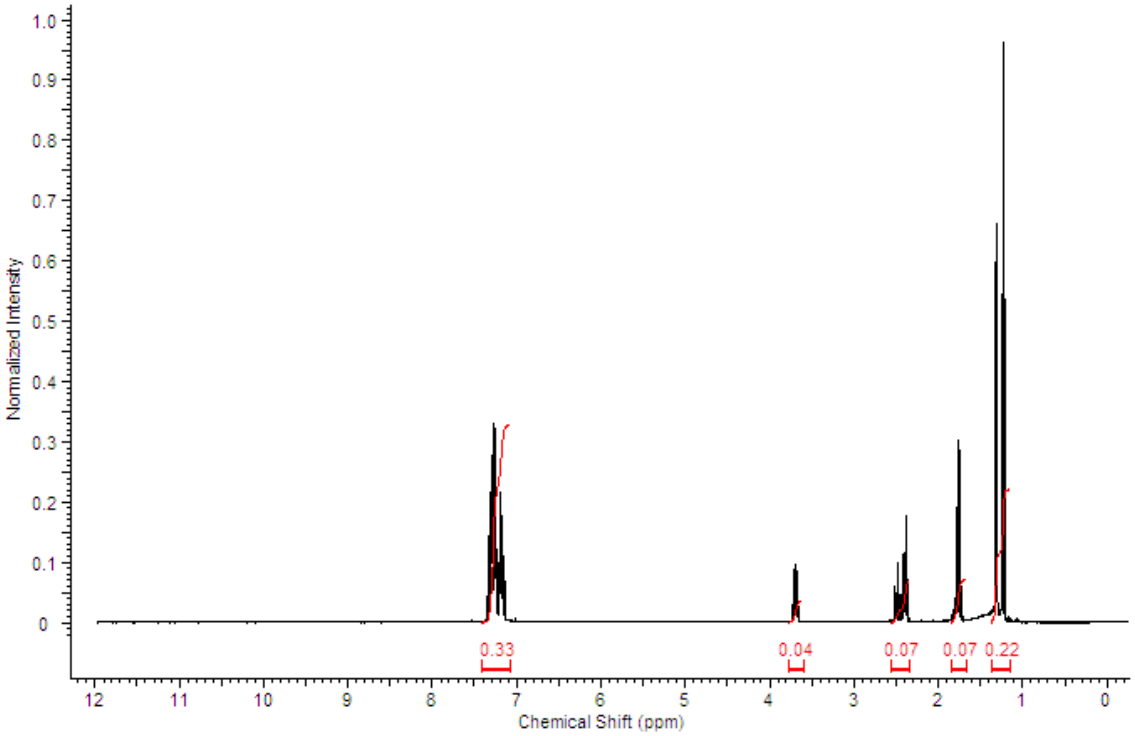

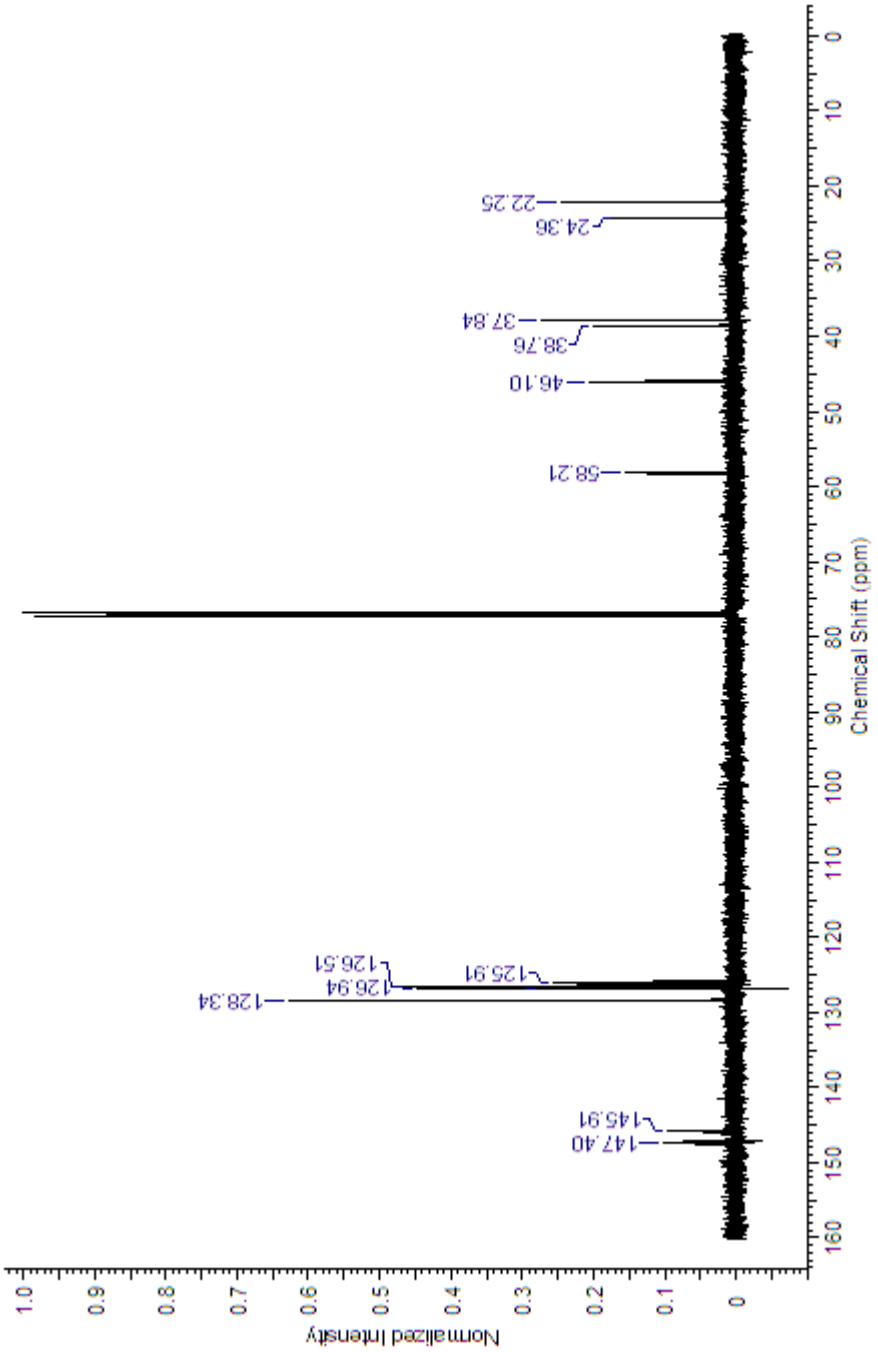
147.40
145.91
128.34
126.94
126.51
125.91
58.21
46.10
38.76
37.84
24.36
22.25
Chemical Shift (ppm)
Normalized Intensity

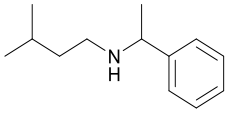

^{1}H NMR (400 MHz, $CDCl_3$): δ = 7.12-7.38 (5H, m, arom.), 3.77 (1H, q, *J* = 6.60 Hz), 2.28-2.57 (2H, m), 1.60 (1H, dq, *J* = 13.39, 6.62 Hz), 1.37 (2H, d, *J* = 6.36 Hz), 1.23 (3H, d, *J* = 6.60 Hz), 0.69-0.93 (6H, m). ^{13}C NMR (100 MHz, $CDCl_3$): δ =145.95, 128.37, 126.78, 126.52, 58.50, 46.00, 39.42, 26.11, 22.82, 22.51. ESI-MS: calcd. for $C_{13}H_{21}NH^+$: 192.18. Found: 192.17 (MH^+).

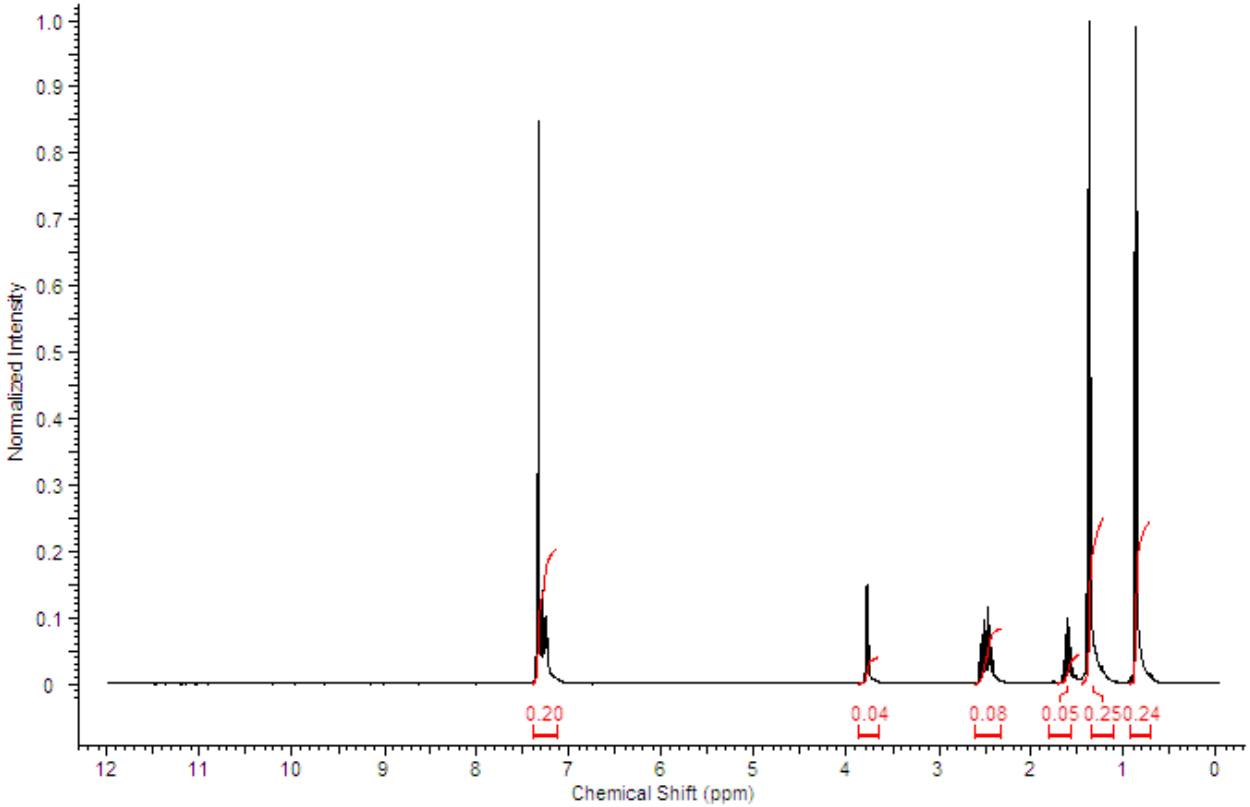

Normalized Intensity
Chemical Shift (ppm)
145.95
128.37
126.52
58.50
46.00
39.42
26.11
22.82
22.51

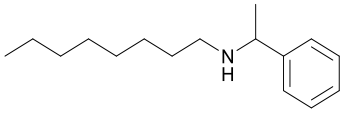

^{1}H NMR (400 MHz, $CDCl_3$): δ = 7.23-7.37 (5H, m, arom.), 3.78 (1H, q, *J* = 6.60 Hz), 2.32-2.62 (2H, m), 1.42-1.57 (2H, m), 1.38 (2H, d, *J* = 6.36 Hz), 1.35 (3H, d, *J* = 6.60 Hz), 1.27 (8H, s), 0.78-0.97 (3H, m). ^{13}C NMR (100 MHz, $CDCl_3$): δ =145.88, 128.38, 126.80, 126.55, 58.42, 47.92, 31.83, 30.29, 29.52, 27.38, 24.34, 22.65, 14.09. ESI-MS: calcd. for $C_{16}H_{27}NH^+$: 234.22. Found: 234.21 (MH^+).

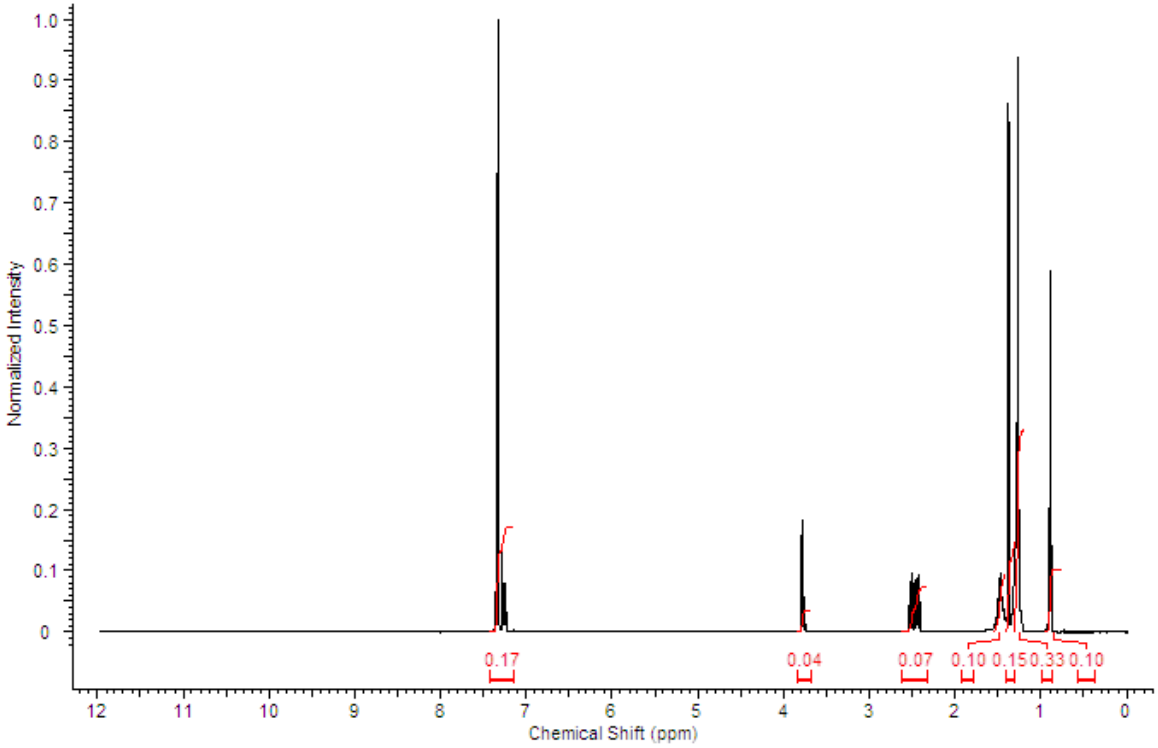

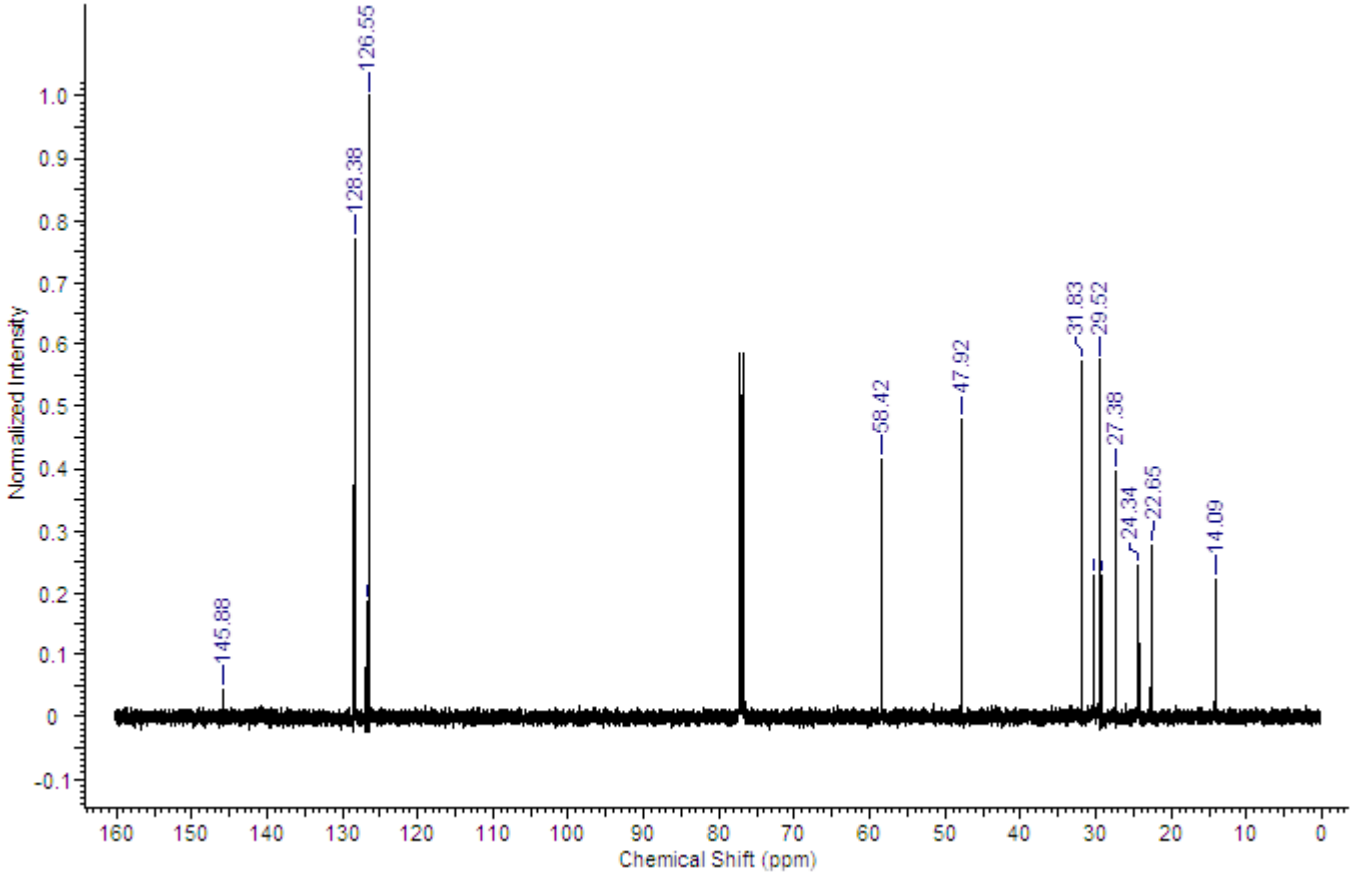
Normalized Intensity
Chemical Shift (ppm)
145.88
128.38
126.55
58.42
47.92
31.83
29.52
27.38
24.34
22.65
14.09

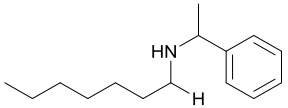

^{1}H NMR (400 MHz, $CDCl_3$): δ = 7.14-7.44 (5H, m, arom.), 3.77 (1H, q, *J* = 6.60 Hz), 2.36-2.55 (2H, m), 1.41-1.55 (2H, m), 1.37 (3H, d, *J* = 6.60 Hz), 1.35 (2H, s), 1.27 (6H, br. s), 0.80-0.93 (3H, m). ^{13}C NMR (100 MHz, CDCl3): δ =145.95, 128.37, 126.54, 58.41, 47.93, 31.82, 30.54, 29.23, 27.34, 22.61, 14.08. ESI-MS: calcd. for $C_{15}H_{25}NH^{+}$: 220.21. Found: 220.20 (MH^{+}).

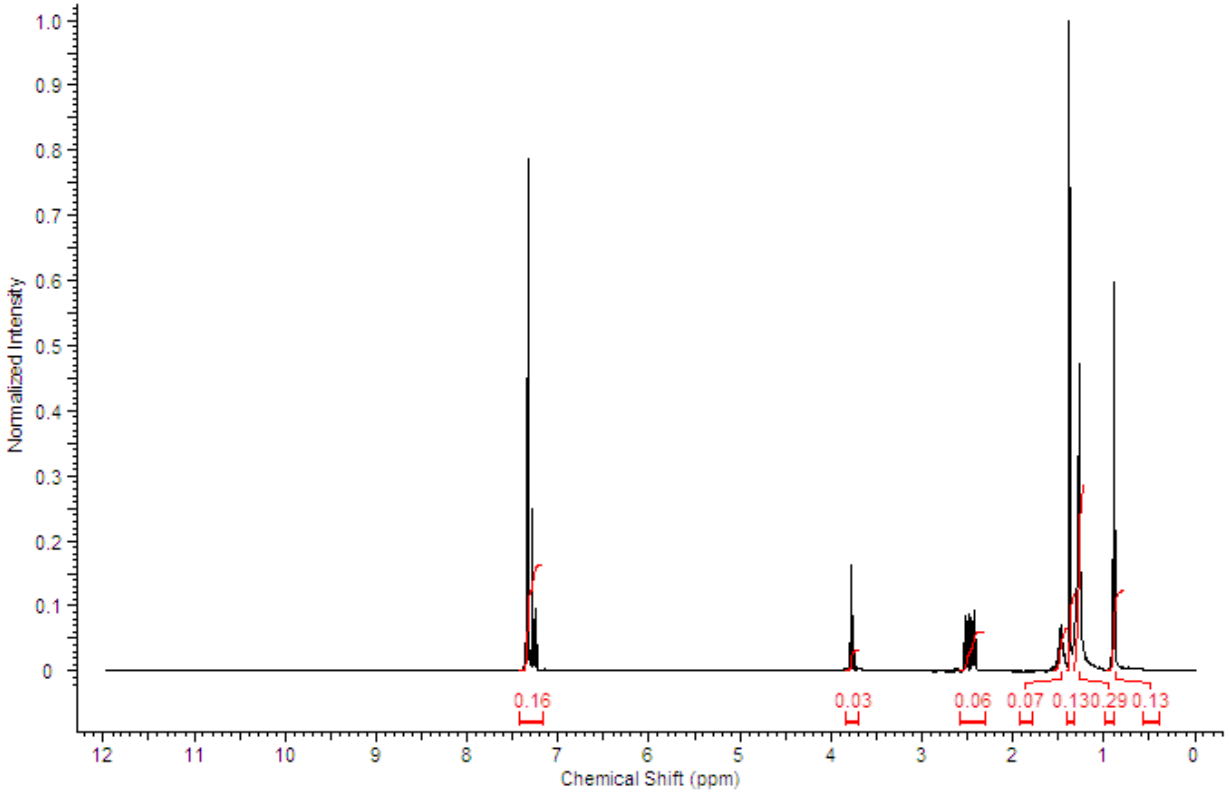

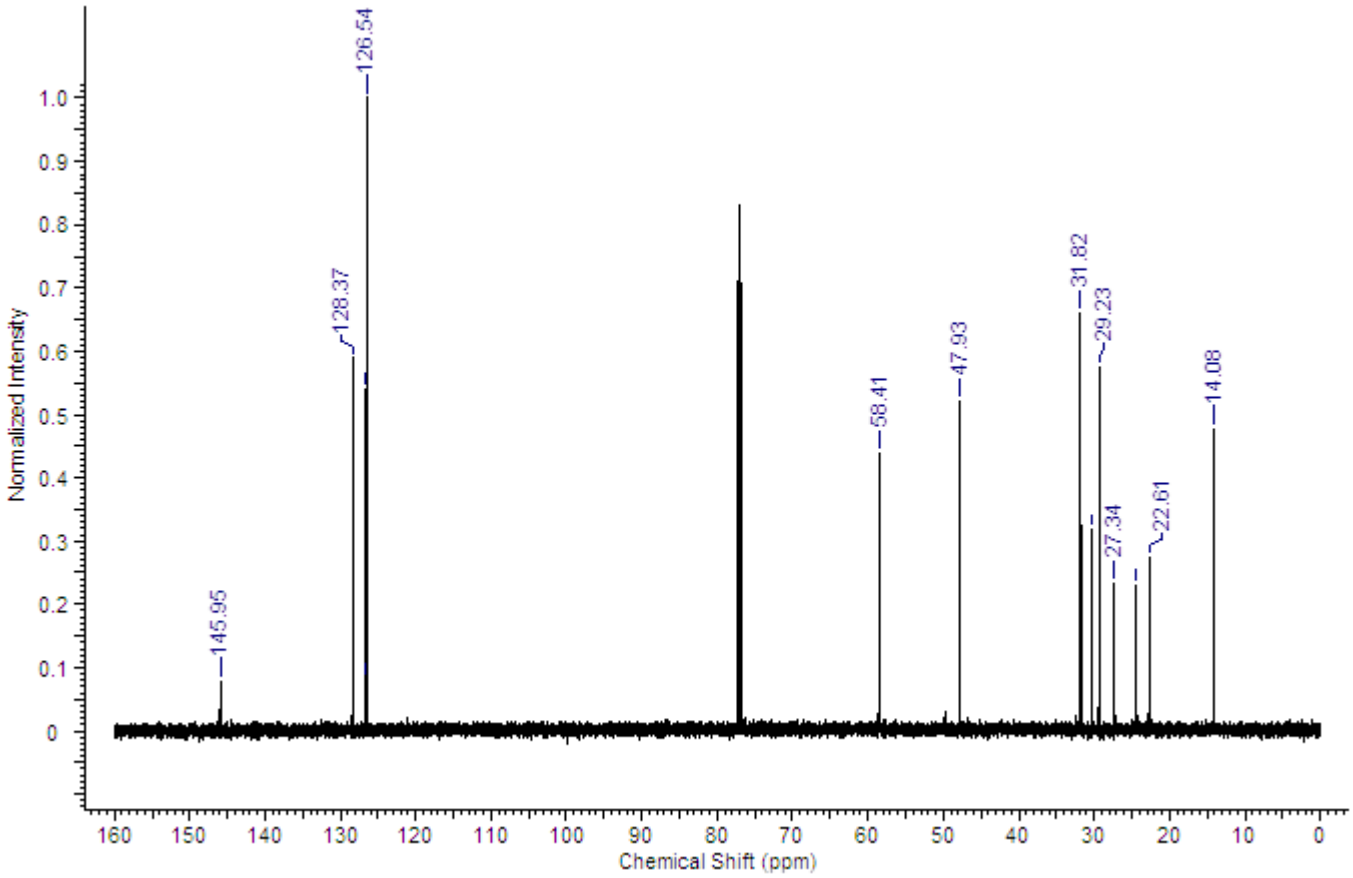
Normalized Intensity
Chemical Shift (ppm)
145.95
128.37
126.54
58.41
47.93
31.82
29.23
27.34
22.61
14.08

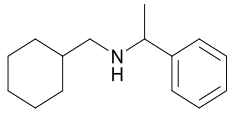

^{1}H NMR (400 MHz, $CDCl_3$): δ = 7.22-7.36 (5H, m, arom.), 3.75 (1H, q, *J* = 6.60 Hz), 2.38-2.55 (2H, m), 1.55-1.80 (2H, m), 1.36 (3H, d, J = 6.60 Hz), 1.10-1.32 (6H, m), 0.81-0.97 (4H, m). ^{13}C NMR (100 MHz, $CDCl_3$): δ =146.13, 128.33, 126.71, 126.55, 58.42, 54.64, 38.21, 31.58, 31.44, 26.71, 26.11, 26.07, 24.55. ESI-MS: calcd. for $C_{15}H_{23}NH^+$: 218.19. Found: 218.18 (MH^+).

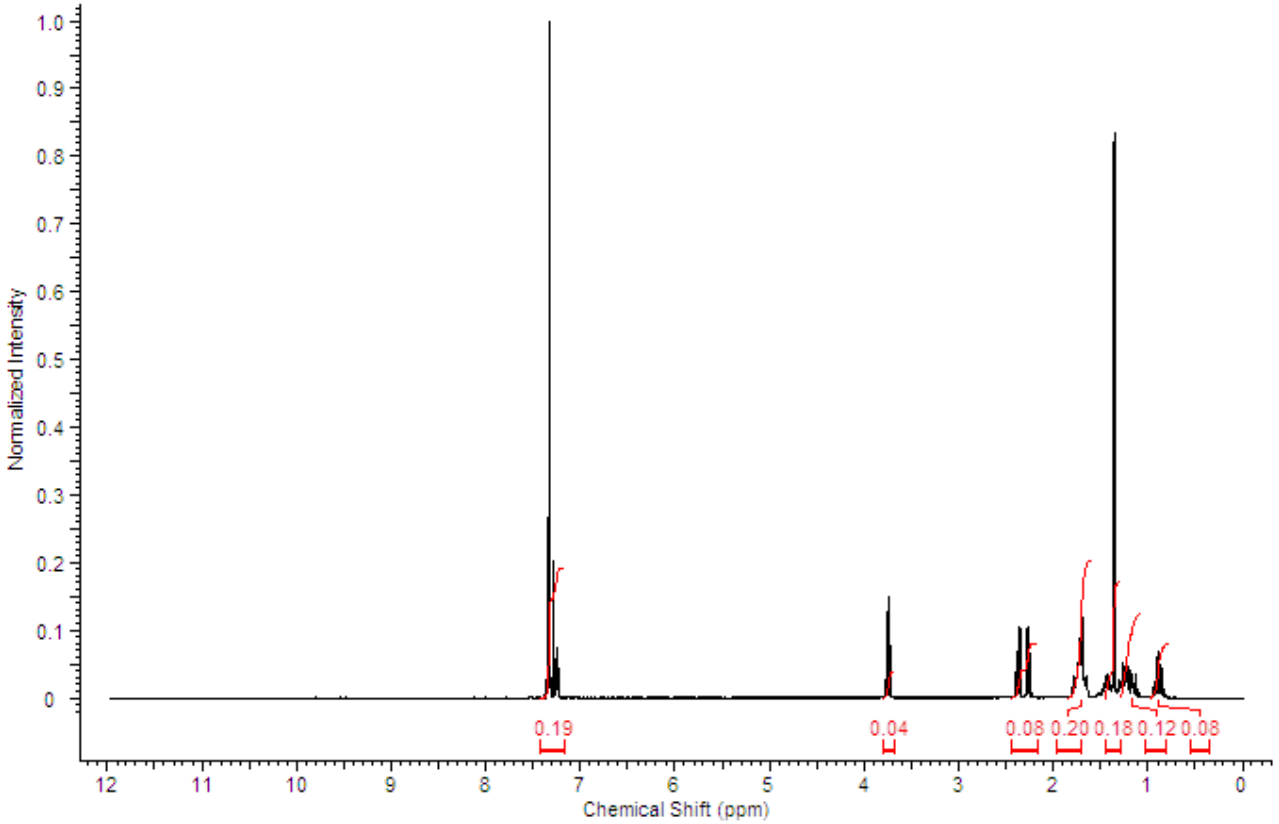

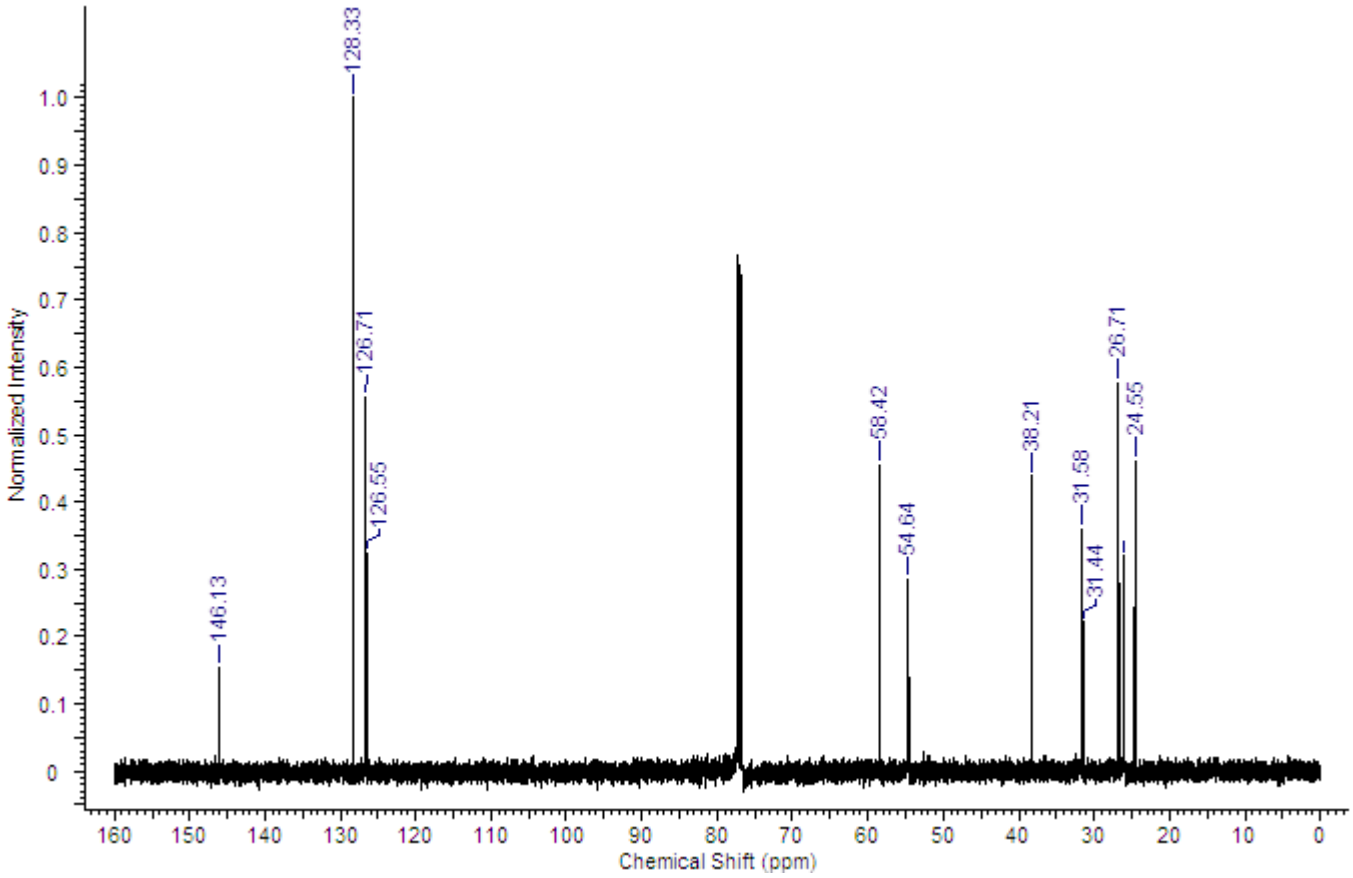
Normalized Intensity
Chemical Shift (ppm)
128.33
126.71
126.55
146.13
58.42
54.64
38.21
31.58
31.44
26.71
24.55

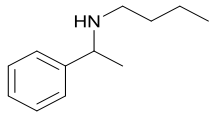

^{1}H NMR (400 MHz, $CDCl_3$): δ = 7.20-7.39 (5H, m, arom.), 3.78 (1H, q, *J* = 6.60 Hz), 2.34-2.64 (2H, m), 1.40-1.51 (2H, m), 1.36 (3H, d, *J* = 6.60 Hz), 1.26-1.34 (2H, m), 0.90 (3H, t, *J* = 7.34 Hz). ^{13}C NMR (100 MHz, $CDCl_3$): δ = 145.97, 128.37, 126.77, 126.53, 58.42, 47.60, 32.46, 24.39, 20.50, 14.00. ESI-MS: calcd. for $C_{12}H_{19}NH^+$: 178.16. Found: 178.15 (MH^+).

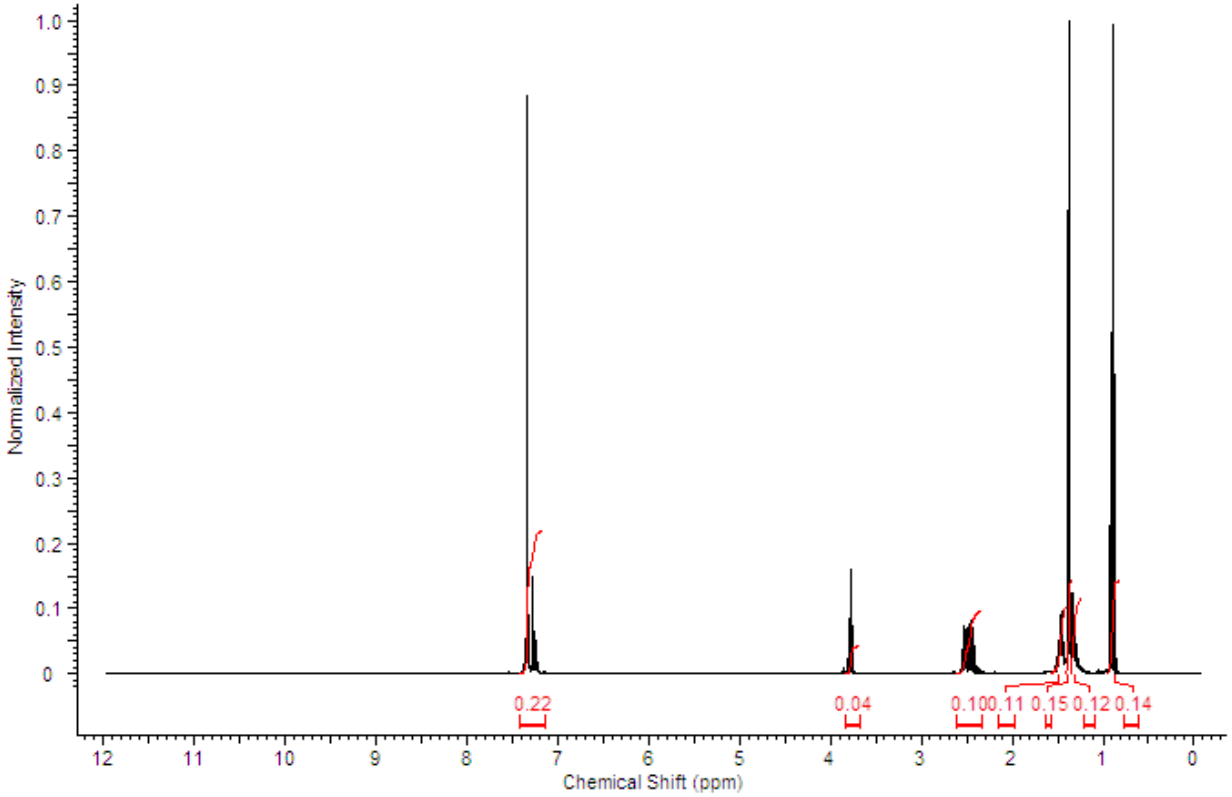

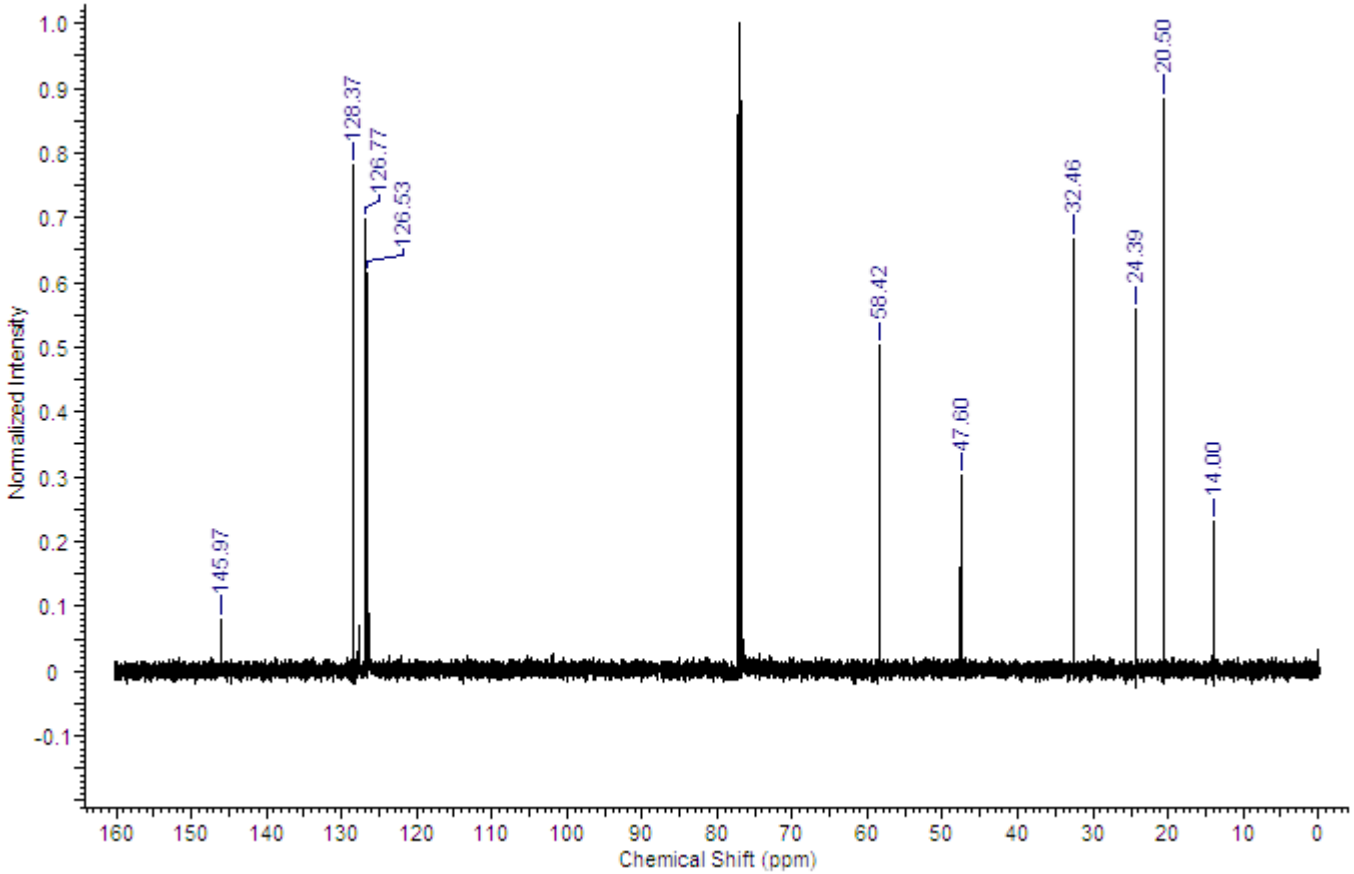
Normalized Intensity
Chemical Shift (ppm)
145.97
128.37
126.77
126.53
58.42
47.60
32.46
24.39
20.50
14.00

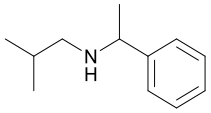

^{1}H NMR (400 MHz, $CDCl_3$): δ = 7.18-7.40 (5H, m, arom.), 3.76 (1H, q, *J* = 6.60 Hz), 2.31-2.43 (1H, m), 2.24 (1H, s), 1.72 (1H, s), 1.38 (3H, d, *J* = 6.60 Hz), 0.78-0.99 (6H, m). ^{13}C NMR (100 MHz, $CDCl_3$): δ = 146.14, 128.33, 126.72, 126.56, 58.38, 55.91, 28.52, 24.56, 20.63. ESI-MS: calcd. for $C_{12}H_{19}NH^+$: 178.16. Found: 178.15 (MH^+).

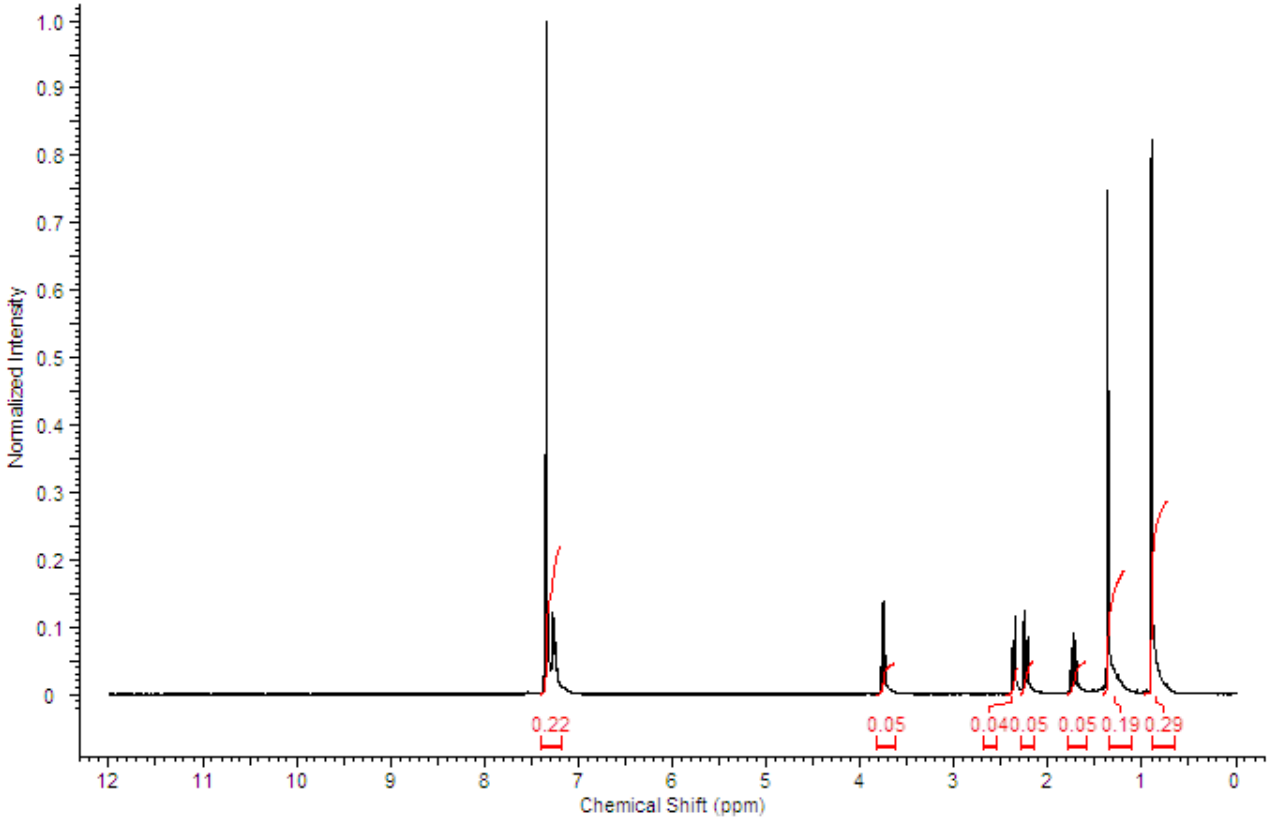

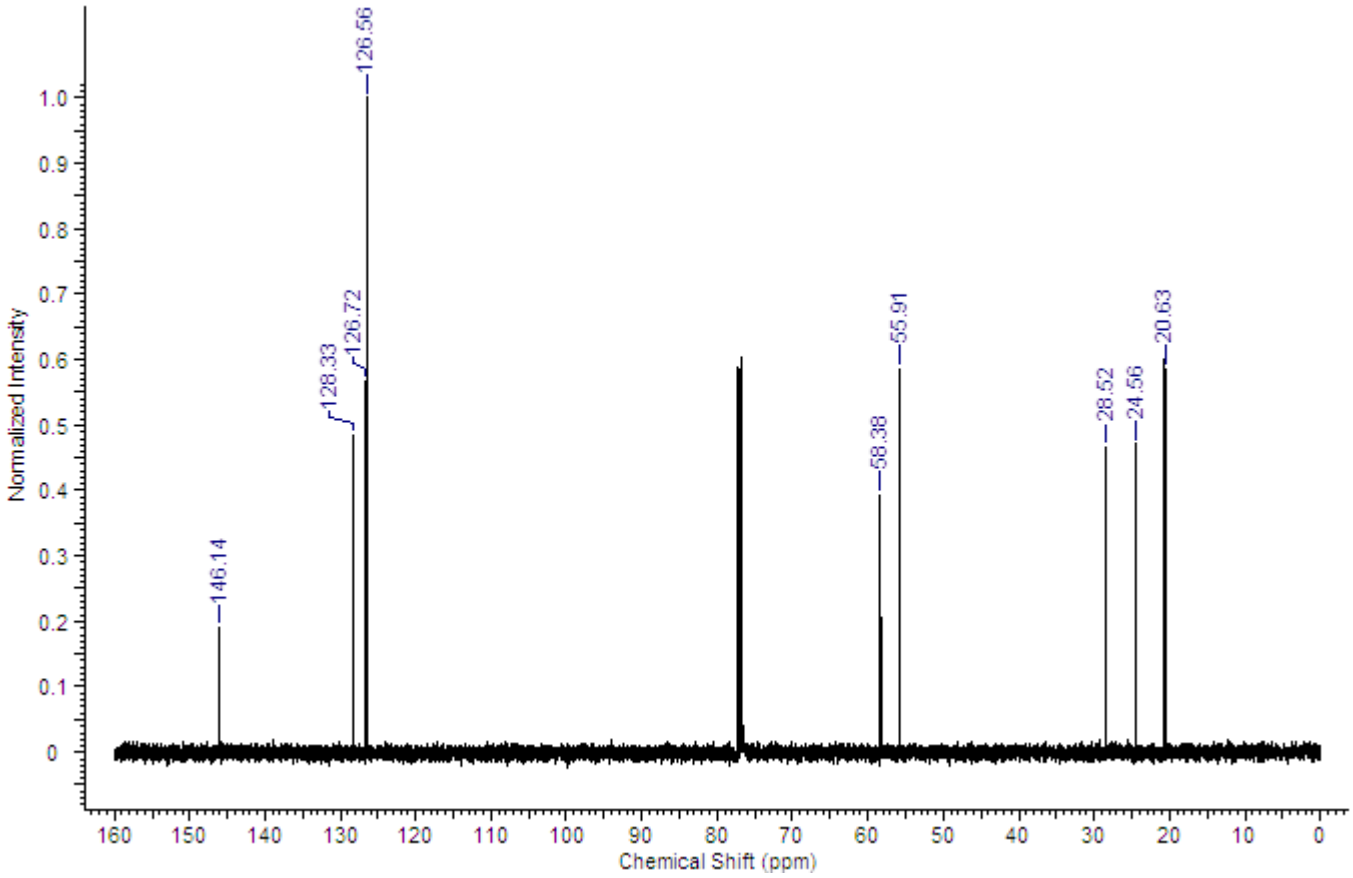
Normalized Intensity
Chemical Shift (ppm)
146.14
128.33
126.72
126.56
58.38
55.91
28.52
24.56
20.63

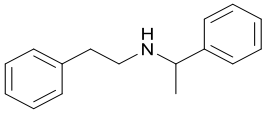

^{1}H NMR (400 MHz, $CDCl_3$): δ = 7.10-7.40 (10H, m, arom.), 3.80 (1H, q, *J* = 6.60 Hz), 2.69-3.00 (4H, m), 1.35 (3H, d, *J* = 6.60 Hz). ^{13}C NMR (100 MHz, $CDCl_3$): δ = 145.64, 140.10, 128.69, 128.41, 127.96, 127.03, 126.54, 126.08, 58.21, 48.94, 36.47, 24.33. ESI-MS: calcd. for $C_{16}H_{19}NH^+$: 226.16. Found: 226.15 (MH^+).

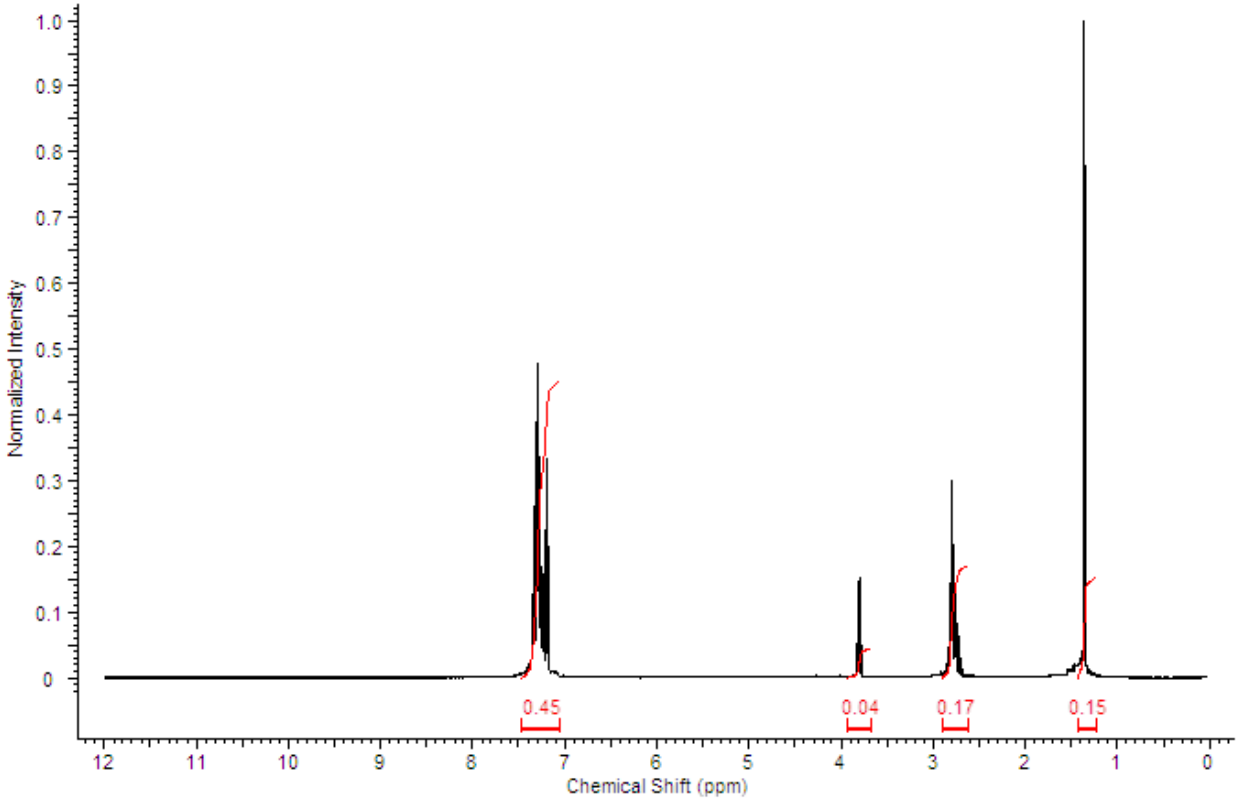

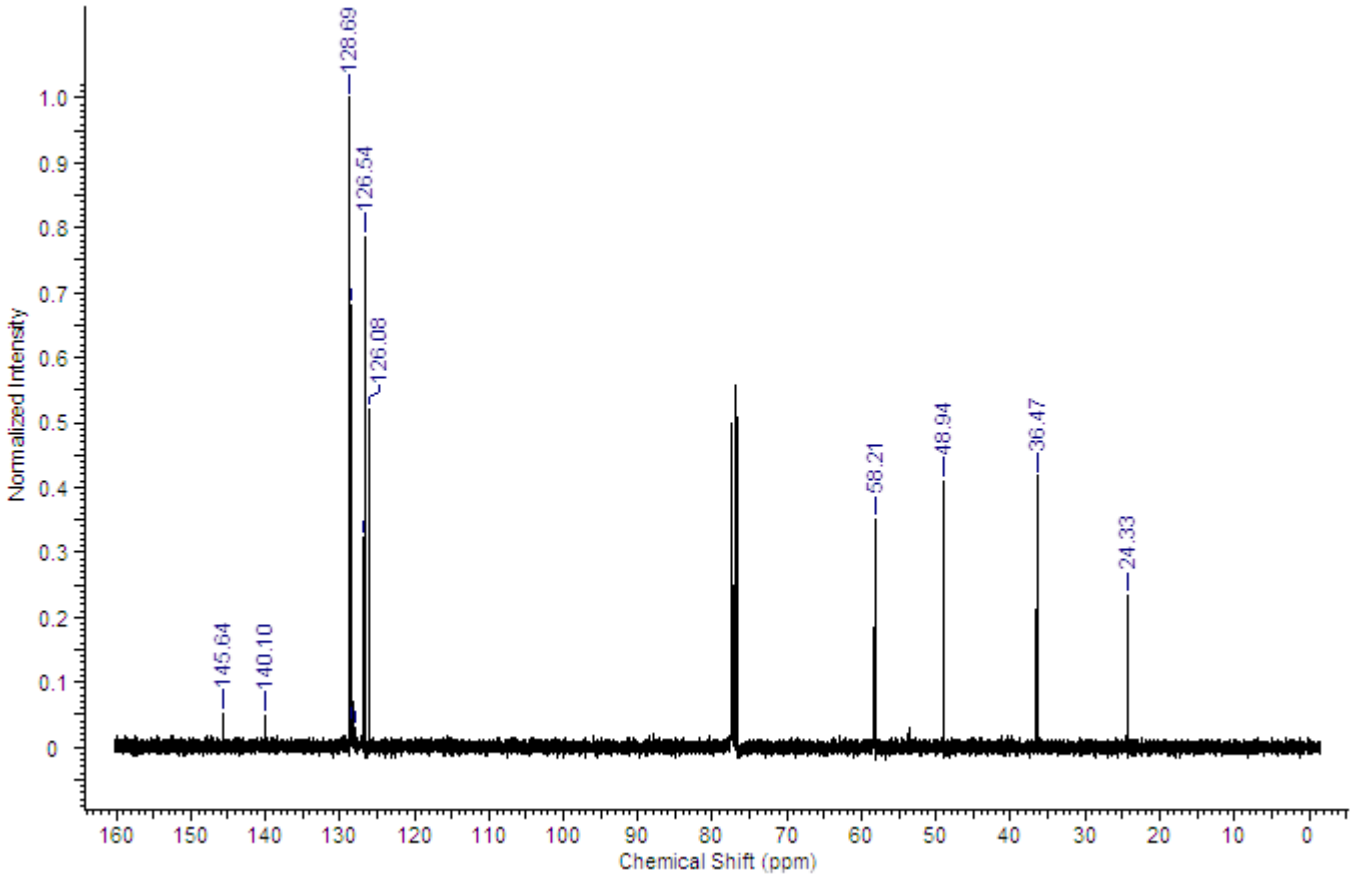
128.69
126.54
126.08
145.64
140.10
58.21
48.94
36.47
24.33
Normalized Intensity
Chemical Shift (ppm)

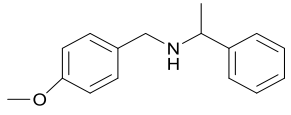

^{1}H NMR (400 MHz, $CDCl_3$): δ = 7.20-7.38 (7H, m, arom.), 6.85-7.02 (2H, m), 3.83-3.85 (2H, m), 3.82 (3H, s), 3.66 (1H, q, *J* = 6.60 Hz), 1.89 (1H, br. s), 1.38 (3H, d, *J* = 6.60Hz). ^{13}C NMR (100 MHz, $CDCl_3$): δ = 158.57, 145.68, 132.85, 129.28, 128.45, 126.89, 126.71, 113.77, 57.41, 55.28, 51.05, 24.50. ESI-MS: calcd. for $C_{16}H_{19}NH^{+}$: 242.15. Found: 242.15 (MH^{+}).

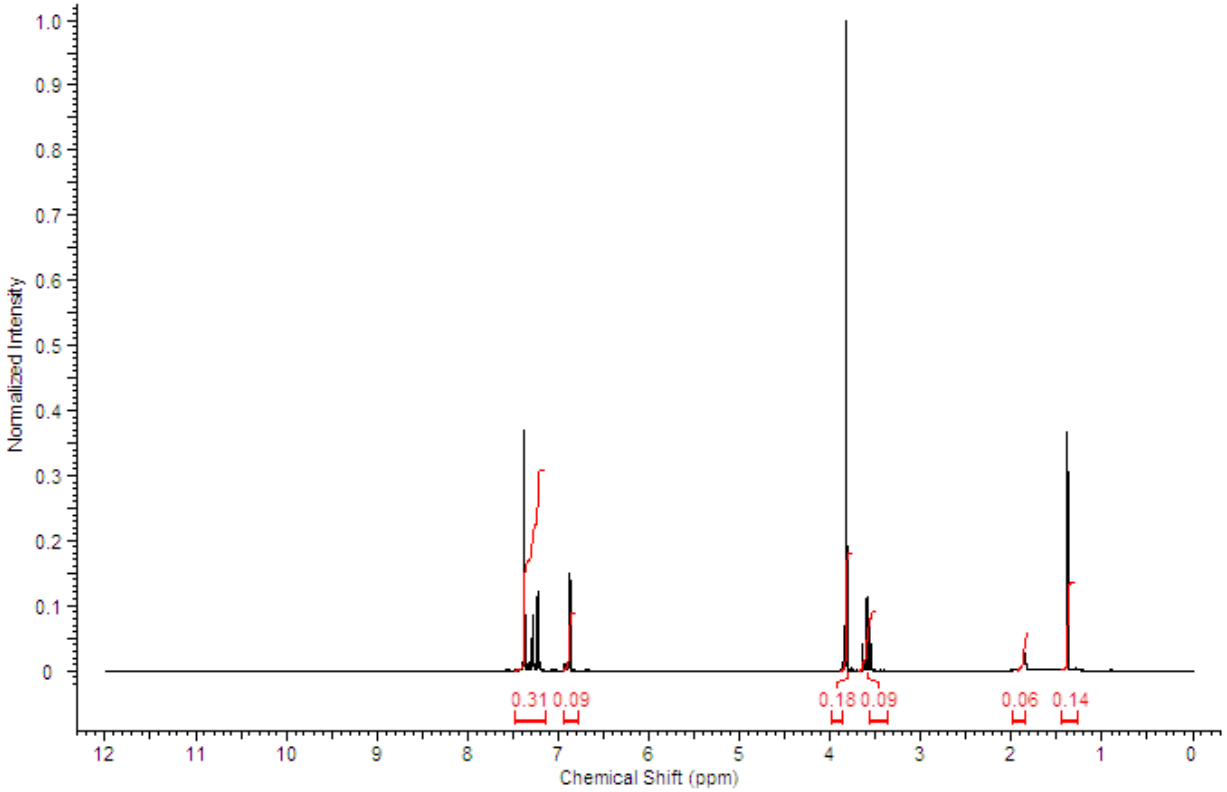

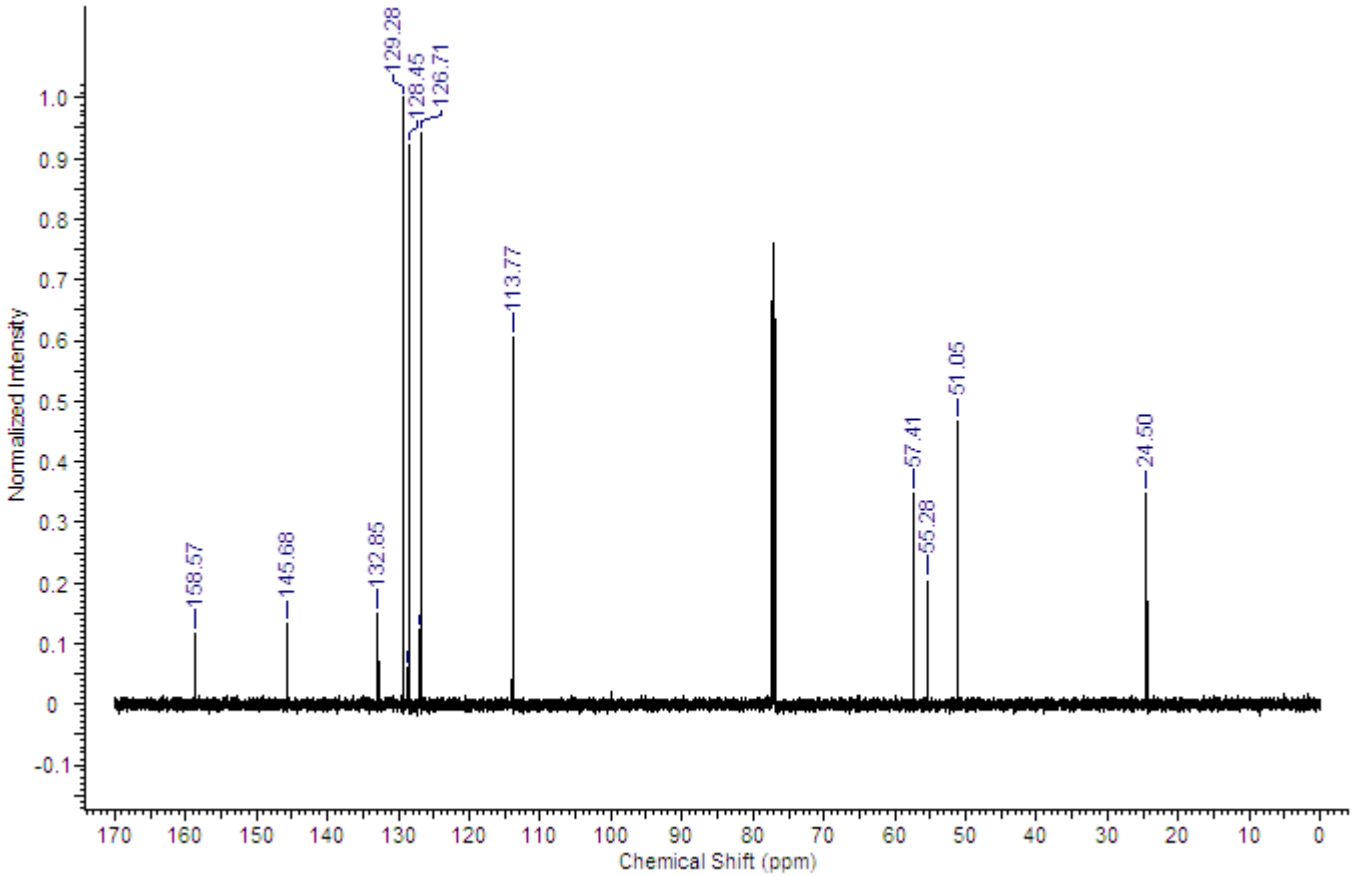
Normalized Intensity
Chemical Shift (ppm)
158.57
145.68
132.85
129.28
128.45
126.71
113.77
57.41
55.28
51.05
24.50

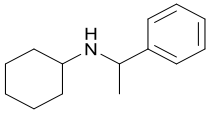

^{1}H NMR (400 MHz, $CDCl_3$): δ = 7.23-7.36 (5H, m, arom.), 3.98 (1H, q, *J* = 6.60 Hz), 2.30-2.34 (1H, m), 1.87-2.04 (2H, m), 1.67-1.74 (1H, m), 1.52 (1H, br. s), 1.36 (3H, d, *J* = 6.60Hz), 1.09-1.15 (3H, m). ^{13}C NMR (100 MHz, $CDCl_3$): δ = 146.26, 128.37, 126.48, 54.46, 53.65, 34.53, 33.19, 26.18, 25.23, 24.95.. ESI-MS: calcd. for $C_{14}H_{21}NH^+$: 204.18. Found: 204.17 (MH^+).

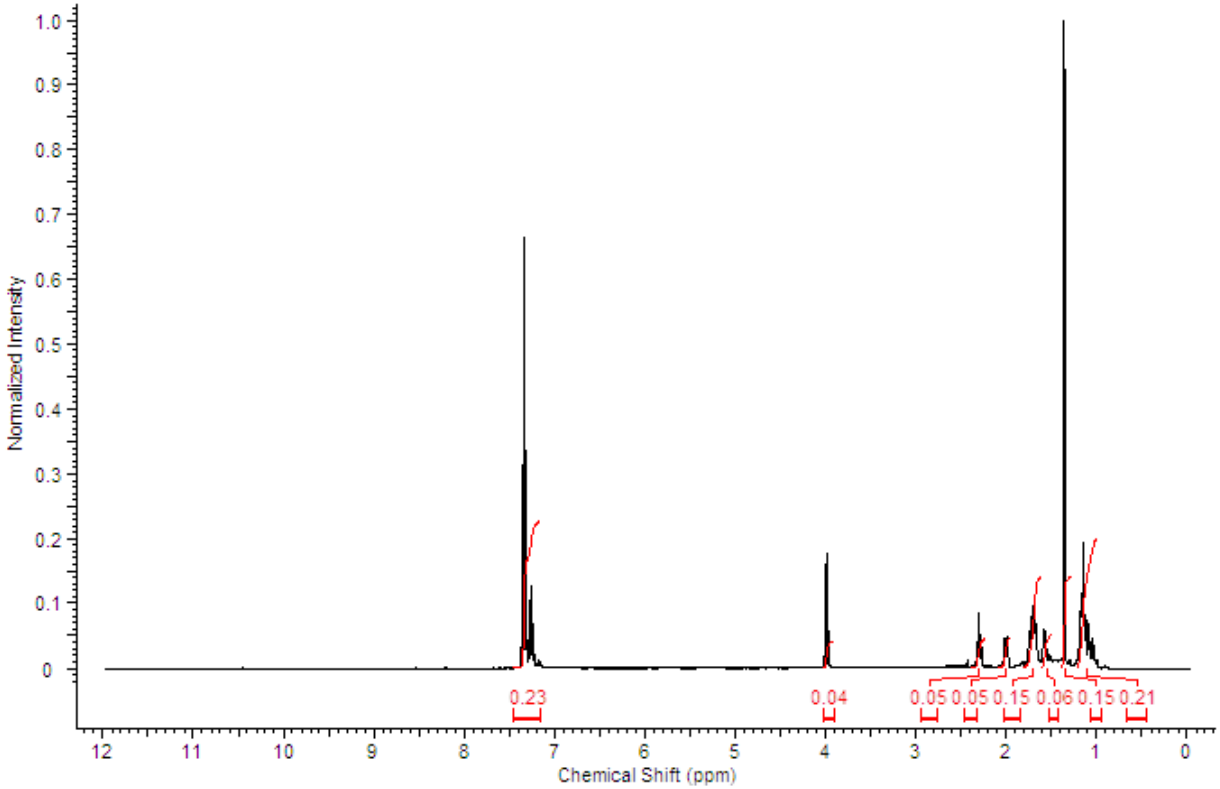

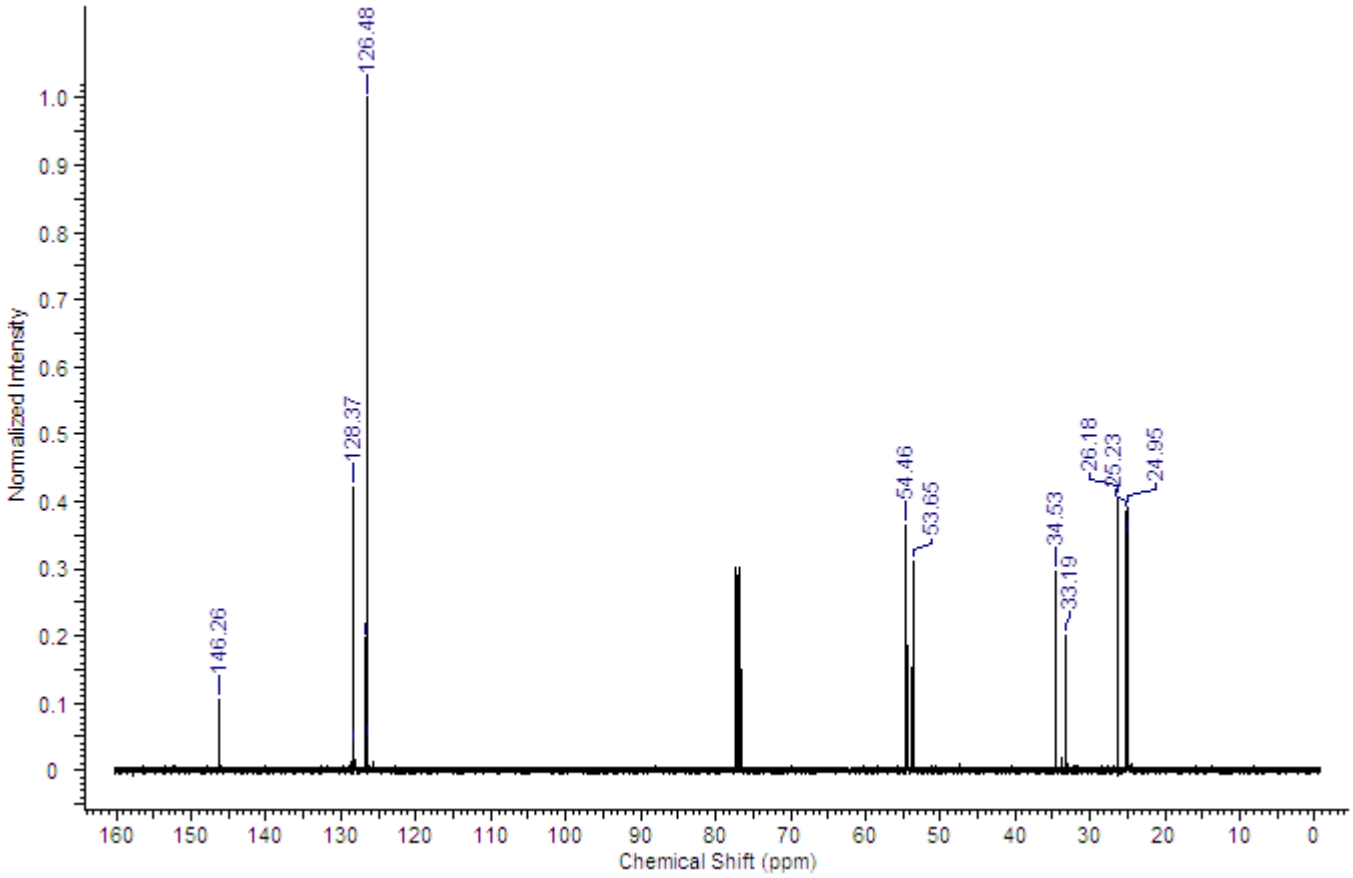
Normalized Intensity
Chemical Shift (ppm)
126.48
128.37
146.26
54.46
53.65
34.53
33.19
26.18
25.23
24.95

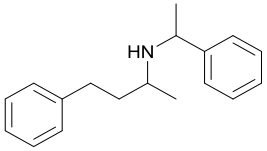

^{1}H NMR (400 MHz, $CDCl_3$): δ = 7.09-7.46 (10H, m, arom.), 4.14 (1H, q, *J* = 6.60 Hz), 2.87-3.04 (1H, m), 2.57-2.79 (2H, m), 1.60-1.77 (2H, m), 1.41 (3H, d, *J* = 6.60Hz), 1.09-1.15 (3H, m). ^{13}C NMR (100 MHz, $CDCl_3$): δ = 147.83, 142.33, 128.48, 128.36, 128.33, 126.79, 125.67, 51.35, 46.58, 41.88, 32.86, 25.71, 24.07. ESI-MS: calcd. for $C_{18}H_{23}NH^+$: 254.19. Found: 254.18 (MH^+).

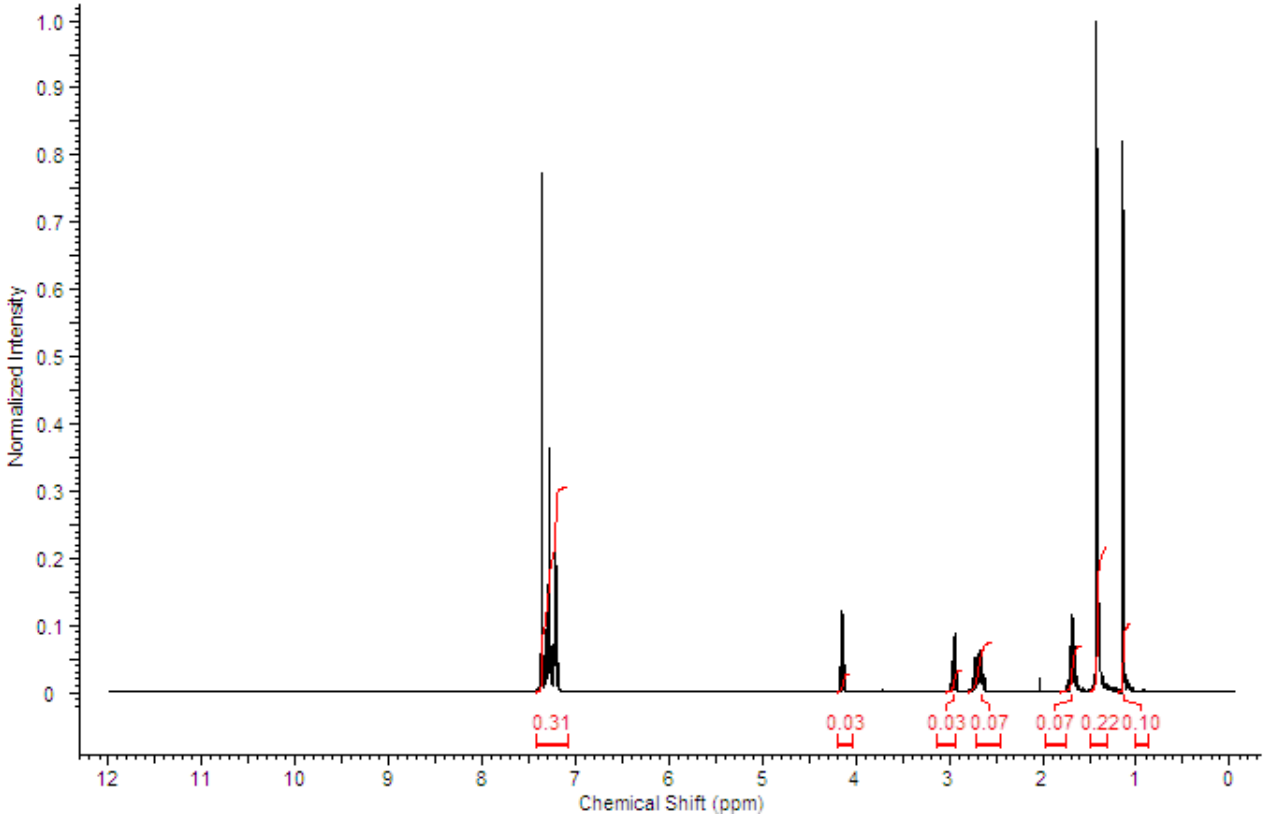

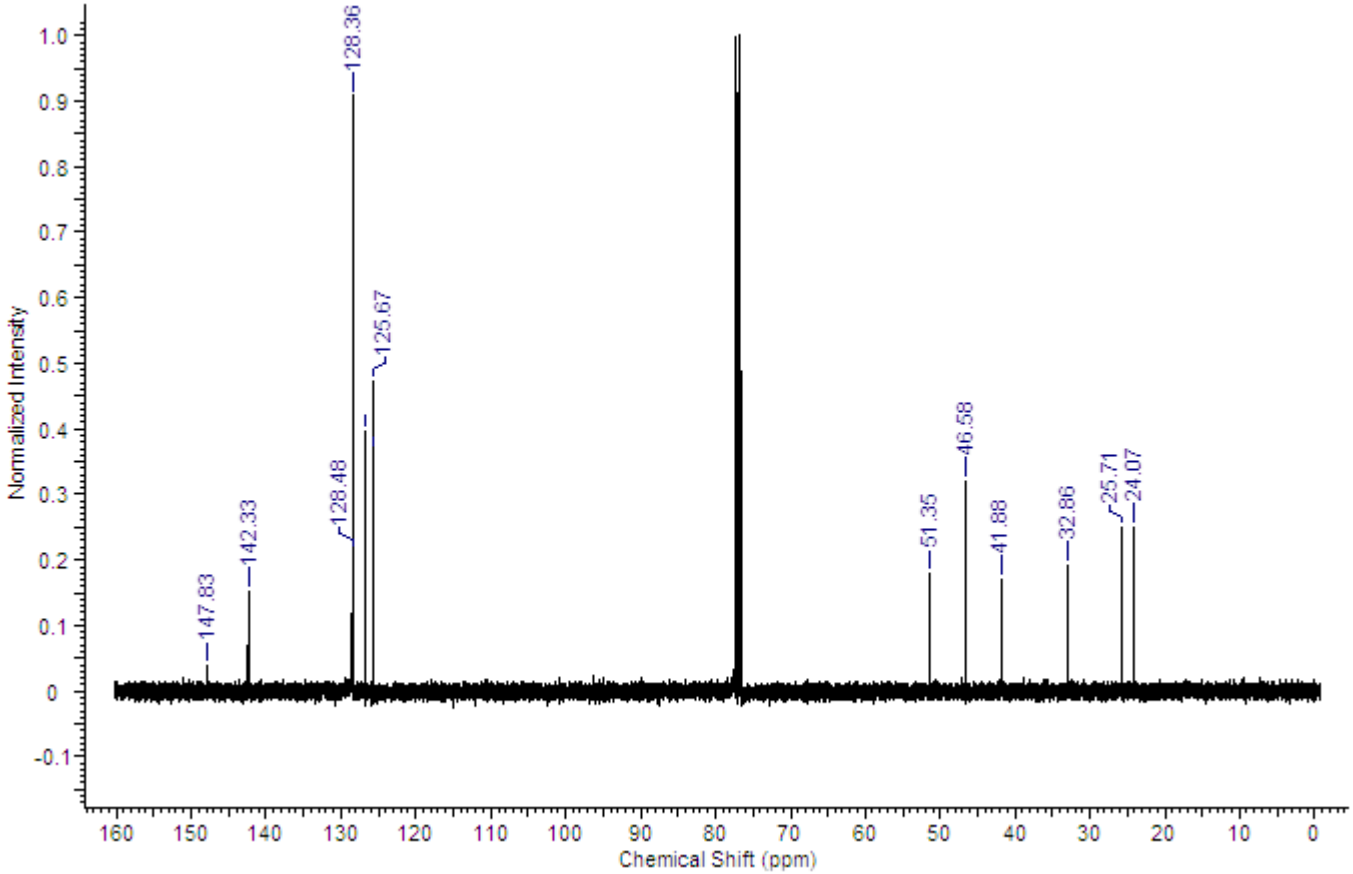
Normalized Intensity
1.0
0.9
0.8
0.7
0.6
0.5
0.4
0.3
0.2
0.1
0
-0.1
128.36
125.67
128.48
147.83
142.33
51.35
46.58
41.88
32.86
25.71
24.07
160
150
140
130
120
110
100
90
80
70
60
50
40
30
20
10
0
Chemical Shift (ppm)

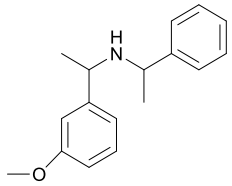

^{1}H NMR (400 MHz, $CDCl_3$): δ = 7.20-7.40 (6H, m), 6.94-7.00 (1H, m), 6.77-6.86 (2H, m), 3.77-3.87 (3H, m), 3.44-3.60 (2H, m), 1.29 (6H, dd, *J* = 6.60, 5.14 Hz). ^{13}C NMR (100 MHz, $CDCl_3$): δ = 159.76, 145.82, 129.38, 129.35, 128.37, 126.82, 126.67, 119.03, 112.92, 112.26, 55.24, 55.19, 55.11, 24.94. ESI-MS: calcd. for $C_{17}H_{21}NH^+$: 256.17. Found: 256.16 (MH^+).

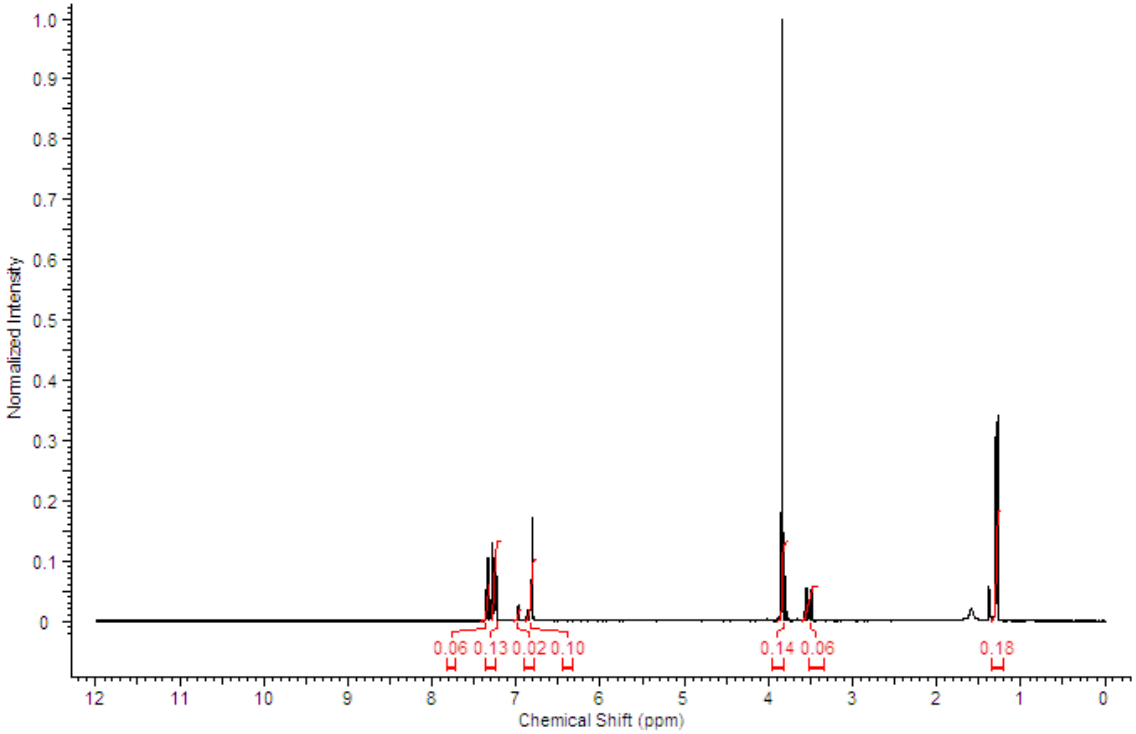

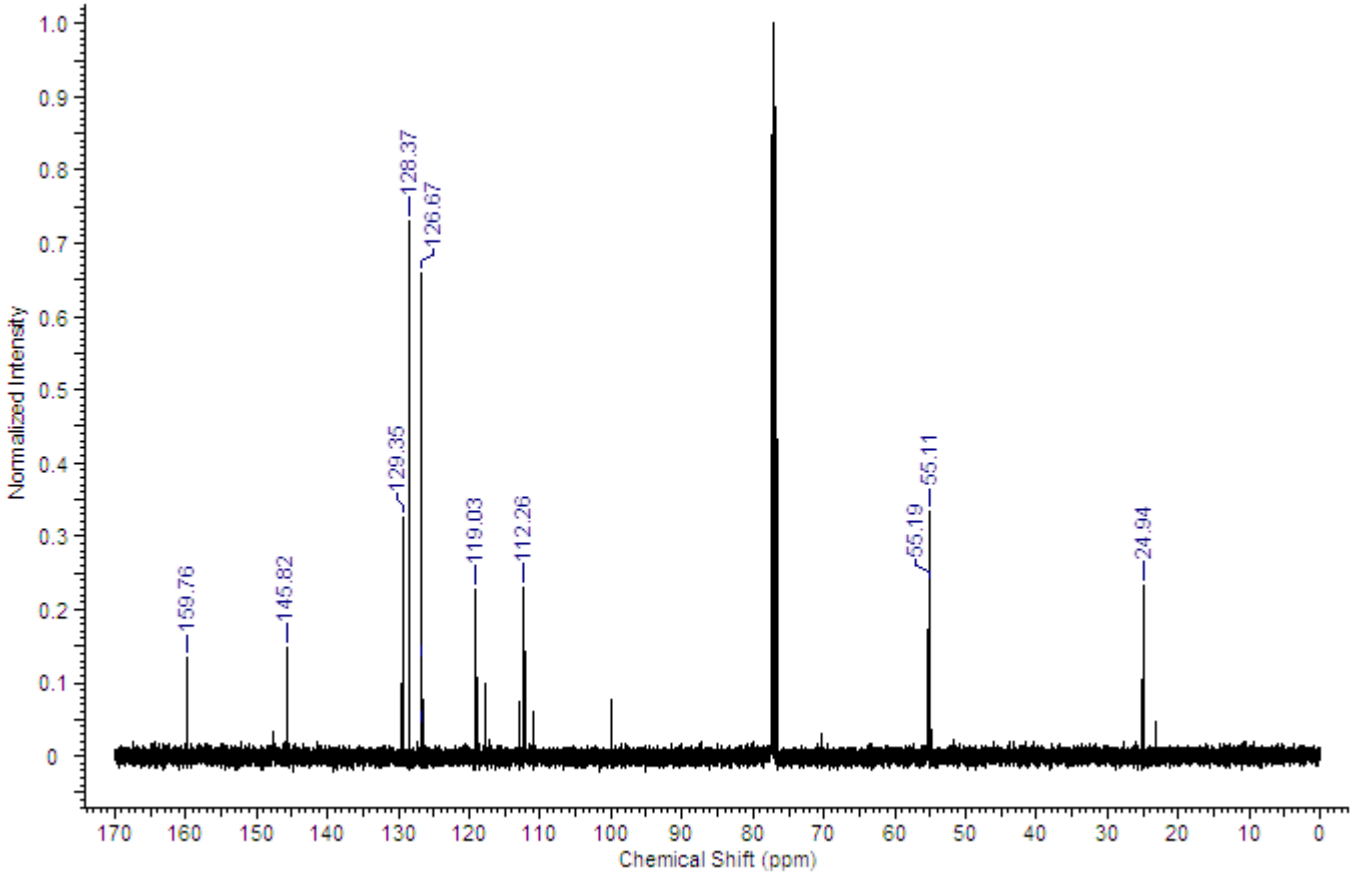
Normalized Intensity
1.0
0.9
0.8
0.7
0.6
0.5
0.4
0.3
0.2
0.1
0
159.76
145.82
129.35
128.37
126.67
119.03
112.26
55.19
55.11
24.94
170
160
150
140
130
120
110
100
90
80
70
60
50
40
30
20
10
0
Chemical Shift (ppm)

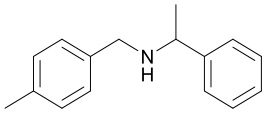

^{1}H NMR (400 MHz, $CDCl_3$): δ = 7.13-7.39 (9H, m, arom.), 3.83 (1H, q, *J* = 6.60 Hz), 3.57-3.68 (2H, m), 2.36 (3H, s), 1.56 (1H, br. s), 1.39 (3H, d, *J* = 6.60Hz). ^{13}C NMR (100 MHz, $CDCl_3$): δ =145.69, 137.64, 136.38, 129.04, 128.44, 128.07, 126.88, 126.72, 57.40, 51.37, 24.51, 21.09. ESI-MS: calcd. for $C_{16}H_{19}NH^+$: 226.16. Found: 226.15 (MH^+).

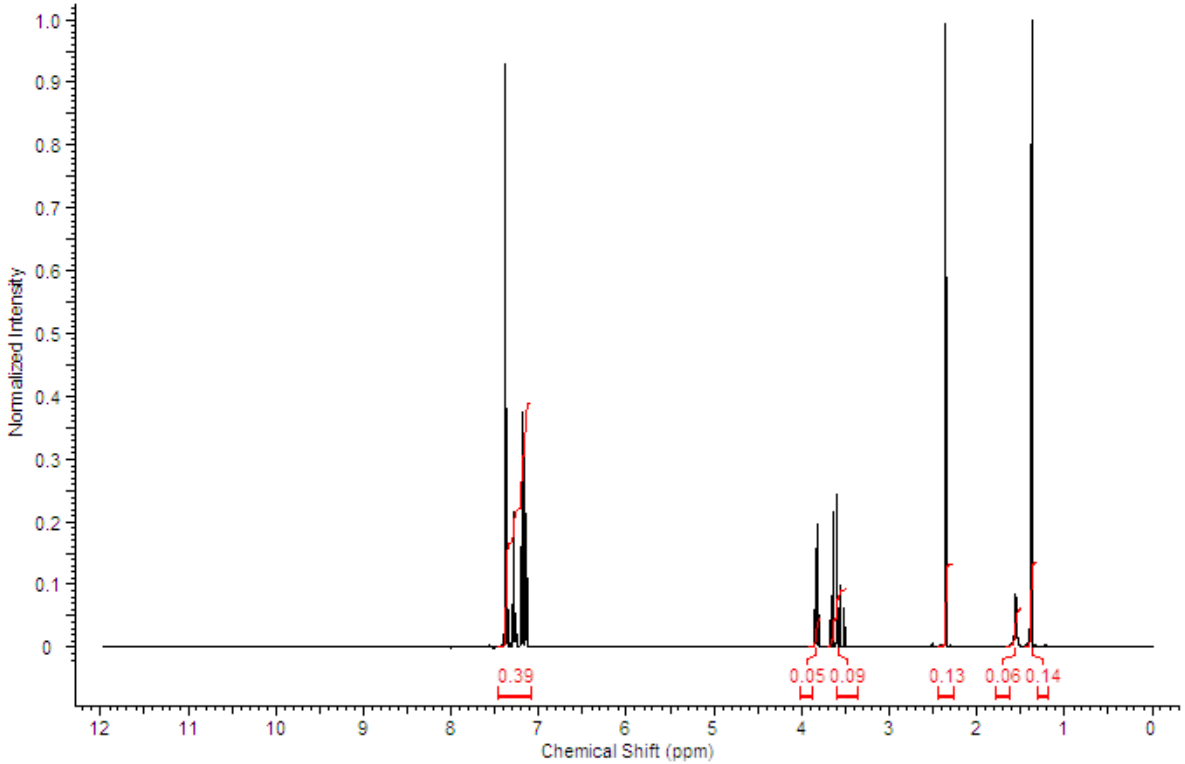

Normalized Intensity
Chemical Shift (ppm)
145.69
137.64
136.38
129.04
128.44
128.07
126.72
57.40
51.37
24.51
21.09

Appendix II

NMR and MS analysis of primary amines

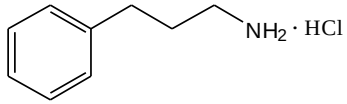

^{1}H NMR (250 MHz, DMSO-d_6): δ = 8.28 (3H, br s, NH_3^+), 7.27-7.33 (2H, m, arom.), 7.16-7.23 (3H, m, arom.), 2.76 (2H, t, *J* = 7.80 Hz), 2.66 (2H, t, *J* = 7.80 Hz), 1.83-1.95 (2H, m). ESI-MS: calcd. for $C_9H_{13}NH^+$: 136.1126. Found: 136.1151 (MH^+).

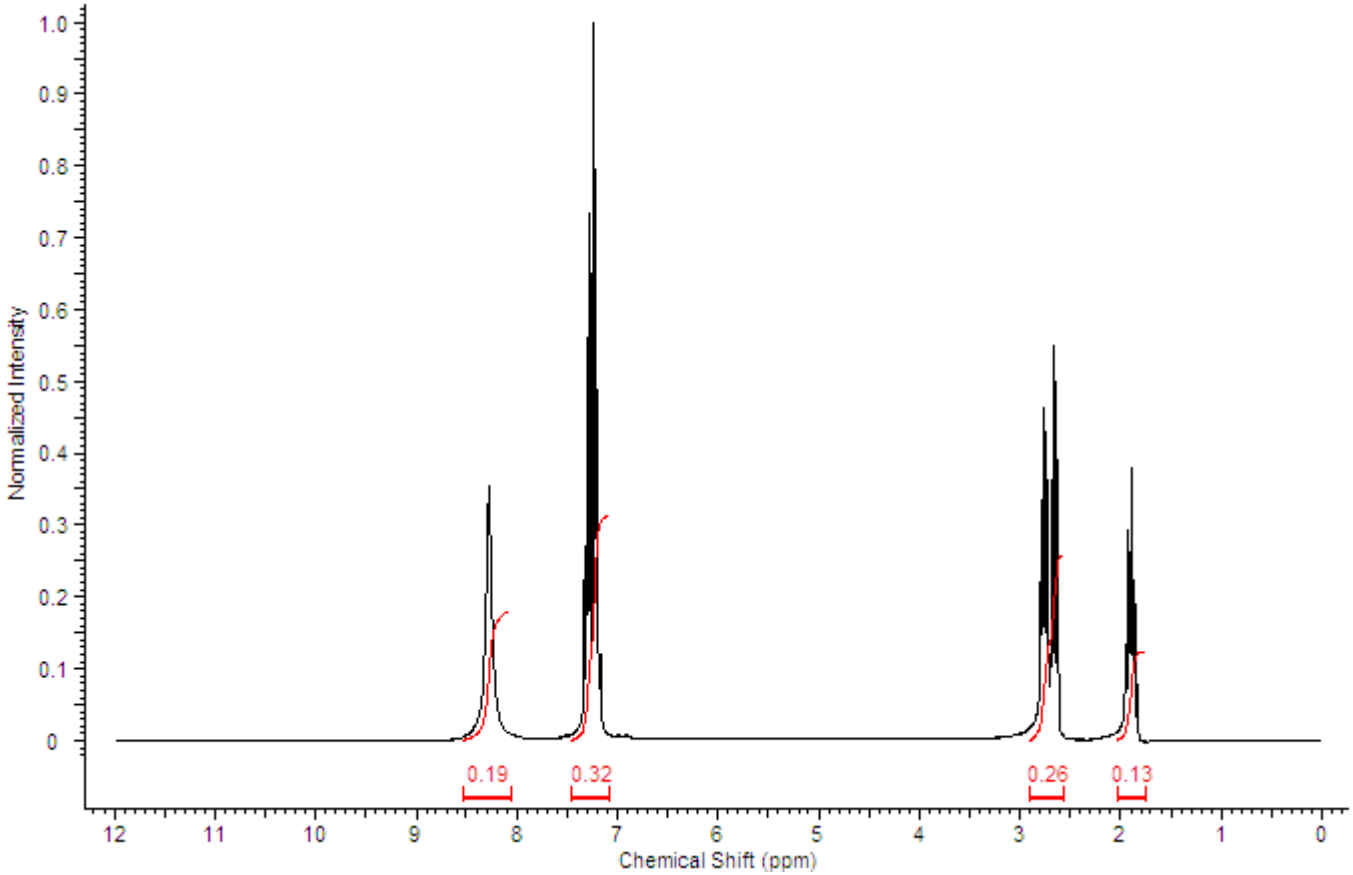

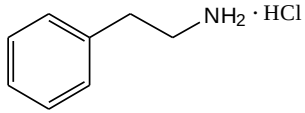

^{1}H NMR (250 MHz, DMSO-*d*$_6$): δ = 8.31 (3H, br s, NH_3^+), 7.12-7.54 (5H, m, arom.), 2.99-3.04 (2H, m), 2.77-2.86 (2H, m). ESI-MS: calcd. for $C_8H_{11}NH^+$: 122.0969. Found: 122.0988 (MH^+).

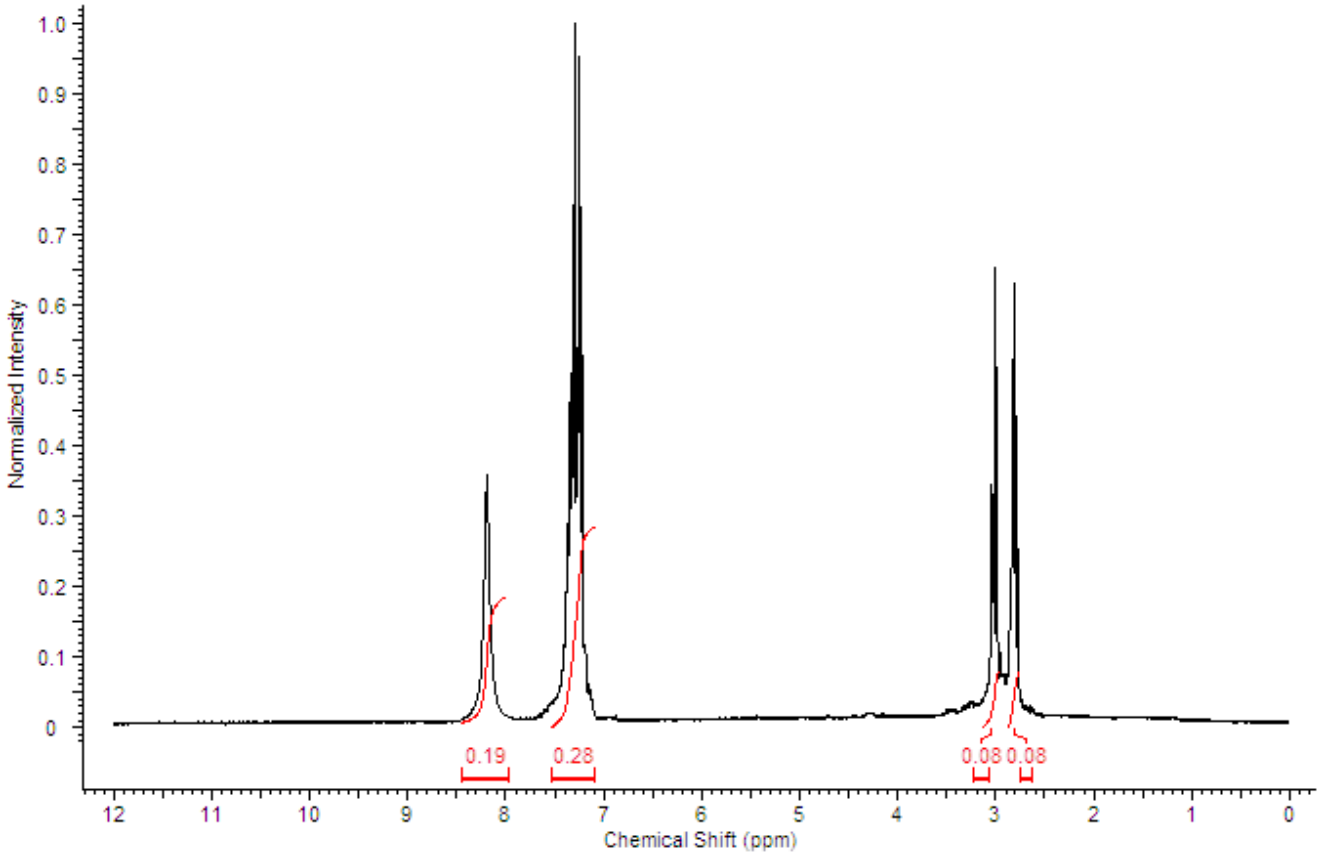

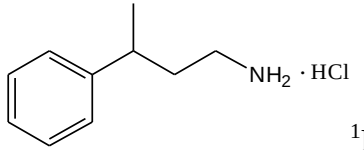

^{1}H NMR (250 MHz, DMSO-*d*$_6$): δ = 8.09 (3H, br s, NH_3^+), 7.14-7.61 (5H, m, arom.), 2.77-2.91 (2H, m), 2.57-2.76 (1H, m), 1.85 (2H,q, J = 7.69 Hz), 1.22 (3H, d, J = 6.95 Hz). ESI-MS: calcd. for $C_{10}H_{15}NH^+$: 150.1282. Found: 150.1289(MH^+).

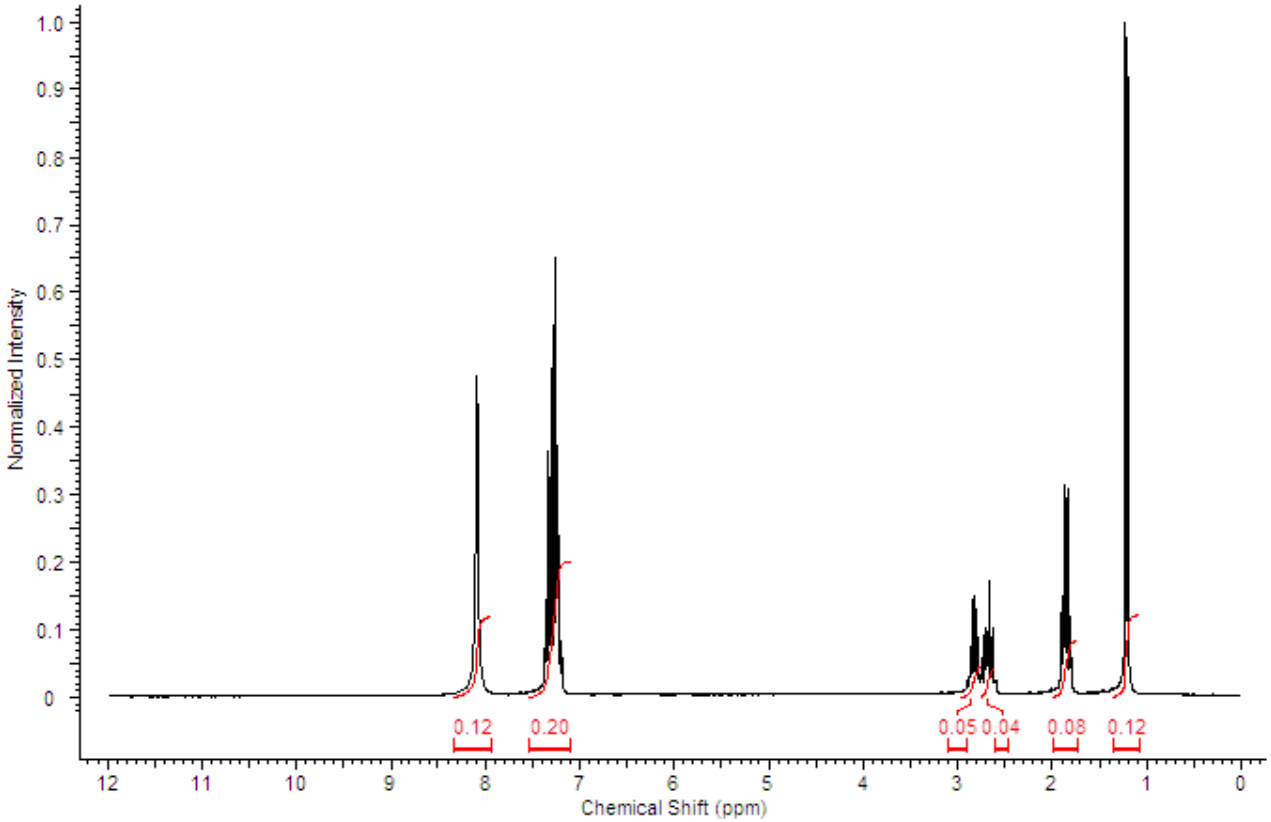

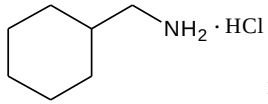

^{1}H NMR (250 MHz, DMSO-d_6): δ = 8.21 (3H, br s, NH_3^+), 2.52-2.59 (2H, m), 1.53-1.73 (2H, m), 1.08-1.25 (5H, m), 0.83-0.96 (4H, m). ESI-MS: calcd. for $C_7H_{15}NH^+$: 114.1282. Found: 114.1294 (MH^+).

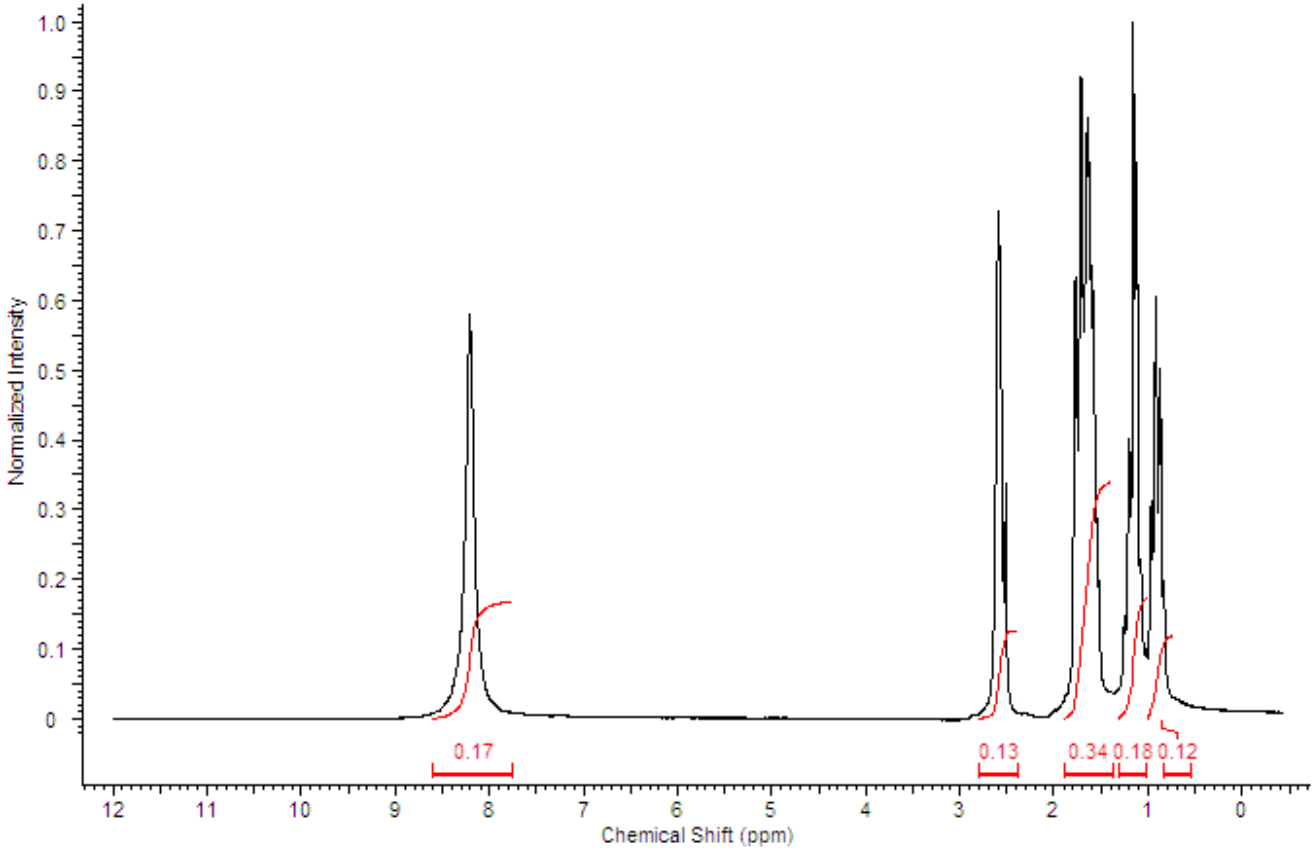

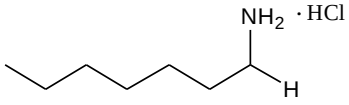

^{1}H NMR (250 MHz, DMSO-*d*$_6$): δ = 8.06 (3H, br s, NH_3^+), 2.62-2.86 (2H, m), 1.52-1.73 (2H, m), 1.27 (8H, br. s), 0.82-1.05 (3H, m). ESI-MS: calcd. for $C_9H_{13}NH^+$: 116.1439. Found: 116.1469 (MH^+).

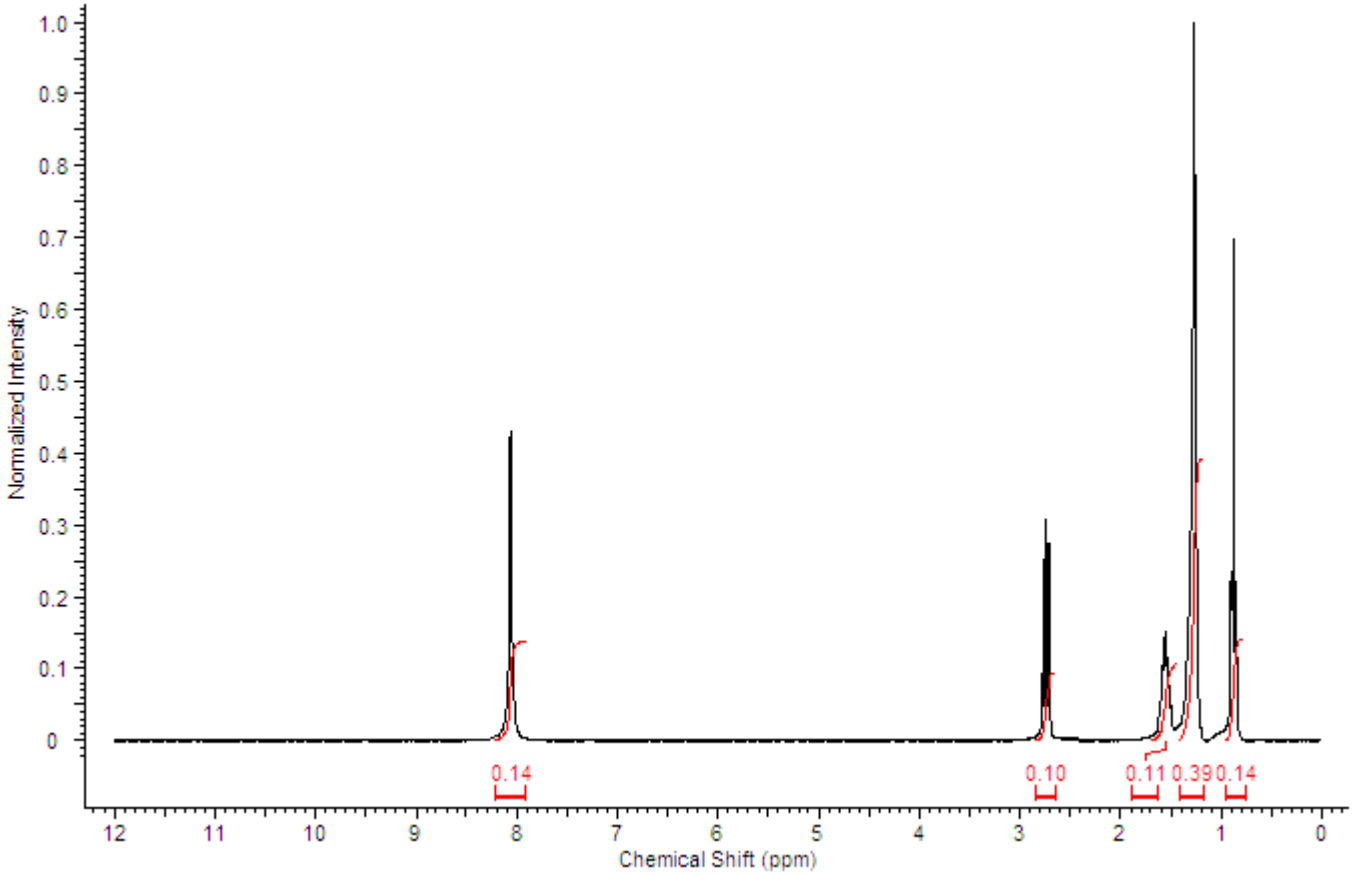

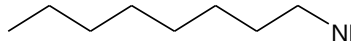

$NH_2 \cdot HCl$ ^{1}H NMR (250 MHz, DMSO-d_6): δ = 8.21 (3H, br s, NH_3^+), 2.49-2.96 (2H, m), 1.38-1.78 (2H, m), 1.24 (10H, s), 0.70-1.06 (3H, m). ESI-MS: calcd. for $C_9H_{13}NH^+$: 130.1595. Found: 130.1602 (MH^+).

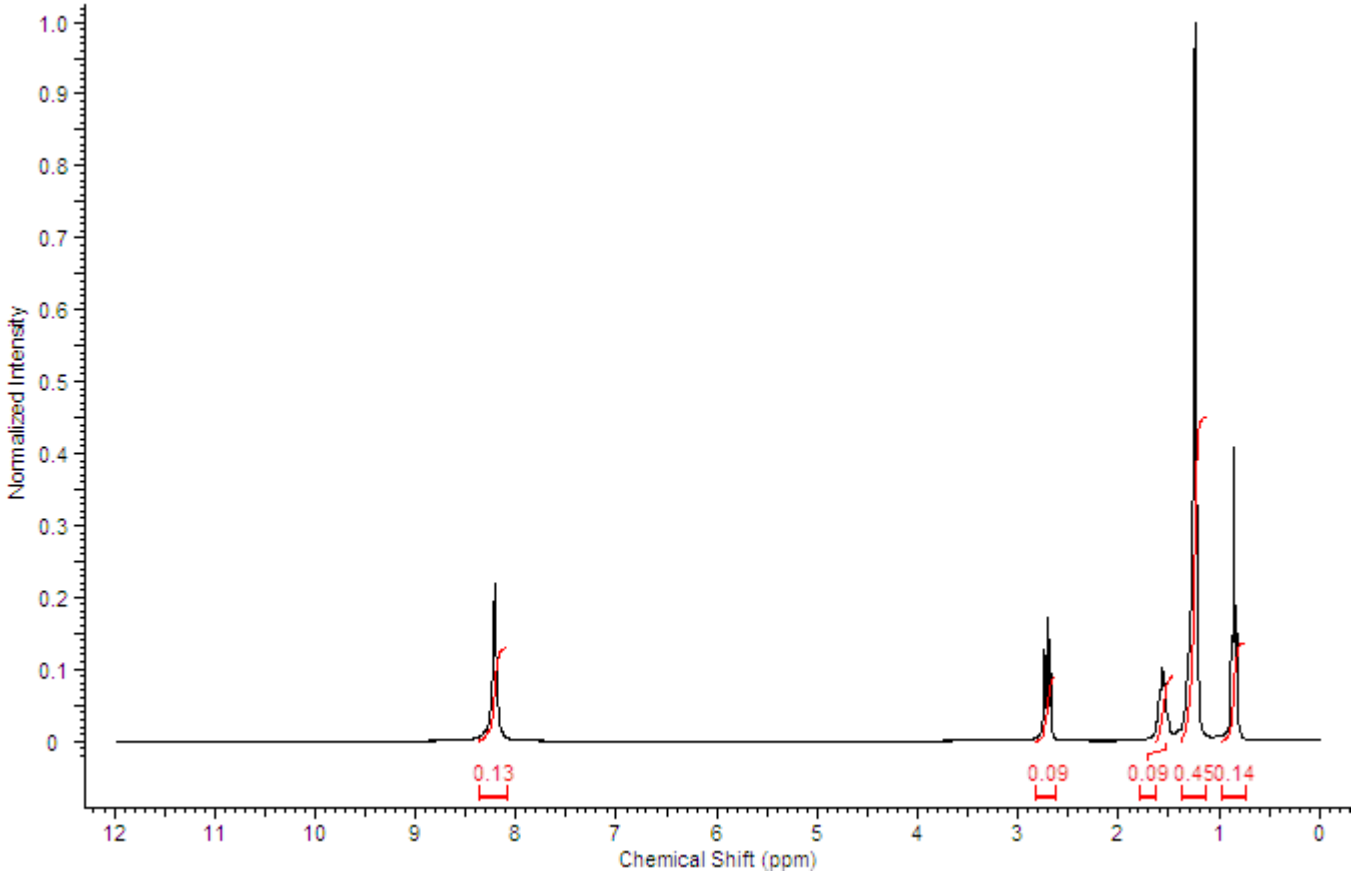

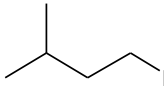

^{1}H NMR (300 MHz, DMSO-*d*$_6$): δ = 8.20 (3H, br s, NH_3^+), 2.69-2.75 (2H, m), 1.56-1.63 (1H, d), 1.40-1.47 (2H, m), 0.84-0.86 (6H, d, *J* = 6.03 Hz). ESI-MS: calcd. for $C_5H_{13}NH^+$: 88.1126. Found: 88.1130 (MH^+).

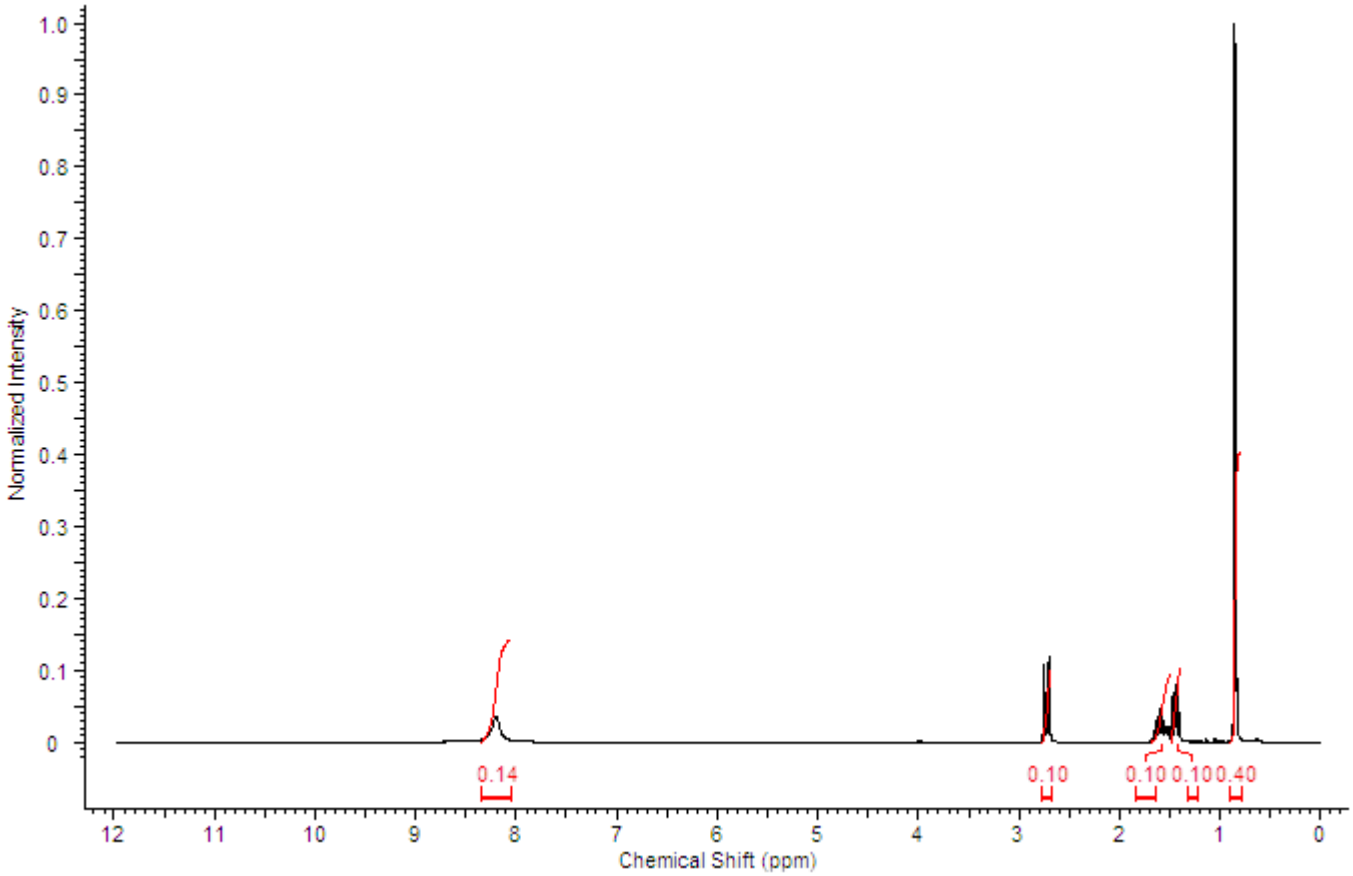

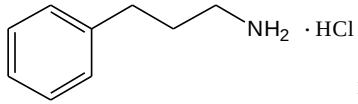

^{1}H NMR (250 MHz, DMSO-*d*$_6$): δ = 8.29 (3H, br s, NH_3^+), 7.27-7.33 (2H, m, arom.), 7.16-7.23 (3H, m, arom.), 2.61-2.82 (4H,m), 1.83-1.99 (2H, m). ESI-MS: calcd. for $C_9H_{13}NH^+$: 136.1126. Found: 136.1194 (MH^+).

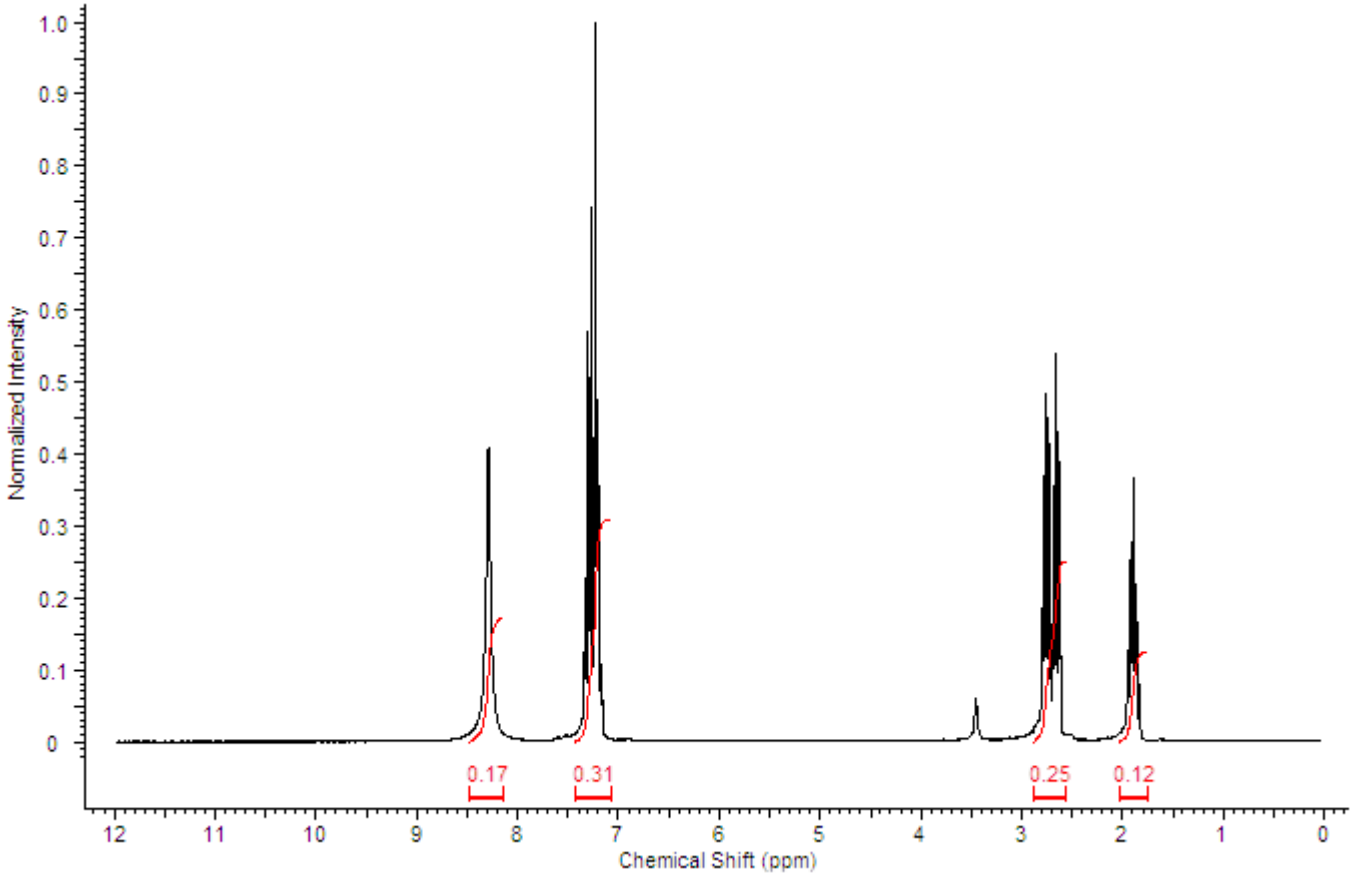

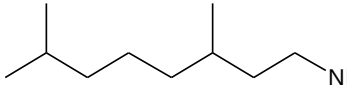

$\cdot$ HCl ^{1}H NMR (250 MHz, DMSO-d_6): δ = 8.16 (3H, br s, NH_3^+), 2.70-2.81 (2H, m), 1.06-1.26 (6H, m), 1.42-1.65 (2H, m), 0.84-0.91 (9H, m). ESI-MS: calcd. for $C_{10}H_{23}NH^+$: 158.1908. Found: 158.1962 (MH^+).

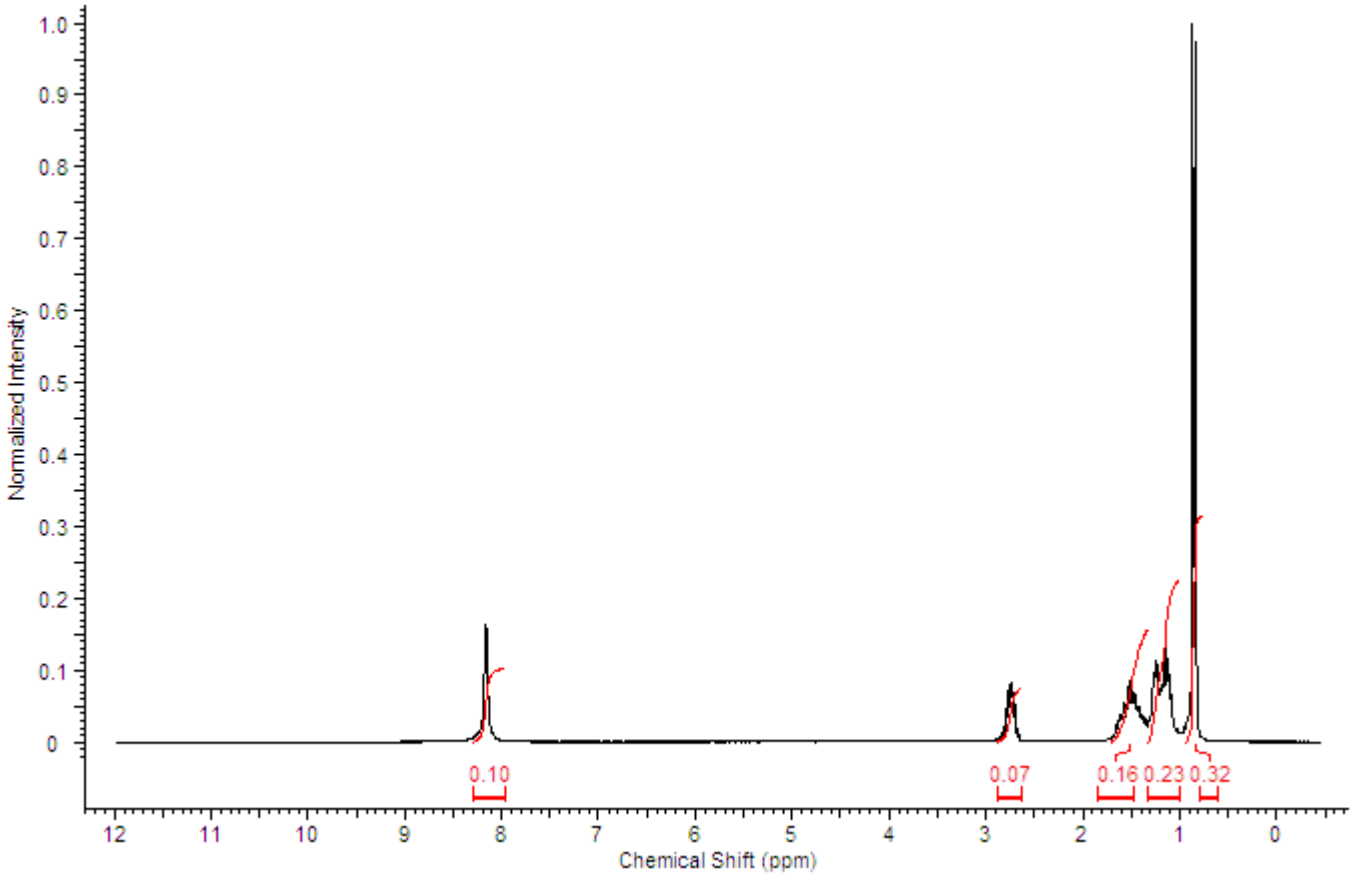

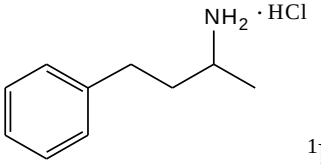

^{1}H NMR (250 MHz, DMSO-d_6): δ = 8.27 (3H, br s, NH_3^+), 7.03-7.44 (5H, m, arom.), 2.98-3.23 (1H, m), 2.58-2.76 (2H, m), 1.85-2.04 (1H, m), 1.64-1.83 (1H, m), 1.25 (3H, d, *J* = 6.63Hz). ESI-MS: calcd. for $C_{10}H_{15}NH^+$: 150.1282. Found: 150.1304 (MH^+).

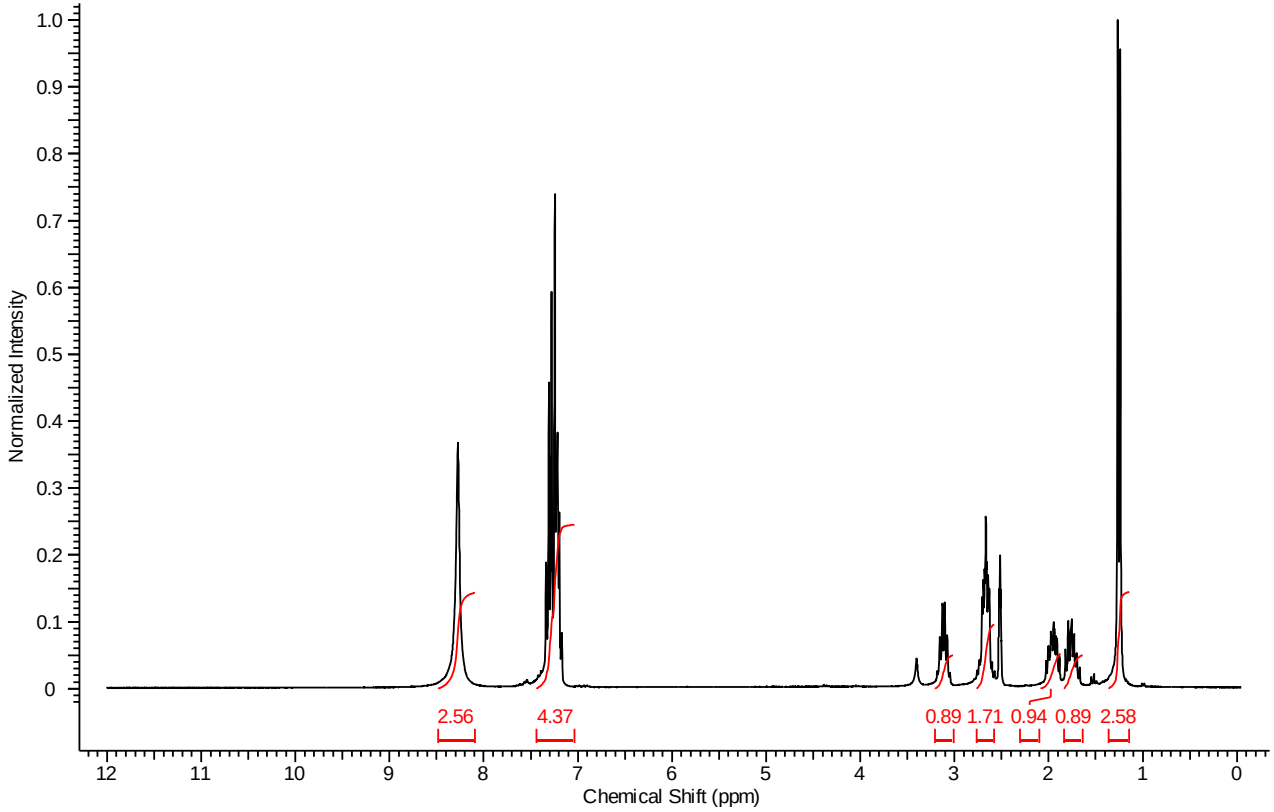

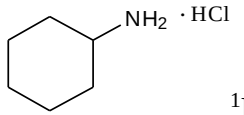
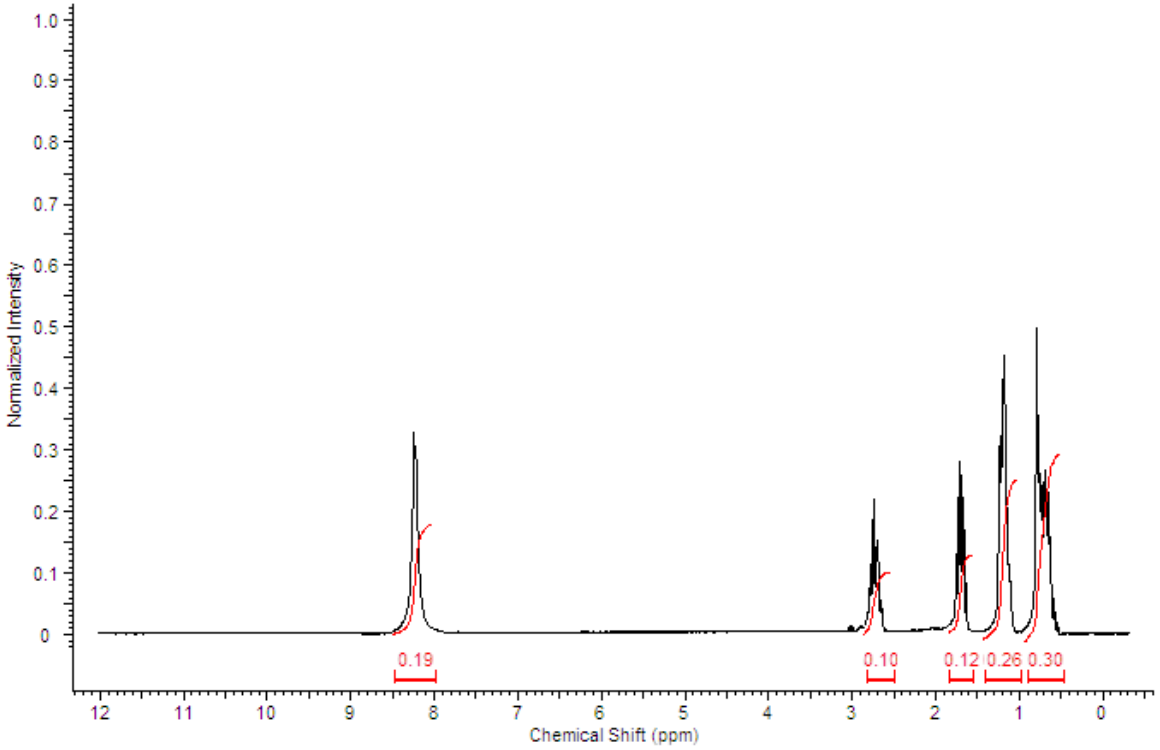
^{1}H NMR (250 MHz, DMSO-*d*$_6$): δ = 8.27 (3H, br. s, NH_3^+), 2.54 (1H, m, *J* = 6.63 Hz), 1.51-1.99 (2H, m), 1.07-1.48 (3H, m), 0.77-1.02 (4H, m). ESI-MS: calcd. for $C_6H_{13}NH^+$: 100.1126. Found: 100.1126 (MH^+).